Understanding the Mechanisms of Neurodegeneration in Amyotrophic Lateral Sclerosis (ALS) using Detailed Magnetic Resonance Neuroimaging

Dr Andrew William Barritt

A thesis submitted in partial fulfilment of the requirements of the University of Brighton for the degree of Doctor of Philosophy

October 2019

revised April 2020

Abstract

Background: Amyotrophic lateral sclerosis (ALS) is a heterogeneous neurodegenerative syndrome comprising rapidly progressive weakness, cognitive impairment and death within several years. Non-invasive magnetic resonance imaging (MRI) modalities sensitive to changes in tissue microstructure have been increasingly undertaken to help understand mechanisms of damage within the nervous system, aiming to establish an objective, sensitive and specific biological marker of disease activity for better diagnosis, prognosis and response to potential treatments *in vivo*. Fractional anisotropy (FA) from diffusion tensor imaging consistently demonstrates changes throughout the corticospinal tract (CST) and corpus callosum (CC) motor pathways compared to controls at group level, although the pathological correlates of FA changes are less certain. Newer MRI modalities including Neurite Orientation Dispersion and Density Imaging (NODDI) and quantitative magnetisation transfer imaging (qMTi) remain relatively unexplored in ALS but their detailed parameters concerning neurite architecture and macromolecular integrity, respectively, hold the potential to broaden understanding of neurodegenerative disease mechanisms. Furthermore, patients who deteriorate fastest possess fewer blood $CD4^+$ $CD25^+$ $FoxP3^+$ Regulatory T Lymphocytes (Tregs) which supports a key role for the immune system in ALS pathogenesis. An ongoing placebo-controlled clinical trial called MIROCALS [Modifying Immune Response and Outcomes in ALS] is testing safety and efficacy of low dose Interleukin-2, to augment Treg numbers, alongside standard treatment with Riluzole in newly-diagnosed patients with ALS. *Methods*: 23 patients with ALS from MIROCALS and 24 healthy controls underwent 1.5 Tesla MRI brain scans using NODDI and qMTi in this cross-sectional study. Neuroimaging analyses were performed at whole brain and region-of-interest levels, including with a novel modification of the NODDI processing pipeline optimised for grey matter neurite indices, in addition to white matter tract-based spatial statistics (TBSS) for the first time using both MRI modalities.

Patients' clinical data included the ALS Functional Rating Scale revised (ALSFRS-R), Edinburgh Cognitive and Behavioural ALS Screen (ECAS), disease duration, rate of disease progression, and blood total CD4 cell count, total Tregs and the Treg:CD4 ratio. Historical cohorts of 23 patients with ALS and 23 healthy controls enabled extended relationships with clinical factors (excluding blood measurements) to be explored. *Results*: Compared to controls, FA was significantly reduced and the NODDI orientation dispersion index (ODI) increased within the CSTs and CC. Reduced NODDI neurite density index (NDI) in these areas was additionally seen in the historical patients. Significantly reduced kf and increased t2f was demonstrated in the historical patients in the CSTs and CC using qMTi but did not reach significance in the MIROCALS patients. Within the CC, Total blood CD4 count showed a negative association with skeletonised FA, a negative association with the skeletonised qMTi f parameter and a positive association with skeletonised ODI, whereas the Treg:CD4 ratio demonstrated a negative association with NDI within the primary motor cortex. In relation to ALSFRS and disease duration, FA and NODDI neurite density index (NDI) consistently showed positive and negative associations, respectively. *Conclusions*: The results suggest that disease associated changes in FA within motor pathways of the CSTs and CC in ALS are not solely due to loss of density of neurite processes, but may also be representative of several architectural alterations, including infiltration of glia or breakdown of normal axon-myelin relationships inferred by NODDI, and accompanied by changes to macromolecular integrity inferred by qMTi. For the first time in ALS, biological measures of systemic immune system function, including blood CD4 and the proportion of Treg cells, have shown relationships to quantitative diffusion and magnetisation transfer imaging modalities within areas of the corpus callosum, thereby supporting a role for cross-talk between peripheral and central immune processes in the disease.

Contents

Abbreviations 12

Acknowledgements 13

Author's Declaration 14

Chapter 1. Introduction and Background

1.1 Human motor systems and Motor Neuron Disease 15

1.2 Epidemiology and genetics of ALS 17

1.3 Clinical presentation and phenotypic heterogeneity of ALS 18

1.3.1 LMN and UMN predominant forms along the 'ALS Spectrum' 19

1.3.2 Extramotor and cognitive involvement in ALS 21

1.4 Diagnosis and Management of ALS 23

1.4.1 Riluzole and other pharmacotherapy 24

1.5 Clinical measures and objective disease biomarkers 25

1.6 How, where and why does ALS arise? 27

1.6.1 What can neuropathology reveal about mechanisms of degeneration in ALS? 28

1.6.2 How do inclusion bodies (IBs) relate to degeneration in ALS? 33

1.6.3 What does neurophysiology suggest about mechanisms of disease in ALS? 36

1.6.4 Do animal models enlighten mechanisms of disease in ALS? 38

1.6.5 A role for the immune system in ALS 41

1.7 Can *in vivo* neuroimaging in patients with ALS aid understanding of the mechanisms of disease?

1.7.1 Limitations of conventional clinical neuroimaging 44

1.7.2 SPECT and PET 45

1.7.3 PET with specific radioligands 46

1.7.4 Task-based functional MRI (fMRI) 48

1.7.5 Resting state functional MRI (rsfMRI) 49

1.7.6 MRI Morphometry 52

1.7.7 Diffusion MRI: Diffusion Tensor Imaging (DTI) 54

1.7.8 Diffusion MRI: Neurite Orientation Dispersion and Density Imaging (NODDI) 58

1.7.9 Quantitative Magnetisation Transfer Imaging (qMTi) 61

1.8 Summary of Key Statements 63

References 65

Chapter 2. Methodology

2.1 Rationale for the Neuroimaging Study 79

2.2 Study Aims and Original Contribution 80

2.3 The choice of Neuroimaging within the study 83

2.4 Participants

2.4.1 Sample size: cross-sectional study 86

2.4.2 Sample size: longitudinal study 87

2.5 Historical cohort of Patients and Controls 89

2.6 Outcome Measures

2.6.1 Primary Outcome Measures 90

2.6.2 Clinical and Fluid Biomarker Measures available for the Doctoral Thesis 91

2.7 Research Questions for the Doctoral Thesis 92

2.8 Outline of analysis techniques and principal brain Regions of Interest (ROIs) 93

2.9 Hypotheses

2.9.1 Diffusion MRI Group Comparisons 96

2.9.2 qMTi Group Comparisons 98

2.9.3 Relationships with Clinical Factors 99

2.9.4 Relationships with Blood CD4 cells 100

2.10 The Neuroimaging Study: Two Studies in One 101

2.10.1 Plan of Investigation: *ANNALS-QuICT Study* 102

2.10.2 Plan of Investigation: *MultiNICS Study* 107

2.11 MRI acquisition and Data Storage 108

2.12 Image Processing and Computation of Parametric Maps for NODDI and qMTi 110

2.12.1 Whole Brain and ROI Statistical Analyses 112

2.12.2 Tract Based Spatial Statistics (TBSS) and Statistical Analyses 113

2.12.3 Precentral motor cortex thickness as a co-variate in NODDI ID=1.1 analyses 114

2.12.4 Quantification of Parameters within Significant Clusters 115

2.13 Subject Demographics and Clinical Data for Doctoral Thesis

2.13.1 Totals of “New Participants” Recruited to ANNALS-QuICT and MultiNICS 116

References 117

Chapter 3. Results: FA from Diffusion Imaging in ALS 120

Participants 122

3.1 Group Differences: FA in New Patients versus New Controls 127

3.2 Relationships between FA and Blood CD4 Cells in the New Patients 130

3.3 Relationships between FA and Clinical Measures in the New Patients 134

3.4 Group Differences: FA in Historical Patients versus Historical Controls 136

3.5 Relationships between FA and Clinical Measures in Historical Patients 139

3.6 Relationships between FA and Clinical Measures: **Combined New + Historical Patients** 144

3.7 Summary of main FA findings in Patients with ALS 150

Chapter 4. Results: NODDI in ALS 151

Participants 152

4.1 Group Differences: NODDI ID=1.7 in New Patients versus New Controls 153

4.2 Relationships between NODDI 1.7 and Blood CD4 cells in the New Patients 156

4.3 Relationships between NODDI 1.7 and Clinical Measures in the New Patients 160

4.4 Group Differences: NODDI 1.7 in Historical Patients versus Historical Controls 161

4.5 Relationships between NODDI 1.7 & Clinical Measures in Historical Patients 169

4.6 Relationships between NODDI 1.7 & Clinical Measures: Combined New + Historical Patients 172

4.7 Summary of main NODDI 1.7 findings in Patients with ALS 176

4.8 Group Differences: NODDI ID=1.1 in New Patients versus New Controls 178

4.9 Relationships between NODDI 1.1 and Blood CD4 cells in the New Patients 178

4.10 Relationships between NODDI 1.1and Clinical Measures in the New Patients 181

4.11 Group Differences: NODDI ID=1.1 in Historical Patients versus Historical Controls 182

4.12 Relationships between NODDI 1.1 & Clinical Measures in Historical Patients 184

4.13 Relationships between NODDI 1.1 & Clinical Measures: Combined Patients 186

4.14 Summary of main NODDI 1.1findings in Patients with ALS 188

Chapter 5. Results: qMTi in ALS 190

Participants 191

5.1 Group Differences: qMTI in New Patients versus New Controls 195

5.2 qMTi relationships with Blood CD4 cells in the New Patients 195

5.3 qMTi relationships with Clinical Measures in New Patients 198

5.4 Group Differences: qMTI in Historical Patients versus Historical Controls 198

5.5 qMTi Relationships with Clinical Measures in the Historical Patients 206

5.6 Relationships between qMTI & Clinical Measures: Combined New + Historical Patients 212

5.7 Summary of main qMTi findings in Patients with ALS 213

Chapter 6. Results: Post hoc analyses 214

6.1 CD4+ Cells and Rate of Disease Progression 214

6.2 Historical versus New MRI scans: Diffusion and qMT Imaging 216

6.3 Effect Sizes for Patient and Control Group Differences 219

6.4 Relationships between FA / NODDI ID=1.7 & Disease Duration with ALSFRS as co-variate 221

Chapter 7. Discussion 223

7.1 Diffusion Imaging in ALS: FA and NODDI 1.7 223

Patients versus Controls 223

Relationships to Clinical Factors 231

Relationships to blood CD4+ cells (New Patients only) 237

7.2 Diffusion Imaging in ALS: NODDI ID=1.1 242

7.3 Quantitative Magnetisation Imaging in ALS 247

7.4 Limitations of the current study 253

7.5 Further work 258

7.6 Conclusion 262

References 264

Appendix. Candidate's Published Work in Relation to the Thesis 273

Review: *Barritt AW, Gabel M, Cercignani M and Leigh PN.* Novel Magnetic Resonance Imaging Techniques and Analysis Methods in Amyotrophic Lateral Sclerosis. *Front Neurol. 9:1065 DOI: 10.3389/fneur.2018.01065.*

Figures and Tables

Chapter 1. Introduction and Background

Figure 1.6.1. Pyramidal tract degeneration in ALS 32

Chapter 2. Methodology

Figure 2.8.1. Whole brain and ROI analyses 95

Figure 2.8.2. TBSS and TBSS ROI analyses 95

Table 2.9.1.1. Hypotheses for FA + NODDI 1.7 in patients relative to controls 97

Table 2.9.1.2 Hypotheses for NODDI 1.1 in patients relative to controls 97

Table 2.9.2.1. Hypotheses for qMTi in patients relative to controls 98

Table 2.9.3.1 Hypotheses FA, NODDI and qMTi parameters versus clinical factors 99

Table 2.9.4.1 Hypotheses FA, NODDI and qMTi parameters versus CD4 and Treg cells 100

Figure 2.10.1. Schematic timeline for MRI brain scans in relation to the MIROCALS Trial 106

Chapter 3. Results: FA from Diffusion Imaging in ALS

Table 3a. New Participant demographics and clinical characteristics 123

Table 3b. Historical Participant demographics and clinical characteristics 124

Table 3c. New and Historical Patient demographics and clinical characteristics 125

Figure 3d. Spread of clinical factors across combined New and Historical Patients 126

Table 3.1.1. Significant group differences in FA between the New Patients and Controls 127

Figure 3.1.2. FA is reduced in New Patients compared to Controls 128

Figure 3.1.3. Skeletonised FA is reduced in New Patients compared to Controls 129

Table 3.2.1. Significant relationships between FA and blood CD4 cells in New Patients 131

Table 3.2.2. Significant relationships between FA and blood CD4 cells with rate as co-variate 131

Figure 3.2.3. Higher total blood CD4 cells associated with reduced skeletonised FA 132

Figure 3.2.4. Higher ratio of Tregs to CD4 cells is associated with increased FA 133

Table 3.3.1. Significant relationships between FA and clinical factors in New Patients 134

Figure 3.3.2. Shorter disease duration associated with reduced FA 135

Table 3.4.1. Significant group differences in FA between Historical Patients and Controls 136

Figure 3.4.2. FA is extensively reduced in Historical Patients compared to Controls 137

Figure 3.4.3. Skeletonised FA is reduced in Historical Patients compared to Controls 138

Table 3.5.1. Significant relationships between FA and clinical factors 140

Figure 3.5.2. Longer disease duration associated with reduced FA 141

Figure 3.5.3. Reduced functional score associated with reduced FA 142

Figure 3.5.4. Reduced ECAS ALS specific score associated with reduced FA 143

Table 3.6.1. Significant relationships between FA and clinical factors in combined Patients 145

Figure 3.6.2. Declining ECAS ALS specific score ($ECAS^{sp}$) associated with reduced FA 146

Figure 3.6.3. Reduced functional score associated with reduced FA 147

Figure 3.6.4. Longer duration of disease associated with extensively reduced FA 148

Figure 3.6.5. Shorter duration of disease associated with reduced FA 149

Chapter 4. Results: NODDI in ALS

Table 4.1.1. Significant differences in NODDI 1.7 between the New Patients and Controls 153

Figure 4.1.2. ODI is increased in New Patients vs Controls 154

Figure 4.1.3. Skeletonised ODI is reduced in New Patients vs Controls 155

Table 4.2.1. Significant relationships between FA and blood CD4 cells in the New Patients 157

Table 4.2.2. Significant relationships between skeletonised FA & CD4 cells in New Patients 157

Figure 4.2.3. Higher total blood CD4 cells associated with increased ODI 158

Figure 4.2.4. Higher total blood CD4 cells associated with increased skeletonised ODI 159

Table 4.4.1. Significant group differences NODDI ID=1.7 between Historical Patients & Controls 162

Figure 4.4.2. NDI is extensively reduced in Historical Patients vs Controls 163

Figure 4.4.3. ODI is increased in Historical Patients compared to Controls 164

Figure 4.4.4. ODI and ISO are decreased in Historical Patients vs controls 165

Figure 4.4.5. Skeletonised NDI extensively reduced in Historical Patients vs Controls 166

Figure 4.4.6. Skeletonised ODI of Motor ROIs increased in Historical Patients vs Controls 167

Figure 4.4.7. Skeletonised ISO is decreased in Historical Patients vs Controls 168

Table 4.5.1. Relationships between NODDI ID=1.7 and clinical factors in Historical Patients 170

Figure 4.5.2. Higher ECAS associated with higher skeletonised NDI and lower ISO 171

Table 4.6.1. Relationships between NODDI ID=1.7 and clinical factors in Combined Patients 174

Figure 4.6.2. Reduced functional score associated with reduced NDI 175

Figure 4.6.3. Increased disease duration associated with reduced NDI 177

Table 4.7.1. Diffusion MRI (FA and NODDI ID=1.7) changes between Patients and Controls 180

Table 4.9.1. Relationships between NODDI ID=1.1 and blood CD4 cells in New Patients 182

Figure 4.9.2. Greater Treg:CD4 ratio associated with lower NDI in left precentral cortex 183

Table 4.11.1. Group differences in NODDI ID=1.1 between Historical Patients and Controls 185

Figure 4.11.2. ODI reduced in New Patients vs Controls within the left primary motor cortex 186

Table 4.12.1. Relationships between NODDI ID=1.1 and clinical factors in Historical Patients 187

Figure 4.12.2. Reduced ECAS ALS Specific score associated with increased NDI 188

Table 4.13.1. Relationships between NODDI ID=1.1 and clinical factors in Combined Patients 189

Figure 4.13.2. Reduced functional score associated with increased NDI 190

Table 4.14.1. Significant NODDI ID=1.1 changes between both Patient & Control groups 192

Chapter 5. Results: qMTi in ALS

Table 5a. New Participant demographics and clinical characteristics 195

Table 5b. Historical Participant demographics and clinical characteristics 196

Table 5c. New and Historical Patient demographics and clinical characteristics 197

Table 5.2.1. TBSS and TBSS Motor ROIs qMTi in New Patients vs blood CD4 cells 199

Figure 5.2.2. Skeletonised f shows a negative association with total blood CD4 count 200

Table 5.4.1. Significant group differences in qMTi between Historical Patients and Controls 202

Figure 5.4.2. Whole brain qMTi comparisons between Historical Participants 203

Figure 5.4.3. Motor ROI qMTi comparisons between Historical Participants 205

Figure 5.4.4. TBSS qMTi comparisons between Historical Participants 207

Figure 5.4.5. TBSS Motor ROIs analyses using qMTi in Historical Participants 208

Table 5.5.1. Whole brain and Motor ROIs qMTi in Historical Patients vs clinical factors 210

Table 5.5.2. TBSS and TBSS Motor ROIs qMTi in Historical Patients vs clinical factors 210

Figure 5.5.3. Whole brain kf shows a significant positive correlation with ALSFRS 211

Figure 5.5.4. Skeletonised f shows significant negative correlation with total ECAS score 212

Figure 5.5.5. Skeletonised f shows significant negative correlation with ECAS ALS Spec. score 213

Figure 5.5.6. Skeletonised kf shows significant positive correlation with ECAS ALS Spec. score 214

Chapter 6. Results: Post hoc analyses

Table 6.1.1. Spearman's rho and significance between Rate of progression & blood CD4 cells 218

Figure 6.1.2. Boxplot of the rate of disease progression in the New Patients 218

Table 6.2.1. Demographics for the Historical Controls and New Controls in the Diffusion 220

Table 6.2.2. Demographics for the Historical Controls and New Controls in the qMTi 220

Figure 6.2.3. Skeletonised ODI increased in the New Controls vs Historical Controls 220

Figure 6.2.4. Subthreshold TBSS qMTi comparisons between New Patients and Controls 221

Table 6.3.1. Effect sizes for significant differences in FA: New Patients vs Controls 222

Table 6.3.2. Effect sizes for significant differences in FA: Historical Patients vs Controls 222

Table 6.3.3. Effect sizes for significant differences in NODDI: New Patients vs Controls 223

Table 6.3.4. Effect sizes for significant differences in NODDI: Historical Patients vs Controls 223

Table 6.3.5. Effect sizes for significant differences in qMTi: Historical Patients vs Controls 223

Figure 6.4.1. Longer disease duration associated with reduced skeletonised FA or NDI 225

Abbreviations

ALS	Amyotrophic Lateral Sclerosis
ALSFRS-R	ALS Functional Rating Scale-Revised
BOLD Signal	Brain Oxygen Level Dependent Signal
C9orf72	Chromosome 9 Open Reading Frame 72 (gene)
CSF	Cerebrospinal Fluid
CNS	Central Nervous System
DTI	Diffusion Tensor Imaging
DWI	Diffusion Weighted Imaging
ECAS	Edinburgh Cognitive and Behavioural Assessment Screen
ENCALS	European Network for the Cure of ALS
fALS	Familial Amyotrophic Lateral Sclerosis
fMRI	Functional Magnetic Resonance Imaging
FSL	FMRIB Software Library
FUS	Fused in Sarcoma (gene)
GABA	Gamma-Aminobutyric Acid
5HT	5-Hydroxytryptophan (Serotonin)
MRC Score	Medical Research Council Score
LMN	Lower Motor Neuron
MNI Space	Montreal Neurological Institute Space
MRI	Magnetic Resonance Imaging
MNDA	Motor Neurone Disease Association
NFL	Neurofilament Light
(p)NFH	(Phosphorylated) Neurofilament Heavy
NICE	National Institute for Health and Clinical Excellence
NifTi	Neuroimaging Informatics Technology Initiative (file format)
NODDI	Neurite Orientation Dispersion and Density Imaging
PET	Positron Emission Tomography
PLS	Primary Lateral Sclerosis
PMA	Progressive Muscular Atrophy
qMTi	Quantitative Magnetisation Transfer Imaging
rsfMRI	Resting State Functional Magnetic Resonance Imaging
sALS	Sporadic Amyotrophic Lateral Sclerosis
SOD1	Superoxide Dismutase 1 (gene)
SPECT	Single-Photon Emission Computed Tomography
TARDBP	Trans Active Response DNA Binding Protein
Teffs	Effector T Cells
Tregs	Regulatory T Cells
tbfMRI	Task-Based Functional Magnetic Resonance Imaging
UMN	Upper Motor Neuron

Acknowledgements

I would like to thank the patients with ALS and the healthy control volunteers - often friends or family members of the patients themselves - who have given up their time to participate in this neuroimaging study and in many cases travelled a significant distance on several occasions in order to do so. This research is dedicated to them in the hope that it may help bring the prospect of better treatment for ALS one step closer

The following colleagues, whose good humour, guidance and wisdom has been instrumental in enabling the neuroimaging study to occur, deserve special thanks:

Professor P Nigel Leigh
Professor Mara Cercignani
Dr Gilbert Bensimon
Dr Christine Payan
Ms Pat Butler
Dr Rebecca Broad
Dr Matt Gabel
Dr Iulia Bogdan
Dr Nick Dowell
Dr Samira Bouyagoub
Dr Charlotte Rae
Dr Matteo Mancini
Dr Timothy Tree
Ms Rachel Thomson
Professor Majid Hafezparast
Dr Greig Jolin
Ms Jan Bush
Mr Stuart Welling
Ms Marta Andrade
Mr James Hunter
Dr Jessica Eccles
Dr Alessandro Colasanti
Dr Neil Harrison
Dr Natasha Sigala
Dr Stephen Bremner

I am very grateful to the entire team at the Clinical Imaging Sciences Centre (CISC) and the Motor Neurone Disease Association (MNDA) for their support of the project.

Declaration

I, Andrew William Barritt, declare that the research contained in this thesis, unless otherwise formally indicated within the text, is the original work of the author. The thesis has not been previously submitted to this or any other university for a degree, and does not incorporate any material already submitted for a degree.

Signed:  **…….**

Dated: **17th April 2020……**

1. Introduction and Background

1.1 Human Motor Systems and Motor Neuron Disease

Volitional movement in humans is complex and requires integration of ascending and descending neural information. The pyramidal tracts, comprising bilateral corticobulbar tracts and corticospinal tracts (or 'direct' CSTs) connecting pyramidal cells of the primary motor cortices to the bulbar nuclei and spinal cord motor neurons, respectively, are considered the most evolutionarily advanced of several descending pathways principally concerned with cranio-spinal motor output.[1] Studies of rodents and primates would suggest that the direct CST serves multiple functions including gating of sensory information and integration of sensorimotor feedback.[2] Upstream inputs arise not only from motor areas in the frontal lobes but also from the primary somatosensory cortex and parietal lobe regions. The important evolutionary advantage in advanced primates of refined limb dexterity, particularly of the upper limb, is mediated through an increased quantity of CST fibres, a greatly expanded cortical input component and a larger proportion of 'corticomotoneuronal' monosynaptic connections between pyramidal cell axon terminals and anterior horn cells themselves (rather than indirect innervation via segmental interneurons or multi-segment propriospinal neurons).[1,3-5] Although a proportion of these corticomotoneuronal cells are the Giant Cells of Betz whose somata are located in cortical layer Vb along with all subcerebrally-projecting glutamatergic pyramidal neurons,[6] a range of cortical neuron sizes appear to contribute to this system. Indeed, primate studies have shown that the distributions for individual muscles overlap each other, with some pyramidal cells even originating in the somatosensory cortex.[1,7]

The CSTs are accompanied by more primitive bilateral subcortical origin pathways which receive significant cortical input themselves and ultimately synapse onto, and modulate, the common output via the motor neurons at cranial or spinal nerve root level.[8] These

include: the rubrospinal tracts arising from the magnocellular midbrain red nuclei which decussate and descend the posterolateral spinal cord with terminations onto interneurons or directly onto upper limb anterior horn cells; the reticulo-, tecto- and vestibulospinal 'ventromedial' tracts which descend the anterolateral spinal cord and synapse onto interneurons or anterior horn cells; and more diffuse pathways including serotonergic and noradrenergic neurons which are believed to modulate motor processing and autonomic function.[1,8,9]

Amyotrophic lateral sclerosis (ALS) is a neurodegenerative syndrome resulting primarily in progressive weakness and loss of movement, and encompasses a spectrum of clinical phenotypes. It is classically attributed to relentless destruction of the cranial motor neurons or anterior horn cells (often referred to as the "lower motor neurons" or "LMNs") and of the CST pyramidal cells (the "upper motor neurons" or "UMNs"), although degeneration in the other descending systems may make relevant contributions to the cumulative burden of patients' symptoms. '**ALS**' was a term first used by Jean-Martin Charcot in 1874 to denote the most common disease pattern of simultaneous UMN and LMN system involvement[10] and is often used synonymously with 'Motor Neuron Disease' (MND). MND technically envelops a broader range of diagnostic entities of which ALS is the most common but includes UMN-dominant (primary lateral sclerosis) and LMN-dominant (progressive muscular atrophy) subtypes. However, in light of electrophysiological, neuroimaging and pathological data they are increasingly considered faces of the same prism, albeit that they may confer different prognoses. With recognition that extra-motor features, particularly frontal dysexecutive, memory and language cognitive impairment,[11,12] may accompany or even precede symptomatic motor involvement, it has become clear that ALS is a multisystem disorder with the susceptibility possibly even intrinsically hard-wired into the wider motor-associated networks.[13] Up to

15% of patients with ALS actually fulfil diagnostic criteria for frontotemporal lobar dementia (FTLD) [11,12,14] and the most common neuropathological hallmark of ALS (ubiquitinated TDP-43 intracellular inclusion bodies) is also found within a subset of patients with FTLD (so-called FTLD-TDP).[15] ALS is thus tricky to stratify simplistically with its pathology, clinical features and underlying causes all lying on a continuum.

1.2 Epidemiology and Genetics of ALS

ALS has a uniform incidence of 2 per 100,000 and a prevalence of roughly three times that, since the average survival from symptom onset is approximately three years.[16,17] There is an overall male to female gender ratio of 3:2 with average age of onset within the 6th or 7th decade.[16] **'Familial ALS'** (fALS) accounts for between 5-10% of cases for which a range of monogenic causes are already identified, including Chromosome 9 open reading frame 72 (C9orf72) in 40%, Superoxide Dismutase 1 (SOD1) in 20%, Fused in Sarcoma (FUS) in 4% and Trans active response DNA binding protein (TARDBP) in 3%.

'Sporadic ALS' (sALS), arising in the absence of an identifiable family history, is believed to account for the remaining 90-95% of cases although **there are no reliably distinguishing characteristics between fALS and sALS on clinical grounds**.[18] Moreover, the boundary between these classifications is becoming increasingly blurred as greater insight is achieved into the extensive cellular processes implicated in disease pathogenesis with which relevance to certain fALS genes is increasingly recognised. It may well be that a threshold of risk in any individual is exceeded by a combination of their own unique genetic susceptibilities and cumulative environmental interactions.[19] Accordingly, genome wide association studies and exome sequencing have suggested that there may be a much larger number of low penetrance genetic variants associated

with the development of ALS,[20] and first degree relatives of patients with sALS have also been found to be at slightly increased risk of developing the disease.[21] Patients with 'sALS' are occasionally found to harbour gene mutations known to cause fALS and, furthermore, so-called pleiotropic genes (such as C9orf72) may intriguingly manifest with either frontotemporal dementia or ALS.[22-27]

1.3 Clinical Presentation and Phenotypic Heterogeneity of ALS

ALS usually presents with progressive painless paralysis in one body region with propagation to adjacent body regions often, but not universally, in a contiguous manner.[18,28,29] Around two thirds of patients have classical 'limb onset' disease with symptoms arising insidiously in an arm or leg,[18,30] whereas difficulty with craniobulbar motor function, such as swallowing, mastication and speech, can be the initial feature in approximately 25-30% and is more commonly associated with the 'pseudobulbar affect' and a faster rate of progression.[14,18,30] Primary neuromuscular respiratory failure is the initial manifestation in only a small minority of patients.[31] By the time the patient presents to medical services the symptoms may have already propagated beyond the site of onset, but compensatory terminal sprouting of surviving LMN axons in the face of a significant loss of anterior horn cells can temporarily sustain function.[18,32-34] The rate of progression is broadly linear on an individual basis but varies considerably between patients - more rapid progression to a second or third body region is indicative of poorer survival.[35]

1.3.1 LMN and UMN Predominant Forms along the 'ALS Spectrum'

Phenotypic subdivision on clinical grounds illustrates just how heterogeneous the 'Motor Neuron Diseases' can be but, paradoxically, may be offering clues as to disparate disease mechanisms. Predominance of proximal weakness and LMN features in the arms or distal weakness and LMN features in the legs for at least 1 year from disease onset is known as the 'flail arm' or 'flail leg' variant, respectively.[18,30] Subtle UMN signs may still be demonstrated in these patients although if they remain absent for between 12-18 months[36,37] (and a diagnosis of ALS remains only 'suspected') bulbar, respiratory or ambulatory function appear to remain intact for longer.[36,37] Flail variants also have demonstrate a longer delay to second region involvement and associate with longer median survival compared to limb- or bulbar-onset ALS.[30]

Similarly, primary muscular atrophy (PMA) represents a purely LMN-restricted disease for at least 4 years,[38] given that upwards of 20% LMN-only cases may go on to develop UMN signs within 2 years of diagnosis and be reclassified as ALS with LMN-onset.[39] Survival rates for PMA and ALS overlap,[30] but there has been data to suggest that patients skewed towards 'PMA' do survive longer irrespective of whether the disease subsequently transformed into ALS.[39] **Intriguingly, in both flail variants[30] and up to 50% patients deemed to have PMA clinically,[39,40] there is neurophysiological, neuroimaging and/or pathological data which confirms the presence of subclinical UMN involvement within the CSTs.**

Conversely, patients in whom UMN features are the sole clinical manifestation for at least 4 years can be diagnosed with primary lateral sclerosis (PLS).[41] Symptom onset is usually in the legs with a spastic paraparesis although upper limb or bulbar onset forms are also encountered.[18] Progression is much slower and function better-preserved

compared to classic ALS, with an 'UMN-predominant ALS' phenotype lying nebulously in between.[41] As time passes PLS may be reclassified as ALS following emergent evidence of LMN involvement, much like for PMA and the emergence of UMN signs. **Nevertheless, neuropathological studies suggest that even the LMNs of 'PLS' patients contain the typical ubiquitinated inclusion bodies (IBs) seen in ALS, despite relatively good preservation of the LMN population as a whole.[42]** Moreover, a similar degree of mainly executive cognitive impairment (see below) can be found in both PLS and ALS, confirming clinical overlap in features outside the motor systems.[43]

It is, therefore, postulated that PLS and PMA are entities at polar ends of the ALS clinicopathological spectrum[26,38,39] which invite further exploration of their important prognostic differences with objective investigative tools to better inform treatment for patients.

1.3.2 Extramotor and cognitive involvement in ALS

In line with neuropathological findings (discussed below), clinical involvement of systems outside of the primary motor tracts is seen in ALS.[28,34,38] Autonomic, extrapyramidal, cerebellar, sensory and cognitive disturbances are recognised, but their presence might reasonably encourage a wider differential diagnosis to be considered. The link between ALS and FTLD is now well-established with identical intracellular ubiquitinated TDP-43 IBs, shared genetics and overlapping clinical phenotypes. Somewhere between 6-15% of patients with ALS are believed to also fulfil diagnostic criteria for frank frontotemporal dementia,[11,12,14] and around 15% of patients with FTD later develop features of ALS.[18] Nevertheless up to half of incident ALS cases may demonstrate cognitive impairment consisting mainly of difficulties with frontal dysexecutive function (reasoning; working memory), verbal fluency, language (including spelling difficulties) and social cognition (theory of mind, recognition of emotions in others) function, in addition to behavioural change such as apathy or irritability.[11,12,44,45] Memory and visuospatial function tends not to be so commonly affected,[45,46] and low mood or anxiety does not appear to significantly drive differences compared to controls.[45,47] Interestingly, both age and site of onset appear to be unrelated to the presence of frank FTLD, although a subgroup with executive dysfunction perhaps tend to be older and experience a more rapid deterioration on the revised ALS Functional Rating Scale (ALSFRS-R) of multi-domain functional impairment[11] and reduced time to survival, although the precise reasons for this are unclear.[48] Indeed, the level of both cognitive and behavioural deficits is worse where motor impairments affect more body regions, as characterised by the King's Staging system.[45] In order to maximise the sensitivity of the range of cognitive and behavioural change in patients with ALS and account for the limitations of physical disability which may skew performance on other assessments,[47] a separate assessment for ALS has been validated. The Edinburgh Cognitive and Behavioural ALS Screen (ECAS)

incorporates patient and caregiver responses to ascertain aptitude within each cognitive domain and identify alterations in behaviour pertinent to everyday interactions,[46] with several versions available for repeated assessment to negate the effects of learning.[49] This is also becoming a very useful tool for use in clinical trials.

Key Statement Box 1

ALS presents with a heterogeneous spectrum of motor and extra-motor (particularly cognitive and behavioural) phenotypes, variable patterns and rates of disease progression between individuals and multiple underlying genetic or, as yet, unidentified ('sporadic') causes.

1.4 Diagnosis and Management of ALS

There is currently no confirmatory test for ALS in life, thus the condition remains a clinical diagnosis with ancillary investigations (if possible and appropriate) assisting the exclusion of potential mimics such as compressive myelopathy, inflammatory motor neuropathies or central neuroinflammatory disease.[50] MR imaging (MRI) of the brain and cervical cord, neurophysiological studies (electromyography and nerve conduction) and blood tests (for muscle cell enzymes) are most commonly undertaken. Diagnostic certainty is often stratified according to the El-Escorial consensus criteria which were initially purposed to regulate research definitions of disease.[38] These criteria subdivide the body into four regions: bulbar, cervical, thoracic and lumbar. A 'definite' ALS diagnosis requires the bulbar plus two spinal areas, or all three spinal areas, to each demonstrate both UMN and LMN signs on neurological examination. It is acknowledged that, depending on the timing of the assessment, even the revised criteria of Awaji-Shima published in 2008 and inclusive of neurophysiological parameters[51] may still relegate a patient to only a 'possible' diagnosis of ALS despite much higher clinical certainty by the treating physician.[38] Furthermore, less typical presentations within the ALS sphere, including those in which the signs are skewed towards either UMN or LMN involvement, challenge the practicality of the criteria as a basis for discussion with patients particularly at the early stages of an evolving presentation. **Ultimately, better diagnostic markers specific for ALS are required.**

Nevertheless, the diagnosis of ALS is devastating news and information on sources of support offered through clinical and charitable services (such as the MND Association) should be made available. The National Institute for Care and Clinical Excellence (NICE) has recently updated its guideline regarding access to and provision of services for patients with ALS, and encompasses the need for holistic assessment of physical and

psychological needs to maintain independence and quality of life.[52] Central to this is that patients with capacity are fully informed and involved in decisions regarding their ongoing requirements and that their wishes for end-of-life care and a desired ceiling of intervention are discussed as early as possible. In particular, attention to bulbar and respiratory function and consideration of timely instigation of non-invasive ventilation (NIV) or insertion of a gastrostomy feeding tube is needed as these measures can improve survival, but may not be appropriate or desired in certain circumstances.

1.4.1 Riluzole and other pharmacotherapy

Riluzole, a drug believed to inhibit glutamatergic signaling, block sodium channels and possibly modulate other intracellular processes,[53] was shown over 20 years ago to prolong survival in ALS by several months but without a significant effect on functional status.[54,55] Its exact mechanisms of action in the disease remain undefined although Riluzole may additionally interact with inclusion bodies.[53] Unless contraindicated, it is standard practice to offer this drug to all patients diagnosed with MND at a dose of 50mg twice daily, although side effects of deranged liver enzymes or worsening weakness may limit use in a proportion of cases. A second drug called Edaravone, a free radical scavenger, recently achieved FDA approval in the United States after a modest-sized trial demonstrated a slowed rate of progression over 6 months.[56] However, as only a subset of patients meeting specific clinical criteria were shown to benefit, and survival data not presented, the European Network for the Cure of ALS (ENCALS) issued a statement that more evidence is needed to justify the rigorous treatment protocol and cost of the drug.[57] Multiple trials of other promising therapies are underway but many others have previously failed to show effect despite encouraging pre-clinical data.[58] **More objective ways to measure (changes in) disease activity in patients are desperately required to accelerate the development of new and effective treatment.**

1.5 Clinical Measures and Objective Disease Biomarkers

Clinical measures remain the most widely used tools to gauge disease severity and provide some indication of the (anticipated) rate of progression or prognosis.[59]. These include functional scales such as the revised ALS Functional Rating Scale (ALSFRS-R; 12 domains scored out of 5, with 48/48 indicative of best function), the Edinburgh Cognitive and Behavioural ALS Screen (ECAS), neurophysiological data and the degree of abnormality denoted by physical examination such as with individual Medical Research Council (MRC) motor scores, the UMN Score, sniff nasal inspiratory pressure and full vital capacity, although each has its own limitations due to technical challenges, rater-dependence or poor sensitivity to change in disease activity.[26] **Changes in functional measures and overall survival also comprise the cornerstone for outcome monitoring in clinical trials in ALS given that there have been no validated and objective quantitative biological markers (so-called "biomarkers") which have a high enough sensitivity and specificity to hold diagnostic, prognostic, therapeutic-predictive or therapeutic-responsive capability**.[26,60] Given the clinical heterogeneity within ALS and infrequency of the condition, this has necessitated larger group sizes and follow-up times to demonstrate significant disease-modifying effects of an experimental intervention.

Objective biomarkers which can not only reflect disease activity and its change with treatment but also, ideally, provide greater insight into the underlying mechanisms of disease, are highly coveted. Several candidates are under investigation, including **quantitative neuroimaging modalities** (discussed in 1.8), neurophysiology and also a wide range of **CSF and/or blood fluid constituents**,[26] to include immune system markers, neurofilament proteins, and a raft of other cell signaling molecules such as neurotrophins.

Key Statement Box 2

There are currently no validated and objective quantitative biomarkers with enough sensitivity and specificity for ALS diagnosis, prognosis, or response to potential disease-modifying therapies although several candidates are under investigation, including measures in blood, cerebrospinal fluid, neurophysiology and quantitative neuroimaging.

1.6. How, where and why does ALS arise?

The central question is whether the UMNs and LMNs are independently or simultaneously affected by the same disease processes, or whether there is causal directionality, in essence a domino effect, with either cell dysfunction originating at the cortical level and 'transmitted' to the anterior horn cells or beginning in the motor units and spreading backwards.[61] Why, where and how a groups of cells first becomes affected is slightly different to asking how the disease spreads between cells, and different again from the stages of cell destruction, but fundamentally tricky to disentangle. Axons often project enormous distances relative to their cell bodies and degeneration may be begin at locations remote to the original insult.

In accordance with the wide-ranging upstream effects suggested by the known genetic influences in ALS, accumulation of dysfunction on the cellular level is believed to arise through interference of a number of organelle functions and intrinsic regulatory pathways including: defective axonal microtubule transport systems; mitochondrial dysfunction; production of free radicals with oxidative stress; excitotoxicity with dysregulated calcium homeostasis; aberrant RNA processing; toxic effects of intracellular inclusion bodies; and neuroinflammation.[18,24,62-64] Nevertheless, the precise mechanisms by which certain neuronal populations succumb to the disease and how they degenerate *in vivo* are unclear. Hypotheses regarding these mechanisms, however, continue to be informed by indirect evidence from animal models of fALS in addition to human neuropathological tissue analyses, neurophysiological measures and investigative neuroimaging. As the same suppositions are used to interpret *how* new exploratory biomarkers might become 'abnormal' in the first place and *why* they may have altered over time (or after intervention) *in vivo*, it is essential to review and critically appraise the data from these resources if improved treatment strategies and outcomes for patients with ALS are to be achieved.

1.6.1 What can neuropathology reveal about mechanisms of degeneration in ALS?

Virtually all understanding about the patterns of degeneration in patients with ALS derives from post-mortem studies. The clear disadvantage is that each histopathological 'snap-shot' generally captures only the most advanced stage of the disease in any individual and cannot be used to *prove* mechanisms or dynamics of disease origin and spread. Moreover, the patients included in most historical neuropathological studies have been those with "classical" ALS (motor) phenotypes thus with poor representation of cases with cognitive impairment or frank ALS dementia.

Pyramidal tracts and anterior horns. Macroscopically the brain and spinal cord often appear normal,[65,66] although the pre-central gyri[65] and medullary pyramids[67] occasionally display a visible loss of volume. On the other hand, the anterior roots reliably appear grey and atrophied, with their target muscles pale and fibrotic.[65,67] Microscopic analyses similarly confirm that loss of anterior horn LMNs is essentially evident in all cases, albeit patchily, whereas loss of cortical pyramidal cell bodies or degeneration of the CSTs can be much less conspicuous,[65,67-69] or sometimes absent.[68] Even in cases where the CSTs show little discernible neuropathological involvement, loss of the giant cells of Betz is consistently observed in the motor cortices,[14,67,68] which may just be dependent on the histological staining method used.[70] The morphology of those Betz cells remaining has been described as abnormally shrunken[71,72] or swollen[73,74] with dendritic stumping, fewer primary branches and their somata encased by astrocytes, believed to reflect asynchronous stages of cell death.[73] Other studies employing three-dimensional stereological techniques to quantify total number[75] and morphology[76] of neocortical motor neuron cell bodies have, conversely, failed to demonstrate any significant difference from control subjects, although the Betz cells were not specifically examined. Smaller-sized

pyramidal motor neurons do succumb to the disease process in the majority of patients and their loss can be detected within both pre- and post-central cortical areas.[14,67,68,73,74,77,78] Indeed, degenerating fibres are not restricted to the precentral gyrus but are found projecting into, or from, the postcentral gyrus and more anterior aspects of the frontal lobe which may partly reflect the broad cortical origins of the CST.[70,77]

Degeneration within the CSTs themselves is suggested by loss of myelin and reduced numbers of axons across a range of diameters often more markedly in the distal compared to proximal tract,[65,68,70,77,79] although comparisons between levels has proved inconsistent.[68] Myelin sheaths can actually appear relatively preserved in motor subcortical areas[65] with tract degeneration in the brain most noticeable more caudally within the posterior aspect of the posterior limb of the internal capsule,[68] which forms a common conduit for several descending motor pathways including the CSTs, cortico-rubro-spinal, and cortico-reticulo-spinal connections[80,81] These findings could, therefore, support a loss of distal CST axon segments before proximal portions.

A range of LMN sizes throughout the anterior quadrants of the ventral horn exhibit reduced numbers and density,[33,71,82] although their loss can be either diffuse or patchy, with islands of normal-appearing cell bodies seen at the same spinal level and an unclear relationship to clinical motor scores.[33,67] Brainstem motor nuclei are similarly depleted, particularly those serving facial and swallowing musculature.[67] Morphology of surviving anterior horn cells is similar to that described in Betz cells whereby the somata can appear shrunken[68,82] and their dendritic arborisations cropped,[83-85] with a few undergoing neuronophagia.[68] Proximal axon swellings, or ‘spheroids’, are seen sometimes in relation

to an otherwise healthy-looking cell body, and are believed to represent axostasis secondary to dysfunction in axonal transport.[65,69,86]

Other motor and non-motor pathways. Data relating specifically to degeneration within other descending motor pathways in ALS is sparse, although myelin pallor within the anterolateral white matter of the spinal cord was reported in over 50% of the historical cases analysed by Brownell and colleagues,[68] which may implicate involvement of the rubrospinal tracts, as does the presence of IBs in at least the parvocellular component of the red nucleus.[87] Systems typically left clinically intact in ALS, such as those controlling sphincter function and extraocular movements, do still demonstrate pathological involvement through either inclusion bodies or frank cell loss in Onuf's nucleus and the brainstem extraocular motor nuclei, respectively.[88,89] Damage to sensory and cerebellar pathways is also seen as evidenced by loss of neurons within Clarke's column (the multilevel nucleus for the dorsal spinocerebellar tract)[33,65] and myelin pallor within the spinocerebellar tracts themselves[90] and the dorsal columns[65,67,68] despite the apparent paucity of symptoms. Interestingly, patients with ALS who have been maintained beyond their natural life expectancy on artificial respiratory support for years demonstrate extensive myelin pallor, neuronal cells loss and cortical gliosis but, despite a complete loss of Betz cells, rostral portions of the CST within the internal capsules and medullary pyramids may still show preservation of myelinated fibres.[91] Proximal portions of some pyramidal neurons may, therefore, endure long epochs during which their distal axons may have degenerated. Inevitably this prompts questions regarding how cells degenerate and what determines the gradient of vulnerability, but also raises hope for potentially restorative therapies.

Non-neuronal involvement. Indeed, ALS is not just a disease of neurons. Non-neuronal cells are involved pathologically and may play important role in propagating or even limiting the spread of disease. Astrocytic gliosis is seen within the ventral horns[82] and around terminal aspects of the CST,[92] the grey-white transition zones between lateral, medial and dorsal funiculi of the spinal cord[79,93] and the brainstem motor nuclei,[67,68] in addition to the superficial and deeper layers of cortical tissue.[71,79,94,95] **Increased numbers of microglia are also similarly seen within the precentral cortex, subcortical white matter, lateral funiculus and anterior horn along with a predominance of $CD8^+$ T-cells and far smaller numbers of $CD4^+$ T-cells[93,94,96] which, as shall be discussed, are believed to play a fundamental role in disease pathogenesis through influencing astrocytic and microglial behaviour.**[95] Moreover, oligodendrocytes[94] in addition to astroglia and microglia[93] show activation by complement which reinforces the non-cell autonomous nature of the disease pathogenesis and influence from immune processes in ALS.

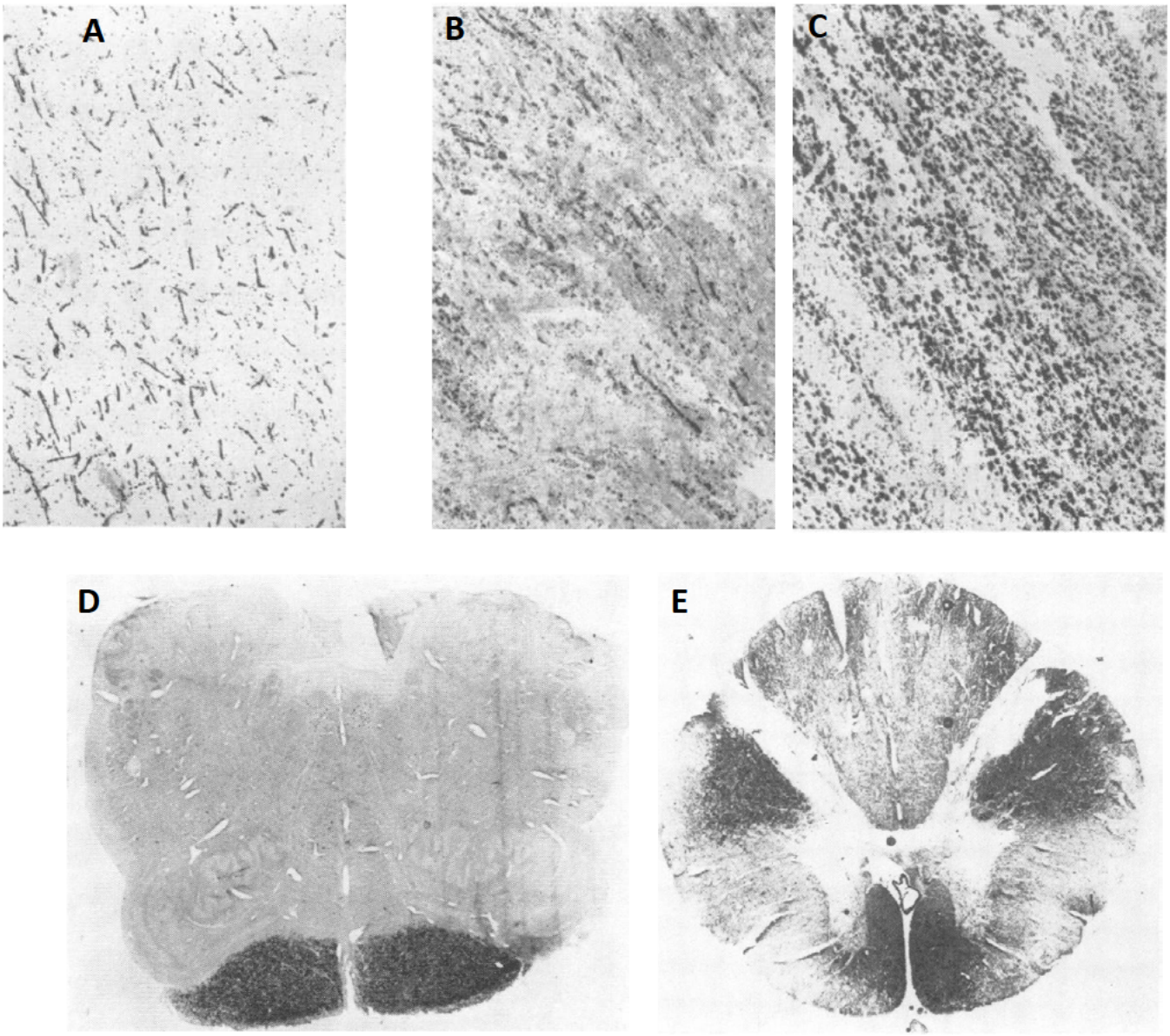

***Figure 1.6.1*. Pyramidal tract degeneration in ALS** shown using the Marchi staining method for degenerating myelin (denoted by black areas) within the corona radiata and internal capsule (A-C; increasing in a rostrocaudal direction), anterior medullary pyramids in the brainstem (D), and both lateral and anterior branches of the corticospinal tract within the thoracic spinal cord (E). *A to C reproduced from Smith et al. 1960;[70] D and E reproduced from Brownell et al. 1970.[68]*

1.6.2 How do inclusion bodies (IBs) relate to degeneration in ALS?

The vast majority of patients with ALS (aside from fALS underpinned by mutations in SOD1 or FUS)[25] and FTLD-TDP dementia harbour abnormal intracellular inclusion bodies (IBs) consisting of ubiquitinated[97] and hyper-phosphorylated C-terminal fragments of the RNA-binding protein TDP-43.[15] TDP-43 is a universally-expressed protein encoded by the Trans active response DNA binding protein (TARDBP) gene, involved in RNA processing and sequesters non-essential RNA molecules in times of cellular stress. Mutations in the TARDBP gene have been shown to increase the propensity of TDP-43 to aggregate,[98] with subsequent neurodegeneration felt to be dependent on its preserved ability to bind and sequester mRNA.[99]

In ALS, IBs are not exclusive to the primary motor pathways but seen additionally within the basal ganglia, nigrostriatal pathways, cerebellum, frontotemporal cortex, amygdala and medulla,[15,100] along with astro- and oligodendroglia.[87,100] It is not clear whether these proteinaceous aggregates are a cause or consequence of the disease process and their quantitative burden cannot distinguish motor neuron disease phenotypes,[14] but they *may* provide clues as to the spread of the disease. It is suggested that IBs propagate between cells by means of axonal and transynaptic transmission, including between glia, in a prion-like fashion and are themselves pathogenic,[3,32,87,101] perhaps accounting for the predominantly contiguous spreading pattern of patients' clinical symptoms.[18,26,29,32] Alternatively, IBs deposition may only serve as an indication that cellular processes are under strain and be independent of symptoms and/or spread. Moreover, the relationship may not be linear anyway owing to compensatory mechanisms of peripheral axon sprouting in the neuromuscular compartment.[33,132]

Analysis of the regional distribution of IBs in selected brain areas of patients with motor-onset ALS has suggested that patients can be grouped into pathological 'Stages': with 'Stage' I representing IBs confined to the corticomotoneurons and anterior horn cells; Stage II accumulation within the reticular formation and precerebelallr nuclei (such as the inferior olive); Stage III accumulation within prefrontal neocortical structures and basal ganglia; and 'Stage' IV involvement of the anteromedial temporal lobe and hippocampus.[3,87] Given that the neurons common to all 'Stages' appear to be the corticomotorneurons or the targets of their projections, it is proposed that these data support the theory of forward disease spread. The IBs generally display a more patchy deposition within the cortical Cells of Betz than within α-motoneurons, although there is some evidence to suggest that abnormal soluble TDP-43 may predominate over insoluble IB aggregates in Betz cells.[102] Nevertheless, both UMN and LMN populations contain IBs simultaneously in all patients rendering it impossible to prove directionality of initial spread using TDP-43 inclusions alone. Indeed, the total quantity of IBs and each pathological stage has not readily shown a relationship to clinical severity or phenotype, disease duration or age at onset.[44,103] MMSE scores were generally lower in 'Stage' IV patients and all demented subjects were classed as 'Stage' III or IV, but cognitive-onset ALS patients were not specifically included.[87]

Clinical manifestations may instead relate to dissemination of IBs throughout the spinal cord rather than the brain. A subsequent study confirmed the most marked burden of pTDP-43 IBs and loss of neurons to be in lamina IX of the anterior horn, whereby upper or lower limb onset disease correlated with involvement of the respective rostral or caudal cord α-motoneuron nuclear columns (as classified by Routal and Pal[104]). However, only several columns bore any relationship to the brain 'Stages' I-IV in the same patients and none with function on the ALS Functional Rating Scale (ALSFRS).[105] IBs were seen

within Onuf's nucleus in nearly a fifth of patients, in addition to involvement of Clarke's column in 'Stages' III and IV, and the oculomotor nucleus in patients already designated as 'Stage' IV in line with neuropathological findings mentioned above.[88,89,105] Interestingly, oligodendrocytes within the anterior horns and CST white matter routinely contained IBs, usually alongside the neuronal cells but sometimes in the absence of obvious neuronal involvement, raising more uncertainty regarding a straightforward "dying forward" neuron-to-neuron theory of disease spread.

Furthermore, although IBs in patients with FTLD-TDP appear also to deposit in a cumulative pattern with prefrontal cortex and amygdala involvement in 'Stage' I through to occipital cortex in 'Stage' IV, the motor cortices and α-motoneurons in the brainstem and cervical cord appear within 'Stage' III where a greater degree of IBs associates accordingly with clinical signs consistent with ALS.[106] IBs within the medulla, midbrain and cervical cord were negatively correlated with duration of disease but did not relate to pathological 'Stage'. **Therefore, despite the shared pathological hallmark and overlapping clinical features between ALS and FTLD-TDP, the apparent 'directionality' implied from an end-stage snap-shot of IB deposition is not clearly associated with retrospective clinical progression or severity, and different deposition patterns logically suggest that factors other than the presence of IBs determine the spectrum of clinical deficits each patient manifests.**

1.6.3 What does neurophysiology suggest about mechanisms of disease in ALS?

Neurophysiological analyses in patients with both fALS[107] and sALS[108] *in vivo*, including measures of cortical and corticospinal tract function with transcranial magnetic stimulation (TMS), including motor threshold, the cortical silent period, intracortical inhibition or facilitation, MEP amplitudes and central motor conduction times (reviewed by Vucic and colleagues[61]), have shown that reduced short-interval intracortical inhibition (SICI) is an early feature within the motor cortex of both limb- and bulbar-onset sALS patients although at a stage when corresponding LMNs were also demonstrably abnormal.[109] Subsequent studies in presymptomatic fALS cases harbouring SOD1 gene mutations revealed that a reduction of SICI is a seen prior to the onset of symptoms or neurophysiological abnormalities in the corresponding contralateral upper limb.[107] Similar findings were recorded in patients with sALS whose corresponding motor units to abductor pollicis brevis muscles were otherwise neurophysiologically normal at the time of recording.[108] Thus hyperexcitability of the motor cortex as an early phenomenon in sALS and fALS, and which may precede the dysfunction of anatomically-linked LMNs, has supported theories that cellular dysfunction in ALS spreads forwards via the corticomotorneuronal system.[61,107-110] The hyperexcitablity is also believed to provide strong evidence for excitotoxicity being fundamental to ALS pathogenesis broadly from either increased glutamatergic excitatory input and aberrant astrocyte neurotransmitter regulatory function,[111,112] and perhaps a target for Riluzole therapy. Conversely, reduced SICI may arise due to deficient cortical inhibitory GABAergic circuitry[110] which is supported by both neuroimaging[113,114] and neuropathological[71,74] data and leads to the alternative hypothesis that ALS disease processes could originate in higher orders of the motor network than within pyramidal or spinal motor cells.

However, LMN electrophysiological normality does not necessarily imply that the cell is unaffected and so, without being able to simultaneously study the anterior horn or pyramidal cells for pathological abnormalities such as aggregates of TDP-43 inclusion bodies, it is still not possible to be truly certain about the order of disease spread. Moreover, if one were to assume that pyramidal corticomotorneurons are affected before LMNs (and thus 'transmit' their disease to lower and adjacent levels of the motor system) the neuropathological evidence suggests they are, conversely, some of the last cells to die and that glial cell involvement in the spinal cord may even precede that of the neurons.

1.6.4 Do animal models enlighten mechanisms of disease in ALS?

Transgenic rodent models of mutant human SOD1 (mSOD1) ALS have enabled potential mechanistic insights into disease pathogenesis, with the caveat that SOD1 mutations account for only 1-2% of human ALS and the experimental mammalian hosts possess far less evolved motor systems. Despite a clear predilection for the LMNs, the UMN compartment is involved with early cortical hyperexcitability[115,116] and even cortical degeneration demonstrable from around postnatal day (P)30.[117] Alterations in layer V pyramidal cell dendritic tree structure from basal expansion[115] to apical regression,[116] with cell shrinkage[117,118] and programmed cell death[117] of corticomotorneuron and other subcerebral projection neuron somata is also evident, and mirrors changes seen in pyramidal and spinal motor neurons in human neuropathology. Degeneration of the corticospinal tract itself is detectable from P60,[117] but suppression of mSOD1 activity in the cortex can delay disease onset and even promote integrity of the LMNs and neuromuscular junctions,[119] suggesting that an upstream deleterious component may be important.

Nevertheless, cellular processes within spinal motor neurons appear to be affected in the first few weeks after birth with cytoplasmic vacuolation, mitochondrial swelling[120] and changes in neuromuscular junction and axon microstructure soon afterwards. Deficiency and dysfunction of neurotransmitter vesicles is reported from P35 followed by deficits in both anterograde and retrograde axonal transport.[82,101] Synaptic breakdown is in progress by P48 prior to an essentially synchronous 'pruning' of peripheral axons proximal to the origin of terminal motor unit branches from P50.[121-123] The LMNs which appear most susceptible are the large diameter, fast fatigable cells followed by the fast fatigue-resistant population, whereas the slow-contracting fibres appear to be extremely resistant.[121] Importantly, this all appears to occur prior to the average onset of clinical

signs of disease around P80, when a critical percentage of axons has been lost, and well before demonstrable loss of cell bodies in the anterior horn around P100.[124] The evidence is, therefore, supportive of a dying back axonopathy with the proximal neuron segment able to endure the longest.

Whether this distal axonopathy arises due to proximal cell body stress and undernourishment of the remote axon terminal or secondary to a direct assault on the peripheral axon itself is not known,[123,125] although the evidence that it takes place in the context of compromised somatic function is difficult to overlook. The cellular pathways which coordinate the initiation and extent of axon pruning in ALS are hypothesised to be similar to, but distinct from, those which execute Wallerian degeneration after axon transection and neuronal pruning throughout normal development, the latter of which is also determined by target synaptic function and neurotrophin signalling.[122] Rather than being protracted, all appear to unfold rapidly over a matter of hours and depend on the ubiquitin-proteasome system, sharing the ultimate sequence of microtubule disassembly, multifocal axonal blebbing (which are distinct from axonal spheroids), fragmentation and phagocyte-mediated clearance irrespective of the different upstream triggers.[122] One might then postulate that the relentless cellular dysfunction and rounds of axon die back continue until the cell body finally succumbs, which is supported by neuropathological evidence revealing preservation of proximal neuron segments long after motor function was lost in life.

Key Statement Box 3

Dynamics and mechanisms of cell death during the course of the human disease remains incomplete, and is inferred from end-stage neuropathology and changes within indirect animal models of the disease. Objective and informative biomarkers of disease activity in patients with ALS *in vivo* are needed.

1.6.5 A role for the immune system in ALS

A role for the immune system in ALS pathogenesis is considered highly likely, more as a determinant of disease propagation rather than the initial trigger.[126,127] Pathological findings and neuroimaging (particularly PET) indicate that activated microglia[94,128-130] and lymphocytes[96,131,132] are present in cortical and subcortical areas in patients with ALS, which influence the rate of disease progression.[130] Depletion of lymphocytes in the mutant SOD1 mouse model, precipitates a pro-inflammatory state and worsened disease outcomes whereas reconstitution, particularly with $CD4^+$ T cells, recovers the clinical progression.[133] Indeed, $CD4^+$ T cells predominate within the rodent CNS throughout earlier stages of disease, until about P120, and then are increasingly surpassed by $CD8^+$ T cell numbers in association with an accelerating burden of symptoms.[134] Specifically, it is the $CD4^+$ T cells positive also for CD25 and high expression of FOXP3, a master transcriptional control gene,[135,136] which appear to mediate this early neuroprotective effect.[126,133,134] $CD4^+$ $CD25^+$ $FoxP3^+$ cells are a subpopulation of 'regulatory' T cells (**Tregs**) which are believed to temper inflammatory responses and maintain immune tolerance.[137,138] Tregs, with the assistance of Th_2 T helper cells, promote a more neuroprotective 'M2' state of CNS microglia,[139] suppress pro-inflammatory T 'effector' cells (**Teffs**) and probably influence the function of other glia such as astrocytes and oligodendrocytes.[140] On the other hand, $CD8^+$ effector cells, alongside Th_1 T helper cells, promote a pro-inflammatory 'M1' microglial phenotype.[141] Accordingly, a rise in pro-inflammatory cytokines is detected alongside the switch to a $CD8^+$ T cell predominance in the latter stages of disease[134] thereby lending support to this microglial transition.[126]

In patients with ALS, lower absolute numbers of blood borne $CD4^+$ $CD25^+$ Tregs and levels of FoxP3 protein in spinal cord tissue are found in those categorized as rapid progressors compared to slow progressors or healthy controls,[142] in addition

to reduced expression of M2 state cytokines within the spinal cord.[134,143] Therefore, significant cross-talk between peripheral circulating Tregs and the CNS compartment is strongly inferred. However, it is not clear whether these cells are specifically trafficked across the blood-brain or CSF-brain barriers, or gain access secondarily as a result of increased permeability of these structures.[127,138] **Nevertheless, manipulation of peripheral Treg number and/or function may be a therapeutic target in ALS.** Successful amelioration of other autoimmune or alloimmune diseases such as Hepatitis C virus-induced cryoglobulinaemic vasculitis,[144] graft versus host disease,[145] systemic lupus erythematosus,[146] corneal transplant survival[147] and alopecia areata[148] has been reported in patients following augmentation of Treg numbers using subcutaneous injections of low dose Interleukin-2 (IL-2) in small open-label studies.[137] Tregs express elevated levels of the cell surface receptor for IL-2, which is produced predominantly by activated $CD4^+$ cells and probably antigen-presenting cells.[149] Higher levels of IL-2 encourage expansion of Teffs in preference to Tregs, and has been historically utilised for treatment of malignancies such as melanoma and renal cell carcinoma with modest success rates yet significant side effect profiles including malaise, flu-like symptoms and vascular leak with third space volume depletion.[137] Conversely, the activation threshold for Tregs is up to 20 times lower meaning that low dose IL-2 supports Treg differentiation and FOXP3 expression, without expanding the pool of Teffs.[137] Deficiency of IL-2 or of its receptor leads to an absence of $CD4^+$ $CD25^+$ $FoxP3^+$ cells and systemic autoimmunity.[149]

Ex vivo expansion of Tregs from ALS patients has indicated that total number and functional state restored to normal,[150] although clinical effects upon re-implantation are uncertain. Various regimes have been used to supplement exogenous low dose IL-2 (ld-IL-2) and sustain an elevated population of Tregs *in vivo* without increasing the risk of

severe infections or inducing significant side-effects previously associated with high dose IL-2. A pulsed administration every few weeks with each dose consisting of between 1-3 million international units per day has been able to selectively maintain Treg levels up to 60% higher than baseline.[137] A phase I trial using ld-IL-2 in ALS (IMODALS) is complete and the ongoing double-blind, randomized-controlled phase II trial (**MIROCALS**) for clinical efficacy is intimately linked to neuroimaging undertaken for this Doctoral Thesis (see Chapter 2).

Key Statement Box 4

The immune system plays a key role in determining the CNS milieu in ALS. Higher levels of blood T regulatory cells (Tregs) are known to associate with a slower rate of progression and is the basis of a new randomised clinical trial (MIROCALS) using low dose Interleukin-2 to augment Treg levels in patients.

1.7 Can *in vivo* neuroimaging in patients with ALS aid understanding of the mechanisms of disease?

1.7.1 Limitations of conventional clinical neuroimaging

Neuroimaging currently available in the clinical environment, including "conventional" MRI sequences T1-, T2-weighted and FLAIR (fluid-attenuated inversion recovery), is used mainly to rule out potential disease mimics, such as cervical myelopathy, rather than to confirm a diagnosis of ALS.[4,26,50,151,152] Hyperintensity of the CST[153-155] or hypointensity of the precentral gyrus grey matter[155,156] on T2 or FLAIR sequences has been reported in patients with ALS. However, this has proven inconsistent[157,158] with limited specificity and poor sensitivity,[158] poor correlation with clinical measures[153-155,158] and evidence that these imaging findings can be observed as part of normal aging.[159] Moreover, a limited degree of pathophysiological information can be inferred from these sequences and so preference has shifted towards more advanced neuroimaging techniques, which can provide quantitative information relating to tissue architecture, biochemical make-up and metabolic function. Although these newer modalities continue to hold an inadequate diagnostic or prognostic role for individuals at this stage (owing to variability in image acquisition/analytical methods and comparisons largely to healthy controls rather than disease mimics), it is anticipated that they may be able to illuminate the underlying mechanisms and dynamics of the degenerative process to help direct future therapeutic approaches. The leading research modalities used in ALS have included functional radionuclide imaging such as single-photon emission computed tomography (SPECT) and positron emission tomography (PET), and functional task-based and resting-state, morphometric and diffusion MRI techniques.

1.7.2 SPECT and PET

Some of the earliest neuroimaging data in patients with ALS derive from single-photon emission computed tomography (SPECT) and positron emission tomography (PET) which illustrated the involvement of both motor and extramotor areas in the disease. Widespread resting cortical hypoperfusion on SPECT has been reported in association with symptom duration[160] and ALSFRS[161] but not with distinct phenotypes. In patients with rapidly progressive frontotemporal dementia and concurrent sigs of ALS (ALS-FTD), SPECT also demonstrated cortical hypoperfusion confined to the frontotemporal regions.[162] PET studies using radiolabelled ^{18}F-fluorodeoxyglucose (FDG) and carbon dioxide ($C[^{15}O]_2$) tracers relating to metabolism and perfusion, respectively, have echoed these findings. Patients with UMN signs compared to those without showed reduced mean cortical FDG uptake greatest in the sensorimotor cortices and putamen, which was somewhat lateralised, proportional to the disease duration and corrected for the effect of atrophy.[163,164] Patients with ALS and impairment of verbal fluency, revealed resting hypoperfusion in areas of the frontal lobes, such as the dorsolateral prefrontal cortex, lateral premotor cortex, medial prefrontal and premotor cortices, whereas a comparison group of ALS patients without cognitive impairment had relatively little perfusion abnormality with respect to controls.[165] Cistaro and colleagues have accordingly reported regional hypometabolism in a group of bulbar-onset, but not limb-onset, ALS patients in the bilateral frontal, right insular, anterior cingulate, precuneus and inferior parietal cortices, with the bulbar-onset group possessing lower scores of executive cognitive function.[166] Hypometabolism in the more expected areas of the premotor cortices and left precentral gyrus was observed but did not reach statistical significance. These and other data would, therefore, imply that cognitive (and possibly substantial UMN) involvement in ALS associates more readily with appreciable differences in perfusion or metabolism of the frontal lobe and subcortical pathways particularly at rest.[167,168]

Interestingly, hypermetabolism has also been reported in areas such as the amygdala and hippocampus, the cerebellum, the midbrain and brainstem,[166-168] in addition to the cervical spinal cord,[169,170] with a possible relationship to clinical severity.[170] It is unclear whether or not these PET findings relate to increased neuronal activity. A large proportion of FDG-glucose uptake is felt to be mediated by astrocytes and other glia,[171] and so it may be that they are representative of reactive cellular processes or infiltration in line with the proposed role of neuroinflammation in disease pathogenesis.

1.7.3 PET with specific radioligands

Accordingly, ligand PET studies using [^{11}C]-PK11195[129] and [^{18}F]-DPA-714,[128] first-generation binders of the TSPO protein on activated microglia, has shown significantly increased binding in subcortical areas of the pons and thalamus as well as the motor and dorsolateral prefrontal cortex in patients with ALS, in addition to PLS.[172] PET with [^{11}C]-PBR28, which binds TSPO with superior specificity, has corroborated these findings in ALS with stable longitudinal uptake in the motor cortices correlating with disease severity in addition to reduced corticospinal tract fractional anisotropy (FA) on diffusion tensor imaging.[173] [^{11}C](L)-deprenyl a binder of monoamine oxidase–B, which primarily resides on astrocytic membranes, similarly showed greater binding in the pons and throughout the cerebral white matter compared to controls[174] supporting the known astrogliosis within brainstem motor nuclei[67,68] and subcortical white matter[71,79] observed in neuropathological studies. PET with a radiolabelled flumazenil ligand against $GABA_A$ has demonstrated significantly decreased binding in the prefrontal cortices, parietal cortices, visual association cortices and left motor and premotor cortex[175] in support of the deficient cortical inhibitory GABAergic circuitry observed neuropathologically[71,74] and a potential

mechanism for primary motor cortical hyperexcitability on neurophysiological examination.[61] Reduced binding of the ^{11}C-WAY100635 ligand to the 5HT1A receptor in frontotemporal regions, cingulate cortex and lateral precentral gyri,[176] may suggest a further mechanism for reduced inhibition of pyramidal cells. Despite the widespread cell loss throughout the cortical layers, notably the Betz cells and other layer V projection neurons, demonstrated on neuropathology[78] expanded areas of sensorimotor cortical blood flow seen with PET[177] and also with functional MRI[178-183] studies during motor task performance in ALS might otherwise indicate reduced inhibition of the remaining pyramidal cells, and/or compensatory reorganisation of remaining cortical circuitry.

Key Statement Box 5

Nuclear medicine neuroimaging has importantly demonstrated reduced cortical metabolism/perfusion, involvement of multiple neurotransmitter systems in disease and provide further evidence for altered glial function in patients with ALS. However, its use is complicated by its radiation exposure and requirement for injectable substances.

1.7.4 Task-based functional MRI (fMRI)

Functional MRI utilises the paramagnetic properties of deoxygenated blood to map a change in blood oxygen level dependent (BOLD) signal upon a task-dependent increase in oxygenated blood flow mediated by neurovascular coupling.[4,184] Although the BOLD signal timing lags behind activity by approximately 4 seconds,[184] the signal can be highly resolved to specific areas of cortical and subcortical structures.[4,185] Motor tasks such as thumb and index finger opposition,[179] button pushing,[181,183] grip strength,[180] repetitive finger movement[178] or manoeuvring a joystick[182] using the right hand have been used to demonstrate changes in cortical activity between patients with ALS and controls, although with a spectrum of results between studies perhaps as a result of differing paradigms and analyses. Overall, an increased area of activation in the contralateral primary motor cortex,[178-183] somatosensory cortex,[178-180,182] supplementary motor area[178-181,183] and parietal cortex[179,182,183] are most consistently observed in patients and controls, but usually *greater* in patients[178,180,182] and/or shifted to a more anterior location.[179] Conversely, reduced areas of activation in the contralateral primary motor, supplementary motor and right parietal cortices relative to controls has also been reported, with activation enlarged elsewhere within the contralateral putamen and (in patients with greater UMN burden) the anterior cingulate and ipsilateral caudate nucleus.[183] Several of these studies have additionally revealed bilateral cortical activation in areas including the sensorimotor, supplementary motor, premotor, and parietal cortices[140,145] with greater ipsilateral involvement in ALS patients versus controls.[178-180,182]

Furthermore, although the *area* of activation may remain large or enlarged, the amplitude of increased signal change from resting baseline in patients may be diminished in line with increasing impairment on the ALSFRS[178] or worsening MRC grade.[180] **Overall, the early expansion, or so-called "boundary shift", of activated cortical areas on task**

performance may be secondary to loss of inhibitory input and/or an effort to compensate for motor system damage using alternative existing connections, in the face of progressive cortical neuron loss which diminishes the degree of BOLD signal change over time[180] and may also underlie cortical hypometabolism often seen on PET and SPECT imaging.

1.7.5 Resting state functional MRI (rsfMRI)

It has been argued that the potential for inconsistency in task performance effort between patients with different degrees of motor impairment renders fMRI data tricky to standardise and, ultimately, interpret.[179,184,186] In recent years, interest has been growing around the spontaneous oscillations in BOLD signal which can be monitored in the brain at wakeful rest. Functionally-linked, yet anatomically disparate, brain regions found to share time-dependent signal fluctuations can be mapped reliably into distinct brain "networks" to include bilateral primary sensorimotor, executive, default mode, primary visual, extra-striate visual and insular-temporal networks, along with the left or right fronto-parietal networks. They are highly reproducible using several different analytical methods for the fMRI data, such as independent component analysis (ICA) and seed-based methods,[187-189] but their respective functions are considered to integrate during normal brain activity rather than function entirely independently of each other.[189] Although the precise origin and function of the background BOLD fluctuations remain uncertain, the majority of the resting state networks also appear to demonstrate overlap with those utilised during active task performance.[188] **Regions of the sensorimotor (SMN), default mode (DMN), left and right fronto-parietal (LFPN and RFPN, respectively) and executive (ExN) networks assessed by independent component analysis have been shown to possess altered connectivity in patients with ALS.**

The most consistent finding is that of reduced connectivity of the primary motor[190,191] or premotor[192] areas of the **SMN**, which otherwise comprises the anterior cingulate, somatosensory and auditory cortices,[187] compared to controls. A study which found no difference in connectivity in this network compared to controls did report that reduced SMN connectivity in the patients correlated with impaired motor function, albeit in regions beyond the typical boundaries of the network.[193] However, increases and decreases in the synchrony of neural activity within individual regions of the SMN relative to controls have also been reported with some of these areas correlating significantly with clinical measures.[194] Coherence within the right postcentral, precentral and superior frontal gyri positively correlated with improved ALSFRS, whereas coherence within the left postcentral gyrus was associated both with faster rate of disease progression and shorter disease duration.[194] The **DMN**, comprising medial frontal, inferior parietal, precunei and medial temporal cortices,[187] has demonstrated increased left precuneus,[195] decreased right orbitofrontal[192,195] or unchanged[190,193] connectivity compared to healthy controls. Positive correlation has been found between ALSFRS and connectivity of each precuneus, and between better frontal executive test scores and the left angular gyrus and precuneus.[195] Conversely, higher ALSFRS has been found to associate negatively with connectivity in the DMN, albeit in areas beyond the typical boundaries of this network.[193] The **LFPN** and **RFPN** have similarly shown areas of both increased[195] or decreased[190,195] connectivity, with increases in the left parietal region not only displaying some overlap with network alteration in behavioural-variant FTD patients but also correlating with improved ALSFRS scores.[195] Less commonly, connectivity of the **ExN** has been investigated in ALS with either a small patch of decreased connectivity within right middle frontal gyrus reported,[191] or no change.[195]

Furthermore, a newer 'multi-echo' acquisition for rsfMRI (ME-rsfMRI) has been proposed to enable screening out a higher percentage of non-BOLD-like signal components and other artefacts which confound the signal such as cardiorespiratory cycles and head movement. ME-rsfMRI can be used to "clean" the BOLD signal by exploiting the expected scaling of BOLD with the echo-time. ME-rsfMRI is felt to be superior to temporal filtering methods used to remove non-BOLD signal from standard single-echo rsfMRI data,[196,197] which has been the technique utilised so far in ALS. Recent findings suggest that ICA on single-echo rsfMRI repeated every 6 months for 2 years demonstrates areas of increased connectivity within the SMN and decreased connectivity within the LFPN, both over time and in relation to ALSFRS.[198] It is, therefore, possible that cross-sectional and longitudinal connectivity analyses using ME-rsfMRI acquisition may better expose the factors governing network function alterations.

Key Statement Box 6

"Single-echo" rsfMRI demonstrates altered connectivity within resting networks (such as the sensorimotor, default mode, fronto-parietal and executive), although findings are highly heterogeneous. "Multi-echo" rsfMRI acquisition may improve the consistency of connectivity differences between patients and controls.

1.7.6 MRI Morphometry

Quantitative information regarding grey and white matter morphology can be derived from high resolution T1-weighted images using automated segmentation tools such as voxel-based morphometry (VBM), providing measures of density and volume, and surface-based morphometry (SBM) which primarily yields measures of cortical thickness and topology.[199,200] Despite a wide spectrum of reported changes using VBM, a recent meta-analysis of 29 studies of non-demented patients with ALS found overall that grey matter volume was globally reduced compared to healthy controls.[201] Confirming the main finding of right precentral gyrus atrophy in an earlier meta-analysis,[202] additional regional atrophy of the left Rolandic operculum, left lenticular nucleus and right anterior cingulate gyrus were also reliably identified and survived the sensitivity analyses.[201] Similarly, SBM analysis has revealed precentral cortical thinning in patients with ALS,[203-206] maximal in either bulbar or limb regions of the motor homunculus based upon patients' respective disease onset pattern.[204,207] Areas of extramotor cortical thinning have included areas of the parietal lobe and primary sensory cortices,[203,206] insular cortex,[206] in addition to the frontal and temporal lobes,[203,205] with the latter possibly associated with a faster disease progression.[205]

Other studies have shown differences in the context of other MND phenotypes or in the presence of cognitive impairment.[74,176-178] Patients with PLS have shown significantly reduced surface area of the primary motor and association motor cortices and subcortical white matter compared to healthy controls alone[208] and patients with ALS, with the latter demonstrating a comparatively smaller, non-significant reduction of the precentral gyri.[85] On the other hand, motor and extramotor regions of cortical atrophy were revealed only in a group of ALS patients with FTD compared to patients with ALS alone, even those with predominant UMN disease.[209] The finding that extramotor frontal or temporal grey

matter can show atrophy in isolation of the primary motor cortex in patients with signs of ALS and demonstrable cognitive difficulty is further indicative of the multisystem and heterogeneous nature of the disease spectrum.[210,211]

Longitudinal studies analysing volumetric changes in ALS over intervals of 3 months to 2 years[198,206,212-214] have reported somewhat differing findings, with one study performing a trio of scans over 6 months failing to demonstrate any change in cortical or deeper grey matter structures,[212] and others detecting change within the precentral gyri,[198,213] frontotemporal cortices[214] and basal ganglia.[198,214] The degree of change in several areas has been shown to be related to reduction in ALSFRS-R[198] or disease duration,[213] although this is not guaranteed.[214] More marked thinning of the precentral cortex has been reported in patients with PLS compared to those with ALS, and yet the ALS showed the largest reduction upon repeat imaging up to two years later.[213]

Key Statement Box 7

Morphometric analyses most consistently report atrophy or reduced thickness of the primary motor cortex in ALS with longitudinal change, if seen at all, in those patients with less UMN involvement at baseline.

1.7.7 Diffusion MRI: Diffusion Tensor Imaging (DTI)

Diffusion MRI is sensitive to the motion of water molecules at the microscopic level. Changes in signal amplitude are measured following the application of a series of pre-determined and spatially-varying magnetic field 'gradients',[215] whereby the amplitude, duration and spacing of the gradient is indicated by the 'b-value'. The effect of the gradients is to introduce some dephasing between randomly moving spins, and therefore a signal attenuation proportional to the water self-diffusion coefficient. As the motion of water is affected by the tissue microstructure, diffusion indirectly characterises tissue configuration. The signal measured is averaged across comparatively large voxel sizes (relative to brain microstructure) and so requires some degree of "modelling". More than one model has been proposed and each typically incorporates slightly differing mathematical assumptions to provide indirect inferences on anatomical configurations. Diffusion Tensor Imaging (DTI) assumes water diffusion obeys Gaussian law and so is primarily powered to detect alterations in highly aligned (and thus highly anisotropic) fibres.[215] From three eigenvalues (or principal diffusivities) and three eigenvectors (directions along which the principal diffusivities are oriented) it is possible to obtain a series of scalar parameters: axial diffusivity (AD) and radial diffusivity (RD) relating to diffusion along and perpendicular to the main axis, respectively; mean diffusivity (MD); and the fractional anisotropy (FA).[200]

Brain DTI consistently shows a reduced FA, often alongside increased MD or RD, within the CST[4,26,186,199,216-225] and body of the corpus callosum.[26,184,186,199,217,218,220,222,226] in patients with ALS. It has been suggested that the posterior limb of the internal capsule, which forms a conduit for several descending motor tracts pathways including the CST, cortico-rubro-spinal, and cortico-reticulo-spinal connections,[80] is where DTI changes are perhaps most reliably encountered in ALS,[200,227] and may even hold a prognostic

significance.[228] Nevertheless, a number of studies have provided average DTI values along the whole intracranial path of the CST,[216,221,223,224,229] either finding no difference between levels,[216] or reporting changes rostrally (in the subcortical white matter, corona radiata and internal capsule),[217,220,230-233] caudally from the level of the posterior limb of the internal capsule to the pons[222,226] and pyramids,[234] or within a number of non-contiguous portions.[219,221,235,236]

Additional areas within the frontal and temporal lobes, including cingulum/cingulate gyrus and insula,[221,237,238] and parietal areas[221,239] have shown reduced FA, all of which is consistent with known regions of neuropathological damage at post mortem[67,68,70] and altered metabolism and function seen on SPECT,[161] PET [166,176,177,240] and fMRI.[183,241] Although these are often referred to as 'extramotor' areas, pyramidal neurons from the cingulate cortex project to the red nucleus and spinal cord and are felt to be heavily integrated into motor functioning.[238,242] Furthermore, pyramidal cells within the somatosensory cortex and parietal lobe contribute directly to the CST[1] and fibre tracking technique has indicated that depeleted fibres originating from the postcentral gyrus underlie a proportion of the reduced FA within the CST.[221]

A relationship between changes in DTI measures and clinical severity on ALS rating scales is also highly variable,[184,199] perhaps in part due to the ALSFRS reflecting more in the way of LMN dysfunction.[234] ALSFRS has been observed to correlate positively with reduced FA[197,201,202,207,212,217,243,244] or negatively with increased MD[245] of the intracranial CST (and in other areas such as the frontal lobe[221] and cerebellum[235]) on cross-sectional DTI, but this is not universal with other studies finding no association with either FA[216,226,228,231,234,246,247] or MD.[221,226,248] Similarly, increased disease duration[235,247,249] or faster progression rate[228,245,250] have been found to correlate with reduced FA[235,247,250] or

measures of increased diffusivity.[228,245,249] On the other hand, increased MD[216] or reduced FA[222,223] of the CST have positively correlated with the UMN clinical score and it may be that patients with a greater burden of UMN involvement clinically, particularly PLS phenotypes, demonstrate a greater degree of change in FA than those with more classic ALS.[186,222,236,250] Even patients with LMN predominant disease, including the PMA variant, have been shown to display CST FA differences compared to healthy controls (albeit less of a change compared to classical ALS[236,248,251] and PLS[236]), some of whom have later manifested UMN signs typical of ALS.[251] Furthermore, it is possible that site of symptom onset also influences the degree of change on diffusion imaging within the CSTs and corpus callosum[231,252] independently of cognitive involvement,[252] with bulbar onset patients showing more extensive differences with respect to controls.

Longitudinal scans in ALS have indicated both the presence[229,230,235,236,253] and absence[216,246] of demonstrable FA change in the CSTs over intervals of between 6-9 months, including at rostral[230,235,236,253] and caudal[236] loci, although the cross-sectional area of the tract may diminish despite a preserved mean FA.[213] Whether these findings suggest a progressive loss of tract fibres between scans or some other process is not clear. A significant reduction in FA of the subcortical CST and corpus callosum has been observed over a six months in patients with PMA, in addition to reductions along the rostro-caudal length of the intracranial CST and corpus callosum in limb- and bulbar-onset ALS, but without change in patients with PLS.[236] These findings would seem to echo the longitudinal volumetric studies of cortical thickness change in ALS and PLS,[206,213] the theme being that UMN-predominant phenotypes may have already accumulated significant CST damage detectable on baseline scans which remains largely ‘saturated’ on follow-up imaging compared to LMN-predominant patients whose CSTs are earlier in the phase of degeneration.

Nevertheless, it is widely accepted that the DTI model loses consistency when fibres bend or fan out, or where otherwise aligned tracts are crossing each other[199] which is common to areas such as the centrum semiovale and even regions of the foliated corpus callosum.[215,254] A reduction in FA may signify increased fibre branching or diameter, reduced axon density or cellular infiltration and thus cannot be used as a surrogate marker for 'loss of fibre integrity',[215] or denote a specific histopathological occurrence.[255] Variations on the diffusion tensor model have been created in an attempt to address these limitations, with one such model being neurite orientation dispersion and density imaging (NODDI).

Key Statement Box 8

DTI consistently demonstrates reduced FA within the CST and corpus callosum. Variable associations with clinical factors may be partly driven by disease heterogeneity. Longitudinal change is sometimes detectable but appears to predominate in patients who have fewer UMN signs at baseline.

1.7.8 Diffusion MRI: Neurite Orientation Dispersion and Density Imaging (NODDI)

NODDI requires acquisition across up to 60 directions and over a longer time than DTI, compartmentalising water diffusion into three geometric spaces encompassing non-Gaussian isotropic (or free), hindered anisotropic and restricted anisotropic components. V_{ISO}, V_{IC} and V_{EC} each broadly correspond to free water/CSF, intra-neurite water (of axons and dendrites) and extra-neurite water (but potentially including glial cells and neuronal somata), respectively.[256-258] The NODDI parameters ISO (isotropic volume fraction), NDI (neurite density index) and ODI (orientation dispersion index; a marker of the geometric complexity of neurites) can then be derived, the latter two of which are considered to provide a more structurally useful breakdown of single FA values.[257] NODDI is able to better delineate white from grey matter, in which normal white matter displays higher NDI and lower ODI with the reverse in grey matter,[259] and differentiate between different grey matter structures although might be more susceptible to changes in field strength in these areas.[258] Compared to DTI, NODDI indices, particularly ODI, have been shown to correlate with histological measures of orientation dispersion in the spinal cord and might also display more inter-subject variability with implications for the sample sizes required for group analyses.[259,260] However, this may not necessarily be an inaccuracy in modelling rather a more accurate depiction of tissue composition.[258] In addition, regions which might be expected to demonstrate considerable axon density and higher NDI values might counterintuitively show higher ISO due to the larger diameter axons enabling more freedom of water movement.[258,260]

NODDI has been used to demonstrate tissue alterations associated with normal ageing[261-263] and in a range of conditions including focal cortical dysplasia,[264] stroke,[265] Wilson's disease,[266] multiple sclerosis,[259] neurofibromatosis type 1[264,267] and neurodegenerative diseases. Reduction in NDI and ODI of the contralateral substantia

nigra pars compacta has been shown to correlate negatively with clinical severity of Parkinson's disease[268] whereas in pre-manifest Huntington's disease reductions in NDI and ODI are seen in a range of white matter tracts with reduced NDI in the corpus callosum correlating positively with markers of severity.[269] In patients with young onset Alzheimer's disease reduction in NDI and ODI is seen corrected for reduced thickness within several relevant cortical areas, with lower NDI values in patients scoring less well on cognitive tests,[270] while in a rodent model NODDI indices correlate more consistently than DTI parameters with the burden of tau pathology harboured by the cortex, corpus callosum and hippocampus.[271]

Use of NODDI imaging in ALS has only recently been undertaken. Whole brain analysis in patients with manifest disease has demonstrated a significant NDI reduction throughout the intracranial CSTs up to the subcortical matter of the precentral gyri and across the corpus callosum, with reduced ODI in the anterior limb of right internal capsule and increased ISO adjacent to the right lateral ventricle relative to healthy controls.[272] NDI within the right corona radiata and precentral subcortical white matter was decreased to a greater extent in those patients with both limb and bulbar involvement compared to limb alone, and longer disease durations correlated with reduced ODI in the precentral gyri, dorsolateral prefrontal cortices and precuneus. Furthermore, at the statistical threshold used, FA was reduced as expected within the CSTs but less extensively than NDI, and changes were not observed within the corpus callosum, implying NODDI may be more sensitive than DTI. Indeed, combined NODDI and DTI has also been performed in pre-manifest C9orf72 mutation carriers alongside first degree relatives not possessing the pathological repeat expansion.[273] The effect size relating to detectable reductions of NDI within 7 of 11 white matter tracts, including the CSTs, is greater than that for DTI metrics (in this case increased axial diffusivity, RD and MD rather than decreased FA) albeit

statistically significant in just two. Therefore, the results appear to corroborate the implication that lowered FA (or increased diffusivity) in the CSTs and corpus callosum results from the loss of axon fibres rather than increased complexity or dispersion within tracts. Longitudinal NODDI scans in ALS have not yet been investigated.

Recent work has also indicated that, when fitting the NODDI model to the diffusion data, optimal calculation of the NDI, ODI and ISO is dependent on whether the parameters are within grey matter structures (such as cortex and basal ganglia) or white matter tracts. Given the greater inherent ease (albeit directionally-restricted) with which intracellular water may diffuse along highly-aligned white matter fibres, it has been suggested that a slightly less generous value for the intrinsic free diffusivity (ID) constant should be used within the NODDI calculation when optimising indices for grey matter. Thus for white matter an ID value of 1.7×10^{-9} $m^2.s^{-1}$ is suggested compared to an ID value of 1.1×10^{-9} $m^2.s^{-1}$ for grey matter.[274,275]

Key Statement Box 9

NODDI may be more sensitive than DTI FA and has recently demonstrated changes within the CSTs in patients with ALS. Further studies are required to explore relationships with clinical measures and longitudinal change.

1.7.9 Quantitative Magnetisation Transfer Imaging (qMTi)

Magnetisation transfer imaging essentially utilises a 'two pool' model in which hydrogen protons are either free (in water molecules) or bound to macromolecules (lipids and proteins) within the semisolid tissue which is dominated by myelin. The bound protons do not directly contribute to the MRI signal and are 'silent' in diffusion sequences (increased radial diffusivity with DTI is not specific for demyelination),[276] but can be indirectly probed thanks to their interaction with the free protons following off-frequency radiofrequency pulses. The exchange in magnetisation between the two compartments allows the state of the semisolid pool (saturated) to affect that of the free protons, resulting in partial saturation and in a decrease of its overall magnetisation.[277] The magnetisation transfer (MT) effect can thereby produce a qualitative magnetisation transfer tissue contrast (MTC) image and is already clinically utilised as part of MR angiography and gadolinium-enhanced T1-weighted sequences, for instance. Indeed, MTC T1 images in patients with ALS have shown hyperintensity along the CST[278,279] and CC[278] in a proportion of cases (and more conspicuously than FLAIR)[279] compared to control subjects which was significantly related to the degree of reduced FA in the same regions and presumed to reflect damage to the white matter tracts, although with no clear association with clinical rating scales or disease duration.[278] Acquiring a proton-density image with and without a MT pulse renders it possible to semi-quantify the MT effect and produce a voxel-wise magnetisation transfer ratio (MTR) to reflect changes in macromolecular integrity. Accordingly, reduced MTR within the brain has been reported within the CSTs,[280] the precentral and other frontal and extramotor gyri,[281,282] in patients with ALS compared to healthy controls, and independently of grey matter atrophy as measured by voxel-base morphometry.[281] However, the MTC and MTR are dependent on a range of imaging variables and their biophysical basis is undefined.[277]

Mathematical models describing the MT-weighted signal as a function of the saturating pulses have enabled more biologically applicable parameters to be derived from quantitative magnetisation transfer imaging (qMTi), including the macromolecular pool fraction [f; modelled to essentially represent myelin content], forward exchange rate of magnetisation transfer [k_f] and transverse relaxation time of the free pool [T_2^F]. Although qMTi is yet to be explored in patients with ALS, studies in multiple sclerosis (MS) have demonstrated reductions in f and k_f, and increased T_2^F in acute inflammatory lesions with a subsequent return to baseline over several months.[283] Compared to healthy controls, normal appearing white matter (NAWM) shows reduced f, kf and MTR,[284] with reduced MTR in chronic MS plaques correlating with greater disability.[285] Reduced MTR in MS is generally considered to be a marker of demyelination. However, a small study found that although reduced MTR at the edge of acute MS lesions correlated with reduced myelin content, in NAWM it may instead result from swollen microglia and axons,[286] highlighting the uncertainty of its interpretation. MTR in normal appearing grey matter is also reduced in patients with relapsing-remitting MS[287-289] and may also correlate with disability, although variable results are reported.[288] Acute increases in kf (but without change in f or T2f) on qMTi have also been found in the insula following a systemic inflammatory stimulus with intramuscular typhoid vaccination and are associated with increased levels of reported fatigue, in addition to a co-localised increase in glucose metabolism measured by FDG-PET.[290] Although mechanisms underlying changes in MT parameters are likely to be very different between diseases, it is plausible that qMTi would be sensitive to structural alterations in ALS given the likely role for the immune system in its pathogenesis.[126,127]

Key Statement Box 10

qMTi is yet to be explored in ALS.

1.8 Summary of Key Statements

- ALS presents with a heterogeneous spectrum of motor and extra-motor (particularly cognitive and behavioural) phenotypes, variable patterns and rates of disease progression between individuals and multiple underlying genetic or, as yet, unidentified ('sporadic') causes.

- There are currently no validated and objective quantitative biomarkers with enough sensitivity and specificity for ALS diagnosis, prognosis, or response to potential disease-modifying therapies although several candidates are under investigation, including measures in blood, cerebrospinal fluid, neurophysiology and quantitative neuroimaging.

- Dynamics and mechanisms of cell death during the course of the human disease remains incomplete, and is inferred from end-stage neuropathology and changes within indirect animal models of the disease. Objective and informative biomarkers of disease activity in patients with ALS *in vivo* are very much needed.

- The immune system plays a key role in determining the CNS milieu in ALS. Higher levels of blood T regulatory cells (Tregs) are known to associate with a slower rate of progression and is the basis of a new randomised clinical trial (MIROCALS) using low dose Interleukin-2 to augment Treg levels in patients.

- Nuclear medicine neuroimaging has importantly demonstrated reduced cortical metabolism/perfusion, involvement of multiple neurotransmitter systems in disease and provide further evidence for altered glial function in patients with ALS. However,

its use is complicated by its radiation exposure and requirement for injectable substances.

- "Single-echo" resting state functional MRI (rsfMRI) demonstrates altered connectivity within resting networks (such as the sensorimotor, default mode, fronto-parietal and executive), although findings are highly heterogeneous. "Multi-echo" rsfMRI acquisition may improve the consistency of connectivity differences between patients and controls.

- MRI Morphometric analyses most consistently report atrophy or reduced thickness of the primary motor cortex in ALS with longitudinal change, if seen at all, in those patients with less UMN involvement at baseline.

- Diffusion Tensor MRI (DTI) consistently demonstrates reduced FA within the CST and corpus callosum. Variable associations with clinical factors may be partly driven by disease heterogeneity. Longitudinal change is sometimes detectable but appears to predominate in patients who have fewer UMN signs at baseline.

- Neurite Orientation Dispersion and Density Imaging (NODDI) may be more sensitive than DTI FA and has recently demonstrated changes within the CSTs in patients with ALS. Further studies are required to explore relationships with clinical measures and its ability to detect longitudinal change.

- Quantitative magnetisation transfer imaging (qMTi) is yet to be explored in ALS.

References

1. Lemon, R.N. Descending pathways in motor control. *Annu Rev Neurosci* **31**, 195-218 (2008).
2. Lemon, R.N. & Griffiths, J. Comparing the function of the corticospinal system in different species: organizational differences for motor specialization? *Muscle Nerve* **32**, 261-279 (2005).
3. Braak, H.*, et al.* Amyotrophic lateral sclerosis--a model of corticofugal axonal spread. *Nat Rev Neurol* **9**, 708-714 (2013).
4. Huynh, W.*, et al.* Assessment of the upper motor neuron in amyotrophic lateral sclerosis. *Clin Neurophysiol* **127**, 2643-2660 (2016).
5. Eisen, A., Turner, M.R. & Lemon, R. Tools and talk: an evolutionary perspective on the functional deficits associated with amyotrophic lateral sclerosis. *Muscle Nerve* **49**, 469-477 (2014).
6. Molyneaux, B.J., Arlotta, P., Menezes, J.R.L. & Macklis, J.D. Neuronal subtype specification in the cerebral cortex. *Nat Rev Neurosci* **8**, 427-437 (2007).
7. Rathelot, J.A. & Strick, P.L. Muscle representation in the macaque motor cortex: an anatomical perspective. *Proc Natl Acad Sci U S A* **103**, 8257-8262 (2006).
8. Kuypers, H.J.G.M. Anatomy of the Descending Pathways. in *Handbook of Physiology - The Nervous System Vol II* (eds. Brooks, V.B., Brookhart, J.M., Mountcastle, V.B. & Geiger, S.R.) 597-666 (Am Physiol Soc, Bethesda, Maryland, 1981).
9. Dentel, C.*, et al.* Degeneration of serotonergic neurons in amyotrophic lateral sclerosis: a link to spasticity. *Brain* **136**, 483-493 (2013).
10. Rowland, L.P. How amyotrophic lateral sclerosis got its name: the clinical-pathologic genius of Jean-Martin Charcot. *Arch Neurol* **58**, 512-515 (2001).
11. Phukan, J.*, et al.* The syndrome of cognitive impairment in amyotrophic lateral sclerosis: a population-based study. *J Neurol Neurosurg Psychiatry* **83**, 102-108 (2012).
12. Ringholz, G.M.*, et al.* Prevalence and patterns of cognitive impairment in sporadic ALS. *Neurology* **65**, 586-590 (2005).
13. Bak, T.H. & Chandran, S. What wires together dies together: verbs, actions and neurodegeneration in motor neuron disease. *Cortex* **48**, 936-944 (2012).
14. Coan, G. & Mitchell, C.S. An Assessment of Possible Neuropathology and Clinical Relationships in 46 Sporadic Amyotrophic Lateral Sclerosis Patient Autopsies. *Neurodegener Dis* **15**, 301-312 (2015).
15. Neumann, M.*, et al.* Ubiquitinated TDP-43 in frontotemporal lobar degeneration and amyotrophic lateral sclerosis. *Science* **314**, 130-133 (2006).
16. McDermott, C.J. & Shaw, P.J. Diagnosis and management of motor neurone disease. *BMJ* **336**, 658-662 (2008).
17. Talbott, E.O., Malek, A.M. & Lacomis, D. The epidemiology of amyotrophic lateral sclerosis. *Handb Clin Neurol* **138**, 225-238 (2016).
18. Ravits, J.*, et al.* Deciphering amyotrophic lateral sclerosis: what phenotype, neuropathology and genetics are telling us about pathogenesis. *Amyotroph Lateral Scler Frontotemporal Degener* **14 Suppl 1**, 5-18 (2013).
19. Al-Chalabi, A.*, et al.* Analysis of amyotrophic lateral sclerosis as a multistep process: a population-based modelling study. *Lancet Neurol* **13**, 1108-1113 (2014).
20. Lattante, S., Ciura, S., Rouleau, G.A. & Kabashi, E. Defining the genetic connection linking amyotrophic lateral sclerosis (ALS) with frontotemporal dementia (FTD). *Trends Genet* **31**, 263-273 (2015).
21. Hanby, M.F.*, et al.* The risk to relatives of patients with sporadic amyotrophic lateral sclerosis. *Brain* **134**, 3454-3457 (2011).

22. White, M.A. & Sreedharan, J. Amyotrophic lateral sclerosis: recent genetic highlights. *Curr Opin Neurol* **29**, 557-564 (2016).
23. Therrien, M., Dion, P.A. & Rouleau, G.A. ALS: Recent Developments from Genetics Studies. *Curr Neurol Neurosci Rep* **16**, 59 (2016).
24. Morgan, S. & Orrell, R.W. Pathogenesis of amyotrophic lateral sclerosis. *Br Med Bull* **119**, 87-98 (2016).
25. Rossi, S., Cozzolino, M. & Carri, M.T. Old versus New Mechanisms in the Pathogenesis of ALS. *Brain Pathol* **26**, 276-286 (2016).
26. Simon, N.G.*, et al.* Quantifying disease progression in amyotrophic lateral sclerosis. *Ann Neurol* **76**, 643-657 (2014).
27. Guerreiro, R., Bras, J. & Hardy, J. SnapShot: Genetics of ALS and FTD. *Cell* **160**, 798 e791 (2015).
28. Ravits, J., Paul, P. & Jorg, C. Focality of upper and lower motor neuron degeneration at the clinical onset of ALS. *Neurology* **68**, 1571-1575 (2007).
29. Gargiulo-Monachelli, G.M.*, et al.* Regional spread pattern predicts survival in patients with sporadic amyotrophic lateral sclerosis. *Eur J Neurol* **19**, 834-841 (2012).
30. Wijesekera, L.C.*, et al.* Natural history and clinical features of the flail arm and flail leg ALS variants. *Neurology* **72**, 1087-1094 (2009).
31. Gautier, G.*, et al.* ALS with respiratory onset: clinical features and effects of non-invasive ventilation on the prognosis. *Amyotroph Lateral Scler* **11**, 379-382 (2010).
32. Kanouchi, T., Ohkubo, T. & Yokota, T. Can regional spreading of amyotrophic lateral sclerosis motor symptoms be explained by prion-like propagation? *J Neurol Neurosurg Psychiatry* **83**, 739-745 (2012).
33. Swash, M., Leader, M., Brown, A. & Swettenham, K.W. Focal loss of anterior horn cells in the cervical cord in motor neuron disease. *Brain* **109 (Pt 5)**, 939-952 (1986).
34. Orsini, M.*, et al.* Amyotrophic Lateral Sclerosis: New Perpectives and Update. *Neurol Int* **7**, 5885 (2015).
35. Fujimura-Kiyono, C.*, et al.* Onset and spreading patterns of lower motor neuron involvements predict survival in sporadic amyotrophic lateral sclerosis. *J Neurol Neurosurg Psychiatry* **82**, 1244-1249 (2011).
36. Orsini, M.*, et al.* Man-in-the-barrel syndrome, a symmetrical proximal brachial amyotrophic diplegia related to motor neuron diseases: a survey of nine cases. *Rev Assoc Med Bras (1992)* **55**, 712-715 (2009).
37. Katz, J.S.*, et al.* Brachial amyotrophic diplegia: a slowly progressive motor neuron disorder. *Neurology* **53**, 1071-1076 (1999).
38. Al-Chalabi, A.*, et al.* Amyotrophic lateral sclerosis: moving towards a new classification system. *Lancet Neurol* **15**, 1182-1194 (2016).
39. Kim, W.K.*, et al.* Study of 962 patients indicates progressive muscular atrophy is a form of ALS. *Neurology* **73**, 1686-1692 (2009).
40. Ince, P.G.*, et al.* Corticospinal tract degeneration in the progressive muscular atrophy variant of ALS. *Neurology* **60**, 1252-1258 (2003).
41. Gordon, P.H.*, et al.* The natural history of primary lateral sclerosis. *Neurology* **66**, 647-653 (2006).
42. Tan, C.F.*, et al.* Primary lateral sclerosis: a rare upper-motor-predominant form of amyotrophic lateral sclerosis often accompanied by frontotemporal lobar degeneration with ubiquitinated neuronal inclusions? Report of an autopsy case and a review of the literature. *Acta Neuropathol* **105**, 615-620 (2003).
43. Grace, G.M.*, et al.* Neuropsychological functioning in PLS: a comparison with ALS. *Can J Neurol Sci* **38**, 88-97 (2011).

44. Goldstein, L.H. & Abrahams, S. Changes in cognition and behaviour in amyotrophic lateral sclerosis: nature of impairment and implications for assessment. *Lancet Neurol* **12**, 368-380 (2013).
45. Crockford, C.*, et al.* ALS-specific cognitive and behavior changes associated with advancing disease stage in ALS. *Neurology* **91**, e1370-e1380 (2018).
46. Abrahams, S., Newton, J., Niven, E., Foley, J. & Bak, T.H. Screening for cognition and behaviour changes in ALS. *Amyotroph Lateral Scler Frontotemporal Degener* **15**, 9-14 (2014).
47. Beeldman, E.*, et al.* The cognitive profile of ALS: a systematic review and meta-analysis update. *J Neurol Neurosurg Psychiatry* **87**, 611-619 (2016).
48. Elamin, M.*, et al.* Executive dysfunction is a negative prognostic indicator in patients with ALS without dementia. *Neurology* **76**, 1263-1269 (2011).
49. Crockford, C.J.*, et al.* ECAS A-B-C: alternate forms of the Edinburgh Cognitive and Behavioural ALS Screen. *Amyotroph Lateral Scler Frontotemporal Degener* **19**, 57-64 (2018).
50. Turner, M.R. & Talbot, K. Mimics and chameleons in motor neurone disease. *Pract Neurol* **13**, 153-164 (2013).
51. de Carvalho, M.*, et al.* Electrodiagnostic criteria for diagnosis of ALS. *Clin Neurophysiol* **119**, 497-503 (2008).
52. NICE. Motor neurone disease: assessment and management. (2016).
53. Bissaro, M. & Moro, S. Rethinking to riluzole mechanism of action: the molecular link among protein kinase CK1delta activity, TDP-43 phosphorylation, and amyotrophic lateral sclerosis pharmacological treatment. *Neural Regen Res* **14**, 2083-2085 (2019).
54. Bensimon, G., Lacomblez, L. & Meininger, V. A controlled trial of riluzole in amyotrophic lateral sclerosis. ALS/Riluzole Study Group. *N Engl J Med* **330**, 585-591 (1994).
55. Lacomblez, L., Bensimon, G., Leigh, P.N., Guillet, P. & Meininger, V. Dose-ranging study of riluzole in amyotrophic lateral sclerosis. Amyotrophic Lateral Sclerosis/Riluzole Study Group II. *Lancet* **347**, 1425-1431 (1996).
56. Safety and efficacy of edaravone in well defined patients with amyotrophic lateral sclerosis: a randomised, double-blind, placebo-controlled trial. *Lancet Neurol* **16**, 505-512 (2017).
57. Al-Chalabi, A.*, et al.* July 2017 ENCALS statement on edaravone. *Amyotroph Lateral Scler Frontotemporal Degener* **18**, 471-474 (2017).
58. Pandya, R.S.*, et al.* Therapeutic neuroprotective agents for amyotrophic lateral sclerosis. *Cell Mol Life Sci* **70**, 4729-4745 (2013).
59. Elamin, M.*, et al.* Predicting prognosis in amyotrophic lateral sclerosis: a simple algorithm. *J Neurol* **262**, 1447-1454 (2015).
60. Turner, M.R., Kiernan, M.C., Leigh, P.N. & Talbot, K. Biomarkers in amyotrophic lateral sclerosis. *Lancet Neurol* **8**, 94-109 (2009).
61. Vucic, S., Ziemann, U., Eisen, A., Hallett, M. & Kiernan, M.C. Transcranial magnetic stimulation and amyotrophic lateral sclerosis: pathophysiological insights. *J Neurol Neurosurg Psychiatry* **84**, 1161-1170 (2013).
62. Carri, M.T., D'Ambrosi, N. & Cozzolino, M. Pathways to mitochondrial dysfunction in ALS pathogenesis. *Biochem Biophys Res Commun* (2016).
63. Blizzard, C.A.*, et al.* Identifying the primary site of pathogenesis in amyotrophic lateral sclerosis - vulnerability of lower motor neurons to proximal excitotoxicity. *Dis Model Mech* **8**, 215-224 (2015).
64. Geevasinga, N., Menon, P., Ozdinler, P.H., Kiernan, M.C. & Vucic, S. Pathophysiological and diagnostic implications of cortical dysfunction in ALS. *Nat Rev Neurol* **12**, 651-661 (2016).

65. Chou, S.M. Pathology of Motor System Disorder. in *Motor Neuron Disease: Biology and Management* (eds. Leigh, P.N. & Swash, M.) 53-92 (Springer-Verlag, London, 1995).
66. Iwanaga, K.*, et al.* Neuropathology of sporadic amyotrophic lateral sclerosis of long duration. *J Neurol Sci* **146**, 139-143 (1997).
67. Martin, J.E. & Swash, M. The Pathology of Motor Neuron Disease. in *Motor Neuron Disease: Biology and Management* (eds. Leigh, P.N. & Swash, M.) 93-118 (Springer-Verlag, London, 1995).
68. Brownell, B., Oppenheimer, D.R. & Hughes, J.T. The central nervous system in motor neurone disease. *J Neurol Neurosurg Psychiatry* **33**, 338-357 (1970).
69. Chou, S.M. & Norris, F.H. Amyotrophic lateral sclerosis: lower motor neuron disease spreading to upper motor neurons. *Muscle Nerve* **16**, 864-869 (1993).
70. Smith, M.C. Nerve Fibre Degeneration in the Brain in Amyotrophic Lateral Sclerosis. *J Neurol Neurosurg Psychiatry* **23**, 269-282 (1960).
71. Nihei, K., McKee, A.C. & Kowall, N.W. Patterns of neuronal degeneration in the motor cortex of amyotrophic lateral sclerosis patients. *Acta Neuropathol* **86**, 55-64 (1993).
72. Kiernan, J.A. & Hudson, A.J. Changes in sizes of cortical and lower motor neurons in amyotrophic lateral sclerosis. *Brain* **114 (Pt 2)**, 843-853 (1991).
73. Hammer, R.P., Jr., Tomiyasu, U. & Scheibel, A.B. Degeneration of the human Betz cell due to amyotrophic lateral sclerosis. *Exp Neurol* **63**, 336-346 (1979).
74. Maekawa, S.*, et al.* Cortical selective vulnerability in motor neuron disease: a morphometric study. *Brain* **127**, 1237-1251 (2004).
75. Gredal, O., Pakkenberg, H., Karlsborg, M. & Pakkenberg, B. Unchanged total number of neurons in motor cortex and neocortex in amyotrophic lateral sclerosis: a stereological study. *J Neurosci Methods* **95**, 171-176 (2000).
76. Toft, M.H., Gredal, O. & Pakkenberg, B. The size distribution of neurons in the motor cortex in amyotrophic lateral sclerosis. *J Anat* **207**, 399-407 (2005).
77. Davison, C. Amyotrophic lateral sclerosis. Origin and extent of the upper motor neuron lesion. *Arch Neurol & Psychiat* **46**, 1039-1056 (1941).
78. Mochizuki, Y., Mizutani, T., Shimizu, T. & Kawata, A. Proportional neuronal loss between the primary motor and sensory cortex in amyotrophic lateral sclerosis. *Neuroscience Letters* **503**, 73-75 (2011).
79. Schiffer, D., Cordera, S., Cavalla, P. & Migheli, A. Reactive astrogliosis of the spinal cord in amyotrophic lateral sclerosis. *J Neurol Sci* **139 Suppl**, 27-33 (1996).
80. Lindenberg, R.*, et al.* Structural integrity of corticospinal motor fibers predicts motor impairment in chronic stroke. *Neurology* **74**, 280-287 (2010).
81. Yagishita, A., Nakano, I., Oda, M. & Hirano, A. Location of the corticospinal tract in the internal capsule at MR imaging. *Radiology* **191**, 455-460 (1994).
82. Stephens, B.*, et al.* Widespread loss of neuronal populations in the spinal ventral horn in sporadic motor neuron disease. A morphometric study. *J Neurol Sci* **244**, 41-58 (2006).
83. Kiernan, J.A. & Hudson, A.J. Changes in shapes of surviving motor neurons in amyotrophic lateral sclerosis. *Brain* **116 (Pt 1)**, 203-215 (1993).
84. Leigh, P.N., Dodson, A., Swash, M., Brion, J.P. & Anderton, B.H. Cytoskeletal abnormalities in motor neuron disease. An immunocytochemical study. *Brain* **112 (Pt 2)**, 521-535 (1989).
85. Kiernan, J.A. & Hudson, A.J. Frontal lobe atrophy in motor neuron diseases. *Brain* **117 (Pt 4)**, 747-757 (1994).
86. Sasaki, S., Maruyama, S., Yamane, K., Sakuma, H. & Takeishi, M. Swellings of proximal axons in a case of motor neuron disease. *Ann Neurol* **25**, 520-522 (1989).

87. Brettschneider, J.*, et al.* Stages of pTDP-43 pathology in amyotrophic lateral sclerosis. *Ann Neurol* **74**, 20-38 (2013).
88. Okamoto, K.*, et al.* Oculomotor nuclear pathology in amyotrophic lateral sclerosis. *Acta Neuropathol* **85**, 458-462 (1993).
89. Pullen, A.H. & Martin, J.E. Ultrastructural abnormalities with inclusions in Onuf's nucleus in motor neuron disease (amyotrophic lateral sclerosis). *Neuropathol Appl Neurobiol* **21**, 327-340 (1995).
90. Swash, M., Scholtz, C.L., Vowles, G. & Ingram, D.A. Selective and asymmetric vulnerability of corticospinal and spinocerebellar tracts in motor neuron disease. *J Neurol Neurosurg Psychiatry* **51**, 785-789 (1988).
91. Mizutani, T.*, et al.* Development of ophthalmoplegia in amyotrophic lateral sclerosis during long-term use of respirators. *J Neurol Sci* **99**, 311-319 (1990).
92. Schiffer, D., Attanasio, A., Chio, A., Migheli, A. & Pezzulo, T. Ubiquitinated dystrophic neurites suggest corticospinal derangement in patients with amyotrophic lateral sclerosis. *Neurosci Lett* **180**, 21-24 (1994).
93. Sta, M.*, et al.* Innate and adaptive immunity in amyotrophic lateral sclerosis: evidence of complement activation. *Neurobiol Dis* **42**, 211-220 (2011).
94. Kawamata, T., Akiyama, H., Yamada, T. & McGeer, P.L. Immunologic reactions in amyotrophic lateral sclerosis brain and spinal cord tissue. *Am J Pathol* **140**, 691-707 (1992).
95. Philips, T. & Robberecht, W. Neuroinflammation in amyotrophic lateral sclerosis: role of glial activation in motor neuron disease. *Lancet Neurol* **10**, 253-263 (2011).
96. Engelhardt, J.I., Tajti, J. & Appel, S.H. Lymphocytic infiltrates in the spinal cord in amyotrophic lateral sclerosis. *Arch Neurol* **50**, 30-36 (1993).
97. Leigh, P.N.*, et al.* Ubiquitin deposits in anterior horn cells in motor neurone disease. *Neurosci Lett* **93**, 197-203 (1988).
98. Johnson, B.S.*, et al.* TDP-43 is intrinsically aggregation-prone, and amyotrophic lateral sclerosis-linked mutations accelerate aggregation and increase toxicity. *J Biol Chem* **284**, 20329-20339 (2009).
99. Li, Y.R., King, O.D., Shorter, J. & Gitler, A.D. Stress granules as crucibles of ALS pathogenesis. *J Cell Biol* **201**, 361-372 (2013).
100. Geser, F.*, et al.* Evidence of multisystem disorder in whole-brain map of pathological TDP-43 in amyotrophic lateral sclerosis. *Arch Neurol* **65**, 636-641 (2008).
101. Pradat, P.F., Kabashi, E. & Desnuelle, C. Deciphering spreading mechanisms in amyotrophic lateral sclerosis: clinical evidence and potential molecular processes. *Curr Opin Neurol* **28**, 455-461 (2015).
102. Braak, H., Ludolph, A.C., Neumann, M., Ravits, J. & Del Tredici, K. Pathological TDP-43 changes in Betz cells differ from those in bulbar and spinal alpha-motoneurons in sporadic amyotrophic lateral sclerosis. *Acta Neuropathol* **133**, 79-90 (2017).
103. Bora, E. Meta-analysis of social cognition in amyotrophic lateral sclerosis. *Cortex* **88**, 1-7 (2017).
104. Routal, R.V. & Pal, G.P. A study of motoneuron groups and motor columns of the human spinal cord. *J Anat* **195 (Pt 2)**, 211-224 (1999).
105. Brettschneider, J.*, et al.* TDP-43 pathology and neuronal loss in amyotrophic lateral sclerosis spinal cord. *Acta Neuropathol* **128**, 423-437 (2014).
106. Brettschneider, J.*, et al.* Sequential distribution of pTDP-43 pathology in behavioral variant frontotemporal dementia (bvFTD). *Acta Neuropathol* **127**, 423-439 (2014).
107. Vucic, S., Nicholson, G.A. & Kiernan, M.C. Cortical hyperexcitability may precede the onset of familial amyotrophic lateral sclerosis. *Brain* **131**, 1540-1550 (2008).

108. Menon, P., Kiernan, M.C. & Vucic, S. Cortical hyperexcitability precedes lower motor neuron dysfunction in ALS. *Clin Neurophysiol* **126**, 803-809 (2015).
109. Vucic, S. & Kiernan, M.C. Novel threshold tracking techniques suggest that cortical hyperexcitability is an early feature of motor neuron disease. *Brain* **129**, 2436-2446 (2006).
110. Eisen, A., Kiernan, M., Mitsumoto, H. & Swash, M. Amyotrophic lateral sclerosis: a long preclinical period? *J Neurol Neurosurg Psychiatry* **85**, 1232-1238 (2014).
111. King, A.E., Woodhouse, A., Kirkcaldie, M.T. & Vickers, J.C. Excitotoxicity in ALS: Overstimulation, or overreaction? *Exp Neurol* **275 Pt 1**, 162-171 (2016).
112. Rothstein, J.D., Martin, L.J. & Kuncl, R.W. Decreased glutamate transport by the brain and spinal cord in amyotrophic lateral sclerosis. *N Engl J Med* **326**, 1464-1468 (1992).
113. Foerster, B.R.*, et al.* Decreased motor cortex gamma-aminobutyric acid in amyotrophic lateral sclerosis. *Neurology* **78**, 1596-1600 (2012).
114. Turner, M.R.*, et al.* Distinct cerebral lesions in sporadic and 'D90A' SOD1 ALS: studies with [11C]flumazenil PET. *Brain* **128**, 1323-1329 (2005).
115. Saba, L.*, et al.* Altered Functionality, Morphology, and Vesicular Glutamate Transporter Expression of Cortical Motor Neurons from a Presymptomatic Mouse Model of Amyotrophic Lateral Sclerosis. *Cereb Cortex* **26**, 1512-1528 (2016).
116. Fogarty, M.J., Noakes, P.G. & Bellingham, M.C. Motor cortex layer V pyramidal neurons exhibit dendritic regression, spine loss, and increased synaptic excitation in the presymptomatic hSOD1(G93A) mouse model of amyotrophic lateral sclerosis. *J Neurosci* **35**, 643-647 (2015).
117. Ozdinler, P.H.*, et al.* Corticospinal motor neurons and related subcerebral projection neurons undergo early and specific neurodegeneration in hSOD1G(9)(3)A transgenic ALS mice. *J Neurosci* **31**, 4166-4177 (2011).
118. Kassa, R.M., Mariotti, R., Bonaconsa, M., Bertini, G. & Bentivoglio, M. Gene, cell, and axon changes in the familial amyotrophic lateral sclerosis mouse sensorimotor cortex. *J Neuropathol Exp Neurol* **68**, 59-72 (2009).
119. Thomsen, G.M.*, et al.* Delayed disease onset and extended survival in the SOD1G93A rat model of amyotrophic lateral sclerosis after suppression of mutant SOD1 in the motor cortex. *J Neurosci* **34**, 15587-15600 (2014).
120. Vinsant, S.*, et al.* Characterization of early pathogenesis in the SOD1(G93A) mouse model of ALS: part II, results and discussion. *Brain Behav* **3**, 431-457 (2013).
121. Pun, S., Santos, A.F., Saxena, S., Xu, L. & Caroni, P. Selective vulnerability and pruning of phasic motoneuron axons in motoneuron disease alleviated by CNTF. *Nat Neurosci* **9**, 408-419 (2006).
122. Saxena, S. & Caroni, P. Mechanisms of axon degeneration: from development to disease. *Prog Neurobiol* **83**, 174-191 (2007).
123. Conforti, L., Adalbert, R. & Coleman, M.P. Neuronal death: where does the end begin? *Trends Neurosci* **30**, 159-166 (2007).
124. Fischer, L.R.*, et al.* Amyotrophic lateral sclerosis is a distal axonopathy: evidence in mice and man. *Exp Neurol* **185**, 232-240 (2004).
125. Dadon-Nachum, M., Melamed, E. & Offen, D. The "dying-back" phenomenon of motor neurons in ALS. *J Mol Neurosci* **43**, 470-477 (2011).
126. Zhao, W., Beers, D.R. & Appel, S.H. Immune-mediated mechanisms in the pathoprogression of amyotrophic lateral sclerosis. *J Neuroimmune Pharmacol* **8**, 888-899 (2013).
127. Schwartz, M. & Baruch, K. Breaking peripheral immune tolerance to CNS antigens in neurodegenerative diseases: boosting autoimmunity to fight-off chronic neuroinflammation. *J Autoimmun* **54**, 8-14 (2014).

128. Corcia, P.*, et al.* Molecular imaging of microglial activation in amyotrophic lateral sclerosis. *PLoS One* **7**, e52941 (2012).
129. Turner, M.R.*, et al.* Evidence of widespread cerebral microglial activation in amyotrophic lateral sclerosis: an [11C](R)-PK11195 positron emission tomography study. *Neurobiol Dis* **15**, 601-609 (2004).
130. Henkel, J.S.*, et al.* Presence of dendritic cells, MCP-1, and activated microglia/macrophages in amyotrophic lateral sclerosis spinal cord tissue. *Ann Neurol* **55**, 221-235 (2004).
131. Troost, D., van den Oord, J.J., de Jong, J.M. & Swaab, D.F. Lymphocytic infiltration in the spinal cord of patients with amyotrophic lateral sclerosis. *Clin Neuropathol* **8**, 289-294 (1989).
132. Troost, D., Van den Oord, J.J. & Vianney de Jong, J.M. Immunohistochemical characterization of the inflammatory infiltrate in amyotrophic lateral sclerosis. *Neuropathol Appl Neurobiol* **16**, 401-410 (1990).
133. Beers, D.R., Henkel, J.S., Zhao, W., Wang, J. & Appel, S.H. CD4+ T cells support glial neuroprotection, slow disease progression, and modify glial morphology in an animal model of inherited ALS. *Proc Natl Acad Sci U S A* **105**, 15558-15563 (2008).
134. Beers, D.R.*, et al.* Endogenous regulatory T lymphocytes ameliorate amyotrophic lateral sclerosis in mice and correlate with disease progression in patients with amyotrophic lateral sclerosis. *Brain* **134**, 1293-1314 (2011).
135. Wan, Y.Y. & Flavell, R.A. Regulatory T-cell functions are subverted and converted owing to attenuated Foxp3 expression. *Nature* **445**, 766-770 (2007).
136. Malek, T.R. & Bayer, A.L. Tolerance, not immunity, crucially depends on IL-2. *Nat Rev Immunol* **4**, 665-674 (2004).
137. Klatzmann, D. & Abbas, A.K. The promise of low-dose interleukin-2 therapy for autoimmune and inflammatory diseases. *Nat Rev Immunol* **15**, 283-294 (2015).
138. Gonzalez, H. & Pacheco, R. T-cell-mediated regulation of neuroinflammation involved in neurodegenerative diseases. *J Neuroinflammation* **11**, 201 (2014).
139. Zhao, W., Xie, W., Xiao, Q., Beers, D.R. & Appel, S.H. Protective effects of an anti-inflammatory cytokine, interleukin-4, on motoneuron toxicity induced by activated microglia. *J Neurochem* **99**, 1176-1187 (2006).
140. Philips, T. & Rothstein, J.D. Glial cells in amyotrophic lateral sclerosis. *Exp Neurol* **262 Pt B**, 111-120 (2014).
141. Tang, Y. & Le, W. Differential Roles of M1 and M2 Microglia in Neurodegenerative Diseases. *Mol Neurobiol* **53**, 1181-1194 (2016).
142. Menon, P.*, et al.* Regulatory T cells in amyotrophic lateral sclerosis: A role for disease modulation. *J Clin Neurosci* **21**, 2050 (2014).
143. Henkel, J.S.*, et al.* Regulatory T-lymphocytes mediate amyotrophic lateral sclerosis progression and survival. *EMBO Mol Med* **5**, 64-79 (2013).
144. Saadoun, D.*, et al.* Regulatory T-cell responses to low-dose interleukin-2 in HCV-induced vasculitis. *N Engl J Med* **365**, 2067-2077 (2011).
145. Kim, N.*, et al.* Therapeutic potential of low-dose IL-2 in a chronic GVHD patient by in vivo expansion of regulatory T cells. *Cytokine* **78**, 22-26 (2016).
146. He, J.*, et al.* Low-dose interleukin-2 treatment selectively modulates CD4(+) T cell subsets in patients with systemic lupus erythematosus. *Nat Med* **22**, 991-993 (2016).
147. Tahvildari, M.*, et al.* In Vivo Expansion of Regulatory T Cells by Low-Dose Interleukin-2 Treatment Increases Allograft Survival in Corneal Transplantation. *Transplantation* **100**, 525-532 (2016).
148. Castela, E.*, et al.* Effects of low-dose recombinant interleukin 2 to promote T-regulatory cells in alopecia areata. *JAMA Dermatol* **150**, 748-751 (2014).

149. Arenas-Ramirez, N., Woytschak, J. & Boyman, O. Interleukin-2: Biology, Design and Application. *Trends Immunol* **36**, 763-777 (2015).
150. Alsuliman, A.*, et al.* A robust, good manufacturing practice-compliant, clinical-scale procedure to generate regulatory T cells from patients with amyotrophic lateral sclerosis for adoptive cell therapy. *Cytotherapy* **18**, 1312-1324 (2016).
151. Foerster, B.R., Welsh, R.C. & Feldman, E.L. 25 years of neuroimaging in amyotrophic lateral sclerosis. *Nat Rev Neurol* **9**, 513-524 (2013).
152. Foerster, B.R.*, et al.* Diagnostic accuracy using diffusion tensor imaging in the diagnosis of ALS: a meta-analysis. *Acad Radiol* **19**, 1075-1086 (2012).
153. Peretti-Viton, P.*, et al.* MRI of the intracranial corticospinal tracts in amyotrophic and primary lateral sclerosis. *Neuroradiology* **41**, 744-749 (1999).
154. Hecht, M.J.*, et al.* MRI-FLAIR images of the head show corticospinal tract alterations in ALS patients more frequently than T2-, T1- and proton-density-weighted images. *J Neurol Sci* **186**, 37-44 (2001).
155. Waragai, M. MRI and clinical features in amyotrophic lateral sclerosis. *Neuroradiology* **39**, 847-851 (1997).
156. Cheung, G.*, et al.* Amyotrophic lateral sclerosis: correlation of clinical and MR imaging findings. *Radiology* **194**, 263-270 (1995).
157. Hofmann, E., Ochs, G., Pelzl, A. & Warmuth-Metz, M. The corticospinal tract in amyotrophic lateral sclerosis: an MRI study. *Neuroradiology* **40**, 71-75 (1998).
158. Rocha, A.J. & Maia Junior, A.C. Is magnetic resonance imaging a plausible biomarker for upper motor neuron degeneration in amyotrophic lateral sclerosis/primary lateral sclerosis or merely a useful paraclinical tool to exclude mimic syndromes? A critical review of imaging applicability in clinical routine. *Arq Neuropsiquiatr* **70**, 532-539 (2012).
159. Ngai, S., Tang, Y.M., Du, L. & Stuckey, S. Hyperintensity of the precentral gyral subcortical white matter and hypointensity of the precentral gyrus on fluid-attenuated inversion recovery: variation with age and implications for the diagnosis of amyotrophic lateral sclerosis. *AJNR Am J Neuroradiol* **28**, 250-254 (2007).
160. Ludolph, A.C.*, et al.* N-isopropyl-p-123I-amphetamine single photon emission computer tomography in motor neuron disease. *Eur Neurol* **29**, 255-260 (1989).
161. Habert, M.O.*, et al.* Brain perfusion imaging in amyotrophic lateral sclerosis: extent of cortical changes according to the severity and topography of motor impairment. *Amyotroph Lateral Scler* **8**, 9-15 (2007).
162. Neary, D.*, et al.* Frontal lobe dementia and motor neuron disease. *J Neurol Neurosurg Psychiatry* **53**, 23-32 (1990).
163. Dalakas, M.C., Hatazawa, J., Brooks, R.A. & Di Chiro, G. Lowered cerebral glucose utilization in amyotrophic lateral sclerosis. *Ann Neurol* **22**, 580-586 (1987).
164. Hatazawa, J., Brooks, R.A., Dalakas, M.C., Mansi, L. & Di Chiro, G. Cortical motor-sensory hypometabolism in amyotrophic lateral sclerosis: a PET study. *J Comput Assist Tomogr* **12**, 630-636 (1988).
165. Abrahams, S.*, et al.* Frontal lobe dysfunction in amyotrophic lateral sclerosis. A PET study. *Brain* **119 (Pt 6)**, 2105-2120 (1996).
166. Cistaro, A.*, et al.* Brain hypermetabolism in amyotrophic lateral sclerosis: a FDG PET study in ALS of spinal and bulbar onset. *Eur J Nucl Med Mol Imaging* **39**, 251-259 (2012).
167. Pagani, M.*, et al.* Functional pattern of brain FDG-PET in amyotrophic lateral sclerosis. *Neurology* **83**, 1067-1074 (2014).
168. Van Laere, K.*, et al.* Value of 18fluorodeoxyglucose-positron-emission tomography in amyotrophic lateral sclerosis: a prospective study. *JAMA Neurol* **71**, 553-561 (2014).

169. Marini, C.*, et al.* A PET/CT approach to spinal cord metabolism in amyotrophic lateral sclerosis. *Eur J Nucl Med Mol Imaging* **43**, 2061-2071 (2016).
170. Yamashita, T.*, et al.* Flow-metabolism uncoupling in the cervical spinal cord of ALS patients. *Neurol Sci* **38**, 659-665 (2017).
171. Belanger, M., Allaman, I. & Magistretti, P.J. Brain energy metabolism: focus on astrocyte-neuron metabolic cooperation. *Cell Metab* **14**, 724-738 (2011).
172. Paganoni, S.*, et al.* Imaging of glia activation in people with primary lateral sclerosis. *Neuroimage Clin* **17**, 347-353 (2018).
173. Alshikho, M.J.*, et al.* Integrated magnetic resonance imaging and [(11) C]-PBR28 positron emission tomographic imaging in amyotrophic lateral sclerosis. *Ann Neurol* **83**, 1186-1197 (2018).
174. Johansson, A.*, et al.* Evidence for astrocytosis in ALS demonstrated by [11C](L)-deprenyl-D2 PET. *J Neurol Sci* **255**, 17-22 (2007).
175. Lloyd, C.M., Richardson, M.P., Brooks, D.J., Al-Chalabi, A. & Leigh, P.N. Extramotor involvement in ALS: PET studies with the GABA(A) ligand [(11)C]flumazenil. *Brain* **123 (Pt 11)**, 2289-2296 (2000).
176. Turner, M.R.*, et al.* [11C]-WAY100635 PET demonstrates marked 5-HT1A receptor changes in sporadic ALS. *Brain* **128**, 896-905 (2005).
177. Kew, J.J.*, et al.* Cortical function in amyotrophic lateral sclerosis. A positron emission tomography study. *Brain* **116 (Pt 3)**, 655-680 (1993).
178. Kollewe, K.*, et al.* Patterns of cortical activity differ in ALS patients with limb and/or bulbar involvement depending on motor tasks. *J Neurol* **258**, 804-810 (2011).
179. Konrad, C.*, et al.* Pattern of cortical reorganization in amyotrophic lateral sclerosis: a functional magnetic resonance imaging study. *Exp Brain Res* **143**, 51-56 (2002).
180. Mohammadi, B., Kollewe, K., Samii, A., Dengler, R. & Munte, T.F. Functional neuroimaging at different disease stages reveals distinct phases of neuroplastic changes in amyotrophic lateral sclerosis. *Hum Brain Mapp* **32**, 750-758 (2011).
181. Schoenfeld, M.A.*, et al.* Functional motor compensation in amyotrophic lateral sclerosis. *J Neurol* **252**, 944-952 (2005).
182. Stanton, B.R.*, et al.* Altered cortical activation during a motor task in ALS. Evidence for involvement of central pathways. *J Neurol* **254**, 1260-1267 (2007).
183. Tessitore, A.*, et al.* Subcortical motor plasticity in patients with sporadic ALS: An fMRI study. *Brain Res Bull* **69**, 489-494 (2006).
184. Kollewe, K., Korner, S., Dengler, R., Petri, S. & Mohammadi, B. Magnetic resonance imaging in amyotrophic lateral sclerosis. *Neurol Res Int* **2012**, 608501 (2012).
185. Brooks, B.R.*, et al.* Functional magnetic resonance imaging (fMRI) clinical studies in ALS--paradigms, problems and promises. *Amyotroph Lateral Scler Other Motor Neuron Disord* **1 Suppl 2**, S23-32 (2000).
186. Verstraete, E. & Foerster, B.R. Neuroimaging as a New Diagnostic Modality in Amyotrophic Lateral Sclerosis. *Neurotherapeutics* **12**, 403-416 (2015).
187. van den Heuvel, M.P. & Hulshoff Pol, H.E. Exploring the brain network: a review on resting-state fMRI functional connectivity. *Eur Neuropsychopharmacol* **20**, 519-534 (2010).
188. Smith, S.M.*, et al.* Correspondence of the brain's functional architecture during activation and rest. *Proc Natl Acad Sci U S A* **106**, 13040-13045 (2009).
189. Damoiseaux, J.S.*, et al.* Consistent resting-state networks across healthy subjects. *Proc Natl Acad Sci U S A* **103**, 13848-13853 (2006).
190. Tedeschi, G.*, et al.* Interaction between aging and neurodegeneration in amyotrophic lateral sclerosis. *Neurobiol Aging* **33**, 886-898 (2012).
191. Trojsi, F.*, et al.* Functional overlap and divergence between ALS and bvFTD. *Neurobiol Aging* **36**, 413-423 (2015).

192. Mohammadi, B., *et al.* Changes of resting state brain networks in amyotrophic lateral sclerosis. *Exp Neurol* **217**, 147-153 (2009).
193. Chenji, S., *et al.* Investigating Default Mode and Sensorimotor Network Connectivity in Amyotrophic Lateral Sclerosis. *PLoS One* **11**, e0157443 (2016).
194. Zhou, F., *et al.* Alterations in regional functional coherence within the sensory-motor network in amyotrophic lateral sclerosis. *Neurosci Lett* **558**, 192-196 (2014).
195. Agosta, F., *et al.* Divergent brain network connectivity in amyotrophic lateral sclerosis. *Neurobiol Aging* **34**, 419-427 (2013).
196. Kundu, P., Inati, S.J., Evans, J.W., Luh, W.M. & Bandettini, P.A. Differentiating BOLD and non-BOLD signals in fMRI time series using multi-echo EPI. *Neuroimage* **60**, 1759-1770 (2012).
197. Dipasquale, O., *et al.* Comparing resting state fMRI de-noising approaches using multi- and single-echo acquisitions. *PLoS One* **12**, e0173289 (2017).
198. Menke, R.A.L., Proudfoot, M., Talbot, K. & Turner, M.R. The two-year progression of structural and functional cerebral MRI in amyotrophic lateral sclerosis. *Neuroimage Clin* **17**, 953-961 (2018).
199. Menke, R.A.L., Agosta, F., Grosskreutz, J., Filippi, M. & Turner, M.R. Neuroimaging Endpoints in Amyotrophic Lateral Sclerosis. *Neurotherapeutics*, 1-13 (2016).
200. Turner, M.R., *et al.* Neuroimaging in amyotrophic lateral sclerosis. *Biomark Med* **6**, 319-337 (2012).
201. Shen, D., *et al.* Voxel-Wise Meta-Analysis of Gray Matter Changes in Amyotrophic Lateral Sclerosis. *Front Aging Neurosci* **8**, 64 (2016).
202. Chen, Z. & Ma, L. Grey matter volume changes over the whole brain in amyotrophic lateral sclerosis: A voxel-wise meta-analysis of voxel based morphometry studies. *Amyotroph Lateral Scler* **11**, 549-554 (2010).
203. Agosta, F., *et al.* The cortical signature of amyotrophic lateral sclerosis. *PLoS One* **7**, e42816 (2012).
204. Schuster, C., *et al.* Focal thinning of the motor cortex mirrors clinical features of amyotrophic lateral sclerosis and their phenotypes: a neuroimaging study. *J Neurol* **260**, 2856-2864 (2013).
205. Verstraete, E., *et al.* Structural MRI reveals cortical thinning in amyotrophic lateral sclerosis. *J Neurol Neurosurg Psychiatry* **83**, 383-388 (2012).
206. Schuster, C., *et al.* Longitudinal course of cortical thickness decline in amyotrophic lateral sclerosis. *J Neurol* **261**, 1871-1880 (2014).
207. Walhout, R., *et al.* Cortical thickness in ALS: towards a marker for upper motor neuron involvement. *J Neurol Neurosurg Psychiatry* **86**, 288-294 (2015).
208. Tartaglia, M.C., *et al.* Brain atrophy in primary lateral sclerosis. *Neurology* **72**, 1236-1241 (2009).
209. Rajagopalan, V. & Pioro, E.P. Distinct patterns of cortical atrophy in ALS patients with or without dementia: an MRI VBM study. *Amyotroph Lateral Scler Frontotemporal Degener* **15**, 216-225 (2014).
210. Mezzapesa, D.M., *et al.* Whole-brain and regional brain atrophy in amyotrophic lateral sclerosis. *AJNR Am J Neuroradiol* **28**, 255-259 (2007).
211. Tsujimoto, M., *et al.* Behavioral changes in early ALS correlate with voxel-based morphometry and diffusion tensor imaging. *J Neurol Sci* **307**, 34-40 (2011).
212. Cardenas-Blanco, A., *et al.* Structural and diffusion imaging versus clinical assessment to monitor amyotrophic lateral sclerosis. *Neuroimage Clin* **11**, 408-414 (2016).
213. Kwan, J.Y., Meoded, A., Danielian, L.E., Wu, T. & Floeter, M.K. Structural imaging differences and longitudinal changes in primary lateral sclerosis and amyotrophic lateral sclerosis. *Neuroimage Clin* **2**, 151-160 (2013).

214. Menke, R.A., *et al.* Widespread grey matter pathology dominates the longitudinal cerebral MRI and clinical landscape of amyotrophic lateral sclerosis. *Brain* **137**, 2546-2555 (2014).
215. Jones, D.K., Knosche, T.R. & Turner, R. White matter integrity, fiber count, and other fallacies: the do's and don'ts of diffusion MRI. *Neuroimage* **73**, 239-254 (2013).
216. Blain, C.R., *et al.* A longitudinal study of diffusion tensor MRI in ALS. *Amyotroph Lateral Scler* **8**, 348-355 (2007).
217. Douaud, G., Filippini, N., Knight, S., Talbot, K. & Turner, M.R. Integration of structural and functional magnetic resonance imaging in amyotrophic lateral sclerosis. *Brain* **134**, 3470-3479 (2011).
218. Turner, M.R. & Verstraete, E. What does imaging reveal about the pathology of amyotrophic lateral sclerosis? *Curr Neurol Neurosci Rep* **15**, 45 (2015).
219. Grolez, G., *et al.* The value of magnetic resonance imaging as a biomarker for amyotrophic lateral sclerosis: a systematic review. *BMC Neurol* **16**, 155 (2016).
220. Muller, H.P., *et al.* A large-scale multicentre cerebral diffusion tensor imaging study in amyotrophic lateral sclerosis. *J Neurol Neurosurg Psychiatry* **87**, 570-579 (2016).
221. Sage, C.A., Peeters, R.R., Gorner, A., Robberecht, W. & Sunaert, S. Quantitative diffusion tensor imaging in amyotrophic lateral sclerosis. *Neuroimage* **34**, 486-499 (2007).
222. Iwata, N.K., *et al.* White matter alterations differ in primary lateral sclerosis and amyotrophic lateral sclerosis. *Brain* **134**, 2642-2655 (2011).
223. Iwata, N.K., *et al.* Evaluation of corticospinal tracts in ALS with diffusion tensor MRI and brainstem stimulation. *Neurology* **70**, 528-532 (2008).
224. Stagg, C.J., *et al.* Whole-brain magnetic resonance spectroscopic imaging measures are related to disability in ALS. *Neurology* **80**, 610-615 (2013).
225. Sarica, A., *et al.* The corticospinal tract profile in amyotrophic lateral sclerosis. *Hum Brain Mapp* **38**, 727-739 (2017).
226. Agosta, F., *et al.* Voxel-based morphometry study of brain volumetry and diffusivity in amyotrophic lateral sclerosis patients with mild disability. *Hum Brain Mapp* **28**, 1430-1438 (2007).
227. Li, J., *et al.* A meta-analysis of diffusion tensor imaging studies in amyotrophic lateral sclerosis. *Neurobiol Aging* **33**, 1833-1838 (2012).
228. Menke, R.A., *et al.* Fractional anisotropy in the posterior limb of the internal capsule and prognosis in amyotrophic lateral sclerosis. *Arch Neurol* **69**, 1493-1499 (2012).
229. Nickerson, J.P., *et al.* Linear longitudinal decline in fractional anisotropy in patients with amyotrophic lateral sclerosis: preliminary results. *Klin Neuroradiol* **19**, 129-134 (2009).
230. Zhang, Y., *et al.* Progression of white matter degeneration in amyotrophic lateral sclerosis: A diffusion tensor imaging study. *Amyotroph Lateral Scler* **12**, 421-429 (2011).
231. Prell, T., *et al.* Diffusion tensor imaging patterns differ in bulbar and limb onset amyotrophic lateral sclerosis. *Clin Neurol Neurosurg* **115**, 1281-1287 (2013).
232. Thivard, L., *et al.* Diffusion tensor imaging and voxel based morphometry study in amyotrophic lateral sclerosis: relationships with motor disability. *J Neurol Neurosurg Psychiatry* **78**, 889-892 (2007).
233. Filippini, N., *et al.* Corpus callosum involvement is a consistent feature of amyotrophic lateral sclerosis. *Neurology* **75**, 1645-1652 (2010).
234. Toosy, A.T., *et al.* Diffusion tensor imaging detects corticospinal tract involvement at multiple levels in amyotrophic lateral sclerosis. *J Neurol Neurosurg Psychiatry* **74**, 1250-1257 (2003).

235. Keil, C.*, et al.* Longitudinal diffusion tensor imaging in amyotrophic lateral sclerosis. *BMC Neurosci* **13**, 141 (2012).
236. van der Graaff, M.M.*, et al.* Upper and extra-motoneuron involvement in early motoneuron disease: a diffusion tensor imaging study. *Brain* **134**, 1211-1228 (2011).
237. Sage, C.A.*, et al.* Quantitative diffusion tensor imaging in amyotrophic lateral sclerosis: revisited. *Hum Brain Mapp* **30**, 3657-3675 (2009).
238. Agosta, F.*, et al.* Structural brain correlates of cognitive and behavioral impairment in MND. *Hum Brain Mapp* **37**, 1614-1626 (2016).
239. Senda, J.*, et al.* Progressive and widespread brain damage in ALS: MRI voxel-based morphometry and diffusion tensor imaging study. *Amyotroph Lateral Scler* **12**, 59-69 (2011).
240. Kew, J.J.*, et al.* The relationship between abnormalities of cognitive function and cerebral activation in amyotrophic lateral sclerosis. A neuropsychological and positron emission tomography study. *Brain* **116 (Pt 6)**, 1399-1423 (1993).
241. Abrahams, S.*, et al.* Word retrieval in amyotrophic lateral sclerosis: a functional magnetic resonance imaging study. *Brain* **127**, 1507-1517 (2004).
242. Devinsky, O., Morrell, M.J. & Vogt, B.A. Contributions of anterior cingulate cortex to behaviour. *Brain* **118 (Pt 1)**, 279-306 (1995).
243. Wang, S.*, et al.* Amyotrophic lateral sclerosis: diffusion-tensor and chemical shift MR imaging at 3.0 T. *Radiology* **239**, 831-838 (2006).
244. Valsasina, P.*, et al.* Diffusion anisotropy of the cervical cord is strictly associated with disability in amyotrophic lateral sclerosis. *J Neurol Neurosurg Psychiatry* **78**, 480-484 (2007).
245. Rajagopalan, V., Yue, G.H. & Pioro, E.P. Brain white matter diffusion tensor metrics from clinical 1.5T MRI distinguish between ALS phenotypes. *J Neurol* **260**, 2532-2540 (2013).
246. Agosta, F.*, et al.* A longitudinal diffusion tensor MRI study of the cervical cord and brain in amyotrophic lateral sclerosis patients. *J Neurol Neurosurg Psychiatry* **80**, 53-55 (2009).
247. Wong, J.C.*, et al.* Spatial profiling of the corticospinal tract in amyotrophic lateral sclerosis using diffusion tensor imaging. *J Neuroimaging* **17**, 234-240 (2007).
248. Graham, J.M.*, et al.* Diffusion tensor imaging for the assessment of upper motor neuron integrity in ALS. *Neurology* **63**, 2111-2119 (2004).
249. Ellis, C.M.*, et al.* Diffusion tensor MRI assesses corticospinal tract damage in ALS. *Neurology* **53**, 1051-1058 (1999).
250. Ciccarelli, O.*, et al.* Investigation of white matter pathology in ALS and PLS using tract-based spatial statistics. *Hum Brain Mapp* **30**, 615-624 (2009).
251. Sach, M.*, et al.* Diffusion tensor MRI of early upper motor neuron involvement in amyotrophic lateral sclerosis. *Brain* **127**, 340-350 (2004).
252. Cardenas-Blanco, A.*, et al.* Central white matter degeneration in bulbar- and limb-onset amyotrophic lateral sclerosis. *J Neurol* **261**, 1961-1967 (2014).
253. Abhinav, K.*, et al.* Use of diffusion spectrum imaging in preliminary longitudinal evaluation of amyotrophic lateral sclerosis: development of an imaging biomarker. *Front Hum Neurosci* **8**, 270 (2014).
254. Budde, M.D. & Annese, J. Quantification of anisotropy and fiber orientation in human brain histological sections. *Front Integr Neurosci* **7**, 3 (2013).
255. Bede, P. The histological correlates of imaging metrics: postmortem validation of in vivo findings. *Amyotroph Lateral Scler Frontotemporal Degener*, 1-4 (2019).
256. Caverzasi, E.*, et al.* Neurite Orientation Dispersion and Density Imaging Color Maps to Characterize Brain Diffusion in Neurologic Disorders. *J Neuroimaging* **26**, 494-498 (2016).

257. Zhang, H., Schneider, T., Wheeler-Kingshott, C.A. & Alexander, D.C. NODDI: practical in vivo neurite orientation dispersion and density imaging of the human brain. *Neuroimage* **61**, 1000-1016 (2012).
258. Chung, A.W., Seunarine, K.K. & Clark, C.A. NODDI reproducibility and variability with magnetic field strength: A comparison between 1.5 T and 3 T. *Hum Brain Mapp* **37**, 4550-4565 (2016).
259. Grussu, F.*, et al.* Neurite dispersion: a new marker of multiple sclerosis spinal cord pathology? *Ann Clin Transl Neurol* **4**, 663-679 (2017).
260. Grussu, F., Schneider, T., Zhang, H., Alexander, D.C. & Wheeler-Kingshott, C.A. Neurite orientation dispersion and density imaging of the healthy cervical spinal cord in vivo. *Neuroimage* **111**, 590-601 (2015).
261. Billiet, T.*, et al.* Age-related microstructural differences quantified using myelin water imaging and advanced diffusion MRI. *Neurobiol Aging* **36**, 2107-2121 (2015).
262. Merluzzi, A.P.*, et al.* Age-dependent differences in brain tissue microstructure assessed with neurite orientation dispersion and density imaging. *Neurobiol Aging* **43**, 79-88 (2016).
263. Nazeri, A.*, et al.* Functional consequences of neurite orientation dispersion and density in humans across the adult lifespan. *J Neurosci* **35**, 1753-1762 (2015).
264. Winston, G.P.*, et al.* Advanced diffusion imaging sequences could aid assessing patients with focal cortical dysplasia and epilepsy. *Epilepsy Res* **108**, 336-339 (2014).
265. Adluru, G.*, et al.* Assessment of white matter microstructure in stroke patients using NODDI. *Conf Proc IEEE Eng Med Biol Soc* **2014**, 742-745 (2014).
266. Song, Y.K.*, et al.* A study of neurite orientation dispersion and density imaging in wilson's disease. *J Magn Reson Imaging* **48**, 423-430 (2018).
267. Billiet, T.*, et al.* Characterizing the microstructural basis of "unidentified bright objects" in neurofibromatosis type 1: A combined in vivo multicomponent T2 relaxation and multi-shell diffusion MRI analysis. *Neuroimage Clin* **4**, 649-658 (2014).
268. Kamagata, K.*, et al.* Neurite orientation dispersion and density imaging in the substantia nigra in idiopathic Parkinson disease. *Eur Radiol* **26**, 2567-2577 (2016).
269. Zhang, J.*, et al.* In vivo characterization of white matter pathology in pre-manifest Huntington's disease. *Ann Neurol* (2018).
270. Parker, T.D.*, et al.* Cortical microstructure in young onset Alzheimer's disease using neurite orientation dispersion and density imaging. *Hum Brain Mapp* **39**, 3005-3017 (2018).
271. Colgan, N.*, et al.* Application of neurite orientation dispersion and density imaging (NODDI) to a tau pathology model of Alzheimer's disease. *Neuroimage* **125**, 739-744 (2016).
272. Broad, R.J.*, et al.* Neurite orientation and dispersion density imaging (NODDI) detects cortical and corticospinal tract degeneration in ALS. *J Neurol Neurosurg Psychiatry* (2018).
273. Wen, J.*, et al.* Neurite density is reduced in the presymptomatic phase of C9orf72 disease. *J Neurol Neurosurg Psychiatry* (2018).
274. Bouyagoub, S., Clarke, C.L., Wood, T.C., Zhang, H. & Cercignani, M. Evaluating NODDI’s a priori □?xed parameters by combining NODDI and mcDESPOT. in *International Society for Magnetic Resonance in Medicine (ISMRM)* (Honolulu, HI, USA, 2017).
275. Fukutomi, H.*, et al.* Neurite imaging reveals microstructural variations in human cerebral cortical gray matter. *Neuroimage* (2018).

276. Cohen-Adad, J. Microstructural imaging in the spinal cord and validation strategies. *Neuroimage* **182**, 169-183 (2018).
277. Cercignani, M., Dowell, N.G. & Tofts, P. Quantitative MRI of the brain : principles of physical measurement. in *Series in medical physics and biomedical engineering* pages cm. (2018).
278. Carrara, G.*, et al.* A distinct MR imaging phenotype in amyotrophic lateral sclerosis: correlation between T1 magnetization transfer contrast hyperintensity along the corticospinal tract and diffusion tensor imaging analysis. *AJNR Am J Neuroradiol* **33**, 733-739 (2012).
279. da Rocha, A.J.*, et al.* Detection of corticospinal tract compromise in amyotrophic lateral sclerosis with brain MR imaging: relevance of the T1-weighted spin-echo magnetization transfer contrast sequence. *AJNR Am J Neuroradiol* **25**, 1509-1515 (2004).
280. Tanabe, J.L.*, et al.* Reduced MTR in the corticospinal tract and normal T2 in amyotrophic lateral sclerosis. *Magn Reson Imaging* **16**, 1163-1169 (1998).
281. Cosottini, M.*, et al.* Mapping cortical degeneration in ALS with magnetization transfer ratio and voxel-based morphometry. *PLoS One* **8**, e68279 (2013).
282. Cosottini, M.*, et al.* Magnetization transfer imaging demonstrates a distributed pattern of microstructural changes of the cerebral cortex in amyotrophic lateral sclerosis. *AJNR Am J Neuroradiol* **32**, 704-708 (2011).
283. Levesque, I.R.*, et al.* Quantitative magnetization transfer and myelin water imaging of the evolution of acute multiple sclerosis lesions. *Magn Reson Med* **63**, 633-640 (2010).
284. Liu, Z.*, et al.* Magnetization transfer ratio measures in normal-appearing white matter show periventricular gradient abnormalities in multiple sclerosis. *Brain* **138**, 1239-1246 (2015).
285. Amann, M.*, et al.* Magnetization transfer ratio in lesions rather than normal-appearing brain relates to disability in patients with multiple sclerosis. *J Neurol* **262**, 1909-1917 (2015).
286. Moll, N.M.*, et al.* Multiple sclerosis normal-appearing white matter: pathology-imaging correlations. *Ann Neurol* **70**, 764-773 (2011).
287. Davies, G.R.*, et al.* Increasing normal-appearing grey and white matter magnetisation transfer ratio abnormality in early relapsing-remitting multiple sclerosis. *J Neurol* **252**, 1037-1044 (2005).
288. Gracien, R.M.*, et al.* Multimodal quantitative MRI assessment of cortical damage in relapsing-remitting multiple sclerosis. *J Magn Reson Imaging* **44**, 1600-1607 (2016).
289. Samson, R.S.*, et al.* Investigation of outer cortical magnetisation transfer ratio abnormalities in multiple sclerosis clinical subgroups. *Mult Scler* **20**, 1322-1330 (2014).
290. Harrison, N.A.*, et al.* Quantitative Magnetization Transfer Imaging as a Biomarker for Effects of Systemic Inflammation on the Brain. *Biol Psychiatry* **78**, 49-57 (2015).

Chapter 2. Methodology

2.1 Rationale for the Neuroimaging Study

ALS remains a devastating clinical diagnosis with relentless physical, and often cognitive, decline to death within several years on average. Almost 25 years after the drug Riluzole was shown to hold a very modest benefit on survival,[1,2] a raft of promising therapies (perhaps with the exception of Edaravone for which efficacy is supported by limited evidence)[3,4] have sadly been unable to demonstrate disease-modifying effects in patients.[5,6] This is despite a huge expansion in knowledge regarding the genetic aberrations and disrupted intra-cellular, inter-cellular and network processes which are implicated in disease pathogenesis. Efforts are likely to have been hampered by several factors, including the clinical and genetic heterogeneity of the patients enrolled into historical drug trials, the uncertainty of whether target engagement within the nervous system has been achieved, and the lack of objective biomarkers which are able to better inform about efficacy earlier than awaiting patient survival data. For these reasons, new consensus guidelines for use in the design of clinical trials in ALS strongly support the use and development of biomarkers in future studies.[6] Furthermore, candidate biomarkers, be they from blood, cerebrospinal fluid, neurophysiology or neuroimaging, offer unique perspectives on disease mechanisms and would be expected to be optimally informative when used in synergy, although preferably with minimal risk to the patient. Neuroimaging, in particular, permits a structural and functional window into the brain *in vivo*, with the objective not just to identify *that* the tissue is affected but also *how* and *why*, which may itself highlight additional therapeutic avenues. Furthermore, MRI techniques are constantly evolving and a range of novel sequences comprising Neurite Orientation Dispersion and Density Imaging (NODDI), Quantitative Magnetisation Transfer Imaging (qMTi) and Resting State Functional MRI (rsfMRI), for instance, can be captured without the need for additional invasive procedures.

2.2 Study Aims and Original Contribution

The overall neuroimaging study forming the basis of this Doctoral Project has been designed specifically to enable brain MRI scans to be performed on healthy controls and a cohort of newly-diagnosed patients with ALS as they are enrolled into a separate double-blind, placebo-controlled phase II clinical trial called MIROCALS [Modifying Immune Response and Outcomes in ALS: www.mirocals.eu; EudraCT 2015-005347-14; International Standard Randomised Controlled Trial Number (ISRCTN): ISRCTN40093015].

MIROCALS is testing the safety and efficacy of low dose Interleukin-2 (ld-IL-2) in addition to standard daily treatment with oral Riluzole and operating clinically within France and the UK. In line with the theory of neuroinflammatory involvement in the pathogenesis of ALS (as discussed in Section 1.6.3) and the association of higher levels of $CD4^+$ $CD25^+$ $FoxP3^+$ T Regulatory Cells (Tregs) with slower rates of clinical progression,[7-11] ld-IL-2 administered subcutaneously in monthly cycles facilitates expansion of Treg cell numbers. The patients enrolled in MIROCALS will be randomly assigned to receive either treatment with ld-IL-2 or placebo (1:1). Novel features of the MIROCALS trial protocol include the integration of repeated measurements of both blood and cerebrospinal fluid (CSF) 'wet' biomarkers at baseline, 3 months and 7 months, anticipated to reflect target response and efficacy, such as Treg cell and neurofilament levels, respectively, alongside validated clinical measures: the ALS Functional Rating Scale revised (ALSFRS-R) and the Edinburgh Cognitive and Behavioural ALS Screen (ECAS).

The primary aim of the overall neuroimaging study is, therefore, to investigate whether brain MRI in patients with ALS and their associations with selected 'wet' biomarkers or clinical measures can reveal new information regarding the mechanisms and dynamics of neurodegeneration.

In taking full advantage of the repeated measurements of these 'wet' biomarkers in MIROCALS over a 7 month period, the neuroimaging study is also seeking to perform MRI sequential brain scanning in the same patients with **the secondary aim to investigate whether the brain scans are sensitive to change over time and how this additionally relates to clinical and 'wet' biomarker measures.**

Ancillary to MIROCALS, but an encapsulated clinical imaging research study in its own right requiring separate Sponsorship and Ethical approval, the neuroimaging study has a biomarker data-sharing agreement through the MIROCALS study's Chief Investigator (Professor P Nigel Leigh) and Coordinator (Dr Gilbert Bensimon) and the MIROCALS Trial Consortium of allied research teams. However, recruitment of patients and follow-up imaging will continue for as long as MIROCALS is recruiting, with longitudinal clinical data and access to which patients received ld-IL-2 or placebo not available until the very end of the trial to avoid the possibility of 'un-blinding' the intervention groups. This will stretch far beyond the shorter timeframe for this Doctoral Project. **Consequently, the focus for this Doctoral Thesis shall be limited to the cross-sectional "baseline" imaging data acquired through the neuroimaging study (and baseline 'wet' biomarker and clinical data acquired through MIROCALS).**

Nevertheless, the neuroimaging study (and Doctoral Thesis) will constitute the first MRI study undertaken as part of a human drug trial in incident ALS cases in tandem with such a range of fluid biomarkers and clinical outcome measures. Integration of detailed neuroimaging within a clinical trial executed to Good Clinical Practice standards of data assurance and quality control has potential to advance the field significantly through greater understanding of links between MRI parameters and these biological compounds in ALS.

2.3 The Choice of Neuroimaging to study

MRI brain imaging is selected as the neuroimaging modality for this study. Unlike SPECT or PET, MRI is not dependent on radioisotope production and has the advantages of being devoid of potentially harmful ionising radiation or contrast media, safe and well-tolerated, and already well-established for use in studies at our research centre (the Clinical Imaging Sciences Centre; CISC). MRI sequences sensitive to alterations in both tissue microstructure and function would be considered ideal to maximise the information yielded from each scan, particularly in the context of the 'wet' biomarker data from MIROCALS.

Diffusion imaging is the only quantitative MRI technique sensitive to the configuration of neurite microstructure and has been extensively explored in ALS, primarily with diffusion tensor imaging (DTI).[12] Fractional anisoptropy (FA) from DTI is reliably reduced within motor areas of the corpus callosum (CC), corticospinal tracts (CSTs) and precentral gyri (PCGs) in patients with ALS but the exact changes in tissue microstructure or macromolecular composition it reflects are unclear. Given that NDI and ODI parameters from NODDI are considered to more closely infer the nature of microstructural change compared to FA and diffusivity indices from DTI,[13] and the recent evidence that NDI may be more sensitive to change in ALS than FA,[14,15] NODDI is chosen as the principal modality for this Doctoral Project. Nevertheless, the NODDI acquisition protocol enables the diffusion tensor model to be fitted to the data retrospectively such that FA and its relationships to novel biomarkers can be rightly explored. NODDI parameters can also be calculated using different values for the intrinsic free diffusivity (ID) constant.

qMTi is yet to be investigated in patients with ALS. Furthermore, its sensitivity to changes in macromolecular content and composition within the brain following inflammatory

events render it an intriguing imaging modality in the context of this project whose patients are being administered ld-IL-2 to potentially modify the peripheral (and thence central nervous system) immune environment. In addition, qMTi acquisition alongside NODDI permits axonal g-ratio (the ratio of axon diameter to its ensheathing myelin) to be estimated which would be entirely new within ALS imaging research and help gather evidence for whether abnormal myelination contributes to the disease.[16] G-ratio is further discussed in Chapter 7.

rsfMRI enables functional connectivity within the brain to be investigated without the need for additional task performance, thereby eliminating inter-subject effort variability, and independent data-driven analyses can be used to generate reproducible resting-state networks. Although rsfMRI captured using single-echo (SE-rsfMRI) acquisition has been performed previously in ALS, this neuroimaging study will be the first to utilise multi-echo rsfMRI acquisition (ME-rsfMRI) which has been shown to minimise artefact from non-BOLD 'noise' signal compared to standard de-noising methods.[17] Furthermore, the ME-rsfMRI analysis pipeline will also output an optimally-combined time-series (before removal of non-BOLD signal components) thus enabling the benefits of de-noising to be evaluated by comparing it against the fully de-noised time-series.

Standard qualitative structural images including the T1-weighted Magnetisation Prepared Rapid Acquisition Gradient Echo (MPRAGE) scan are essential for the alignment and processing of rsfMRI and qMTi data, but are themselves able to yield analyses of cortical thickness and brain morphometry which are often regionally altered in the disease.[18] T1- and T2-weighted image contrasts are also useful for the qualitative assessment by clinical radiologists, relevant in the case of unexpected findings. **An imaging protocol comprising conventional unenhanced T1/MPRAGE and T2 sequences alongside NODDI, qMTi and rsfMRI sequences within the brain has, therefore, been undertaken within the neuroimaging study**, constituting the same content and total duration (50 minutes) previously tolerated by patients with ALS at our research centre.[14]

2.4.1 Participant Sample Size: Cross-sectional Study

Two new cohorts of participants are required in the neuroimaging study to address the primary aim:

- a group of **"New Patients"** with ALS who are also enrolled into the MIROCALS trial (see Section 2.10.1 - the ANNALS-QuICT study) who undergo a baseline scan and a repeat scan, after an appropriate interval. Given that DTI has been reported to demonstrate changes within the motor system over 6-8 months,[19-22] and the repeat sampling of blood and CSF 'wet' biomarkers in MIROCALS will occur at baseline (Inclusion), after 3 months (upon randomisation to 'treatment') and at 7 months (after 4 months on 'treatment'), **the scans will be performed as close to MIROCALS Inclusion and after Month 7**. See Figure 2.10.1 for schematic timeline.

- a group of age-matched healthy **"New Controls"** for comparison (see Section 2.10.2 - the MultiNICS study) who will undergo imaging once, given that longitudinal studies of DTI in healthy controls have demonstrated no appreciable change over a period of 6-8 months.[22,23]

At the time of prospectively planning estimates of required group sizes, no prior studies had been published using our primary imaging outcome, NODDI, in ALS. Power calculations were thus based on previous diffusion tensor imaging (DTI) MRI analyses from Blain et al.[23] on the basis that fractional anisotropy (FA) and mean diffusivity (MD) parameters derived from DTI were broadly equivalent to neurite density index (NDI) and orientation dispersion index (ODI) derived from NODDI. Using their study's normally-distributed data with $Z\alpha$ set at 1.96 (corresponding to a type I error of 5%) and a power

of 80% (Zβ set at 0.842) the group size was calculated as **24.5 per group**. Preliminary cross-sectional data analyses using NODDI in patients with ALS have subsequently shown highly significant changes in imaging parameters with a sample size of 16 subjects in each group[24,25] followed by a full analysis comprising 23 patients and 23 controls,[14] thus confirming our original power calculation estimate of around 24-25 subjects per group for the cross-sectional (baseline) analyses. Only participants recruited to MIROCALS in the UK will be considered for the neuroimaging study. Furthermore, the UK Centres are anticipated to include 72-90 of the 240 envisaged participant total, meaning that a minimum a take-up for the neuroimaging study of roughly 33% would be sufficient to meet the primary aim.

To meet the primary aim of the neuroimaging study (and of the Doctoral Thesis):
23-25 New Patients with ALS and 23-25 age-matched New Controls are required

2.4.2 Participant Sample Size: Longitudinal Study

The secondary aim of the neuroimaging study will be addressed essentially through a pilot study. No longitudinal NODDI and qMTi studies (and only one small study using single-echo rsfMRI)[26] have been performed in patients with ALS [and certainly none using these MRI modalities to detect a therapeutic drug response].

Longitudinal studies in ALS patient cohorts with DTI report attrition rates due to drop-out (or even death) throughout a 6-12 period to be between 25-60%.[19,23,27,28] By virtue of the neuroimaging study design, MRI brain scans will be separated minimally by 5 and maximally by 9 months, allowing for reasonable leeway in arranging attendances (see 2.10.1 for schematic timeline), and in line with the interval periods in studies using DTI.[19-

[22] Indeed, longitudinal change within the CST has been reported repeating DTI within as few as 7-15 subjects[19,20] and so an anticipated baseline group size of 23-25 patients and controls would remain justified. Thus, the primary and secondary aims of the neuroimaging study will be met with a 33% recruitment from UK MIROCALS participants.

Although the Doctoral Thesis will not focus on a possible ld-IL-2 treatment effect for the reasons outlined above, with respect to planning the wider neuroimaging study in the context of MIROCALS, the patient group recruited for brain imaging will comprise participants randomised to receive ld-IL-2 and those assigned to receive placebo. Taking into account the inevitable division of the patient group into a presumed roughly equal split and the estimated longitudinal patient attrition rate of up to 60%, also presumed to affect the placebo and ld-IL-2 groups equally, the neuroimaging study will therefore aim to recruit up to 2 x 25 = 50 patients from MIROCALS to maximise treatment group sizes.

To meet the secondary aim of the neuroimaging study
(beyond the scope of the Doctoral Thesis):
23-25 patients with ALS from a maximum of 50 with an attrition rate of <60%
between scans and 23-25 age-matched healthy controls are required

2.5 Historical Cohort of Patients and Controls

23 patients with ALS recruited from Brighton and Sussex University Hospitals NHS Trust and 23 appropriately age-matched healthy controls have recently been recruited within a cross-sectional imaging study at our research centre (the Clinical Imaging Sciences Centre, CISC). The scans were conducted using identical MRI protocols and the same scanning machine, with clinical measures undertaken. Inclusion Criteria for imaging were: El Escorial definite, probable, laboratory-supported or possible ALS; age 18 to 70 years-of-age; FVC>60% predicted; unrestricted length of disease. Although these patients with ALS will not have been part of the MIROCALS trial, and thus will have no fluid biomarker data, they will enable extended group comparisons to be made with respect to relationships with markers of clinical severity. These groups shall be referred to from here on as the "**Historical Patients**" and "**Historical Controls**", respectively.

In order to interpret and discuss entirely novel associations between imaging parameters and blood immune cells in the cohort of New Patients aligned to MIROCALS, and to explore why differences between patient cohorts may arise, it has been decided to demonstrate the group comparisons between the Patient groups and their respective Control groups separately. The patient groups will be combined to enable extended comparisons with respect to relationships between imaging parameters and markers of clinical severity held in common.

2.6.1 Primary outcome Measures

The primary outcome measures from the overall neuroimaging study are quantitative data parameters from cross-sectional scans in patients with ALS and healthy controls in this order of preference to maximise complete data sets for diffusion, followed by qMTi and then rsfMRI modalities across all participants:

- **High resolution T1/MPRAGE** to enable essential processing steps for the remaining MRI sequences and to calculate cortical thickness.
- **DTI** parameter: Fractional Anisotropy [FA];
- **NODDI** parameters: Orientation Dispersion Index [ODI], Neurite Density Index [NDI] and Isotropic Volume Fraction [ISO]. Calculated with the intrinsic diffusivity (ID) constant set to:
    - 1.7×10^{-9} $m^2.s^{-1}$ **"NODDI 1.7"** for white matter parameters;
    - 1.1×10^{-9} $m^2.s^{-1}$ **"NODDI 1.1"** for grey matter parameters.[29,30]
- **qMTi** parameters: the bound proton fraction [f-value], forward-exchange rate constant [kf value] and T_2 of free water component [T_2f value];
    - **MRI G-ratio** calculated using the NDI and ISO from NODDI, and the f-value from qMTi;[31]
- **ME-rsfMRI** temporal fluctuations in BOLD signal in order to measure functional connectivity and generate resting state networks;

The Doctoral Thesis shall focus only on the baseline diffusion (**DTI and NODDI**) and **qMTi** scans and their relationships to baseline clinical measures and 'wet' biomarker data available from MIROCALS. From hereon the Methodology will be tailored to this.

2.6.2 Clinical and Fluid Biomarker Measures available for the Doctoral Thesis

Clinical and fluid biomarker measures in patients with ALS will be provided for the neuroimaging study under the data sharing agreement with the MIROCALS Consortium and include their Inclusion (baseline):

- ALS Functional Rating Scale revised (ALSFRS-R)
- Edinburgh Cognitive and Behavioural ALS Screen (ECAS)
- Duration of disease
- Rate of disease progression
- Baseline total blood CD4 count, total blood $CD4^+$ $CD25^+$ $FoxP3^+$ (Treg) count, or the Treg:CD4 ratio. Lymphocyte data provided courtesy of Dr Timothy Tree (Reader in Immunology, Department of Immunobiology, King's College London). *Additional blood and cerebrospinal fluid biomarkers will not be available until un-blinding of the MIROCALS trial.*

2.7 Research Questions for the Doctoral Thesis

The Doctoral Thesis seeks to address the following fundamental questions to enlighten the understanding of the mechanisms of neurodegeneration in ALS:

1. Are there significant differences in brain FA, NODDI and qMTi, measurements between patients with ALS and healthy controls, and what aspects of tissue change might they represent? **

2. Is NODDI processed with intrinsic diffusivity (ID) assumed = 1.1 x 10^{-9} $m^2.s^{-1}$ ["NODDI 1.1"] able to more readily detect changes in the grey matter (notably the PMCs but also the deep grey matter structures such as the thalamus) compared to "NODDI 1.7"? **

3. Does the total blood CD4 count, total blood $CD4^+$ $CD25^+$ $FoxP3^+$ Treg count, or the Treg:CD4 Ratio demonstrate significant associations with brain FA, NODDI and qMTi parameters in patients with ALS? ***

4. How do clinical measures including ALSFRS, Disease Duration, Rate of Progression, and ECAS relate to brain FA, NODDI and qMTi parameters in patients with ALS? **

5. In light of the above, what further studies would enable clarification of the relevance and basis of these MRI changes in the brain?

** Analysis of both the **New** and **Historical** participant cohorts can be explored.

*** Analysis of the **New** participant cohorts only.

2.8 Outline of analysis techniques & principal brain Regions of Interest (ROIs)

Whole brain image analysis enables both grey and white matter regions of significant difference between patients and controls to be ascertained without stipulating any *a priori* hypotheses and has been utilised in numerous studies in ALS.[20,21,32-35] However, a greater correction for multiple comparisons across voxels is required compared to a more hypothesis-driven **ROI analysis**, but which itself might overlook other areas affected by the disease. Although ROI-analysis can be performed in native space, standardisation implies that both approaches require the participants' scans to be warped (or "normalised") into a "standard" space so that cohorts of scans can be meaningfully compared. However, potential discrepancies in true anatomical alignment may result from this warping. Furthermore, there is a variability regarding some image pre-processing practices such as "smoothing" which aims to increase signal-to-noise.

A technique of **Tract Based Spatial Statistics (*TBSS*)** has been proposed to address these challenges as a more consistent like-with-like comparison of brain regions between subjects. TBSS creates a group-specific "skeleton" of the principal brain white matter tracts onto which the subject's particular imaging parameter is then projected (described below in 2.12.2), and has been undertaken widely in studies using DTI in ALS to investigate tract 'integrity'.[36-43] The number of voxels compared between participants, and thus correction for multiple comparisons, is minimised and, similarly to whole brain analyses, voxels from across the entire parameter "skeleton" can be compared or restricted to a pre-selected ROI.

Although reductions in FA using whole brain or TBSS analyses are most consistently seen between patients and controls within the motor pathways of the corpus callosum (CC) and bilateral corticospinal tracts (CSTs) extending into the precentral gyri (PCGs), there is some uncertainty as to the tissue microstructural or macromolecular changes FA represent. Relationships to clinical measures have also been variable, reflective of the clinical heterogeneity. The first study using NODDI at the whole brain level in symptomatic ALS was recently been undertaken,[14] although NODDI TBSS has not been performed. Furthermore, qMTi has not been explored in patients with ALS and potential associations between FA, NODDI or qMTi across the brain and CD4 cell populations is a novel undertaking.

In order to optimise interpretation of NODDI and qMTi analyses in light of the more established DTI changes in ALS, image analysis will be performed using:

- **Whole Brain** parameter maps;
- **TBSS** skeletonised parameters;
- Parameters within **Regions of Interest** (ROIs):

"**Motor ROIs**" = Corpus Callosum +
Bilateral CSTs (extending into the subcortical white matter of the PCGs) +
Bilateral Precentral Motor Cortices.

"**PCGs ROI**" = Precentral Motor Cortices only.

The parameter maps for FA, NODDI and qMTi will not undergo any form of Gaussian smoothing throughout the study. The spatial extent of NODDI (particularly using TBSS) and qMTi change are unknown and may be more focal than those seen previously with FA, albeit this approach may increase the likelihood of false positive results.

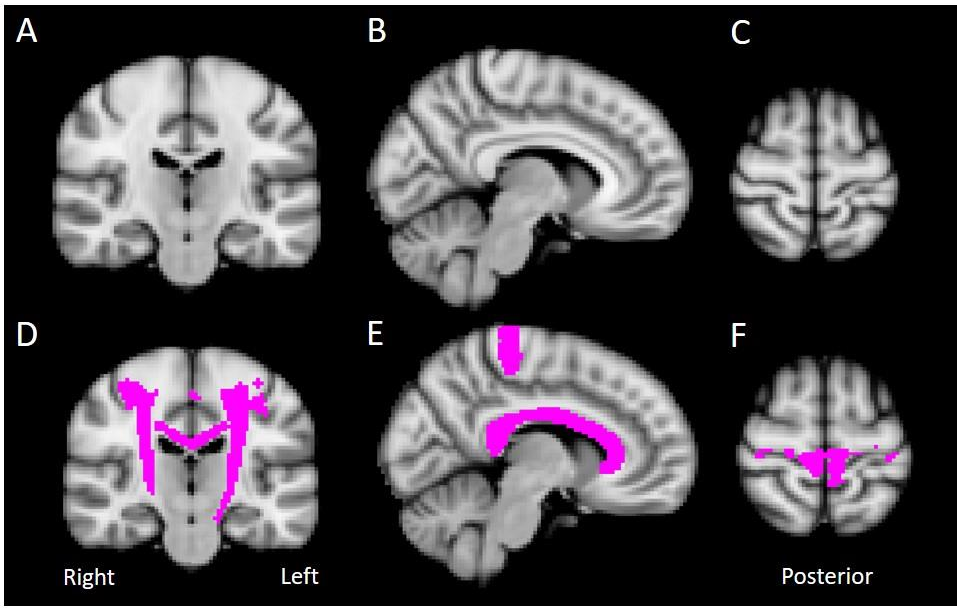

Figure 2.8.1. **Whole brain and ROI analyses.** Diffusion and qMTi parameters are selected across the whole brain (represented by T1 images in standard MNI space in A-C) or restricted to within the Motor ROIs mask (inclusive of the precentral gyri, corpus callosum and bilateral corticospinal tracts in purple D-F).

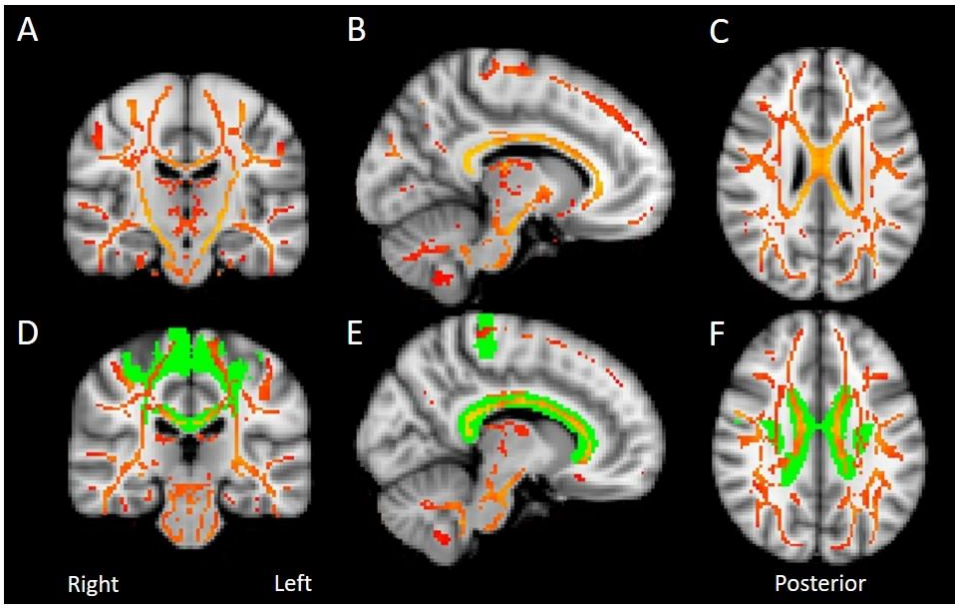

Figure 2.8.2. **TBSS and TBSS ROI analyses.** Skeletonised diffusion and qMTi parameters are selected across the entire TBSS skeleton (in red/yellow overlain onto T1 brain images in standard MNI space in A-C) or restricted to within the Motor ROIs mask (demonstrated in green D-F).

2.9 Hypotheses

2.9.1 Group Comparisons: brain FA and NODDI parameters are predicted to show significant differences between patients with ALS compared to controls in the baseline scans. Specifically it is hypothesised that:

(i) DTI: FA will be reduced within the CSTs, CCs, PCGs and PMCs using whole brain, TBSS and Motor ROIs analyses.

(ii) NODDI with ID 1.7 (optimised for white matter): in line with recently published NODDI in ALS:[14,15] NDI will be reduced within the CSTs, CC, PCGs white matter and PMCs; ODI reduced within the PMCs and PCGs white matter, and reduced/unchanged within the CSTs and CC; ISO unchanged in these areas although may be increased in peri-ventricular white matter[14] (see Table 2.9.1.1).

(iii) NODDI with ID 1.1 (optimised for grey matter): parameter changes will be as above for NODDI 1.7 but change more evident in the PMCs using NODDI 1.1 (see Table 2.9.1.2).

Brain Area	FA	NDI	ODI	ISO
CSTs	↓	↓	↔/↓	↔
CC	↓	↓	↔/↓	↔
PCGs white matter	↓	↓	↓	↔
PMCs (PCGs ROI)	↓	↓	↓	↔

Table 2.9.1.1. Hypotheses for FA + NODDI 1.7 in patients relative to controls within motor areas.

Brain Area		NDI	ODI	ISO
CSTs		↓	↔/↓	↔
CC		↓	↔/↓	↔
PCGs white matter		↓	↓	↔
PMCs (PCGs ROI)		↓	↓	↔

Table 2.9.1.2. Hypotheses for NODDI 1.1 in patients relative to controls within motor areas.

2.9.2 **Group Comparisons**: brain qMTi parameters will show significant differences between patients with ALS compared to controls in the baseline scans. Specifically it is hypothesised that:

(i) as ALS is not considered to be a demyelinating disease, **f** will be unchanged in the white matter, or possibly reduced owing to loss of myelinated CST fibres.

(ii) **kf** may be expected to be reduced in the white matter given kf decreases in demyelinating inflammatory lesions[44] although may, conversely, be raised in the grey matter given the response to a mild peripheral (systemic) immune challenge.[45]

(iii) **T2f** may be increased in the CST, CC and PCGs due to increased free water content secondary to inflammatory responses or tissue disruption. See Table 2.9.2.1.

Brain Area	f	Kf	T2f
CSTs	↓/↔	↓	↑/↔
CC	↓/↔	↓	↑/↔
PCGs	↓/↔	↓	↑/↔
PMCs (PCGs ROI)	↓/↔	↑/↔	↑/↔

Table 2.9.2.1. Hypotheses for qMTi parameters in patients relative to controls

2.9.3 Relationships with Clinical Factors: Brain NODDI, FA, and qMTi parameters from the baseline scans will correlate significantly with the baseline measures of clinical severity, as measured through the ALSFRS-R, disease duration, rate of progression, ECAS and the ECAS ALS Specific sub score.

On the assumption that the *direction* of change in each parameter between patients with the disease and controls without the disease described above (in **1**) are correct, it would be hypothesised that as the *degree* of change becomes greater, the less favourable the clinical picture (such as a lowered ALSFRS score, a longer duration, faster progression and a reduced ECAS score) as in Table 2.9.3.1. However, even if group differences in a certain parameter are not detected, associations with clinical factors within the patient group may still be possible.

	FA	NDI	ODI	ISO	f	kf	T2f
ALSFRS	Pos	Pos	Pos	Neg/ -	Pos/ -	Pos/ -	Neg/ -
Disease duration	Neg	Neg	Neg	Pos/ -	Neg/ -	Neg/ -	Pos/ -
Rate of progression	Neg	Neg	Neg	Pos/ -	Neg/ -	Neg/ -	Pos/ -
ECAS	Pos	Pos	Pos	Neg/-	Pos/ -	Neg/ -	Neg/ -
ECAS ALS Specific	Pos	Pos	Pos	Neg/-	Pos/ -	Neg/ -	Neg/ -

Table 2.9.3.1. Hypotheses FA, NODDI and qMTi parameters versus clinical factors.

2.9.4 Relationships with Blood CD4 cells: brain NODDI, FA, and qMTi parameters from the baseline scans will correlate significantly with the baseline total blood CD4 count, total blood $CD4^+$ $CD25^+$ $FoxP3^+$ Treg count, or the Treg:CD4 ratio.

On the assumption that the *direction* of change in each parameter between patients with the disease and controls without the disease described above (in **1**) are correct, it would be hypothesised that as the *degree* of change becomes greater, the fewer CD4 cells (and specifically the Treg cells) circulating in the blood, as in Table 2.9.4.1. However, even if group differences in a certain parameter are not detected, associations with clinical factors within the patient group may still be possible.

	FA	NDI	ODI	ISO	f	kf	T2f
CD4 count	Pos/ -	Pos/ -	Pos/ -	Neg/ -	Pos/ -	Pos/ -	Neg/ -
$CD4^+$ $CD25^+$ $FoxP3^+$ Tregs	Pos	Pos	Pos	Neg	Pos	Pos	Neg
Treg:CD4 ratio	Pos	Pos	Pos	Neg	Pos	Pos	Neg

Table 2.9.4.1. Hypotheses FA, NODDI and qMTi parameters versus CD4 and Treg cells.

2.10 The Neuroimaging Study: Two Studies in One

For Sponsorship reasons, the neuroimaging study forming the basis of the Doctoral Thesis were split into two:

- The **ANNALS-QuICT** ["Analysing Neuroinflammation and Neurodegeneration in Amyotrophic Lateral Sclerosis (ALS): Quantitative Imaging in a Clinical Trial"] study recruiting patients with ALS from MIROCALS to undergo MRI brain scans as close to the Inclusion *[and Month 7]* timepoint intimately related to the fluid biomarker analysis schedule within MIROCALS (see schematic diagram in Figure 2.10.1). The Sponsor for the MIROCALS study (CHU de Nimes, Paris) is providing Sponsorship for the neuroimaging on patients and Ethical approval achieved as a significant amendment to the MIROCALS protocol.

- The **MultiNICS** ["Multimodal NeuroImaging in Control Subjects"] study recruiting healthy controls to undergo a MRI brain scan once. These subjects have no connection to MIROCALS and are sponsored separately by the University of Sussex with local Ethical approval.

ANNALS-QuICT and MultiNICS have both been conducted at the Clinical Imaging Sciences Centre in Falmer, University of Sussex, Brighton.

2.10.1 Plan of Investigation: *ANNALS-QuICT Study*

Sponsorship and Ethical Approvals

- Ethical approval from the MHRA, HRA and London Central REC for ANNALS-QuICT as a significant amendment to the MIROCALS protocol: ACHIEVED March 2017.
- Sponsorship secured from CHU de Nimes, Paris: ACHIEVED March 2017.
- Funding for participant and carer travel from MNDA: ACHIEVED November 2016 with no-cost extensions January 2018 and March 2019 (until May 2020).
- Site Initiation Visits at UK MIROCALS recruitment sites: ACHIEVED July 2017.

Recruitment. Subjects enrolled into MIROCALS at official MIROCALS recruitment centres in London, Sheffield, Manchester and Brighton are informed of the optional neuroimaging study as part of the MIRCOALS Inclusion Visit protocol. Patients indicating interest provide consent for their contact details (or those of a carer / next-of-kin) to be passed to the ANNALS-QuICT Investigators, Dr Andrew Barritt and Professor Nigel Leigh.

Contact is made by telephone or email, given that patients are recruited from geographically disparate sites across the UK, and each sent: a Welcome Letter; a Patient Information Sheet to explain the purpose of the ANNALS-QuICT study; a Screening Questionnaire to ensure the inclusion and exclusion criteria are satisfied; a MRI Patient Information leaflet; a MRI safety checklist as standard for all patients undergoing scans at the Clinical Imaging Sciences Centre (CISC); and directions to the CISC. A second contact with the participant is arranged so that intent to enrol can be ascertained and any issues highlighted from the MRI safety ANNALS-QuICT information can be addressed

prior to their journey to Sussex. All eligible participants provide formal written consent for their involvement prior to any scan taking place on the same day as their MRI.

Recruitment to ANNALS-QuICT is continuing for as long as MIROCALS is recruiting (from July 2017 and envisaged for 26 months) with follow up scans occurring 5-9 months later. The schematic in Figure 2.10.1 below represents the timeline of follow up scanning for each participant in ANNALS-QuICT, aligned with collection of the fluid biomarkers within MIROCALS. Therefore, the total duration of the neuroimaging study will be 26 + 9 (max) = 35 months. **As discussed, a sub-group analysis on the baseline imaging only is being performed for this Doctoral Thesis.**

Visit One to the CISC: Baseline MRI Brain scans (for Doctoral Thesis)

Participants undergo their baseline scan as soon as possible after Inclusion to MIROCALS (and certainly within the 3 month Riluzole only "run-in" period) and are asked to arrive 20-30 minutes prior to their scheduled appointment time to discuss any further questions and to check through the ANNALS-QuICT Screening Questionnaire, MRI Safety Checklist and the ANNALS-QuICT Consent Form (signed by the patient and Dr Andrew Barritt). One of the Radiographers also confirms MRI safety information with the patient directly. During the scan patients wear ear protection as recommended by the National Institute for Occupational Safety and Health (NIOSH) and lie still without performing any task. The MRI sequences are prioritised over 50 minutes:

1. Conventional T2-weighted and FLAIR imaging (5 minutes).
2. High resolution T1-weighted MPRAGE (7 minutes)
3. NODDI (17 minutes)
4. Quantitative magnetization transfer (12 minutes)
5. resting-state functional MRI (9 minutes)

The participant is reviewed before they leave CISC and feedback on their experience received. A plan to contact them in advance of the follow up scan is made.

Visit Two to the CISC: Follow Up MRI (beyond scope of Doctoral Thesis)

Participants undergo the follow-up scan 4-6 months after randomisation to 'treatment' of either additional ld-IL-2 or placebo. The ANNALS-QuICT Screening Questionnaire and MRI Safety Checklist are re-evaluated and consent confirmed. The MRI sequences are performed exactly as previously.

Inclusion and Exclusion Criteria. For baseline brain MRI within ANNALS-QuICT all participants must fulfil MIROCALS (a-g) and ANNALS-QuICT (h-j) Inclusion Criteria, without satisfying any Exclusion Criteria. For follow-up brain MRI in ANNALS-QuICT all participants must still be enrolled in MIROCALS, continue to satisfy ANNALS-QuICT criteria (h-j).

a. Patients of either sex;
b. 18 to 75 years of age (inclusive);
c. Probable, laboratory probable or definite ALS [El Escorial revised diagnostic criteria];
d. Disease duration ≤ 24 months;
e. Vital capacity ≥ 80% of predicted;
f. No prior or present Riluzole treatment;
g. Patient able to provide signed informed consent;
h. Patient able to lie flat in comfort for up to 50 minutes;
i. No contraindication to MRI such as cardiac pacemaker.
j. Able to journey to the University of Sussex campus in Falmer for the MRI scan.

ANNALS-QuICT Exclusion Criteria

Other causes of neuromuscular weakness; presence of other neurodegenerative diseases; significant cognitive impairment, clinical dementia or psychiatric illness; severe cardiac or pulmonary disease; other diseases precluding functional assessments; contra indication for lumbar puncture; other life-threatening diseases; documented auto-immune disorders except asymptomatic Hashimoto thyroiditis; women of child-bearing age without contraception or pregnant or breast feeding; any clinically significant laboratory abnormality; other concurrent investigational medications; unable to take Riluzole; patient unable to lie flat in comfort for up to 50 minutes for scan; contraindication to MRI such as cardiac pacemaker; patient unable to provide informed consent.

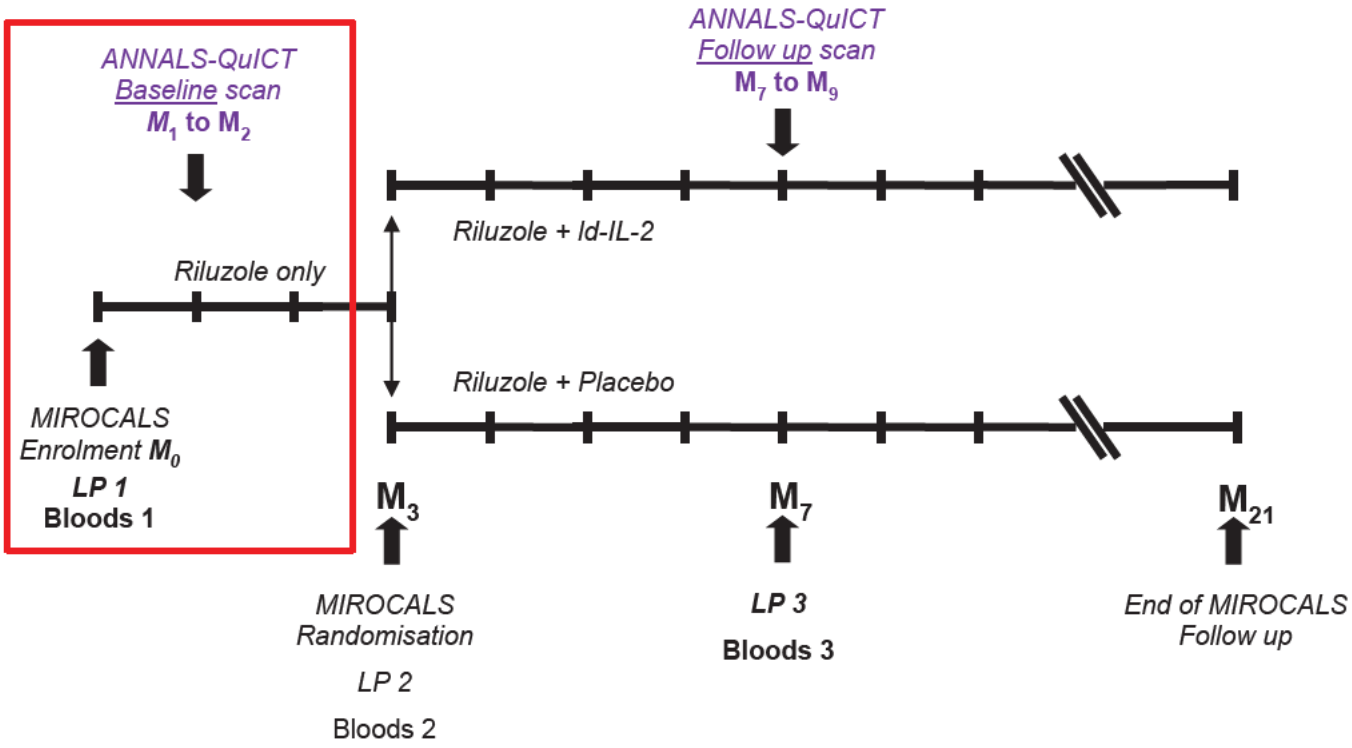

Figure 2.10.1. **Schematic timeline for MRI brain scans in relation to the MIROCALS Trial for an individual participant.** Enrolment to MIROCALS is accompanied by LP and bloods, repeated at month (M) 3 and M7. The baseline MRI brain scan is aimed to occur within M1-M2, and the follow up scan M7-M9 (4-6 months after randomisation to treatment). **The Doctoral Thesis shall only focus on the baseline MRI brain scans and MIROCALS Inclusion clinical + 'wet' biomarker data (red box).**

2.10.2 Plan of Investigation: *MultiNICS Study*

Sponsorship and Ethical Approvals

- Ethical approval from the BSMS RGEC: ACHIEVED January 2017.
- Funding for participant travel from MNDA: ACHIEVED November 2016.
- Minor amendment for no cost increase to sample population: ACHIEVED May 2019.

Recruitment. Healthy subjects have been recruited largely by participation of family members, friends, and contacts of people diagnosed with ALS and is a recruitment method previously proven to be effective in previous studies of patients with ALS conducted at CISC, and also supported by the MND Association.

Participant Experience. Participants for MultiNICS were contacted by telephone, email or in person, sent the approved Information Sheet, Screening Questionnaire to ensure the inclusion and exclusion criteria are satisfied, a MRI Information leaflet and a MRI safety checklist as standard for all patients undergoing scans at Clinical Imaging Sciences Centre (CISC). The scans occurred as in ANNALS-QuICT but only once.

MultiNICS Inclusion Criteria:

a. Participants of either gender;
b. 18 - 75 years of age (inclusive);
c. Participants able to provide signed informed consent;
d. Participants able to lie flat in comfort for up to 50 minutes;
e. No contraindication to MRI such as cardiac pacemaker.
f. Able to journey to the University of Sussex campus for the MRI scan.

MultiNICS Exclusion Criteria as for ANNALS-QuICT but also no diagnosis of ALS/MND.

2.11 MRI acquisition and Data Storage

MRI raw data has been captured over approximately 50 minutes using the 1.5 Tesla Siemens Magnetom Avanto scanner at the Clinical Imaging Sciences Centre (CISC) in the standard Digital Imaging and Communications in Medicine (DICOM) format, and stored anonymously and confidentially on the University of Sussex DICOM server under a unique numerical identifier. The following sequences have been taken:

a. Dual-echo T2-weighted (TEs = 11ms and 86ms; TR=3040ms; echo-train length = 6; field of view = 240 x 210mm^2; matrix = 256 x 224; slice thickness = 5mm);

b. Fast fluid-attenuated inversion recovery (FLAIR) (TE = 89ms, TR = 9720ms; TI = 2578: echo-train length = 16, field of view = 240 x 210mm^2; matrix = 256 x 224; slice thickness = 5mm);

c. Volumetric T1-weighted high resolution MPRAGE (TE = 3.57ms, TR = 2730ms; TI = 100ms; flip angle = 7^0; field of view = 256 x 240mm^2; matrix = 254 x 240; slice thickness = 1mm and voxel size 1 x 1 x 1 mm);

d. Multi-shell diffusion-weighted acquired with single-shot, twice re-focused pulse-gradient spin-echo EPI,[46] using three b values (9 directions for b=300 smm^{-2}, 30 directions with b=800 smm^{-2}, and 60 diffusion directions with b=2400 smm^{-2}), optimised for NODDI.[13] Ten non-diffusion weighted (b=0) volumes are acquired. Additional acquisition parameters are: TE = 99 ms, TR = 8400; field of view = 240 x 240mm^2; matrix = 96 x 96; slice thickness = 2.5mm and voxel size 2.5 x 2.5 x 2.5 mm.

e. Quantitative MT imaging is based on balanced steady-state free precession (bSSFP) model of MT.[47] The acquisition sequence consists of a 3D True Fast Imaging with Steady-state Precession (True FISP) sequence (field of view 240 x 180mm^2, matrix 256 x 96, slices 32, slice thickness = 5 mm) with voxel size 0.9375 x 1.875 x 5mm, modified to allow the duration of the radiofrequency pulse to be varied. Twenty-four volumes are acquired varying either the flip angle (between 5º and 40º) or the repetition time (between 3.66ms and 5.96ms) and the pulse duration. In addition, 3D fast low-angle shot (FLASH) volumes are acquired for T1-mapping, with repetition time 30ms and echo time 5ms. The excitation flip angles are varied between volumes (5º, 15º, 25º). The same field of view, matrix, and number of slices as the True FISP are used.

f. [Resting state functional MRI consisting of 200 volumes of a multiple gradient-echo echo planar imaging (EPI) T2*-weighted sequence (TR = 2570 ms; TEs = 15, 34, 54ms; flip angle = 90°; matrix size = 64 x 64; field of view = 31 axial slices; field of view 236mm thickness 4.5mm, interslice gap 0mm) and voxel size 3.3 x 3.3 x 3.3 mm are obtained. Subjects are instructed to lie with their eyes open and not think about anything in particular during the scan.] *Analysis and results reported outside of this Thesis.*

2.12 Image Processing and Computation of Parametric Maps for NODDI and qMTi

Diffusion MRI: NODDI. The raw data DICOM files are converted to NifTi format using *mcverter* (available from the Lewis Centre for Neuroimaging, University of Oregon) then corrected for eddy-current distortions and for involuntary movement, using the following pipeline: a "within-b-value" co-registration is performed, and average b=0, b=300, b=800, and b=2400 images created for the concatenated DWI image files; each of these averages is co-registered to the mean b=0 image to obtain the transformation matching them; each DW volume is then realigned to the mean DW image with the same b-value, and the final transformation matching each DW volume with the b=0 image obtained by combining the matrices from either step. The b-matrices are rotated accordingly.[48] The resulting data are analysed using the software implemented in *Matlab* and distributed by the developers of NODDI (http://www.nitrc.org/projects/noddi_toolbox) to yield NDI, ODI, and ISO maps for each participant (as per Zhang et al. 2012).[13] For parameter maps destined predominantly for white matter statistical analyses the intrinsic free water diffusivity is set at 1.7 x 10^{-9} $m^2.s^{-1}$ whereas parameter maps predominantly for grey matter analyses are generated with a slightly less generous intrinsic free water diffusivity of 1.1 x 10^{-9} $m^2.s^{-1}$ prior to normalisation.[29,30] Finally, subject-specific NODDI parameter maps were warped into the Montreal Neurological Institute (MNI)152 standard 2mm space using Advanced normalisation Tools (*ANTS*) and *WarpImageMultiTransform 3* ready for whole brain and region of interest (ROI) statistical analyses using *randomise_parallel* as outlined below in Section 2.12.1.

Diffusion MRI: DTI. The raw data DICOM files are converted to NifTi format using *mcverter*. FA parameter maps are generated by applying a diffusion tensor model to each voxel within the NODDI b vectors and b values files (corrected for eddy-current distortions and involuntary movement) using FSL *DTIFIT* software. Pre-normalised maps

were used for Tract Based Spatial Statistics (TBSS; see below). Subject-specific FA maps were non-linearly warped into the MNI152 standard space using the same transformation matrices as used for the NODDI maps in Advanced normalisation Tools (*ANTS*), ready for whole brain and ROI statistical analyses using Randomise (see below).

qMTi. The raw data DICOM files are converted to NifTi format using *mcverter*. The T1/MPRAGE are segmented into white and gray matter and cerebrospinal fluid using Statistical Parametric Mapping (*SPM;* version 12) to yield a parenchymal mask. The "True FISP" (Trufi format) steady-state coherent files, in which *balanced gradients* are used along all three axes, and gradient-echo structural images are realigned to subject-specific T1/MPRAGE space using SPM12 (Wellcome Trust Centre for Neuroimaging, University College London, UK; http://www.fil.ion.ucl.ac.uk/spm). A T1 map was calculated for all data sets by fitting the theoretical spoiled gradient-echo as a function of the flip angle to the signal measured by the three-dimensional fast low-angle shot sequences. The qMTi parameters are then calculated by performing a voxel-wise nonlinear least-squares fitting (Levenberg-Marquardt method) to a binary spin bath model for balanced steady-state free precession.[47] The quantitative maps are then masked to remove background noise and warped into (MNI)152 standard 1mm space using *ANTS* and the segmentation deformation fields ready for whole brain and region of interest (ROI) statistical analyses using Randomise (see below).

2.12.1 Whole Brain and ROI Statistical Analyses

Whole brain voxel-based analysis enables regions of significant difference between subjects to be ascertained without stipulating any *a priori* hypotheses, although does require a greater correction for multiple comparisons than ROI analysis. Both methods have been selected to look for differences between patients with ALS and controls, in addition to associations between patients' MRI parameters and clinical/biomarker measures by performing permutation-based non-parametric statistical analyses to safeguard against the possibility that MRI parameter distributions between subjects are non-Gaussian, in line with previous studies.[36,40,49-51] The Juelich Histological Atlas (JHU) was used to produce either a whole brain (grey and white matter) or Motor ROI (the CSTs, corpus callosum and PCGs) mask with 25% probability thresholds in Montreal Neurological Institute standard space.

5000 permutations within the framework of the general linear model (*Glm*; FMRIB Software Library version 6.0), and with age as a co-variate throughout, were undertaken on 4D group-wise image files for FA, NODDI and qMTi using *randomise_parallel* (FSL software) and applying threshold-free cluster enhancement (TFCE) in 3 dimensions as the test statistic. TFCE optimises detection of clusters of voxels within the imaging data without needing to specify cluster-defining characteristics in advance.[52] A statistical significance threshold of $p<0.05$ after correction for multiple comparisons [family-wise error (FWE)] was used. Therefore, the output 1-p image was thresholded at 0.95(min)-1.0(max) with the summary p value referring to the voxel with the maximum significance across the cluster(s). The anatomical location all cluster maxima separated by at least 8mm was then calculated in MNI space (co-ordinates in mm), along with its size (K) in voxels and individual maximum significance, using *Cluster* and the Juelich Histological Atlas in *Atlasquery* (FSL software).

2.12.2 Tract Based Spatial Statistics (TBSS) and Statistical Analyses.

Given the potential discrepancies in anatomical alignment after using standard normalisation techniques when aiming to compare parameters in specific areas between subjects, and the variability in parameter smoothing practices to increase signal to noise, Tract Based Spatial Statistics (*TBSS*) was proposed as a way to identify areas of commonality (in the principal brain white matter tracts) amongst subjects on which to project the subject specific imaging parameters for more consistent like-with-like comparison. By means of an adaptation to the original FSL TBSS processing pipeline,[53] the ANTS-normalised FA maps were merged using *fslmerge* and used to create a mean FA image and brain mask in *fslmaths*. Using *tbss_skeleton,* the mean FA image was thinned to create a mean FA 'skeleton' representative of the centres of the main white matter tracts common to the group and a threshold of 0.2 applied following visual inspection in *fslview* to exclude voxels with poor tract correspondence or of low likelihood of being representative of white matter. Each subject's aligned FA data was projected onto this mean skeleton to create a 4D image file. Once the TBSS pipeline had been performed on the FA parameter maps, the non-FA parameter maps from NODDI (generated using intrinsic diffusivity set to 1.7×10^{-9} $m^2.s^{-1}$) and qMTi were similarly skeletonised utilising the masks created for the FA images, although mean FA data files needed to be 'upsampled' into 1mm cubed voxel size using *flirt* prior to qMTi parameters skeletonisation. The 4D skeletonised parameter files were then entered into voxel-wise statistical analysis using *randomise_parallel*, but this time applying TFCE in 2 dimensions only (as recommended for TBSS).[51,54] P values were considered significant if ≤0.05 after correction for multiple comparisons at the cluster level.

2.12.3 Precentral cortex thickness as a co-variate in NODDI ID=1.1 analyses

Given the potential for precentral cortical thinning in patients with ALS[55-59] and for potential variation in parameter calculation within cortical structures due to partial voluming with white matter or CSF,[30,60] cortical reconstruction and volumetric segmentation was performed within the FreeSurfer image analysis suite (v.6.0.0 freely available for download at http://surfer.nmr.mgh.harvard.edu/) using the T1 MPRAGE files in order to calculate average thickness of the precentral cortex for each participant. An average of the left and right cortices was taken. These values were then entered as a co-variate within Glm (FMRIB Software Library version 6.0) permutation testing using TFCE for analyses using NODDI ID=1.1 which found significant voxel clusters within the primary motor cortices.

Other potential co-variates such as handedness and gender were not included in the statistical analyses as they have been found elsewhere not to significantly influence MRI diffusion parameters in ALS.[60,61]

2.12.4 Quantification of Parameters within Significant Clusters

For those TFCE comparisons at the Whole Brain, TBSS or Motor ROIs levels which revealed significant results, the corresponding 1-p image was itself converted into a mask using *fslmaths* to threshold at 0.95 and to binarise the remaining (significant) voxels within the clusters. This mask then enabled the mean (μ) parameter value and its standard deviation (σ) within the same clusters to be individually calculated from each of the participants' 3D images in *fslstats*.

For comparisons between patients and controls, the group parameter means from each group were plotted graphically with error bars for the 95% confidence intervals using IBM SPSS Statistics (SPSS; version 24). Each group's μ and σ were used to calculate the **Cohen's *d* measure of effect size** using the following formula:

$$\text{Cohen's } d = [\mu_2 - \mu_1] / \sqrt{[(\sigma_1^2 + \sigma_2^2) / 2]}$$

For associations between patients' mean imaging parameters and their clinical factors or blood CD4 cell groups, Tukey Boxplots of the mean parameter values within the significant cluster were produced and inspected for outliers. Outlier values lying >1.5 x Interquartile Range (IQR) were designated an asterisk small circle, whereas an asterisk denoted extreme outliers >3.0 x IQR. These outliers were removed prior to displaying the values against the relevant clinical/biochemical measure on a scatterplot, performing Regression analyses, plotting the regression line and calculating the adjusted R^2 using SPSS.

2.13 Subject Demographics and Clinical Data for Doctoral Thesis

2.13.1 Totals of "New Participants" Recruited to ANNALS-QuICT and MultiNICS

- ANNALS-QuICT patients with El-Escorial definite, probable or laboratory-supported ALS ("**New Patients**"): n=23 (17 men and 6 women; median age 59 years; mean age 58 years with standard deviation 9.7; range 31–70 years) were recruited in total for the Doctoral Thesis, of whom 23 have complete data sets for DTI (FA) and NODDI, and 20 have complete data sets for qMTi owing to a technical issue affecting several scans. The mean time from Inclusion to MIROCALS and the baseline MRI scan in ANNALS-QuICT was 39 days in both these data sets of n=20 and n=23.

- MultiNICS subjects ("**New Controls**"): n=27 (14 men and 13 women; median age 65 years; mean age 63.5 years with standard deviation 6.8; range 47–72 years) were recruited in total. Several early scans were also affected by the technical issue with qMTi and additional participants were offered scans. Thus, all 27 of these participants have complete data sets for Structural MRI, NODDI and rsfMRI, and 24 have complete data sets for qMTi owing to a technical issue affecting several scans.

Each subsequent results chapter details the exact participants whose brain scans are used in each of the analyses with full demographic and clinical information.

References

1. Bensimon, G., Lacomblez, L. & Meininger, V. A controlled trial of riluzole in amyotrophic lateral sclerosis. ALS/Riluzole Study Group. *N Engl J Med* **330**, 585-591 (1994).
2. Lacomblez, L., Bensimon, G., Leigh, P.N., Guillet, P. & Meininger, V. Dose-ranging study of riluzole in amyotrophic lateral sclerosis. Amyotrophic Lateral Sclerosis/Riluzole Study Group II. *Lancet* **347**, 1425-1431 (1996).
3. Safety and efficacy of edaravone in well defined patients with amyotrophic lateral sclerosis: a randomised, double-blind, placebo-controlled trial. *Lancet Neurol* **16**, 505-512 (2017).
4. Al-Chalabi, A.*, et al.* July 2017 ENCALS statement on edaravone. *Amyotroph Lateral Scler Frontotemporal Degener* **18**, 471-474 (2017).
5. Pandya, R.S.*, et al.* Therapeutic neuroprotective agents for amyotrophic lateral sclerosis. *Cell Mol Life Sci* **70**, 4729-4745 (2013).
6. van den Berg, L.H.*, et al.* Revised Airlie House consensus guidelines for design and implementation of ALS clinical trials. *Neurology* **92**, e1610-e1623 (2019).
7. Beers, D.R.*, et al.* Endogenous regulatory T lymphocytes ameliorate amyotrophic lateral sclerosis in mice and correlate with disease progression in patients with amyotrophic lateral sclerosis. *Brain* **134**, 1293-1314 (2011).
8. Henkel, J.S.*, et al.* Regulatory T-lymphocytes mediate amyotrophic lateral sclerosis progression and survival. *EMBO Mol Med* **5**, 64-79 (2013).
9. Menon, P.*, et al.* Regulatory T cells in amyotrophic lateral sclerosis: A role for disease modulation. *J Clin Neurosci* **21**, 2050 (2014).
10. Schwartz, M. & Baruch, K. Breaking peripheral immune tolerance to CNS antigens in neurodegenerative diseases: boosting autoimmunity to fight-off chronic neuroinflammation. *J Autoimmun* **54**, 8-14 (2014).
11. Zhao, W., Beers, D.R. & Appel, S.H. Immune-mediated mechanisms in the pathoprogression of amyotrophic lateral sclerosis. *J Neuroimmune Pharmacol* **8**, 888-899 (2013).
12. Turner, M.R.*, et al.* Neuroimaging in amyotrophic lateral sclerosis. *Biomark Med* **6**, 319-337 (2012).
13. Zhang, H., Schneider, T., Wheeler-Kingshott, C.A. & Alexander, D.C. NODDI: practical in vivo neurite orientation dispersion and density imaging of the human brain. *Neuroimage* **61**, 1000-1016 (2012).
14. Broad, R.J.*, et al.* Neurite orientation and dispersion density imaging (NODDI) detects cortical and corticospinal tract degeneration in ALS. *J Neurol Neurosurg Psychiatry* (2018).
15. Wen, J.*, et al.* Neurite density is reduced in the presymptomatic phase of C9orf72 disease. *J Neurol Neurosurg Psychiatry* (2018).
16. Barritt, A.W., Gabel, M.C., Cercignani, M. & Leigh, P.N. Emerging Magnetic Resonance Imaging Techniques and Analysis Methods in Amyotrophic Lateral Sclerosis. *Front Neurol* **9**, 1065 (2018).
17. Dipasquale, O.*, et al.* Comparing resting state fMRI de-noising approaches using multi- and single-echo acquisitions. *PLoS One* **12**, e0173289 (2017).
18. Shen, D.*, et al.* Voxel-Wise Meta-Analysis of Gray Matter Changes in Amyotrophic Lateral Sclerosis. *Front Aging Neurosci* **8**, 64 (2016).
19. Keil, C.*, et al.* Longitudinal diffusion tensor imaging in amyotrophic lateral sclerosis. *BMC Neurosci* **13**, 141 (2012).
20. Sage, C.A., Peeters, R.R., Gorner, A., Robberecht, W. & Sunaert, S. Quantitative diffusion tensor imaging in amyotrophic lateral sclerosis. *Neuroimage* **34**, 486-499 (2007).

21. Zhang, Y.*, et al.* Progression of white matter degeneration in amyotrophic lateral sclerosis: A diffusion tensor imaging study. *Amyotroph Lateral Scler* **12**, 421-429 (2011).
22. van der Graaff, M.M.*, et al.* Upper and extra-motoneuron involvement in early motoneuron disease: a diffusion tensor imaging study. *Brain* **134**, 1211-1228 (2011).
23. Blain, C.R.*, et al.* A longitudinal study of diffusion tensor MRI in ALS. *Amyotroph Lateral Scler* **8**, 348-355 (2007).
24. Broad, R.*, et al.* Neurite Orientation Dispersion and Density Imaging (NODDI) demonstrates microstructural changes associated with Amyotrophic Lateral Sclerosis. in *MNDA Symposium* (Orlando, Florida, 2015).
25. Broad, R.*, et al.* Neurite Orientation Dispersion and Density Imaging: Correlation Analysis in Amyotrophic Lateral Sclerosis. in *MNDA Symposium* (Dublin, Ireland, 2016).
26. Menke, R.A.L., Proudfoot, M., Talbot, K. & Turner, M.R. The two-year progression of structural and functional cerebral MRI in amyotrophic lateral sclerosis. *Neuroimage Clin* **17**, 953-961 (2018).
27. Agosta, F.*, et al.* A longitudinal diffusion tensor MRI study of the cervical cord and brain in amyotrophic lateral sclerosis patients. *J Neurol Neurosurg Psychiatry* **80**, 53-55 (2009).
28. de Albuquerque, M.*, et al.* Longitudinal evaluation of cerebral and spinal cord damage in Amyotrophic Lateral Sclerosis. *Neuroimage Clin* **14**, 269-276 (2017).
29. Bouyagoub, S., Clarke, C.L., Wood, T.C., Zhang, H. & Cercignani, M. Evaluating NODDI's a priori □?xed parameters by combining NODDI and mcDESPOT. in *International Society for Magnetic Resonance in Medicine (ISMRM)* (Honolulu, HI, USA, 2017).
30. Fukutomi, H.*, et al.* Neurite imaging reveals microstructural variations in human cerebral cortical gray matter. *Neuroimage* (2018).
31. Stikov, N.*, et al.* In vivo histology of the myelin g-ratio with magnetic resonance imaging. *Neuroimage* **118**, 397-405 (2015).
32. Agosta, F.*, et al.* Voxel-based morphometry study of brain volumetry and diffusivity in amyotrophic lateral sclerosis patients with mild disability. *Hum Brain Mapp* **28**, 1430-1438 (2007).
33. Iwata, N.K.*, et al.* White matter alterations differ in primary lateral sclerosis and amyotrophic lateral sclerosis. *Brain* **134**, 2642-2655 (2011).
34. Muller, H.P.*, et al.* A large-scale multicentre cerebral diffusion tensor imaging study in amyotrophic lateral sclerosis. *J Neurol Neurosurg Psychiatry* **87**, 570-579 (2016).
35. Sach, M.*, et al.* Diffusion tensor MRI of early upper motor neuron involvement in amyotrophic lateral sclerosis. *Brain* **127**, 340-350 (2004).
36. Cardenas-Blanco, A.*, et al.* Structural and diffusion imaging versus clinical assessment to monitor amyotrophic lateral sclerosis. *Neuroimage Clin* **11**, 408-414 (2016).
37. Ciccarelli, O.*, et al.* Investigation of white matter pathology in ALS and PLS using tract-based spatial statistics. *Hum Brain Mapp* **30**, 615-624 (2009).
38. Douaud, G., Filippini, N., Knight, S., Talbot, K. & Turner, M.R. Integration of structural and functional magnetic resonance imaging in amyotrophic lateral sclerosis. *Brain* **134**, 3470-3479 (2011).
39. Menke, R.A.L., Agosta, F., Grosskreutz, J., Filippi, M. & Turner, M.R. Neuroimaging Endpoints in Amyotrophic Lateral Sclerosis. *Neurotherapeutics*, 1-13 (2016).

40. Sage, C.A., *et al.* Quantitative diffusion tensor imaging in amyotrophic lateral sclerosis: revisited. *Hum Brain Mapp* **30**, 3657-3675 (2009).
41. Stagg, C.J., *et al.* Whole-brain magnetic resonance spectroscopic imaging measures are related to disability in ALS. *Neurology* **80**, 610-615 (2013).
42. Alruwaili, A.R., *et al.* A combined tract-based spatial statistics and voxel-based morphometry study of the first MRI scan after diagnosis of amyotrophic lateral sclerosis with subgroup analysis. *J Neuroradiol* **45**, 41-48 (2018).
43. Alruwaili, A.R., *et al.* Tract integrity in amyotrophic lateral sclerosis: 6-month evaluation using MR diffusion tensor imaging. *BMC Med Imaging* **19**, 19 (2019).
44. Levesque, I.R., *et al.* Quantitative magnetization transfer and myelin water imaging of the evolution of acute multiple sclerosis lesions. *Magn Reson Med* **63**, 633-640 (2010).
45. Harrison, N.A., *et al.* Quantitative Magnetization Transfer Imaging as a Biomarker for Effects of Systemic Inflammation on the Brain. *Biol Psychiatry* **78**, 49-57 (2015).
46. Reese, T.G., Heid, O., Weisskoff, R.M. & Wedeen, V.J. Reduction of eddy-current-induced distortion in diffusion MRI using a twice-refocused spin echo. *Magn Reson Med* **49**, 177-182 (2003).
47. Gloor, M., Scheffler, K. & Bieri, O. Quantitative magnetization transfer imaging using balanced SSFP. *Magn Reson Med* **60**, 691-700 (2008).
48. Leemans, A. & Jones, D.K. The B-matrix must be rotated when correcting for subject motion in DTI data. *Magn Reson Med* **61**, 1336-1349 (2009).
49. Cardenas-Blanco, A., *et al.* Central white matter degeneration in bulbar- and limb-onset amyotrophic lateral sclerosis. *J Neurol* **261**, 1961-1967 (2014).
50. Filippini, N., *et al.* Corpus callosum involvement is a consistent feature of amyotrophic lateral sclerosis. *Neurology* **75**, 1645-1652 (2010).
51. Menke, R.A., *et al.* Fractional anisotropy in the posterior limb of the internal capsule and prognosis in amyotrophic lateral sclerosis. *Arch Neurol* **69**, 1493-1499 (2012).
52. Smith, S.M. & Nichols, T.E. Threshold-free cluster enhancement: addressing problems of smoothing, threshold dependence and localisation in cluster inference. *Neuroimage* **44**, 83-98 (2009).
53. Smith, S.M., *et al.* Tract-based spatial statistics: voxelwise analysis of multi-subject diffusion data. *Neuroimage* **31**, 1487-1505 (2006).
54. FSL. TBSS User Guide. (https://fsl.fmrib.ox.ac.uk/fsl/fslwiki/TBSS/UserGuide).
55. Agosta, F., *et al.* The cortical signature of amyotrophic lateral sclerosis. *PLoS One* **7**, e42816 (2012).
56. Schuster, C., *et al.* Focal thinning of the motor cortex mirrors clinical features of amyotrophic lateral sclerosis and their phenotypes: a neuroimaging study. *J Neurol* **260**, 2856-2864 (2013).
57. Schuster, C., *et al.* Longitudinal course of cortical thickness decline in amyotrophic lateral sclerosis. *J Neurol* **261**, 1871-1880 (2014).
58. Verstraete, E., *et al.* Structural MRI reveals cortical thinning in amyotrophic lateral sclerosis. *J Neurol Neurosurg Psychiatry* **83**, 383-388 (2012).
59. Walhout, R., *et al.* Cortical thickness in ALS: towards a marker for upper motor neuron involvement. *J Neurol Neurosurg Psychiatry* **86**, 288-294 (2015).
60. Schmitz, J., *et al.* Hemispheric asymmetries in cortical gray matter microstructure identified by neurite orientation dispersion and density imaging. *Neuroimage* **189**, 667-675 (2019).
61. Toosy, A.T., *et al.* Diffusion tensor imaging detects corticospinal tract involvement at multiple levels in amyotrophic lateral sclerosis. *J Neurol Neurosurg Psychiatry* **74**, 1250-1257 (2003).

Chapter 3. Results: FA from Diffusion Imaging in ALS

In this first results chapter, cross-sectional image analysis of fractional anisotropy (FA) from diffusion tensor imaging (DTI) within the New and Historical cohorts of participants will be presented, including the differences between patients with ALS and healthy controls, relationships with measures of clinical severity in patients and the completely novel associations with 'wet' blood biomarkers [CD4 cells and Regulatory T Cells (Tregs)] in the New Patients. FA is a well-established diffusion MRI parameter found across many studies to be reduced within motor areas of the corpus callosum (CC), corticospinal tracts (CSTs) and precentral gyri (PCGs) in patients with ALS. Nevertheless, there is some ambiguity as to the tissue microstructural or macromolecular alterations the change in FA may represent, as discussed in Chapters 1 and 2. FA analyses, therefore, constitute a logical prelude to the subsequent chapters presenting NODDI (Chapter 4) and novel qMTi (Chapter 5) analyses in these patients from which it is aimed to understand more about the nature of the parameter changes revealed. The findings will ultimately be discussed in Chapter 7.

As described in Chapter 2, non-parametric permutation testing with age included as a co-variate throughout using Threshold-Free Cluster Enhancement (TFCE) was undertaken to identify clusters of voxels whose parameters significantly differed between groups or in association with clinical and 'wet' biomarker blood measures:

- At Whole Brain level;
- Using skeletonised parameters through Tract Based Spatial Statistics (TBSS);
- Within the Motor ROIs. This analysis was performed voxel-wise within the search volume defined by the motor ROIs mask either as a whole, or skeletonised;

Rate of disease progression was included as a covariate in analyses involving the 'wet' biomarker blood cell levels. P value outputs within each analysis are quoted with correction for multiple comparisons at cluster level and considered significant where $p \leq 0.05$.

Participants

Sections 3.1-3.3: 23 patients with El Escorial definite, probable or laboratory-supported ALS recruited within ANNALS-QuICT (mean age 58.0 years; n=17 male; n=20 limb onset) and 24 healthy controls recruited within MultiNICS (mean age 62.4 years; n=11 male). FA was calculated using *dtifit*, as described in Chapter 2. Demographics and patients' clinical characteristics are summarised in Table 3a with statistical analyses performed SPSS. Shapiro-Wilk Testing revealed statistical evidence of non-normality in age distribution in patients (p=0.02). A Mann-Whitney U (MWU) Test demonstrated no significant differences in group medians (p=0.1). A Pearson-Chi Square test, however, demonstrated a borderline statistical difference of gender mix differences between the two groups (p=0.05).

Sections 3.4-3.5: 23 Historical patients with El Escorial definite, probable or laboratory-supported ALS (mean age 64.4 years; n=16 male; n=20 limb onset) and 23 Historical healthy controls (mean age 61.5 years; n=14 male). Shapiro-Wilk Testing revealed evidence of non-normality in patients' age distribution (p=0.002). MWU Test confirmed no significant differences in group medians (p=0.286). A Pearson-Chi Square test demonstrated no significantly different gender mix (p=0.536). See Table 3b.

Section 3.6: all 46 participants with ALS. Evidence of non-normality was found in one or other group and so non-parametric tests were employed throughout. The New Patient group were younger than the Historical patients by a mean 6.4 years (MWU p=0.008), had significantly shorter disease duration by a mean 7.2 months (MWU p=0.004) and less impaired function on the ALSFRS by a mean 3 points (MWU p=0.018). The gender mix, sites of onset, rates of disease progression, total ECAS and ALS-specific ECAS sub scores did not differ significantly between patient groups (see Table 3c).

	MultiNICS Healthy Controls [n=24]§	ANNALS-QuICT Patients with ALS [n=23]	Statistics
Age in years Mean (SD) Range Median	 62.4 (6.5) 47-71 65	 58 (9.7) 31-70 59	**Shapiro-Wilk Test** Controls: p=0.074 ALS: p=0.022 **MWU Test** p=0.096
Sex Male Female	 11 13	 17 6	Pearson Chi-Square p=0.05
Disease site of onset Limb Bulbar		 20 3	
Disease duration Mean (SD) Range Median		 12.1 (6.4) 4-23 10	
Total ALSFRS (max. 48) Mean (SD) Range Median		 43 (3.2) 34-47 44	
Rate of change of ALSFRS* Mean (SD) Range Median		 0.5 (0.43) 0.09-1.83 0.33	
Total ECAS (max.136) Mean (SD) Range Median		 111.8 (13.7) 77-132 116	
ALS-specific ECAS (max.100)† Mean (SD) Range Median		 82.8 (11.6) 57-98 86	
Blood Treg cell levels Mean absolute Tregs (SD) Range Median Mean absolute CD4 (SD) Range Median Mean % of total CD4 (SD) Range Median		 707.3 (385.8) 303 - 1679 576 10843 (5144) 4384 - 22783 9525 6.72 (2.51) 4.07 - 15.50 5.8	
MIROCALS inclusion to scan Mean days (SD) Range Median		 39.7 (19.8) 7-84 36	

Table 3a. New Participant demographics and clinical characteristics for diffusion (FA and NODDI) MRI analyses. *MWU=Mann Whitney U Test; * points lost per month duration; † sub-total of language, verbal fluency and executive scores.*

	Historical Controls [n=23]	Historical Patients with ALS [n=23]	Statistical Comparison
Age in years Mean (SD) Range Median	 61.5 (9.3) 43-76 64	 64.4 (8.0) 45-73 67	**Shapiro-Wilk Test** Controls: p=0.162 ALS: p=0.002 **Mann-Whitney U Test** p=0.286
Sex Male Female	 14 9	 16 7	Pearson Chi-Square p=0.536
Disease site of onset Limb Bulbar		 20 3	
Disease duration (months) Mean (SD) Range Median		 19 (8.9) 9-39 17	
Total ALSFRS (max. 48) Mean (SD) Range Median		 40 (5.2) 25-46 40	
Rate of change of ALSFRS* Mean (SD) Range Median		 0.44 (0.29) 0.09-1.33 0.37	
Total ECAS (max.136) Mean (SD) Range Median		 112.5 (13.7) 83-135 113	
ALS-specific ECAS (max.100)† Mean (SD) Range Median		 86.0 (8.8) 65-100 87	

Table 3b. Historical Participant demographics and clinical characteristics for diffusion (FA and NODDI) MRI analyses. *MWU=Mann Whitney U Test; * points lost per month duration; † sub-total of language, verbal fluency and executive scores.*

	Historical Patients with ALS [n=23]	ANNALS-QuICT Patients with ALS [n=23]	Statistical Comparison
Age in years Mean (SD) Range Median	 64.4 (8.0) 45-73 67	 58.0 (9.7) 31-70 59	**Shapiro-Wilk Test** Historical: p=0.002 ANNALS: p=0.022 **MWU Test p=0.008**
Sex: Male Female	 16 7	 17 6	Pearson Chi-Square p=0.743
Site of onset Limb Bulbar	 20 3	 20 3	Pearson Chi-Square p=1.0
Disease duration Mean (SD) Range Median	 19.3 (8.9) 9-39 17	 12.1 (6.4) 4-23 10	**Shapiro-Wilk Test** Historical: p=0.025 ANNALS: p=0.037 **MWU Test p=0.004** Cohen's *d* **= 0.93**
Total ALSFRS (max. 48) Mean (SD) Range Median	 40 (5.2) 25-46 40	 43 (3.2) 34-47 44	**Shapiro-Wilk Test** Historical: p=0.023 ANNALS: p=0.016 **MWU Test p=0.018** Cohen's *d* **= 0.69**
Rate of change of ALSFRS* Mean (SD) Range Median	 0.44 (0.29) 0.1-1.33 0.37	 0.5 (0.43) 0.09-1.83 0.33	**Shapiro-Wilk Test** Historical: p=0.001 ANNALS: p=0.000 **MWU Test p=0.93**
Total ECAS (max.136) Mean (SD) Range Median	 112.5 (13.7) 83-135 113	 111.8 (13.7) 77-132 116	**Shapiro-Wilk Test** Historical: p=0.76 ANNALS: p=0.016 **MWU Test p=0.97**
ALS-specific ECAS (max.100)† Mean (SD) Range Median	 86.0 (8.8) 65-100 87	 82.8 (11.6) 57-98 86	**Shapiro-Wilk Test** Historical: p=0.27 ANNALS: p=0.008 **MWU Test p=0.44**

Table 3c. New and Historical Patient demographics and clinical characteristics for diffusion (FA and NODDI) MRI analyses. The groups demonstrated statistically significant differences in age, disease duration and functional impairment as measured by ALSFRS. Histograms of the distribution of values are shown in Figure 3d. *MWU = Mann Whitney U Test; * = points lost per month duration; † = sub-total of language, verbal fluency and executive scores.*

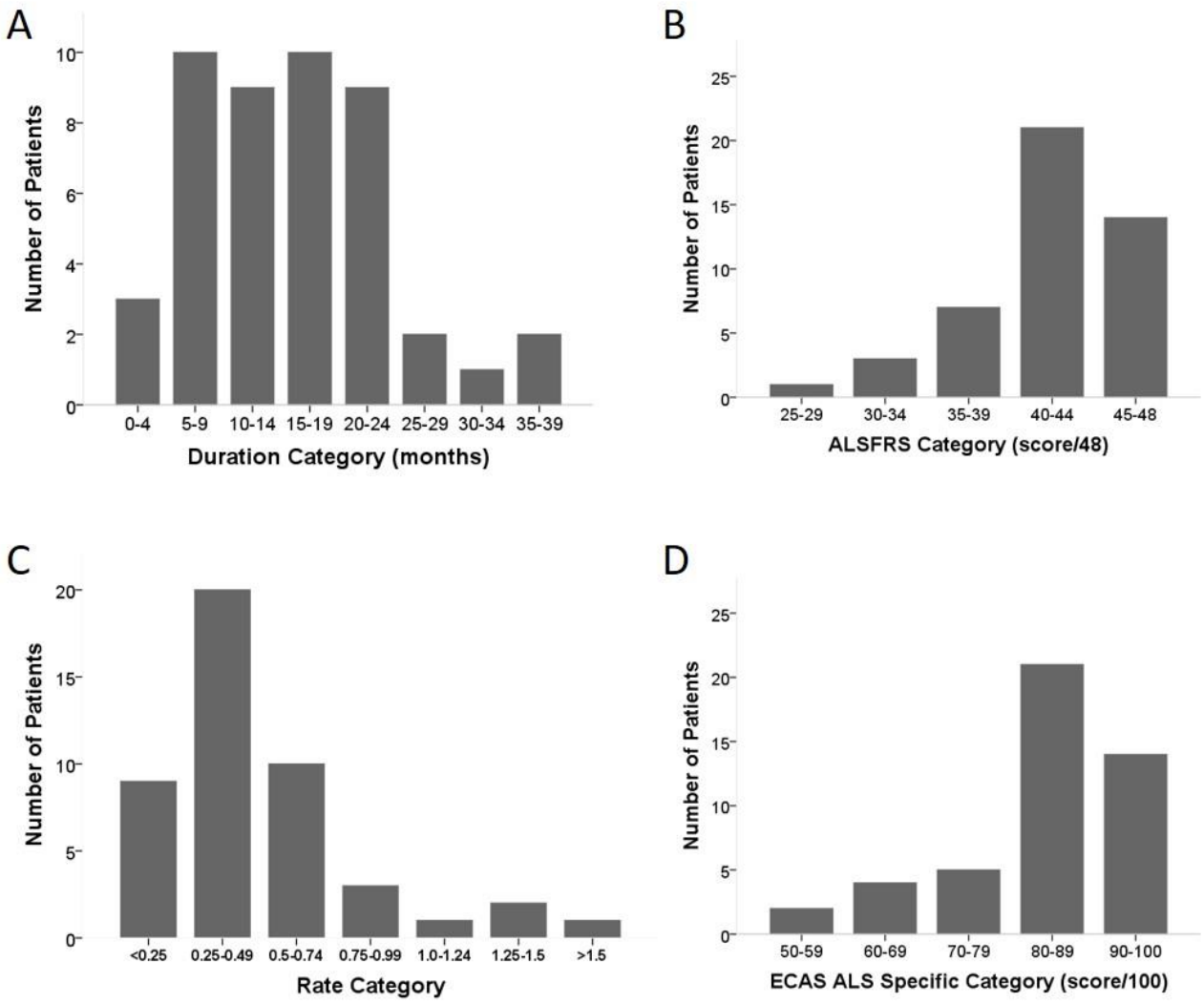

Figure 3d. **Spread of clinical factors across combined New and Historical Patients** showing histograms of categorised variables for the disease duration (A), ALSFRS (B), Rate of progression (C) and the ECAS ALS Specific score (D).

3.1 Group Differences: FA in New Patients versus New Controls

Whole brain and Motor ROIs. A significant decrease in FA (p=0.03) in patients compared to controls was seen within the CSTs and left CC body (Fig. 3.1.2 A-C) following Motor ROIs analysis, and confirmed using quantification of the mean FA within these regions (Fig. 3.1.2 D). No other comparative decreases or increases in FA were seen (Table 3.4.1).

TBSS and TBSS Motor ROIs. A significant decrease (p=0.045) in skeletonised FA within the rostral CSTs and CC was seen in patients compared to controls (Fig. 3.1.3 A-C), and again (p=0.013) following analysis using the Motor ROIs mask (Fig. 3.1.3 D-F), also confirmed using quantification of the mean FA within these regions (Fig. 3.1.3 G and H, respectively). Cohen's *d* effect sizes were 0.99 and 0.85, respectively. No other comparative differences in FA were seen (Table 3.1.1).

Table 3.1.1	FA in New Patients vs New Controls			
	Whole Brain	Motor ROIs	TBSS Entire Skeleton	TBSS Motor ROIs
Controls>ALS		p=0.032	p=0.045	p=0.013
ALS>Controls				

Table 3.1.1. **Summary of significant group differences in FA between the New Patients and Controls** using TFCE at Whole brain, Motor ROIs, TBSS and TBSS Motor ROIs levels. The main finding is of reduced FA within the CC and CSTs.

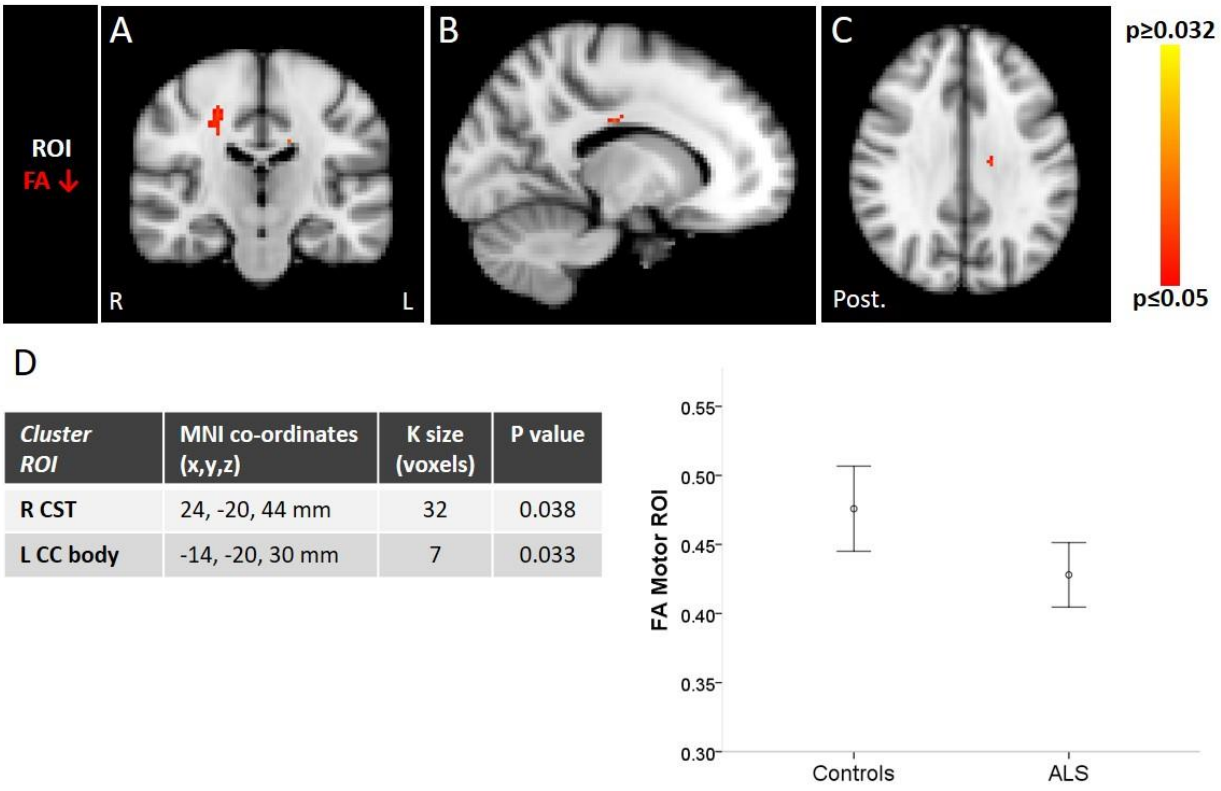

Cluster ROI	MNI co-ordinates (x,y,z)	K size (voxels)	P value
R CST	24, -20, 44 mm	32	0.038
L CC body	-14, -20, 30 mm	7	0.033

Figure 3.1.2. **FA is reduced in New Patients compared to Controls** within the right CST and left CC body at Motor ROIs level (panels A-C). The location, size ("K") and significance of each cluster maximum is listed in panel D with the mean FA across these clusters plotted. Colour column represents range of p values and error bars represent 95% confidence intervals. *R=right; L=left; Post=posterior.*

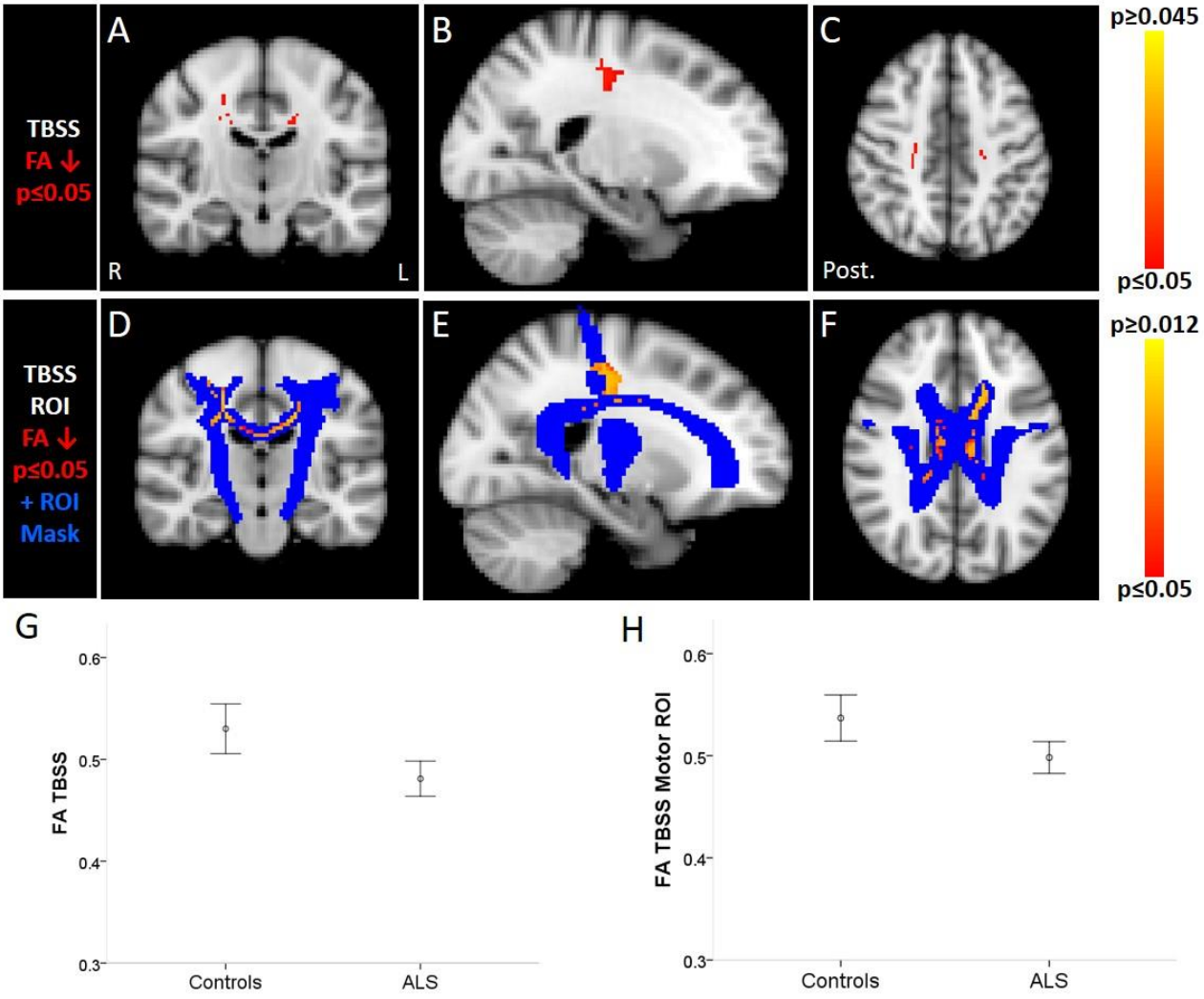

Cluster Peak TBSS	MNI co-ordinates (x,y,z)	K size (voxels)	P value
L CC body	-10, 4, 28 mm	80	0.045
R CST	22, -20, 44 mm	60	0.045
L CST	-22, -22, 36 mm	14	0.048

Cluster Peak TBSS ROI	MNI co-ordinates (x,y,z)	K size (voxels)	P value
CC body	-14, -16, 32 mm	595	0.012

Figure 3.1.3. **Skeletonised FA is reduced in New Patients compared to Controls** within the CSTs and CC using the entire (A-C) and Motor ROIs only (D-F; Motor ROIs mask overlaid in blue) TBSS skeleton. The location, size and significance of each cluster maximum is shown in panels G and H, respectively, with mean FA across the clusters plotted. Colour columns represent range of p values and error bars represent 95% confidence intervals. *R=right; L=left; Post=posterior.*

3.2. Relationships between FA and Blood CD4 Cells in the New Patients

Whole brain and Motor ROIs. No significant positive or negative associations were seen between FA and total blood CD4 count, total blood $CD4^+$ $CD25^+$ $FoxP3^+$ Treg count, or the Treg:CD4 Ratio (Table 3.2.1).

TBSS and TBSS Motor ROIs. A significant negative (p=0.016) association was revealed between total blood CD4 count and masked skeletonised FA within the central and anterior corpus callosum (Fig. 3.2.3 A-C) at the Motor ROI level. FA values within these significant regions demonstrated a weak negative association with total blood CD4 on scatterplot (Fig. 3.2.3 H) and adjusted R^2=0.1. No other significant positive or negative associations were seen between FA and total blood CD4 count, total blood $CD4^+$ $CD25^+$ $FoxP3^+$ Treg count, or the Treg:CD4 Ratio (Table 3.2.1).

When adding the rate of disease progression as an additional co-variate (to age), the significant negative association between skeletonised FA within the CC of the Motor ROIs and the total blood CD4 count was again replicated, although also emerged (p=0.043) without the use of the Motor ROIs mask (Fig. 3.2.3 A-C).

Furthermore, a new positive association between FA within a small subcortical white matter area of the left superior parietal lobule and the Treg:CD4 Ratio was seen on whole brain analysis (Fig. 3.2.4 A-C). FA values within these regions demonstrated a moderate negative association with Treg:CD4 total on scatterplot (Fig. 3.2.4 E) and adjusted R^2=0.31. No other new associations were seen (Table 3.2.2).

Table 3.2.1	FA versus Blood CD4 Cells and Tregs in New Participants							
	Whole Brain		Motor ROIs		TBSS Entire Skeleton		TBSS Motor ROIs	
	Pos	Neg	Pos	Neg	Pos	Neg	Pos	Neg
Blood CD4 total								p=0.016
Blood Treg total								
Treg:CD4 Ratio								

Table 3.2.1. **Summary of relationships between FA and blood CD4 cells** in the New Patients using TFCE at Whole brain, Motor ROIs, TBSS and TBSS Motor ROIs levels, with age as the only co-variate. Significant group differences shown bold/underlined.

Table 3.2.2	FA versus Blood CD4 Cells and Tregs in New Participants with Rate covariate							
	Whole Brain		Motor ROIs		TBSS Entire Skeleton		TBSS Motor ROIs	
	Pos	Neg	Pos	Neg	Pos	Neg	Pos	Neg
Blood CD4 total						p=0.043		p=0.025
Blood Treg total								
Treg:CD4 Ratio	p=0.009							

Table 3.2.2. **Summary of significant relationships between FA and blood CD4 cells** in the New Patients with age and rate of disease progression as co-variates. The association with FA within the CC and the total CD4 cell count now emerged on unmasked TBSS TFCE, along with a new positive relationship within the left parietal cortex and the percentage of Treg cells.

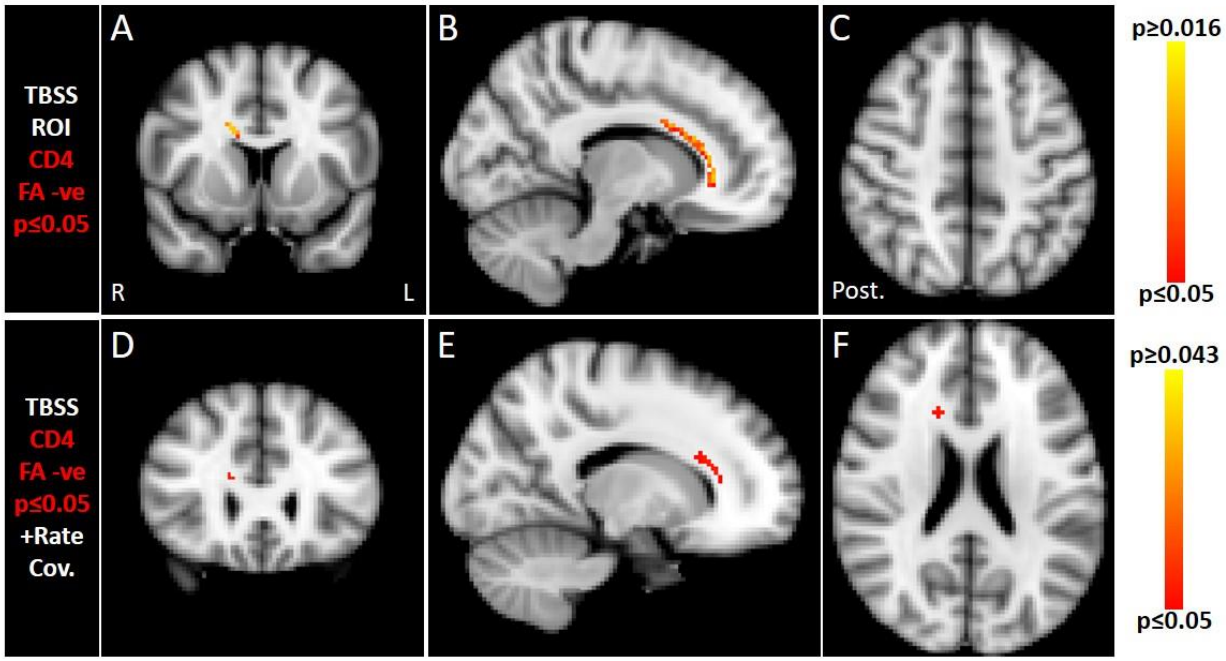

G

Cluster Peak TBSS ROI	MNI co-ordinates (x,y,z)	K size (voxels)	P value
CC Body	16, 30, 16mm	161	0.016

H

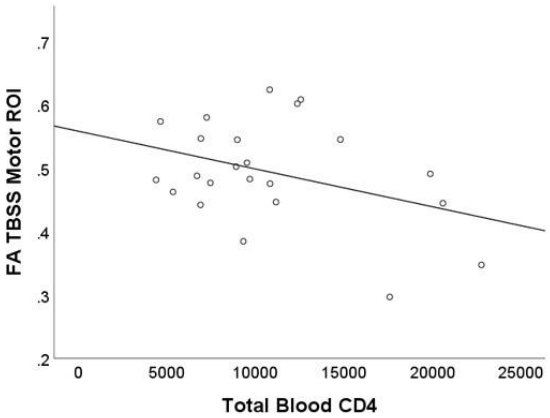

Figure 3.2.3. **Higher total blood CD4 cells associated with reduced skeletonised FA** within the central and anterior CC on Motor ROIs analysis (A-C; see table G for location, size and significance of cluster maximum), and emerges on entire skeleton analysis when including Rate of disease progression as a covariate (D-F). FA within the significant regions shown in A-C demonstrate a weak negative association with total blood CD4 on scatterplot (H; adjusted R^2=0.1). Colour bar represents range of p values. *R=right; L=left; Post=posterior.*

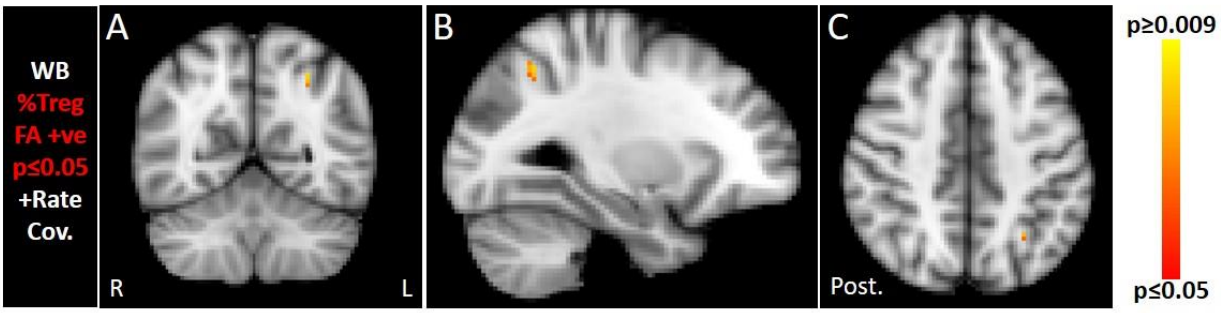

D

Cluster Peak Whole Brain	MNI co-ordinates (x,y,z)	K size (voxels)	P value
Sup. Parietal lob.	-28, -58, 48 mm	8	0.009

E

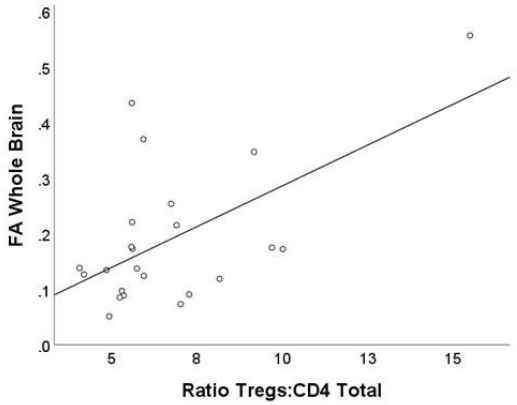

Figure 3.2.4. **Higher ratio of Tregs to CD4 cells is associated with increased FA** within a small subcortical white matter region of the superior parietal lobule (A-C) with location, size ("K") and significance of the cluster maximum listed in the table. FA within the significant regions shown in A-C demonstrates a moderate negative association with Treg:CD4 total on scatterplot (E; adjusted R^2=0.31). Colour bar represents range of p values. *R=right; L=left; Post=posterior.*

3.3 Relationships between FA and Clinical Measures in the New Patients

A significant positive association between FA within a small area spanning the junction between the right parietal and occipital cortices and Disease Duration was found (Fig. 3.3.2 A-C). FA values within this cluster demonstrated a strong negative association with disease duration on scatterplot (Fig. 3.3.2 E) with adjusted R^2=0.62. Otherwise, no significant positive or negative associations were found between FA and clinical measures ALSFRS, Rate of Progression or Disease Duration at the level of Whole Brain, Motor ROIs, TBSS whole skeleton or TBSS Motor ROIs (Table 3.3.1).

Table 3.3.1

FA versus Clinical Measures in New Patients								
	Whole Brain		Motor ROIs		TBSS Entire Skeleton		TBSS Motor ROIs	
	Pos	Neg	Pos	Neg	Pos	Neg	Pos	Neg
ALSFRS								
Rate								
Duration	p=0.028							
ECAS								
ECAS ALS Spec								

Table 3.3.1. **Summary of significant relationships between FA and clinical factors** in the New Patients using TFCE at Whole brain, Motor ROIs, TBSS and TBSS Motor ROIs levels.

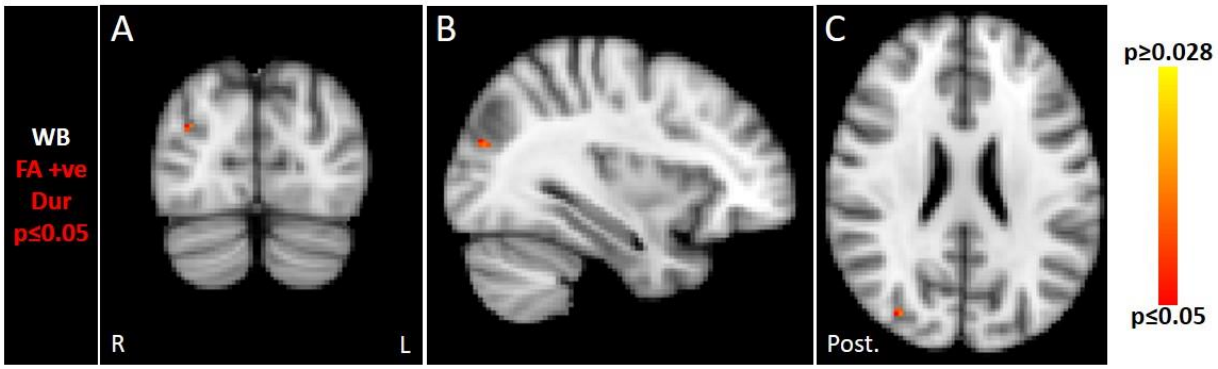

D

Cluster Peak Whole Brain	MNI co-ordinates (x,y,z)	K size (voxels)	P value
Inf. Parietal Lobule	34, -78, 22mm	8	0.028

E

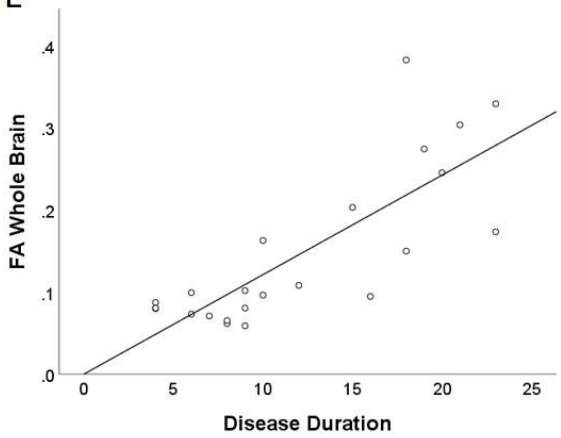

Figure 3.3.2. **Shorter disease duration associated with reduced FA** within a cortical area of the right inferior parietal lobule (A-C) with location, size ("K") and significance of the cluster maximum listed in the table. FA within the significant regions shown in A-C demonstrate a strong negative association with disease duration on scatterplot (E; adjusted R^2=0.62). Colour bar represents range of p values. *R=right; L=left; Post=posterior.*

3.4 Group Differences: FA in Historical Patients versus Historical Controls

Whole brain and Motor ROIs FA. Voxel clusters exhibiting significant decreases in FA (p=0.005 and p=0.001, respectively) were seen extensively within the CSTs, CC and PCGs in patients compared to controls before (Fig. 3.4.2 A-C) and after (Fig. 3.4.2 D-F) masking for the Motor ROIs. Quantifying the mean FA in these areas corroborated the reduction in the patient group (Fig. 3.4.2 G and H, respectively). Cohen's *d* effect sizes were 1.63 and 1.41, respectively. No significant increases in FA were seen (Table 3.4.1).

TBSS and TBSS Motor ROIs. Skeletonised FA throughout the central body and anterior aspect of the corpus callosum along with the forceps minor bilaterally demonstrated a significant decrease (p=0.009 and p=0.002, respectively) in patients compared to controls before (Fig. 3.4.3 A-C) and after (Fig. 3.4.3 D-F) masking with the Motor ROIs. Quantifying mean FA in these areas also confirmed the reduction in the patient group (Fig. 3.4.3 G and H, respectively). No significant increases in FA were seen (Table 3.9.1).

Table 3.4.1

	FA in Historical Patients vs Historical Controls			
	Whole Brain	Motor ROIs	TBSS Entire Skeleton	TBSS Motor ROIs
Controls>ALS	p=0.005	p=0.001	p=0.009	p=0.002
ALS>Controls				

Table 3.4.1. **Summary of significant group differences in FA between Historical Patients and Controls** using TFCE at Whole brain, Motor ROIs, TBSS and TBSS Motor ROIs levels. The main finding is of reduced FA within the CC and CSTs.

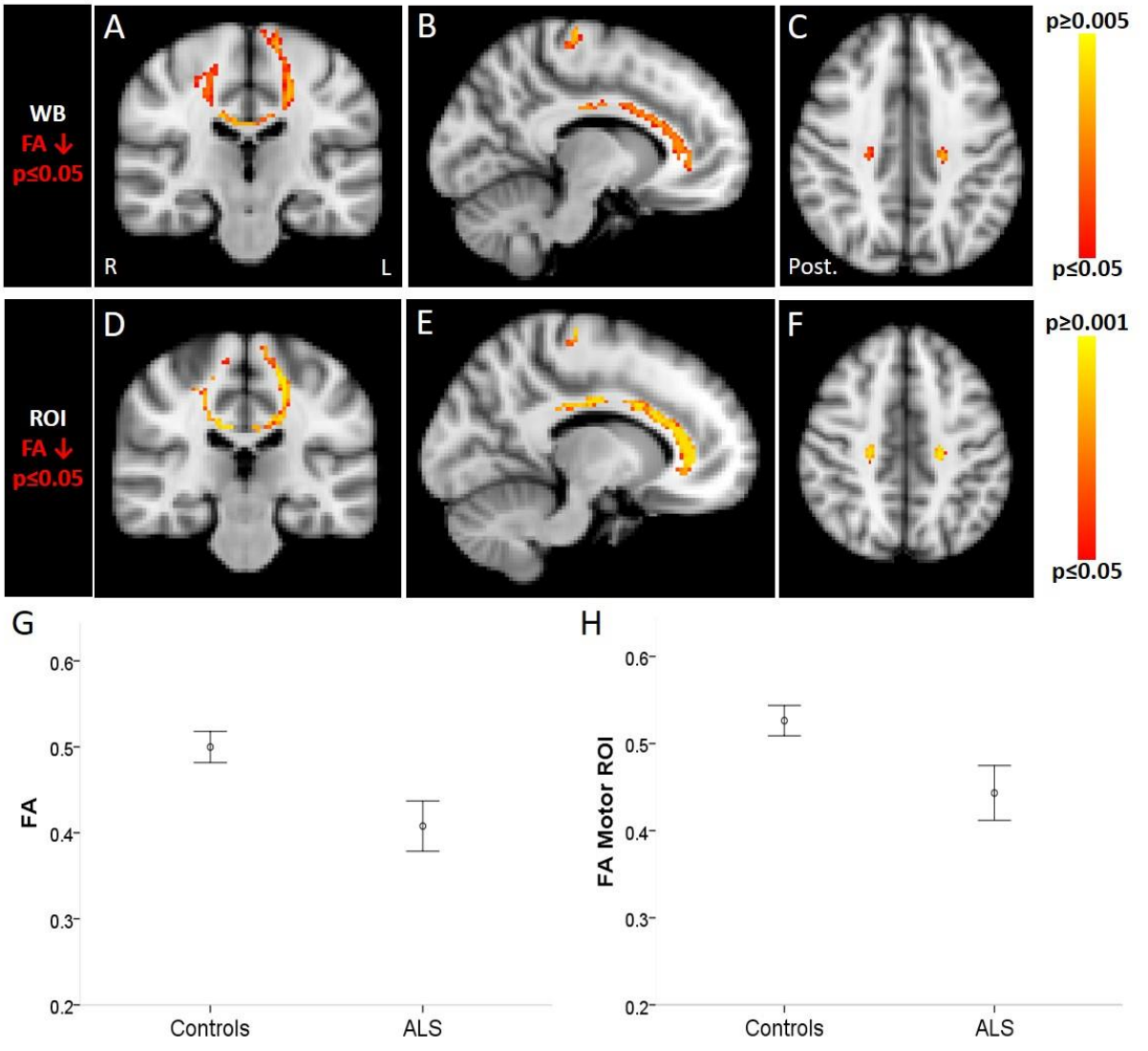

Cluster Peak WB	MNI co-ordinates (x,y,z)	K size (voxels)	P value
Body CC	16, 30, 16 mm	1521	0.005
R CST	22, -22, 44 mm	127	0.028

Cluster Peak ROI	MNI co-ordinates (x,y,z)	K size (voxels)	P value
Body CC	16, 30, 16 mm	2049	0.001
R CST	12, -24, 62 mm	6	0.034

Figure 3.4.2. **FA is extensively reduced in Historical Patients compared to Controls** throughout the CSTs extending into the PCGs and across the corpus callosum using TFCE at the whole brain (A-C) and Motor ROIs (D-F) levels, giving a characteristic 'horseshoe' appearance and confirmed by quantifying mean FA in these areas (G and H, respectively). Location, size ("K") and significance of each cluster maximum listed in the tables. Colour columns represent range of p values and error bars represent 95% confidence intervals. *R=right; L=left; Post=posterior.*

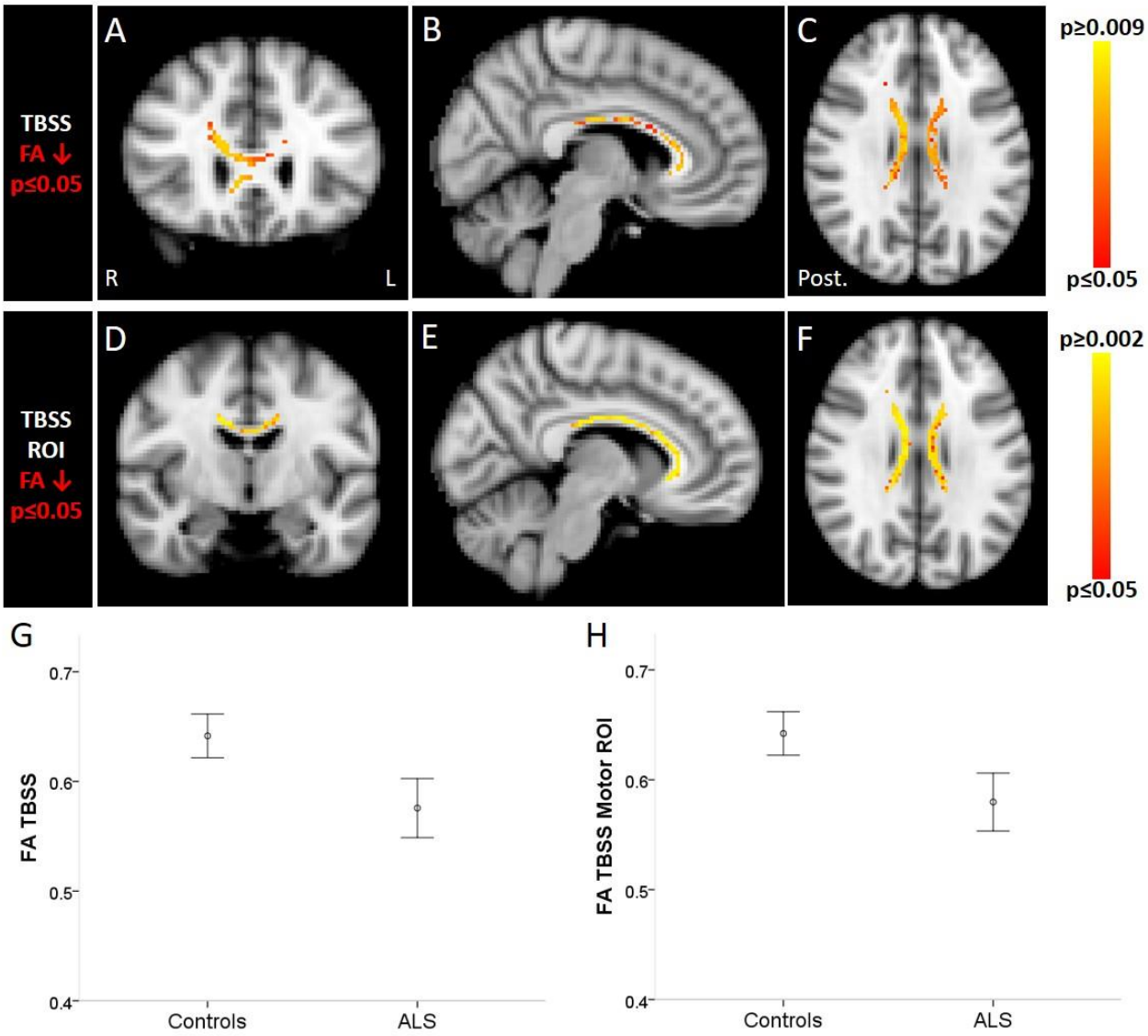

Cluster Peak WB	MNI co-ordinates (x,y,z)	K size (voxels)	P value
Body CC	16, 30, 16 mm	1521	0.005
R CST	22, -22, 44 mm	127	0.028

Cluster Peak ROI	MNI co-ordinates (x,y,z)	K size (voxels)	P value
Body CC	16, 30, 16 mm	2049	0.001
R CST	12, -24, 62 mm	6	0.034

Figure 3.4.3. **Skeletonised FA is reduced in Historical Patients compared to Controls** throughout the central and anterior CC using entire TBSS skeleton TFCE (A-C) and Motor ROIs only TFCE (D-F), confirmed by quantifying mean FA in these areas (G and H, respectively). Location, size ("K") and significance of each cluster maximum listed in the tables. Colour columns represent range of p values and error bars represent 95% confidence intervals. *R=right; L=left; Post=posterior.*

3.5 Relationships between FA and Clinical Measures in Historical Patients

Whole brain and Motor ROIs FA. A significant negative association between FA within a small area of the right forceps major and Disease Duration was found using TFCE at the Motor ROIs level (Fig. 3.5.2 A-C). FA values within this area accordingly demonstrated a moderate linear relationship (Fig. 3.5.2 I) with adjusted R^2=0.46.

TBSS and TBSS Motor ROIs. A significant negative association (p=0.017) between skeletonised FA within the body of the CC and Disease Duration was demonstrated using the entire TBSS skeleton (Fig. 3.5.2 D-F), and reproduced at higher significance following use of the Motor ROI mask (p=0.005; not shown). However, the area in the right forceps minor did not re-emerge. FA values within these areas demonstrated a moderate linear relationship with disease duration on scatterplot (Fig. 3.5.2 J) with adjusted R^2=0.51).

A significant positive association (p=0.039) between skeletonised FA throughout the rostral CSTs, CC and subcortical white matter of the PCGs and the ALSFRS score was observed using the entire TBSS skeleton (Fig. 3.5.3 A-C), and reproduced at slightly higher significance following use of the Motor ROI mask (p=0.035; not shown). FA values within these areas demonstrated a moderate linear relationship with disease duration on scatterplot (Fig. 3.5.3 E) with adjusted R^2=0.58.

A significant positive association (p=0.027) was also observed between FA within the right central and anterior CC and the ECAS ALS Specific score using the Motor ROIs only TBSS skeleton (Fig. 3.5.4 A-C), visualised as a weak linear relationship using mean FA (Fig. 3.5.4 E) with adjusted R^2=0.32.

No other significant positive or negative associations were found between FA and ALSFRS, Rate of Progression, Disease Duration, total ECAS score and ECAS ALS Specific score at the level of Whole Brain, Motor ROIs, TBSS whole skeleton or TBSS Motor ROIs (Table 3.5.1).

Table 3.5.1	FA versus Clinical Measures in Historical Patients							
	Whole Brain		Motor ROIs		TBSS Entire Skeleton		TBSS Motor ROIs	
	Pos	Neg	Pos	Neg	Pos	Neg	Pos	Neg
ALSFRS					p=0.039		p=0.035	
Rate								
Duration				p=0.036		p=0.017		p=0.005
ECAS								
ECAS ALS Spec							p=0.027	

Table 3.5.1. **Summary of significant relationships between FA and clinical factors** in the Historical Patients using TFCE at Whole brain, Motor ROIs, TBSS and TBSS Motor ROIs levels.

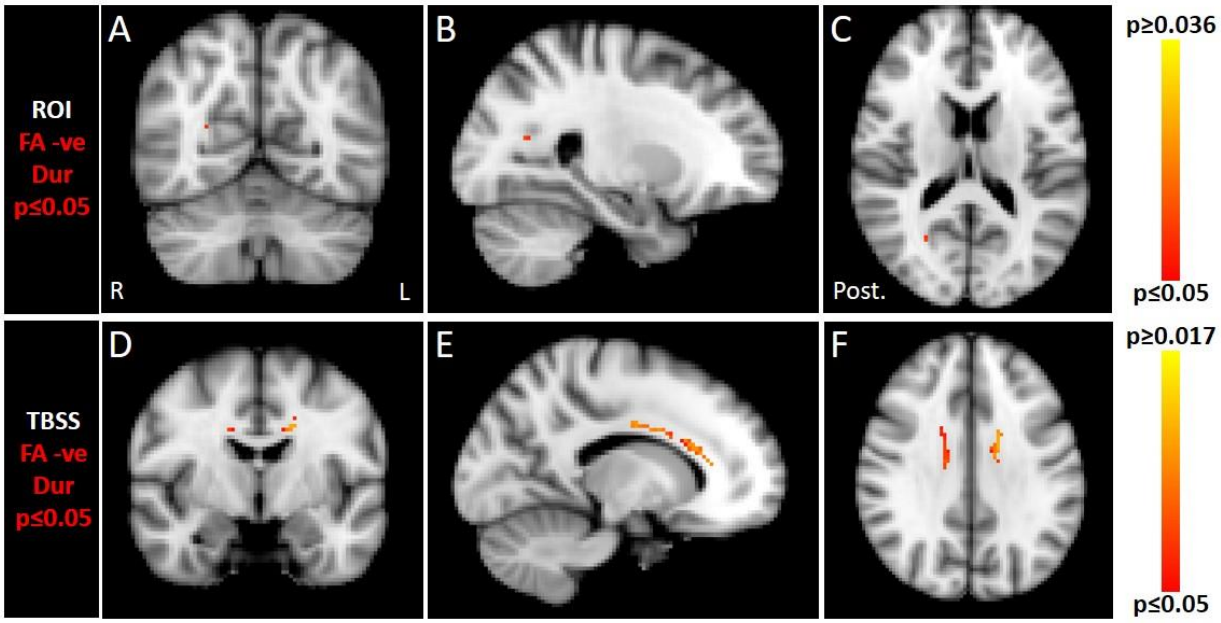

G

Cluster Peak ROI	MNI co-ordinates (x,y,z)	K size (voxels)	P value
Posterior Body CC	26, -64, 16mm	2	0.036

H

Cluster Peak TBSS	MNI co-ordinates (x,y,z)	K size (voxels)	P value
Body CC	-16, 4, 32 mm	118	0.016
Body CC	18, -14, 34 mm	58	0.031

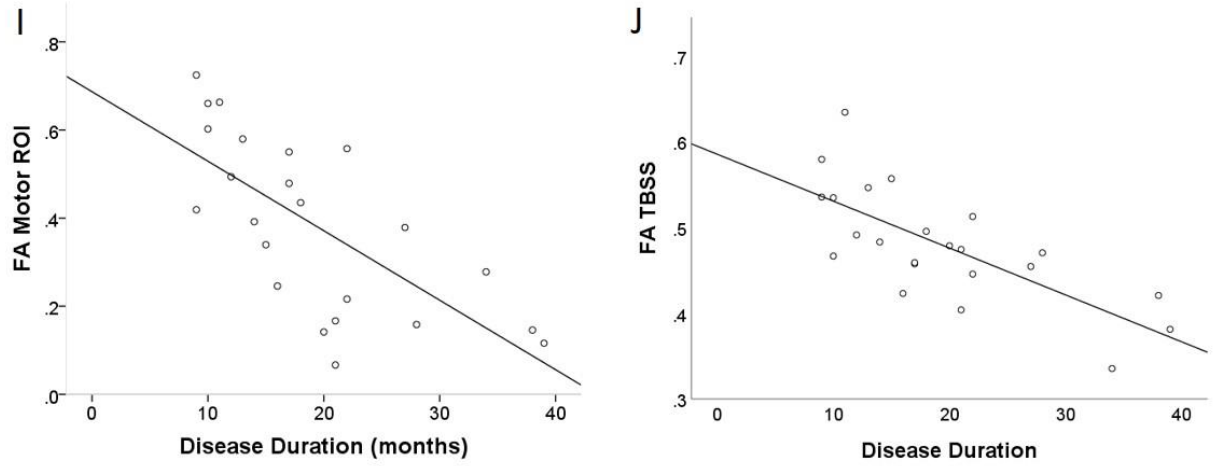

Figure 3.5.2. **Longer disease duration associated with reduced FA** within the right forceps major on Motor ROIs (A-C) and within the body of the CC using TBSS (D-F) TFCE analysis. Location, size ("K") and significance of cluster maxima listed in the tables (G and H). FA within these respective areas demonstrated moderate linear relationships with disease duration on scatterplot (I + J; adjusted R^2=0.46 & 0.51, respectively). Colour bars = range of p values. *R=right; L=left; Post=posterior.*

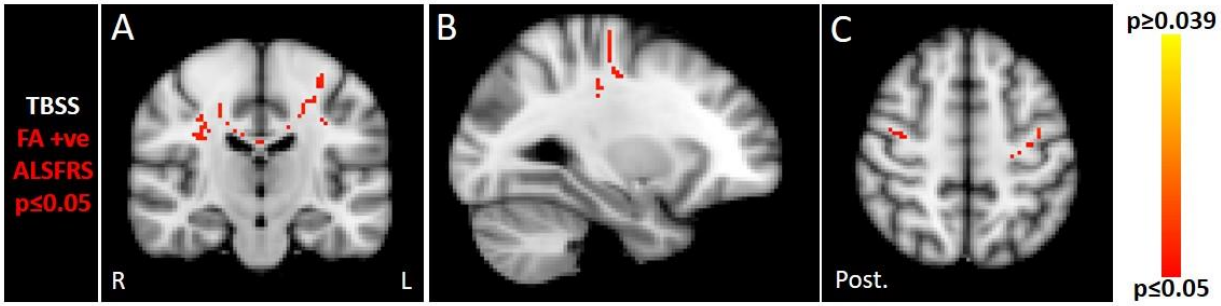

D

Cluster Peak TBSS	MNI co-ordinates (x,y,z)	K size (voxels)	P value
L CST	-38, -8, 50mm	229	0.039
CC body	18, -22, 32mm	201	0.043
R CST	38, -10, 50mm	18	0.046
R CST	32, -30, 60mm	12	0.048

E

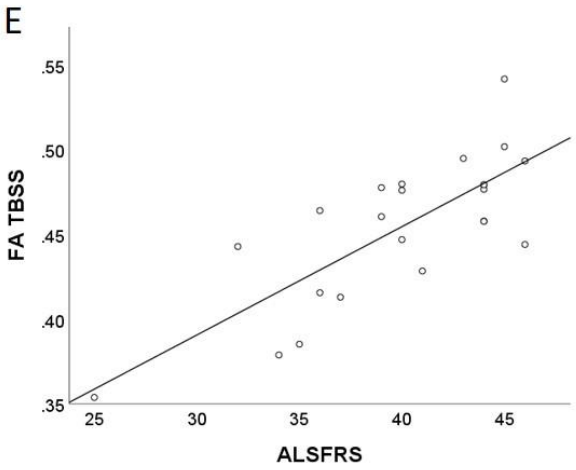

Figure 3.5.3. **Reduced functional score associated with reduced FA** within the rostral CSTs, CC and subcortical white matter of the PCGs using TBSS TFCE (A-C) with the location, size ("K") and significance of each cluster maximum listed in the table. FA within these respective areas demonstrated a moderate linear relationship with disease duration on scatterplot (E; adjusted R^2=0.58). Colour bars represent range of p values. *R=right; L=left; Post=posterior.*

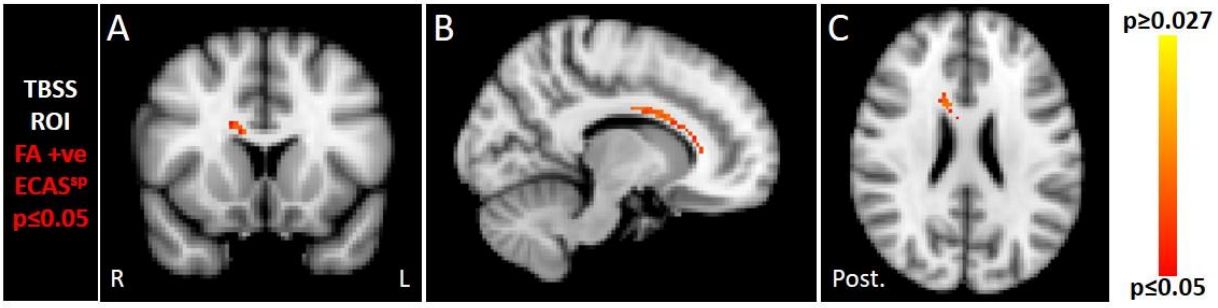

D

Cluster Peak TBSS	MNI co-ordinates (x,y,z)	K size (voxels)	P value
CC body	14, 12, 24mm	138	0.027

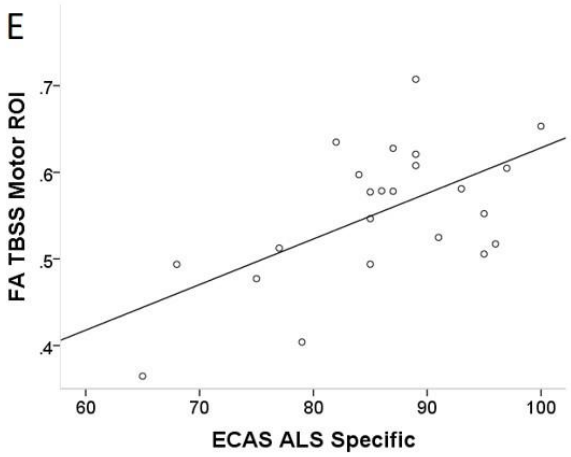

Figure 3.5.4. **Reduced ECAS ALS specific score associated with reduced FA** within the right central and anterior CC using TBSS Motor ROIs TFCE (A-C). Location, size ("K") and significance of cluster maximum is detailed in table D. FA within this area demonstrated a weak linear relationship with ALSFRS (E; adjusted R^2=0.32). Colour bars represent range of p values. *R=right; L=left; Post=posterior.*

3.6 Relationships between FA and Clinical Measures

Combined New + Historical Patients

Whole brain and Motor ROIs. A significant positive association between FA within a small region of the right inferior parietal lobe and ECAS ALS Specific score was found at whole brain level TFCE (Fig. 3.6.2 A-C). A weak linear relationship was demonstrated between the two variables (Fig. 3.6.2 E) with adjusted R^2=0.28.

TBSS and TBSS Motor ROIs. A significant positive association (p=0.038) between skeletonised FA throughout the CC, rostral CSTs and bilateral PCGs subcortical white matter and the ALSFRS score was observed using entire TBSS skeleton TFCE (Fig. 3.6.3 A-C), and reproduced at slightly higher significance (p=0.02) following Motor ROIs TBSS TFCE (Fig. 3.6.3 D-F), with a weak-moderate linear relationship on scatterplot (Fig. 3.6.3 I) and adjusted R^2=0.39.

A significant negative association (p=0.024) between extensive clusters of skeletonised FA throughout the CC, rostral CSTs and bilateral PCGs subcortical white matter and Disease Duration was observed using entire TBSS skeleton TFCE (Fig. 3.6.4 A-C), and reproduced at slightly higher significance (p=0.015) following Motor ROIs TBSS TFCE (Fig. 3.6.4 D-F). A weak linear relationship was demonstrated on scatterplot of skeletonised FA values within the clusters found on TFCE TBSS ROI and duration of disease (Fig. 3.6.4 I) with adjusted R^2=0.22.

A significant positive correlation (p=0.022) between a small cluster of skeletonised FA within the right temporal fusiform cortex and Disease Duration was observed using entire TBSS skeleton TFCE (Fig. 3.6.5 A-C). FA values within this cluster demonstrated a weak linear relationship with duration of disease (Fig. 3.6.5 E) and adjusted R^2=0.24).

No other positive or negative associations between FA and ALSFRS, Disease Duration, Rate of Disease Progression, ECAS and ECAS ALS Specific score were found (Table 3.12.1).

Table 3.6.1	FA versus Clinical Measures in Combined New and Historical Patients							
	Whole Brain		Motor ROIs		TBSS Entire Skeleton		TBSS Motor ROIs	
	Pos	Neg	Pos	Neg	Pos	Neg	Pos	Neg
ALSFRS					p=0.038		p=0.02	
Rate								
Duration					p=0.022	p=0.024		p=0.015
ECAS								
ECAS ALS Spec	p=0.036							

Table 3.6.1. **Summary of significant relationships between FA and clinical factors** in the combined New and Historical Patients using TFCE at Whole brain, Motor ROIs, TBSS and TBSS Motor ROIs levels. The main findings are of a positive association with ALSFRS and a negative association with Disease Duration, with some small extra-motor positive associations with Duration and the ECAS ALS Specific score.

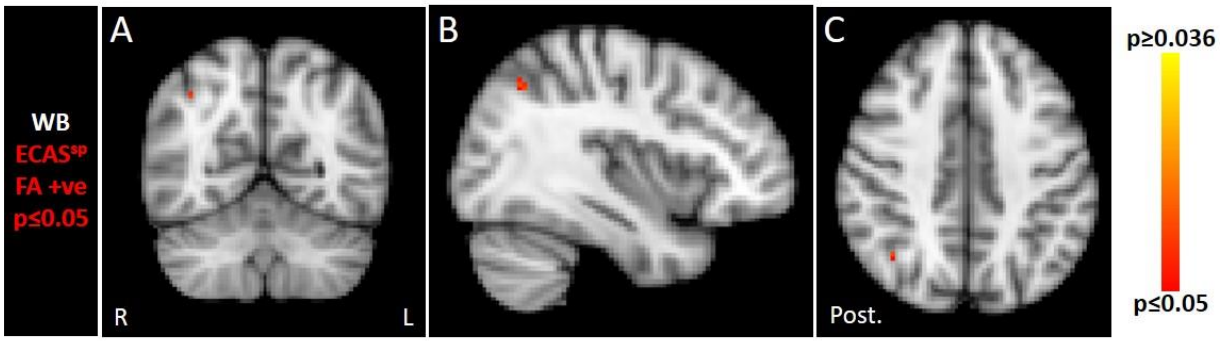

D

Cluster Peak Whole Brain	MNI co-ordinates (x,y,z)	K size (voxels)	P value
Anterior IPS	38, -60, 42 mm	5	0.036

E

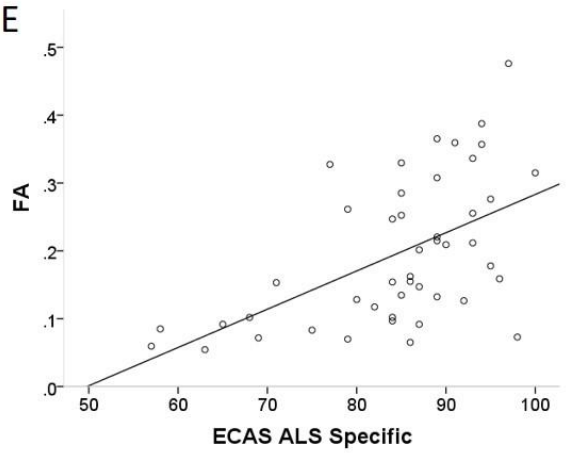

Figure 3.6.2. **Lower ECAS ALS specific score (ECAS^{sp}) associated with reduced FA** within the anterior intraparietal sulcus using whole brain TFCE (A-C). Location, size ("K") and significance of cluster maximum is detailed in table D. FA within this area demonstrated a weak linear relationship with cognitive scores (E; adjusted R^2=0.28). Colour bars represent range of p values. *R=right; L=left; Post=posterior.*

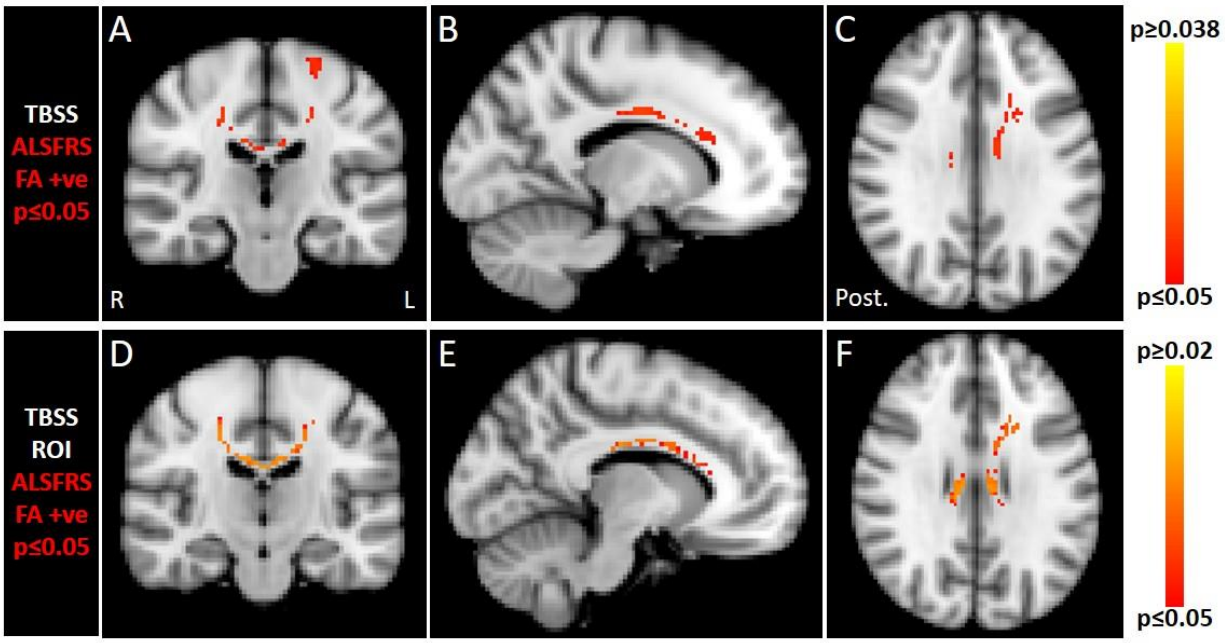

G

Cluster Peak TBSS	MNI co-ordinates (x,y,z)	K size (voxels)	P value
Body CC	-14, -10, 34mm	323	0.038
L PCG	-22, -22, 68mm	16	0.041
L CST	-36, -10, 46mm	8	0.047

H

Cluster Peak TBSS ROI	MNI co-ordinates (x,y,z)	K size (voxels)	P value
Body CC	-14, -10, 34mm	387	0.02
L CST	-40, -10, 46mm	17	0.039

H

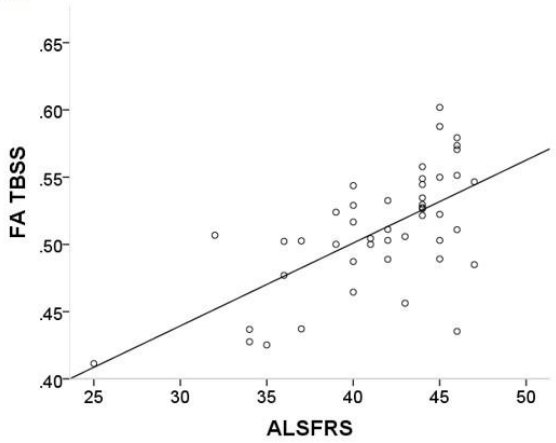

Figure 3.6.3. **Reduced functional score associated with reduced FA** within the rostral CSTs, CC and subcortical white matter of the PCGs using TFCE TBSS (A-C) and Motor ROIs TBSS (D-E). Location, size ("K") and significance of the cluster maxima are detailed in tables G and H, respectively. FA within the areas using TFCE TBSS demonstrated a weak-moderate linear relationship with ALSFRS scores (I; adjusted R^2=0.39). Colour bars represent range of p values. *R=right; L=left; Post=posterior.*

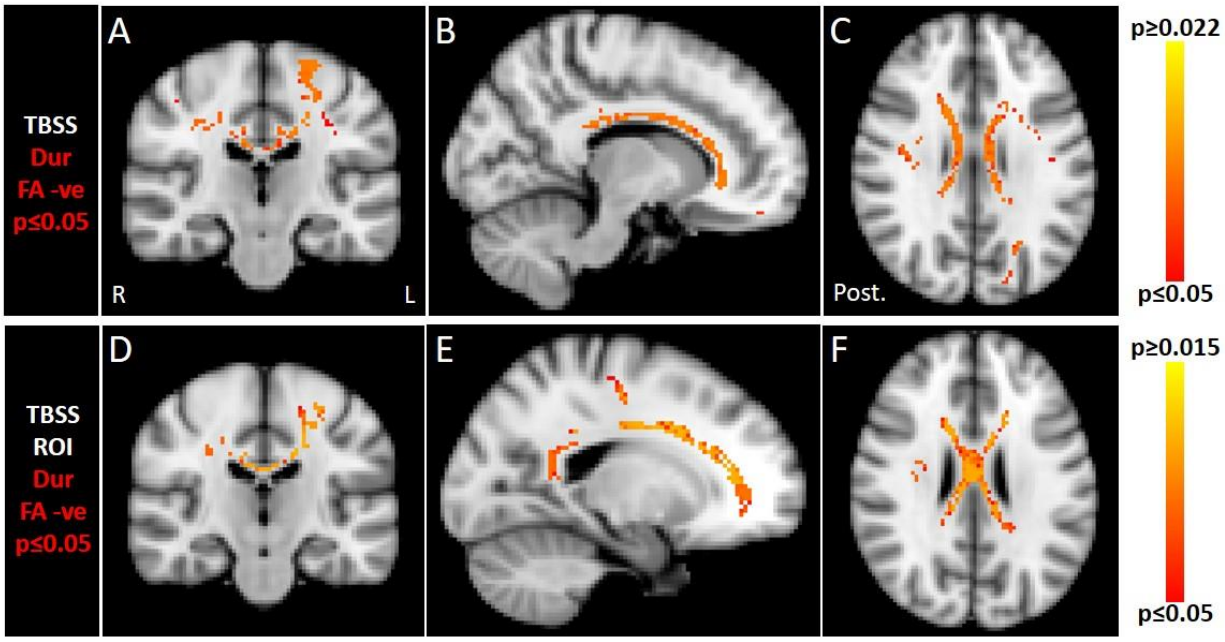

G

Cluster Peak TBSS	MNI co-ordinates (x,y,z)	K size (voxels)	P value
Body CC	-10, -8, 30	2174	0.022
Body CC	-26, 34, 4mm	78	0.047
L CST	-32, -22, 36mm	18	0.049
R CST	50, -2, 24mm	13	0.049

H

Cluster Peak TBSS ROI	MNI co-ordinates (x,y,z)	K size (voxels)	P value
Body CC	-16, -2, 34mm	1461	0.015

I

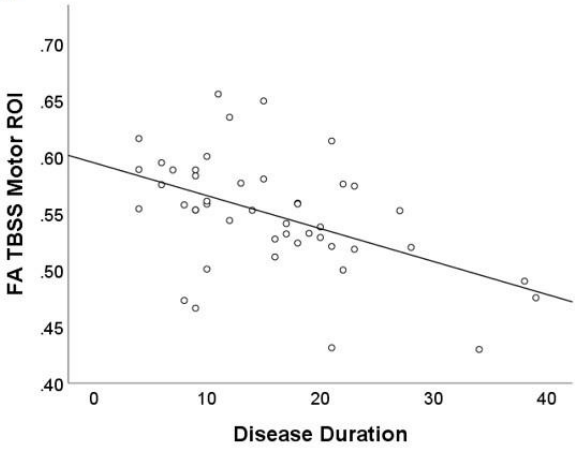

Figure 3.6.4. **Longer duration of disease associated with extensively reduced FA** within the rostral CSTs, CC and subcortical white matter of the PCGs using TFCE TBSS (A-C) and Motor ROIs TBSS (D-E). Location, size ("K") and significance of the cluster maxima are detailed in tables G and H, respectively. FA values within the clusters found on TFCE TBSS ROI demonstrated a weak linear relationship with duration of disease (I; adjusted R^2=0.22). Colour bars represent range of p values. *R=right; L=left; Post=posterior.*

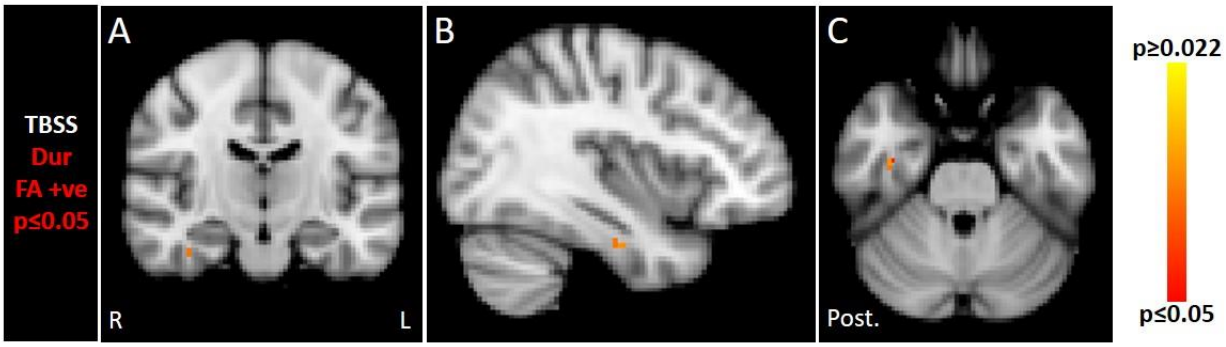

D

Cluster Peak TBSS	MNI co-ordinates (x,y,z)	K size (voxels)	P value
R Fusiform	38, -14, -28 mm	5	0.022

E

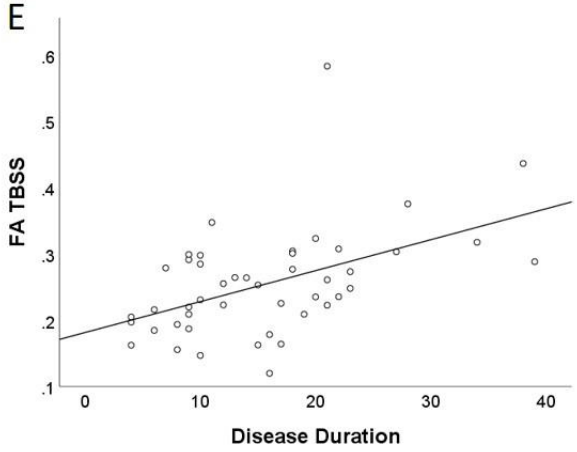

Figure 3.6.5. **Shorter duration of disease associated with reduced FA** within the white matter of the right temporal fusiform cortex using TFCE TBSS (A-C). Location, size ("K") and significance of the cluster maximum is detailed in table D. FA values within this cluster demonstrate a weak linear relationship with duration of disease (E; adjusted R^2=0.24). Colour bars represent range of p values. *R=right; L=left; Post=posterior.*

3.7 Summary of main FA findings in Patients with ALS

A. FA is reliably reduced within the CSTs and CC compared to controls, albeit to a greater extent and significance in the Historical Patients compared to the New Patients, particularly on TBSS and TBSS Motor ROIs analyses.

B. ALSFRS and Disease Duration demonstrate the most consistent positive and negative associations, respectively, with FA within the CSTs, CC and PCGs as seen in the Historical Patients and clearly maintained in Combined patient group analyses which was principally revealed using TBSS analyses. Interestingly, these are the two clinical measures which differ significantly between the patient groups.

C. FA within an extra-motor cortical (grey matter) area in the temporal lobe demonstrates a positive association with the ECAS ALS Specific score across the Combined patient group.

D. Total blood CD4 cell count demonstrates a negative association with FA within the CC on TBSS analyses, which was more readily demonstrated after accounting for the Rate of disease progression.

E. The ratio of blood Tregs:CD4 cells demonstrates a weak positive association with FA within the parietal lobe after accounting for the Rate of disease progression.

Chapter 4. Results: NODDI in ALS

In this results chapter, cross-sectional image analysis of Neurite Orientation Dispersion and Density Imaging (NODDI) parameters within the New and Historical cohorts of participants will be presented, using NODDI parameters generated with **intrinsic diffusivity (ID)** 1.7 proposed as being optimised for white matter and then with **ID=1.1** proposed as being optimised for the grey matter. Given that both patient groups have demonstrated reductions in FA within at least the corpus callosum (CC) and corticospinal tracts (CSTs) compared to controls, the potential contribution of NDI, ODI and ISO to these FA changes can now be explored. Their own relationships with measures of clinical severity may also help to further elucidate the microstructural nature of the FA associations, particularly with ALSFRS and Duration of Disease identified in Chapter 3, in addition to the novel associations with total blood CD4 count and FA in the CC, and Treg:CD4 ratio with FA in the parietal lobe.

As described in Chapter 2, non-parametric permutation testing with age included as a co-variate throughout using Threshold-Free Cluster Enhancement (TFCE) was undertaken to identify clusters of voxels whose parameters significantly differed between groups or in association with clinical and 'wet' biomarker blood measures:

- At Whole Brain level (**ID=1.7** and **ID=1.1**);
- Using Tract Based Spatial Statistics (TBSS) skeletonised parameters (**ID=1.7 only**);
- Within the Motor ROIs (**ID=1.7** and **ID=1.1**);

Rate of disease progression was included as a covariate in analyses involving the 'wet' biomarker blood cell levels. P values within each analysis are quoted with correction for multiple comparisons at cluster level and considered significant where $p \leq 0.05$.

Participants for analyses with NODDI ID=1.7

Sections 4.1-3.3: 23 patients recruited within ANNALS-QuICT and 24 healthy controls recruited within MultiNICS as summarised in Chapter 3 Table 3a.

Sections 4.4-4.5: 23 Historical patients and 23 Historical healthy controls as summarised in Chapter 3 Table 3b.

Section 4.6: all 46 participants with ALS as summarised in Chapter 3 Table 3c.

[Section 4.7: SUMMARY]

Participants for analyses with NODDI ID=1.1

Sections 4.8-4.10, 4.11-4.12 and **4.13** as above.

[Section 4.14: SUMMARY]

4.1 Group Differences: New Patients versus New Controls NODDI ID=1.7

Whole brain and Motor ROIs. A clusters of significantly increased ODI (p=0.02) in patients compared to controls were seen within the left CC (Fig. 4.1.2 A-C) following Motor ROIs analysis, reflected by quantification of the mean ODI within these regions (Fig. 4.1.2 D). This contrasts with the similar change seen in FA albeit in the *right* CST (refer to Fig. 3.1.2). No other differences in FA were seen (Table 4.1.1).

TBSS and TBSS Motor ROIs. A significant increase in skeletonised ODI (p=0.001) throughout the central and anterior CC, the CSTs extending superiorly into the subcortical white matter (WM) of the PCGs, the forceps minor bilaterally, and the subcortical WM of the superior frontal gyrus, frontal pole and right post-central gyrus (Fig. 4.1.3 A-C) was seen in patients compared to controls. The significant increases were replicated (p=0.001) extensively throughout the CC and the rostral CSTs extending superiorly into the subcortical white matter of the PCGs following analysis using the Motor ROIs mask (Fig. 4.1.3 D-F), confirmed using quantification of the mean ODI within these regions (Fig. 4.1.3 G and H, respectively). The extent and significance of ODI change is much more marked compared to the similar group comparisons of skeletonised FA (refer back to Figure 3.1.3). No other differences in NDI, ODI or ISO were seen.

Table 4.1.1

	Whole Brain			Motor ROIs			TBSS Entire Skeleton			TBSS Motor ROIs		
	NDI	ODI	ISO	NDI	ODI	ISO	NDI	ODI	ISO	NDI	ODI	ISO
Controls>ALS												
ALS>Controls					p=0.025			p=0.001			p=0.001	

Table 4.1.1. **Summary of significant differences in NODDI 1.7 between the New Patients and Controls** using TFCE at Whole brain, Motor ROIs, TBSS and TBSS Motor ROIs levels. The main finding is of increased ODI within the CC and CSTs.

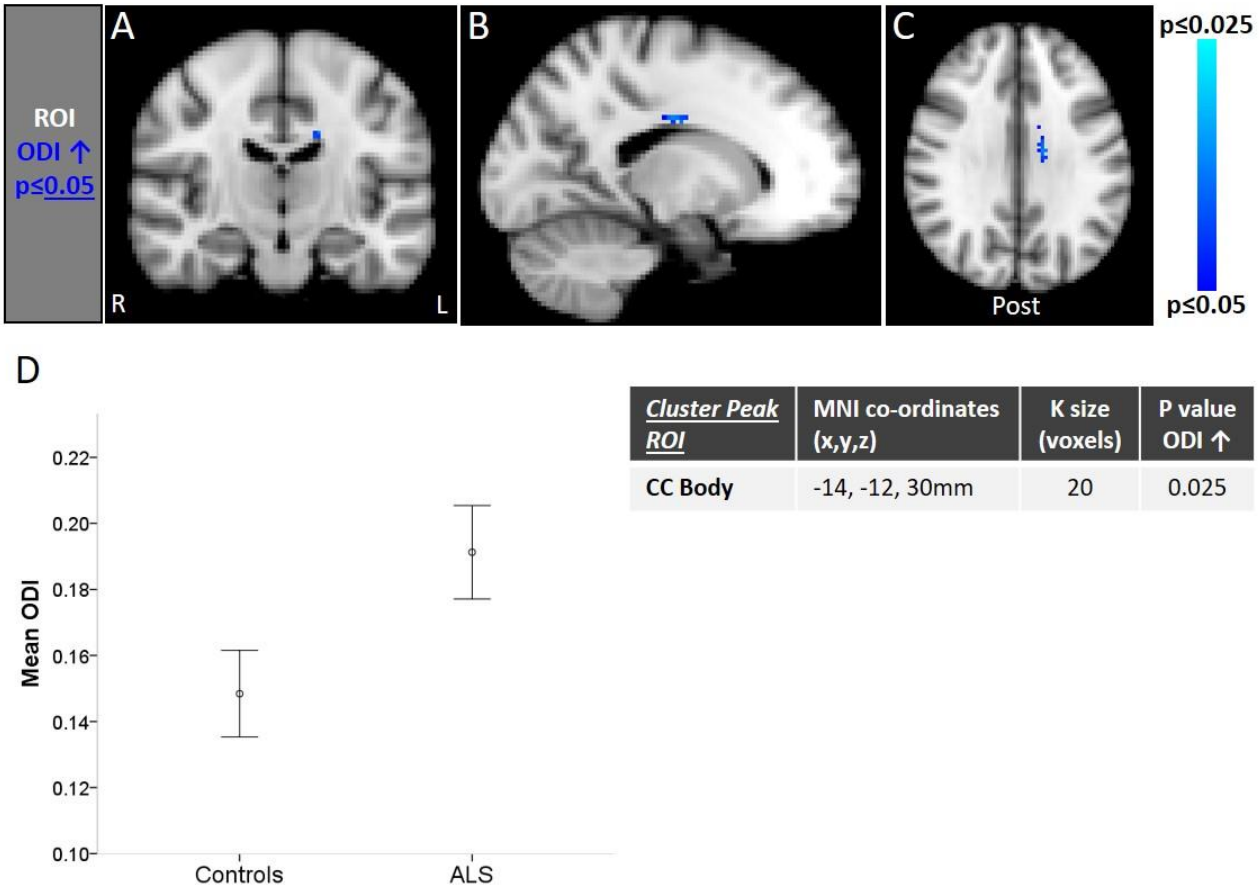

Cluster Peak ROI	MNI co-ordinates (x,y,z)	K size (voxels)	P value ODI ↑
CC Body	-14, -12, 30mm	20	0.025

Figure 4.1.2. **ODI is increased in New Patients compared to Controls** within the left CC at Motor ROIs level (A-C), confirmed by quantifying mean ODI in these areas (D). Location, size ("K") and significance of the cluster maximum is outlined in the table. Colour column represents range of p values and error bars represent 95% confidence intervals. Effect size = 1.22. *R=right; L=left; Post=posterior.*

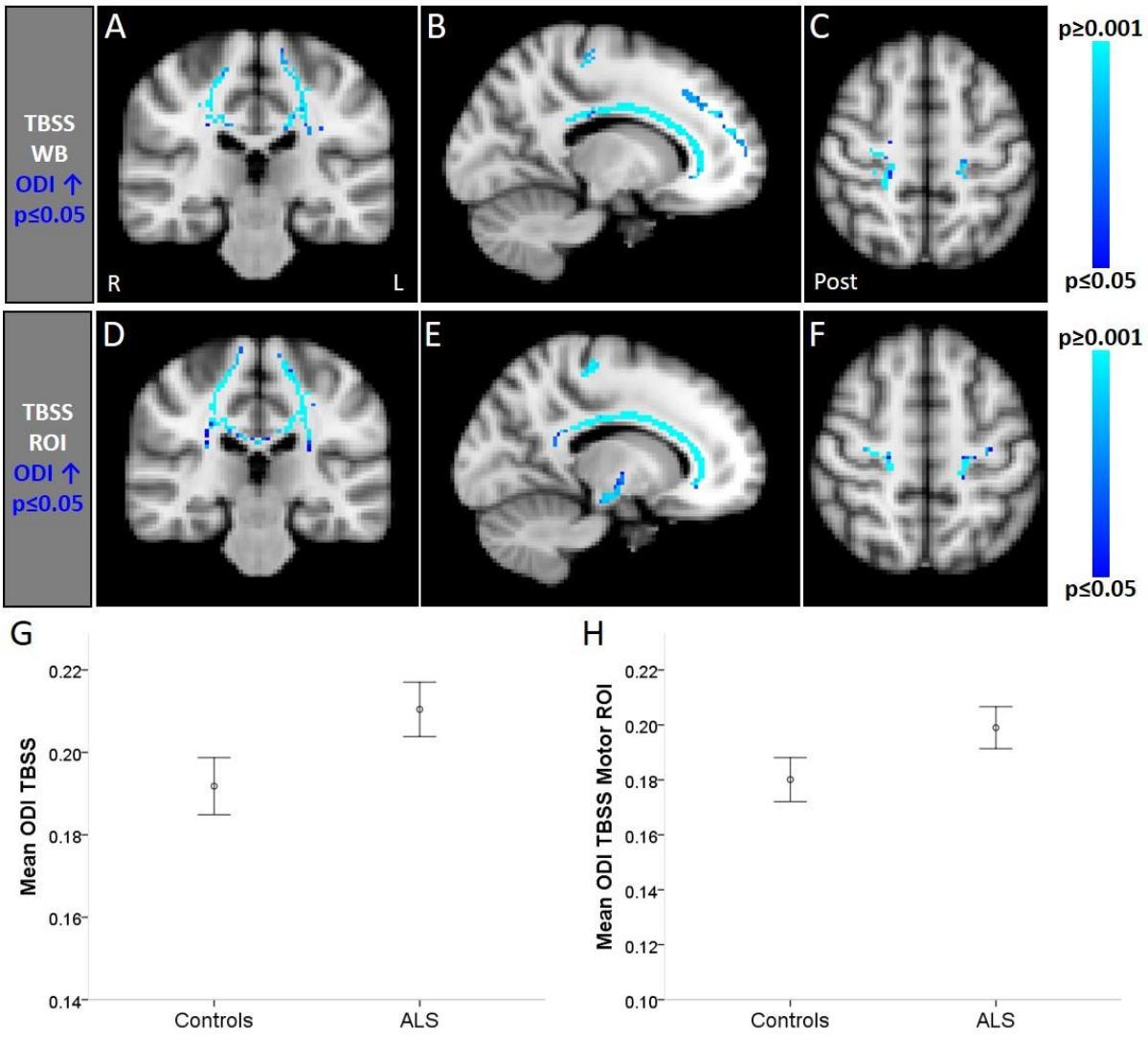

Cluster Peak TBSS	MNI co-ordinates (x,y,z)	K size (voxels)	P value ODI ↑
CC Body	-16, 20, 22mm	1658	<0.001
R CST	22, -16, 0mm	33	0.039

Cluster Peak TBSS ROI	MNI co-ordinates (x,y,z)	K size (voxels)	P value ODI ↑
CC Body	-18, 28, 20mm	1172	<0.001

Figure 4.1.3. **Skeletonised ODI is increased in New Patients compared to Controls** extensively along the CSTs and within the CC using the entire (A-C) and Motor ROIs only (D-F) TBSS skeleton, confirmed by quantifying mean ODI in these areas (G and H, respectively). Effect sizes were 0.97 and 0.80, respectively. Location, size ("K") and significance of the cluster maxima are outlined in the tables. Colour columns represent range of p values and error bars represent 95% confidence intervals. *R=right; L=left; Post=posterior.*

4.2 Relationships between NODDI ID=1.7 and Blood CD4 cells in the New Patients

Whole brain and Motor ROIs. A significant positive association between ODI and total blood CD4 count (p=0.042) was seen within the body and anterior aspect of the corpus callosum before (Fig. 4.2.3 A-C) and following (Fig. 4.2.3 D-F) masking for the Motor ROIs, neither of which had been observed in the FA analysis. ODI within these latter significant regions demonstrated a weak positive association with total blood CD4 cells on scatterplot (Fig. 4.2.3 I) with adjusted R^2=0.2. No other significant associations were seen (Table 4.2.1).

TBSS and TBSS Motor ROIs. A significant positive association (p=0.013) between total blood CD4 count and unmasked skeletonised ODI was seen within the right corpus callosum (Fig.4.2.4 A-C), and similarly following use of the Motor ROIs mask (not shown) which accompanies the negative association with FA also shown within the CC (see Fig. 3.2.3). Skeletonised ODI within these significant clusters demonstrated a weak positive association with total blood CD4 cells on scatterplot (Fig.4.2.4 E) with adjusted R^2=0.2. No other significant associations with skeletonised NDI, ODI or ISO were seen (Table 4.2.2).

When adding the rate of disease progression as an additional co-variate (to age), the significant positive associations between entire skeleton and Motor ROIs skeletonised ODI within the CC and the total blood CD4 count were again replicated (p=0.028 each), in agreement with the findings reported using FA TBSS, whereas the associations seen using whole brain ODI and Motor ROIs mask disappeared.

Table 4.2.1	Whole Brain						Motor ROIs					
	NDI		ODI		ISO		NDI		ODI		ISO	
	Pos	Neg	Pos	Neg	Pos	Neg	Pos	Neg	Pos	Neg	Pos	Neg
Blood CD4 total			p=0.042						p=0.03			
Blood Treg total												
Treg:CD4 Ratio												

Table 4.2.1. **Summary of significant relationships between FA and blood CD4 cells** in the New Patients using TFCE at Whole brain and Motor ROIs levels, with age as the only co-variate. These relationships did not survive correction for Rate of Progression.

Table 4.2.2	TBSS Entire Skeleton						TBSS Motor ROIs					
	NDI		ODI		ISO		NDI		ODI		ISO	
	Pos	Neg	Pos	Neg	Pos	Neg	Pos	Neg	Pos	Neg	Pos	Neg
Blood CD4 total			p=0.013						p=0.015			
Blood Treg total												
Treg:CD4 Ratio												

Table 4.2.2. **Summary of significant relationships between skeletonised FA and blood CD4 cells** in the New Patients using TFCE at TBSS and TBSS Motor ROIs levels, with age as the only co-variate. These relationships did survive correction for Rate of Progression and thus mirror the findings reported using FA TBSS (see Table 3.2.2).

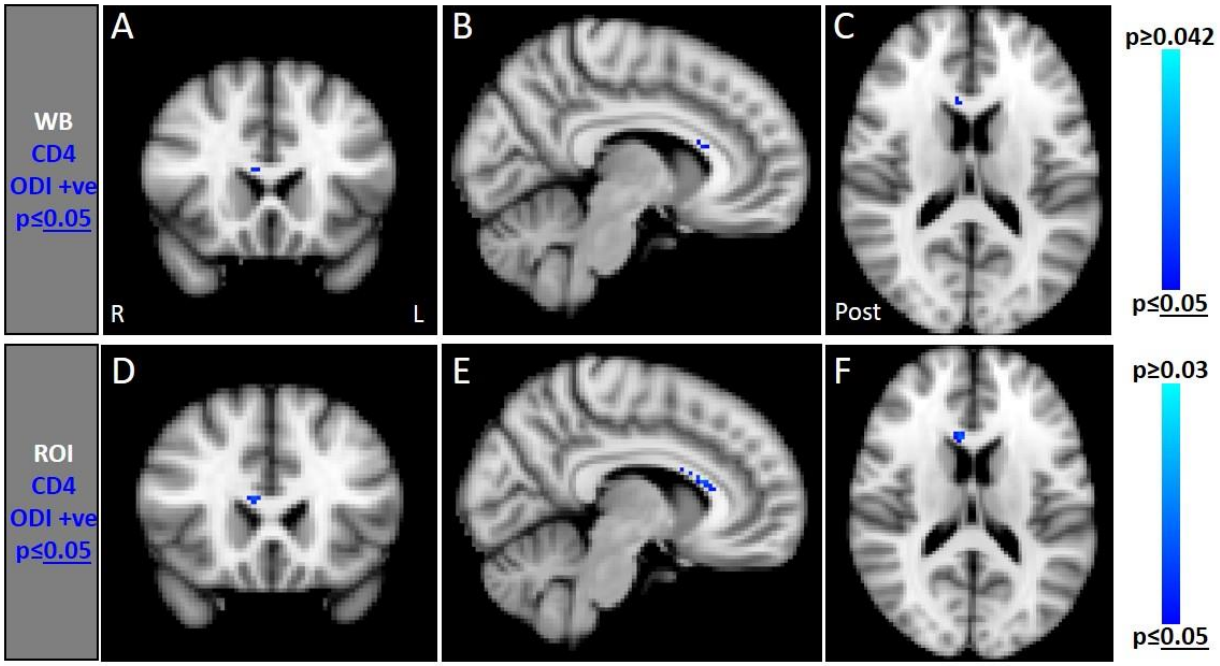

G

Cluster Peak Wholebrain	MNI co-ordinates (x,y,z)	K size (voxels)	P value ODI+ve
CC Body	8, 20, 16mm	4	0.042

H

Cluster Peak ROI	MNI co-ordinates (x,y,z)	K size (voxels)	P value ODI+ve
CC Body	8, 20, 16mm	14	0.03
CC Body	8, 14, 20mm	3	0.04

I

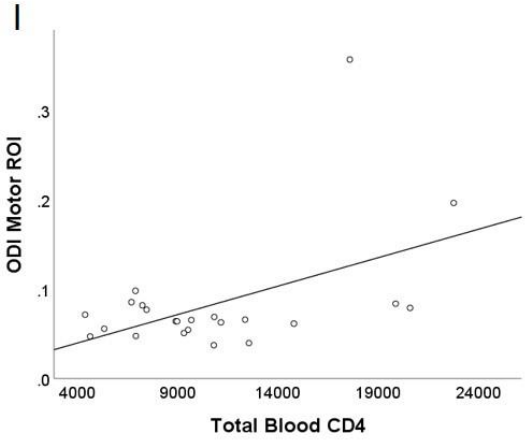

Figure 4.2.3. **Higher total blood CD4 cells associated with increased ODI** within the body and anterior right aspect of the corpus callosum at whole brain (A-C) and Motor ROIs analysis. Location, size ("K") and significance of the cluster maxima are outlined in tables G and H, respectively. ODI within the regions shown in D-E demonstrates a weak positive association with total blood CD4 cells on scatterplot (I; adjusted R^2=0.2). *R=right; L=left; Post=posterior.*

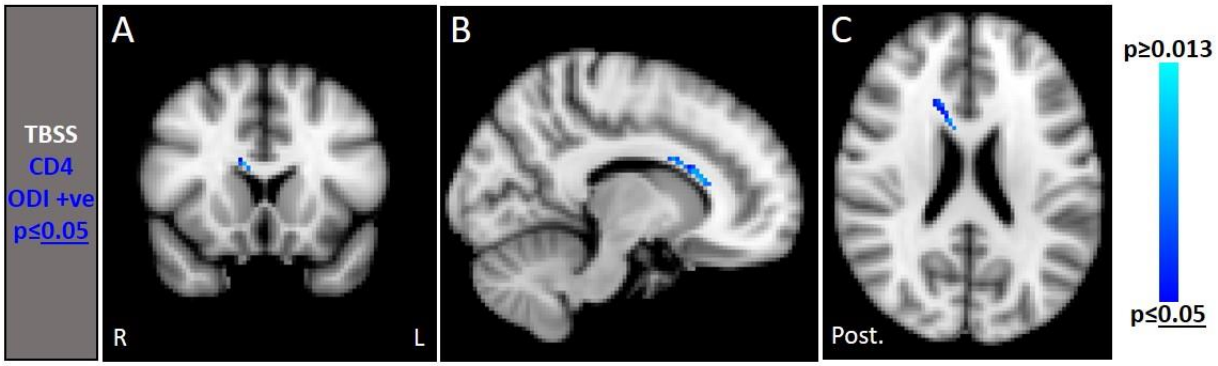

D

Cluster Peak TBSS	MNI co-ordinates (x,y,z)	K size (voxels)	P value ODI+ve
CC Body	10, 18, 18mm	80	0.013

E

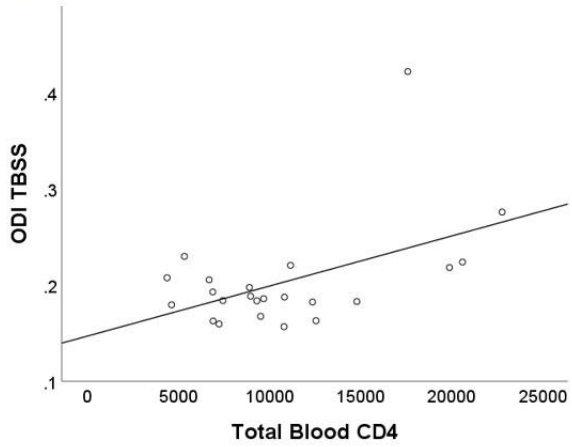

Figure 4.2.4. **Higher total blood CD4 cells associated with increased skeletonised ODI** within the body and anterior right aspect of the corpus callosum (A-C). Location, size ("K") and significance of the cluster maximum is outlined in table D, respectively. ODI within the regions shown in A-C demonstrates a weak positive association with total blood CD4 cells on scatterplot (E; adjusted R^2=0.2). Colour column represents range of p values. *R=right; L=left; Post=posterior.*

4.3 Relationships between NODDI ID=1.7 and Clinical Measures in the New Patients

No significant positive or negative associations were found between NDI, ODI or ISO and clinical measures ALSFRS, Disease Duration, Rate of Disease Progression, ECAS and ECAS ALS Specific score at the level of the Whole Brain and Motor ROIs, or the TBSS whole skeleton and TBSS Motor ROIs. In particular, no association with Disease Duration was replicated as was reported with whole brain FA.

4.4 Group Differences: NODDI ID=1.7 in Historical Patients versus Controls

Whole brain and Motor ROIs. Extensive and contiguous clusters of significantly decreased NDI were seen throughout the CSTs and corpus callosum in patients using TFCE before (Fig. 4.4.2 A-C) and after (Fig. 4.4.2 D-F) masking with the Motor ROIs. Mean NDI in these clusters corroborated the reduction in the patient group (Fig. 4.4.2 G and H, respectively),. The areas of reduced NDI are mirrored by, but more extensive than, those detected with FA (see Fig. 3.4.2). Significantly increased ODI was seen in the right anterior corpus callosum extending into the right forceps minor (Fig.4.4.3 A-C) in patients at whole brain level, and more extensively within the left CST and body and anterior aspect of the CC at Motor ROIs level (D-F), indicated by the mean ODI in these clusters (Fig.4.4.3 G and H, respectively). These areas are shared by, though less widespread than, those detected with FA in the Historical participants.

A small cluster of decreased ODI in the right putamen on whole brain (Fig. 4.4.4 A-C) and two single-voxel 'clusters' of decreased ISO within the right CST on Motor ROIs analysis (Fig. 4.4.4 D-F) were also seen, with effect sizes of 1.83 and 1.33, respectively. Regarding these single-voxel 'clusters' of reduced ISO, relaxing the significance threshold of the TFCE output file to corrected p values of <0.1 revealed enlarging clusters remaining within only the right CST of 19 and 6 voxels, respectively. At a threshold of <0.2 the clusters merged into an isolated right CST cluster of 61 voxels. Reduced ISO within the right CST was also observed using TBSS (as below).

TBSS and TBSS Motor ROIs. Skeletonised NDI throughout the rostro-caudal length of the CSTs, the PCGs and the corpus callosum was significantly decreased in patients using TFCE across the entire skeleton (Fig. 4.4.5 A-C with wider regions of the corona

radiata and superior longitudinal fasciculus involved bilaterally) and with Motor ROIs analysis (Fig. 4.4.5 D-F), reflected by mean NDI from these areas (Fig.4.4.5 G and H, respectively). Once again, the location of NDI changes overlap with, and are much more extensive than, those detected with FA (see Fig. 3.4.3). Significantly increased ODI within the body and right anterior corpus callosum extending into the right forceps minor was seen using Motor ROIs analysis (Fig. 4.4.6 A-C), albeit present at lower thresholds using the entire skeleton (not shown). Furthermore, the ODI increases were less extensive than the skeletonised changes in FA.

Clusters of skeletonised ISO demonstrated significant decreases within the rostral right CST, corona radiata and superior longitudinal fasciculus on entire TBSS analysis (Fig. 4.4.7 A-C) with less extensive clusters restricted to the right CST on Motor ROIs analysis, as had been picked up on whole brain analysis above. Conversely, a cluster of significantly increased skeletonised ISO was also found within the body and anterior aspect of the CC (Fig. 4.4.7 D-E).

Table 4.4.1

	Whole Brain			Motor ROIs			TBSS Entire Skeleton			TBSS Motor ROIs		
	NDI	ODI	ISO	NDI	ODI	ISO	NDI	ODI	ISO	NDI	ODI	ISO
Controls>ALS	p=0.001	p=0.034		p=0.001		p=0.043	p=0.001		p=0.024	p=0.001		p=0.041
ALS>Controls		p=0.017			p=0.003						p=0.014	p=0.035

Table 4.4.1. **Summary of significant group differences in NODDI ID=1.7 between Historical Patients and Controls** using TFCE at Whole brain, Motor ROIs, TBSS and TBSS Motor ROIs levels. The main findings are of reduced NDI, increased ODI and reduced ISO within the CC and CSTs.

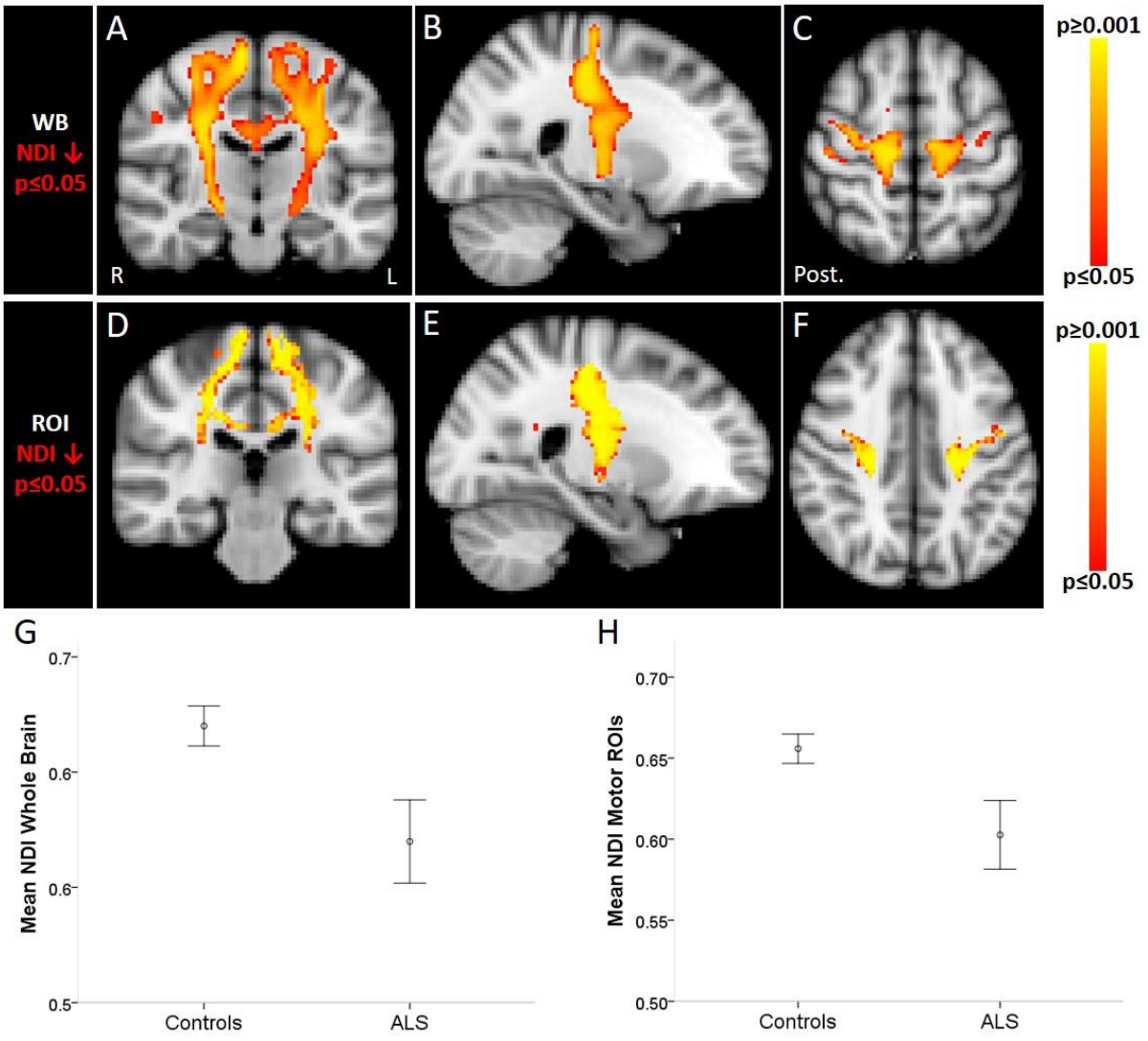

Cluster Peak WB	MNI co-ordinates (x,y,z)	K size (voxels)	P value NDI ↓
R CST	10, -22, 62 mm	5832	0.001
R CST (medulla)	2, -36, -50 mm	212	0.028

Cluster Peak ROI	MNI co-ordinates (x,y,z)	K size (voxels)	P value NDI ↓
R CST	24, -22, 40 mm	2327	<0.001
Body CC	-20, -48, 18 mm	18	0.036
Body CC	20, -48, 20 mm	16	0.041
R PMCtx	-6, -36, 68 mm	2	0.047

Figure 4.4.2. **NDI is extensively reduced in Historical Patients compared to Controls** extensively throughout the CSTs, PCGs and corpus callosum using TFCE at the whole brain (A-C) and Motor ROIs (D-F) levels, confirmed by quantifying mean NDI in these areas (G and H, respectively). Location, size ("K") and significance of the cluster maxima are outlined in the tables. Colour columns represent range of p values and error bars represent 95% confidence intervals. *R=right; L=left; Post=posterior.*

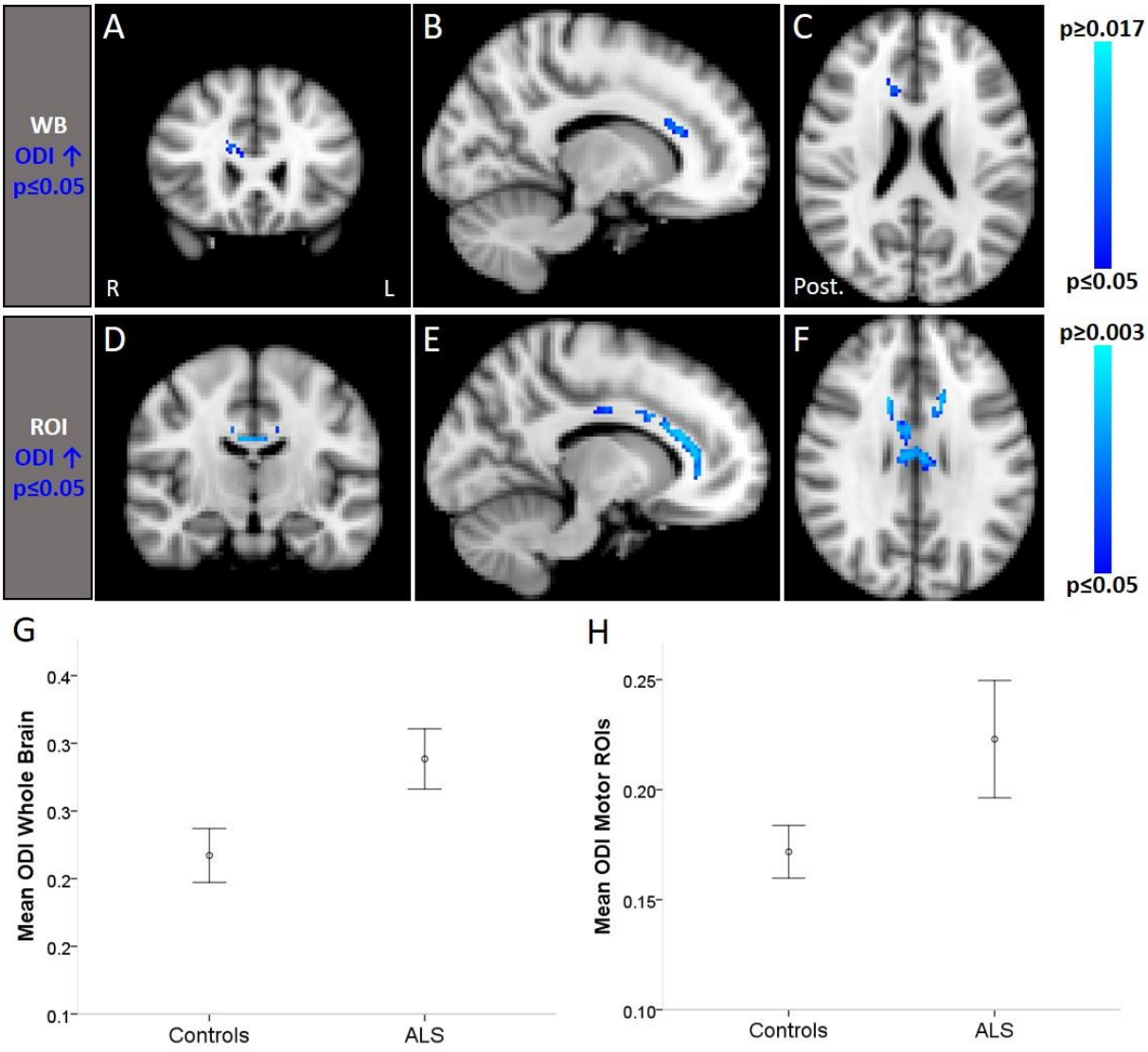

Cluster Peak WB	MNI co-ordinates (x,y,z)	K size (voxels)	P value ODI ↑
CC Body	16, 30, 18mm	75	0.017
CC Body	8, 28, 14mm	1	0.048

Cluster Peak ROI	MNI co-ordinates (x,y,z)	K size (voxels)	P value ODI ↑
Body CC	16, 30, 18mm	736	0.003
L CST	-20, -22, 42mm	8	0.048

Figure 4.4.3. **ODI is increased in Historical Patients compared to Controls** within the corpus callosum extending into the right forceps minor using TFCE at the whole brain level (A-C), and more extensively within the left CST along with the CC using Motor ROIs analysis (D-F), confirmed by quantifying mean ODI in these areas (G and H, respectively). Location, size ("K") and significance of the cluster maxima are outlined in the tables. Colour columns represent range of p values and error bars represent 95% confidence intervals. *R=right; L=left; Post=posterior.*

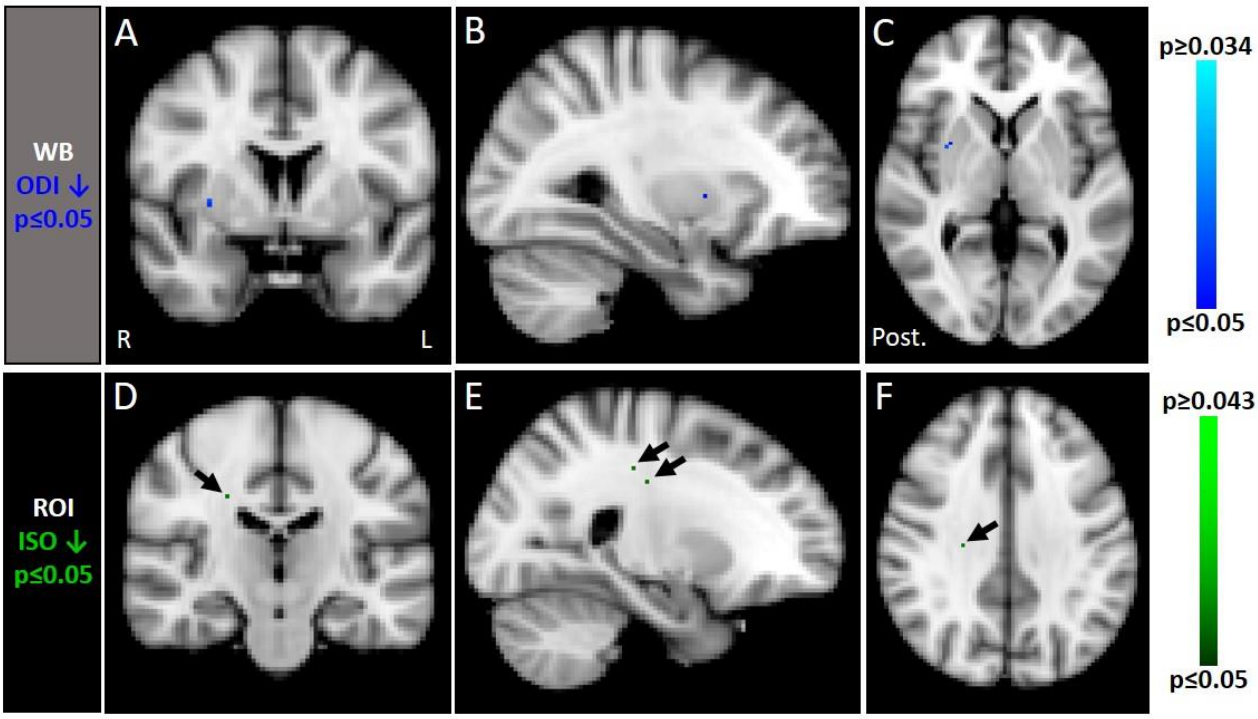

Cluster Peak WB	MNI co-ordinates (x,y,z)	K size (voxels)	P value ODI ↓
R Putamen	32, 2, 2mm	3	0.034

Cluster Peak ROI	MNI co-ordinates (x,y,z)	K size (voxels)	P value ISO ↓
R CST	24, -26, 40mm	1	0.043
R CST	24, -20, 34mm	1	0.043

Figure 4.4.4. **ODI and ISO are decreased, within the right putamen (A-C) and right CST (D-F), respectively,** in Historical Patients compared to controls using TFCE at the whole brain level and Motor ROIs levels, respectively. Location, size ("K") and significance of the cluster maxima are outlined in the tables. Colour columns represent range of p values and error bars represent 95% confidence intervals. *R=right; L=left; Post=posterior.*

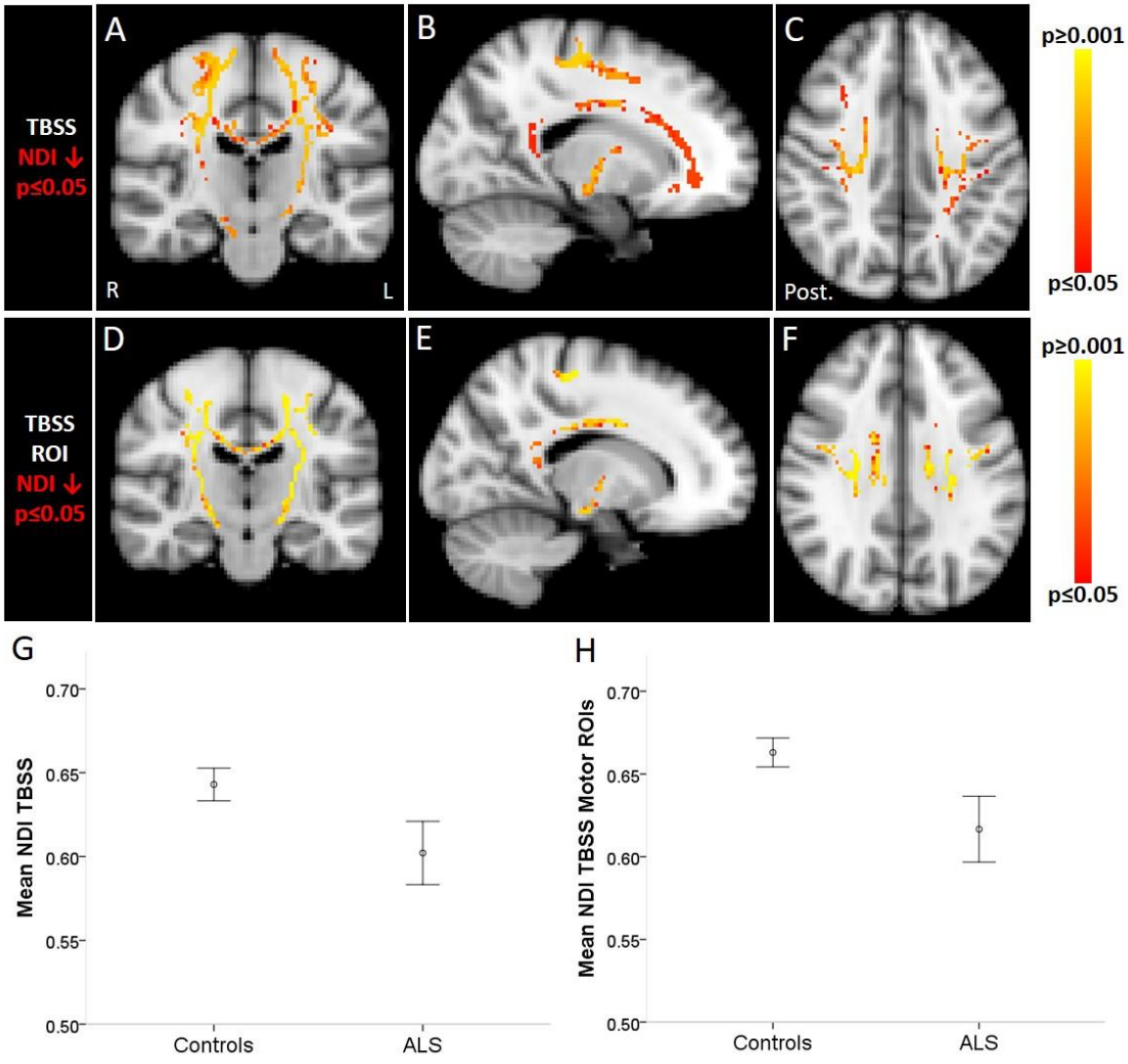

Cluster Peak TBSS	MNI co-ordinates (x,y,z)	K size (voxels)	P value NDI ↓
R CST	22, -24, 48mm	3433	0.001
R Inf. Parietal	52, -14, 26mm	36	0.049

Cluster Peak TBSS ROI	MNI co-ordinates (x,y,z)	K size (voxels)	P value NDI ↓
R CST	22, -24, 46mm	1765	0.001

Figure 4.4.5. **Skeletonised NDI is extensively reduced in Historical Patients compared to Controls** throughout the CSTs, PCGs, CC, bilateral coronae radiatae and superior longitudinal fasciculi using TFCE across the entire skeleton (A-C) and the CSTs, PCGs, CC using TFCE within Motor ROIs only (D-F). Location, size ("K") and significance of the cluster maxima are outlined in the tables. Mean NDI in these areas was accordingly decreased (G and H, respectively). Colour columns represent range of p values and error bars represent 95% confidence intervals. *R=right; L=left; Post=posterior.*

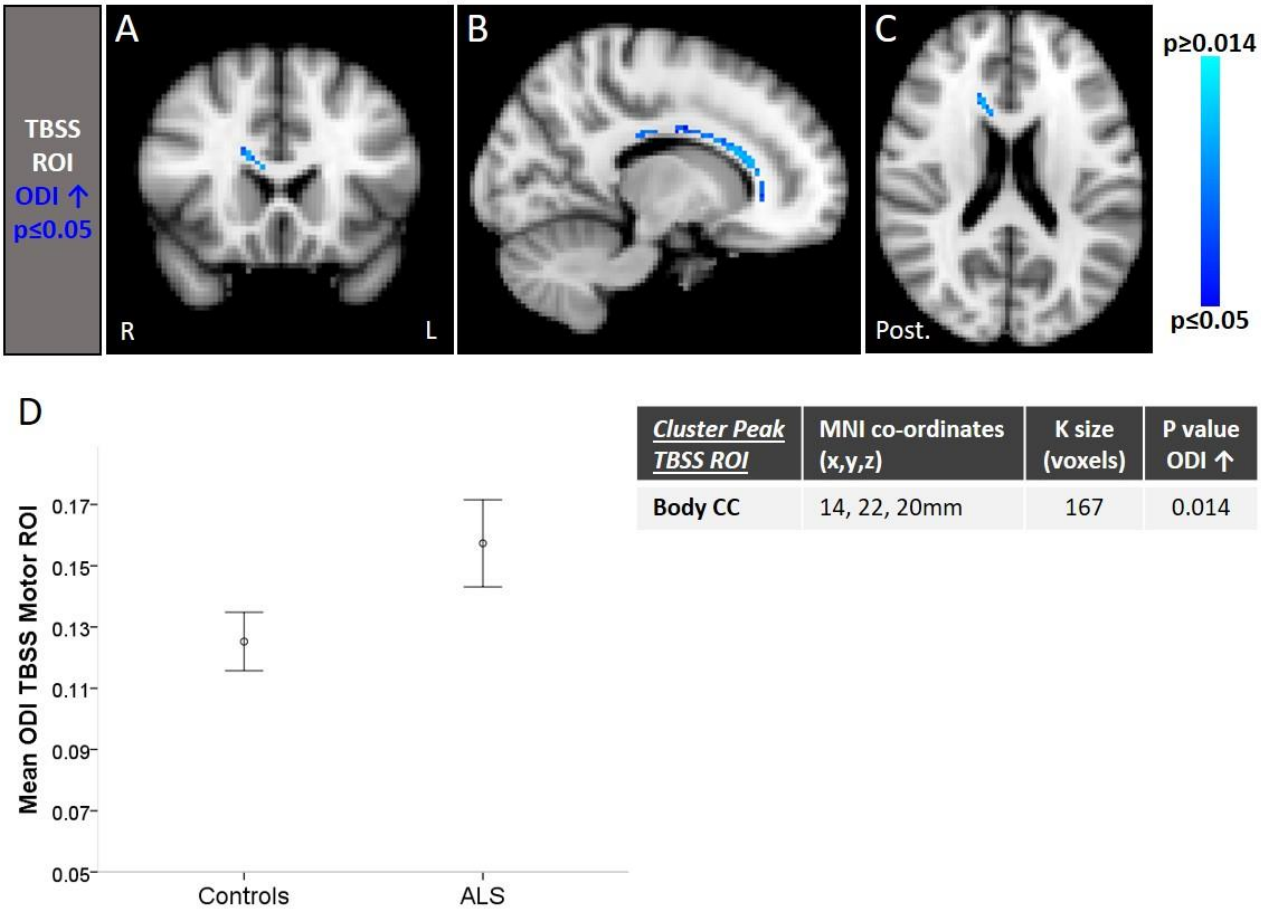

Cluster Peak TBSS ROI	MNI co-ordinates (x,y,z)	K size (voxels)	P value ODI ↑
Body CC	14, 22, 20mm	167	0.014

Figure 4.4.6. **Skeletonised ODI of the Motor ROIs is increased in Historical Patients compared to Controls** within the central body and right anterior corpus callosum extending into the right forceps minor using TFCE (A-C), confirmed by quantifying mean ODI in these areas (D). Location, size ("K") and significance of the cluster maximum is outlined in the table. Colour columns represent range of p values and error bars represent 95% confidence intervals. *R=right; L=left; Post=posterior.*

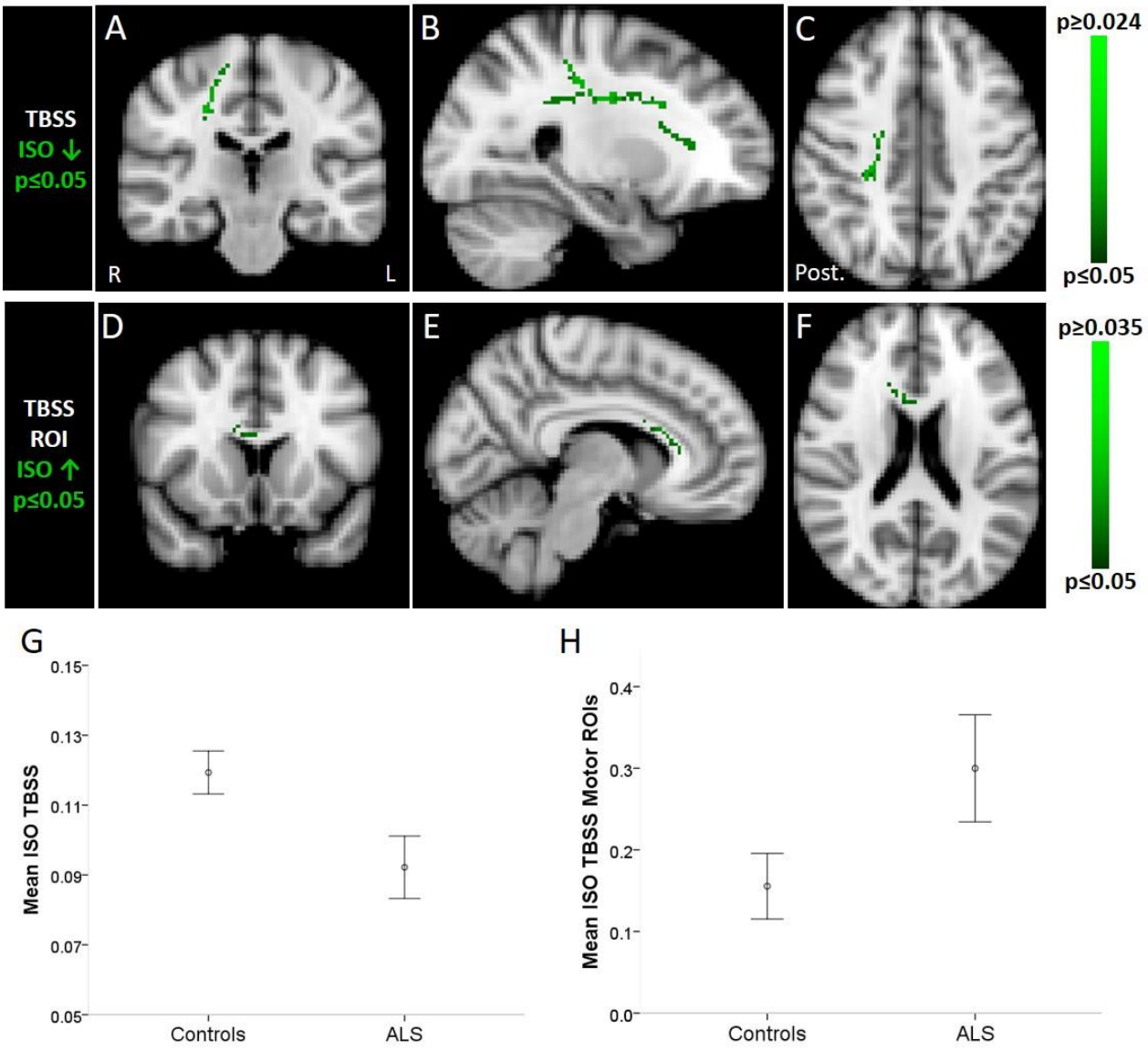

Cluster Peak TBSS	MNI co-ordinates (x,y,z)	K size (voxels)	P value ISO ↓
R CST	26, -16, 32mm	287	0.024

Cluster Peak TBSS ROI	MNI co-ordinates (x,y,z)	K size (voxels)	P value ISO ↑
CC Body	8, 20, 18mm	43	0.035

Figure 4.4.7. **Skeletonised ISO is decreased in Historical Patients compared to Controls** within the right CST, superior longitudinal fasciculus and right CST on entire skeleton analyses (A-C; mean ISO quantified in G). **Conversely, ISO is increased** in the body and anterior CC (D-F; mean ISO in H). Location, size ("K") and significance of each respective cluster maxima are outlined in the tables. Colour columns = range p value and error bars = 95% confidence intervals. *R=right; L=left; Post=posterior.*

4.5 Relationships between NODDI ID=1.7 & Clinical Measures in Historical Patients

Whole brain and Motor ROIs. No significant associations were found between NDI, ODI or ISO and the ALSFRS, Rate of Progression, Disease Duration total ECAS score and ECAS ALS Specific score at the level of Whole Brain or Motor ROIs.

TBSS and TBSS Motor ROIs. A significant positive association between skeletonised NDI and the ECAS ALS specific score was found within an extensive area of the left CST extending from the subcortical white matter of the PCG via the posterior limb of the internal capsule, in addition to the left CC and deep anterior frontal lobe white matter (Fig. 4.5.2 A-C). A strong linear relationship was seen on scatterplot (Fig. 4.5.2 H) with adjusted R^2=0.37. The same association failed to reach significance (p=0.06) following TBSS Motor ROIs analysis though the same areas of the left CST and CC emerged upon lowering the threshold. A small area of skeletonised ISO within the anterior CC also demonstrated a significantly negative association with the total ECAS score (Fig. 4.5.2 D-F) with a strong linear relationship on scatterplot (Fig. 4.5.2 J) and adjusted R^2=0.43.

No other significant associations were found with ALSFRS, Rate of Progression, Disease Duration total ECAS score and ECAS ALS Specific score using TBSS or TBSS Motor ROIs analyses (Table 4.5.1). Of note, the positive and negative associations between FA and the ALSFRS and Disease Duration, respectively, were not observed (refer back to Table 3.5.1).

	TBSS Entire Skeleton						TBSS Motor ROIs					
	NDI		ODI		ISO		NDI		ODI		ISO	
	Pos	Neg	Pos	Neg	Pos	Neg	Pos	Neg	Pos	Neg	Pos	Neg
ALSFRS												
Rate												
Duration												
ECAS												p=0.048
ECAS ALS Spec	p=0.033											

Table 4.5.1. **Summary of significant relationships between NODDI ID=1.7 and clinical factors** in the Historical Patients using TFCE at TBSS and TBSS Motor ROIs levels.

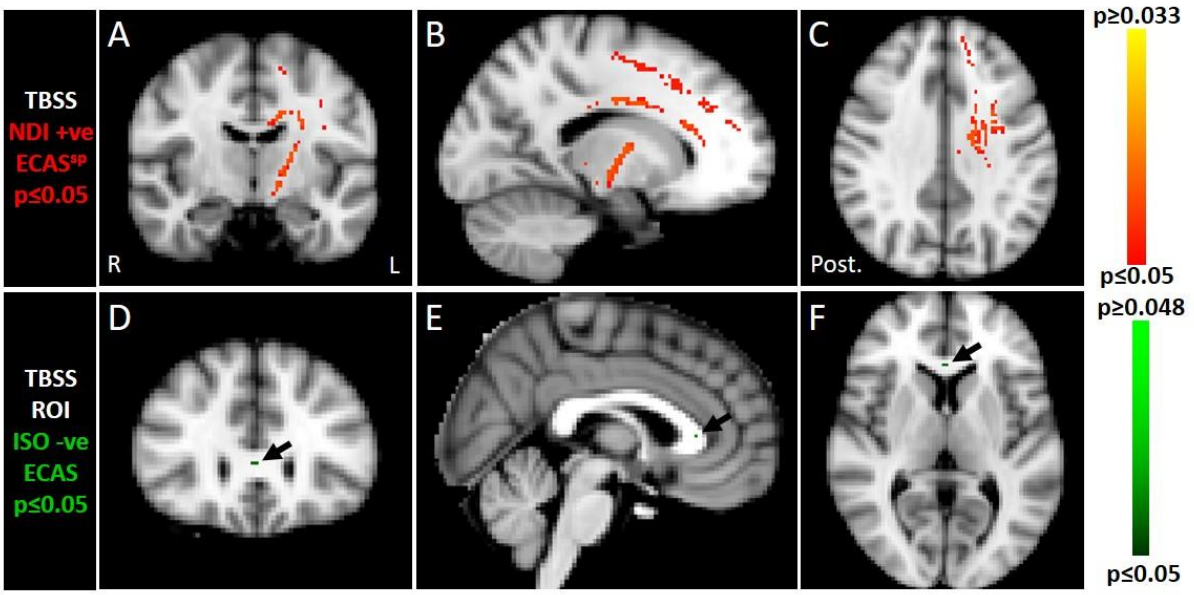

G

Cluster Peak TBSS	MNI co-ordinates (x,y,z)	K size (voxels)	P value NDI+ve
CC Body	-18, -4, 34mm	1169	0.033

H

Cluster Peak TBSS ROI	MNI co-ordinates (x,y,z)	K size (voxels)	P value ISO-ve
CC Body	2, 28, 6mm	2	0.048

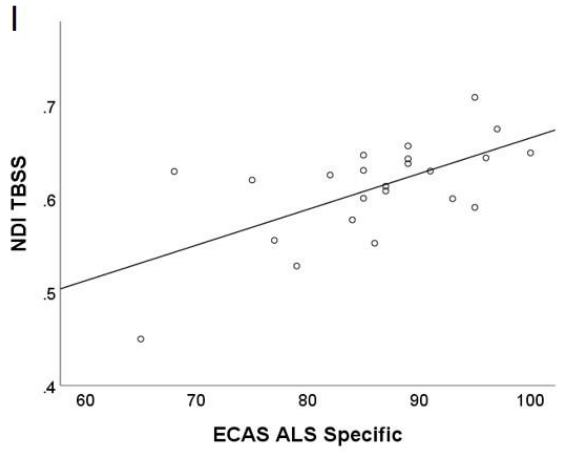

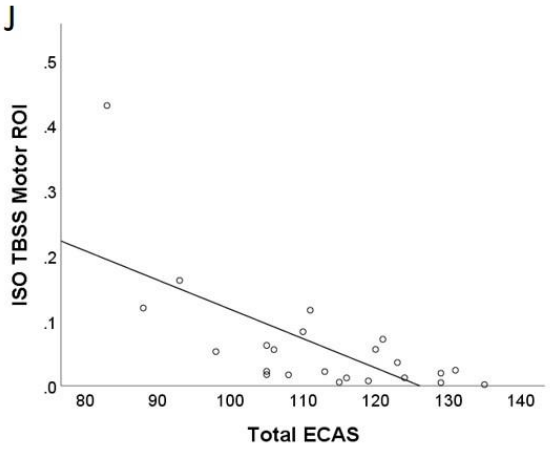

Figure 4.5.2. **Higher performance on the ECAS associated with higher skeletonised NDI and lower ISO.** A-C show the positive relationship between NDI along the left CST, PCG, CC and frontal lobe white matter and the ECAS ALS Specific score, with a strong linear relationship on scatterplot (H; adjusted R^2=0.37). D-F demonstrate the negative association between ISO in the CC and the total ECAS score, with a strong linear relationship on scatterplot (J; adjusted R^2=0.43). Location, size ("K") and significance of each cluster maximum are outlined in tables G and H, respectively. Colour bars = p value range. *R=right; L=left; Post=posterior.*

4.6 Relationships between NODDI ID=1.7 and Clinical Measures

Combined New + Historical Patients

Whole brain and Motor ROIs. No significant associations between NDI, ODI or ISO and ALSFRS, Duration of Disease, Rate of Disease Progression, ECAS total score or ECAS ALS-specific score were found. In particular, no positive association was found with the ECAS ALS-specific score in the right parietal lobe as was seen with whole brain FA (see Fig. 3.6.2).

TBSS and TBSS Motor ROIs. A significant positive association (p=0.048) between skeletonised NDI within the CC and right rostral CST and the ALSFRS score was found using entire TBSS skeleton TFCE (Fig. 4.6.2 A-C). NDI values within these clusters demonstrated a moderate linear relationship with ALSFRS on scatterplot (Fig. 4.6.2 I) with adjusted R^2=0.24. The significant positive association was reproduced at slightly higher significance (p=0.036) following Motor ROIs TBSS TFCE (Fig. 4.6.2 D-F). Conversely, a significant negative association (p=0.023) between extensive skeletonised NDI throughout the CC, PCGs, rostro-caudal length of the CSTs including the posterior limbs of the internal capsules, bilateral superior longitudinal fasciculi and the corona radiatae and Duration of Disease was found using entire TBSS skeleton TFCE (Fig. 4.6.3 A-C). NDI within these clusters demonstrated a moderate linear relationship with ALSFRS score on scatterplot (Fig. 4.6.3 I) with adjusted R^2=0.19. The association was reproduced at slightly higher significance (p=0.011) following Motor ROIs TBSS TFCE (Fig. 4.6.3 D-F). These results with NDI echo respective positive and negative associations, between FA and ALSFRS (Fig. 3.6.3) and Disease Duration (see Fig. 3.6.4).

However, no positive association was found with Disease Duration in the right temporal lobe as was seen with skeletonised FA (see Fig. 3.6.5).

Table 4.6.1	NODDI versus Clinical Measures in Combined Doctoral and Historical Patients											
	TBSS Entire Skeleton						TBSS Motor ROIs					
	NDI		ODI		ISO		NDI		ODI		ISO	
	Pos	Neg	Pos	Neg	Pos	Neg	Pos	Neg	Pos	Neg	Pos	Neg
ALSFRS	p=0.048						p=0.036					
Rate												
Duration		p=0.023						p=0.011				
ECAS												
ECAS ALS Spec												

Table 4.6.1. **Summary of significant relationships between NODDI ID=1.7 and clinical factors** in the Combined Patients using TFCE at TBSS and TBSS Motor ROIs levels. The positive association between NDI and the ALSFRS, and the negative association between NDI and the Disease Duration mirror the main findings with FA (see Table 3.6.1).

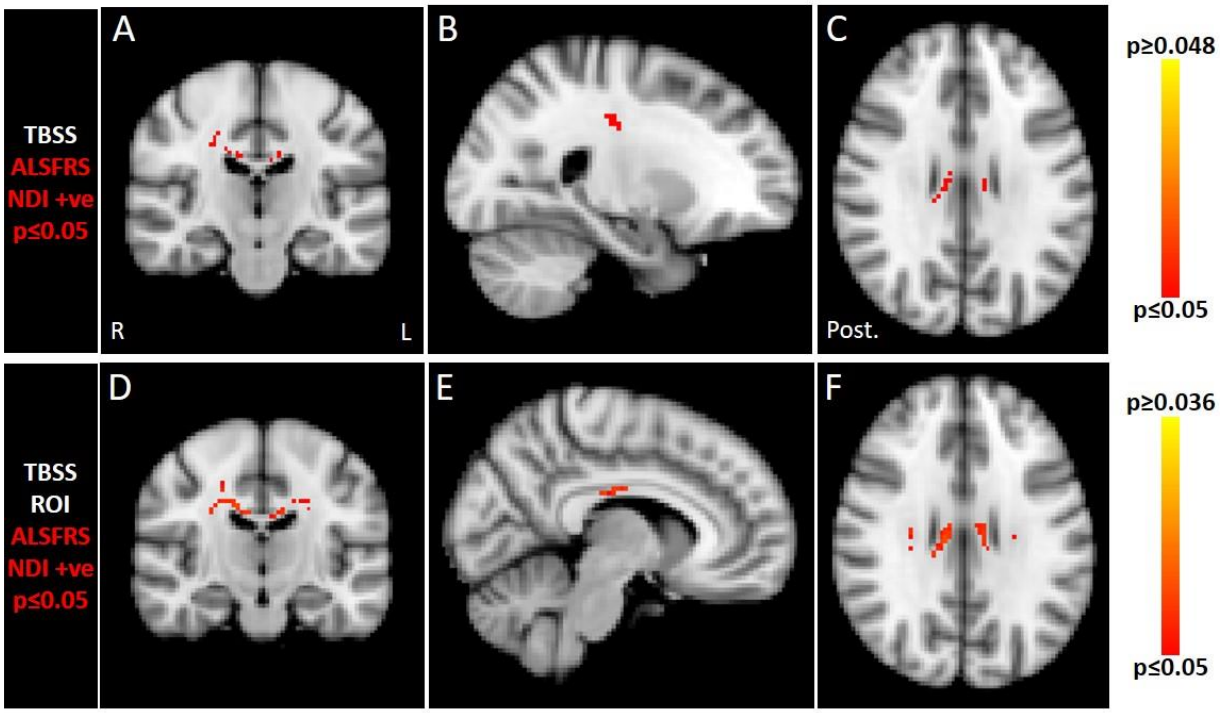

G

Cluster Peak TBSS	MNI co-ordinates (x,y,z)	K size (voxels)	P value NDI+ve
CC Body	10, -20, 28mm	33	0.048
R CST	24, -22, 34mm	17	0.049
CC Body	-10, -22, 28mm	4	0.049

H

Cluster Peak TBSS ROI	MNI co-ordinates (x,y,z)	K size (voxels)	P value NDI+ve
CC Body	10, -20, 28mm	171	0.036
L CST	-24, -20, 34mm	39	0.043

I

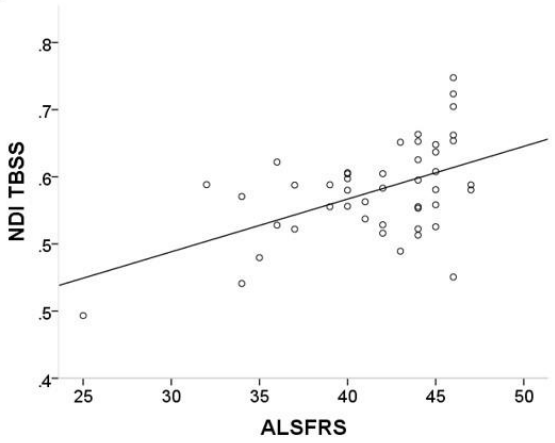

Figure 4.6.2. **Reduced functional score associated with reduced NDI** within the CC and right rostral CST using TFCE TBSS (A-C) and extending into both CSTs on Motor ROIs TBSS analysis in Combined Patients (D-F) which are strikingly similar to the areas associated with reduced FA (see Fig. 3.6.3). Location, size ("K") and significance of the cluster maxima are outlined in tables G and H, respectively. NDI within the areas in A-C demonstrates a moderate linear relationship with ALSFRS on scatterplot (I; adjusted R^2=0.24). Colour bars = p value range. *R=right; L=left; Post=posterior.*

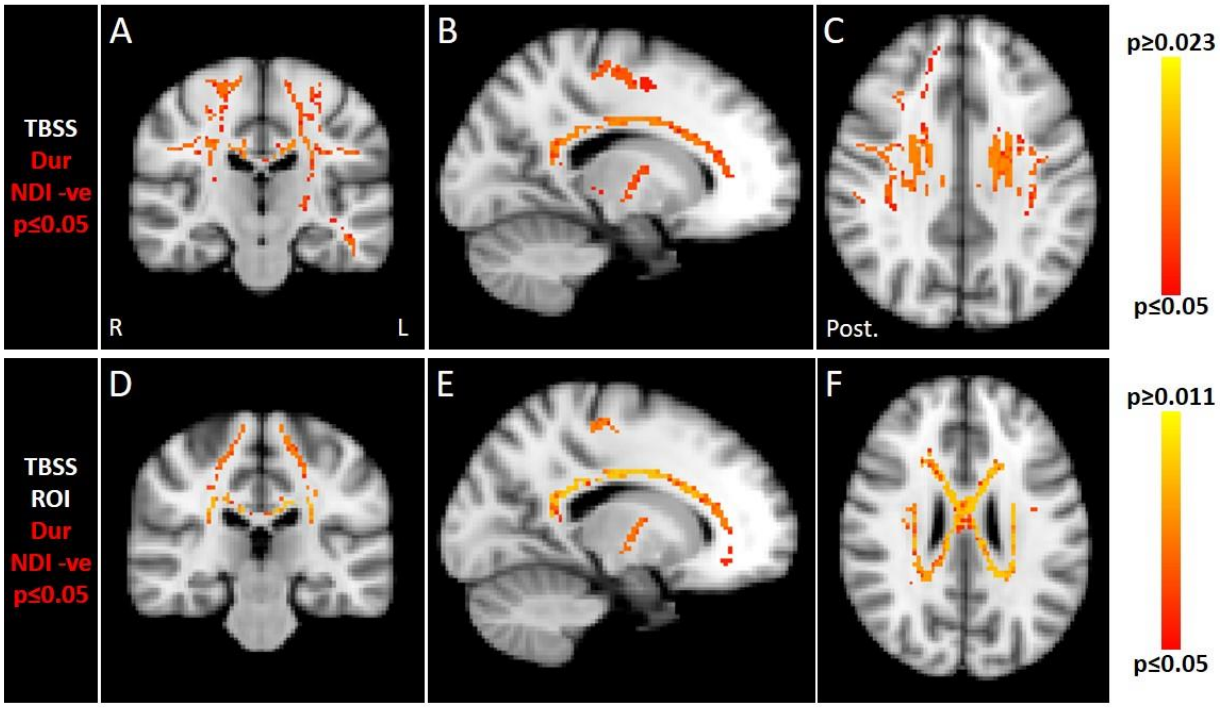

G

Cluster Peak TBSS	MNI co-ordinates (x,y,z)	K size (voxels)	P value NDI-ve
CC Body	-10, 8, 24mm	4517	0.023

H

Cluster Peak TBSS ROI	MNI co-ordinates (x,y,z)	K size (voxels)	P value NDI-ve
CC Body	-14, -24, 30mm	2258	0.011

I

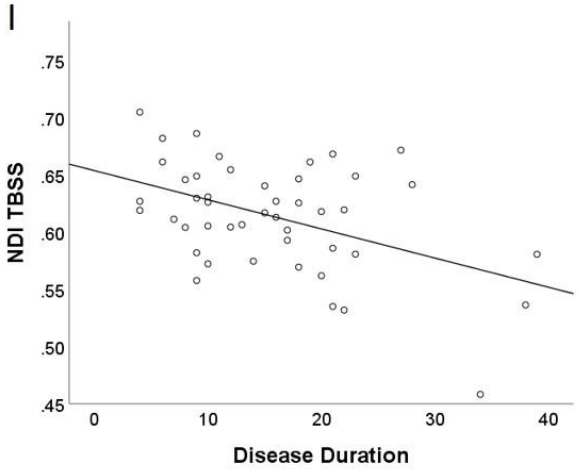

Figure 4.6.3. **Increased disease duration associated with reduced NDI** within the CC, PCGs, rostro-caudal length of the CSTs traversing the posterior limbs of the internal capsules, bilateral superior longitudinal fasciculi and the corona radiatae using TFCE TBSS (A-C) and extensively throughout the CSTs and CC on Motor ROIs TBSS analysis (D-F). These are strikingly similar to the areas associated with reduced FA (see Fig. 3.6.4). Location, size ("K") and significance of each cluster maximum are outlined in tables G and H, respectively. NDI within the areas in A-C demonstrate the moderate linear relationship with ALSFRS score on scatterplot (I; adjusted R^2=0.19). Colour bars = p value range. *R=right; L=left; Post=posterior.*

4.7 Summary of main NODDI ID=1.7 findings in Patients with ALS

A. NDI is reduced (exclusively in the Historical Patients) and ODI increased (predominantly in the New Patients) within the CSTs and CC compared to controls, particularly on TBSS and TBSS Motor ROIs analyses. This mirrors the location of reduced FA seen in both Patient groups, albeit more extensive in the Historical Patients.

B. Increased ISO in the CC +/- the CSTs *may* also contribute to the lowered FA in these regions. See Table 4.7.1 for a summary of Patient versus Control group differences.

C. ALSFRS and Disease Duration demonstrate consistent positive and negative associations, respectively, with NDI within the CSTs, CC and PCGs in the Combined patient group analyses (rather than the New or, particularly, the Historical group alone) most strikingly revealed using TBSS analyses. To reiterate, these are the two clinical measures which also differ significantly between the patient groups.

D. Associations between skeletonised ISO or NDI and the ECAS or ECAS ALS Specific scores, respectively, were limited to the Historical group only.

E. Total blood CD4 cell count consistently demonstrates a positive association with ODI within the CC, which persists after accounting for the Rate of disease progression, and this is the same region in which a negative association was found with FA.

Table 4.7.1. **Summary of significant Diffusion MRI (FA and NODDI ID=1.7) changes between Patient & Control groups.** Coloured boxes highlight similarities. *CC=corpus callosum; CSTs=corticospinal tracts; PCGs=precentral gyri; Cor=corona radiata.*

4.8 Group Differences: New Patients versus New Controls NODDI ID=1.1

No significant differences were found in NDI, ODI or ISO between patients and controls at the level of the Whole Brain and PCGs ROI, particularly within any grey matter regions. Furthermore, the increased ODI seen in patients with NODDI 1D=1.7 was not seen.

4.9 Relationships between NODDI ID=1.1 and Blood CD4 cells in the New Patients

Whole brain and PCGs ROI. A significant negative association (p=0.023) between NDI within the left precentral gyrus cortical grey matter and the Blood Treg:CD4 Ratio was found on whole brain TFCE analysis. The association emerged with greater significance (p=0.015) following correction for average precentral gyrus cortical thickness (Fig. 4.9.2 A-C). NDI values within this cluster showed a moderate linear association on scatterplot (Fig. 4.9.2 E) with adjusted R^2=0.18.

A borderline significant positive association between total blood CD4 count and unmasked ODI (p=0.05) was seen within the anterior corpus callosum, similarly to that demonstrated within the significance threshold using whole brain NODDI ID=1.7 data.

No other associations were found between NDI, ODI or ISO and total blood CD4 count, total blood $CD4^+$ $CD25^+$ $FoxP3^+$ Treg count, or the Treg:CD4 Ratio (Table 4.9.1). **Adding rate of disease progression as an additional co-variate** (to age) rendered all associations beneath the significance threshold.

Table 4.9.1	Whole Brain						PCGs ROI					
	NDI		ODI		ISO		NDI		ODI		ISO	
	Pos	Neg	Pos	Neg	Pos	Neg	Pos	Neg	Pos	Neg	Pos	Neg
Blood CD4 total												
Blood Treg total												
Treg:CD4 Ratio								p=0.023				
							PCGs thickness corr.	p=0.015				

Table 4.9.1. **Summary of significant relationships between NODDI ID=1.1 and blood CD4 cells** in the New Patients using TFCE at Whole brain and PCGs ROI level, with age as the only co-variate.

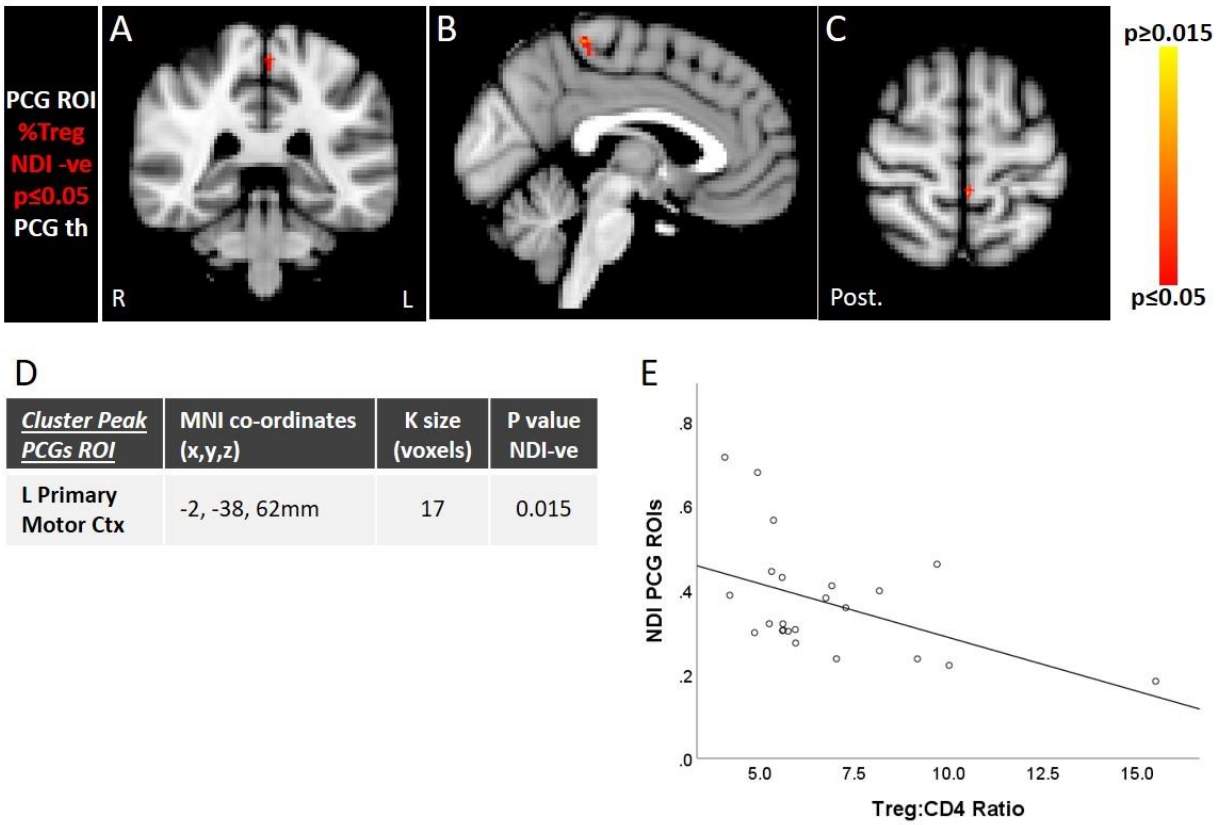

Cluster Peak PCGs ROI	MNI co-ordinates (x,y,z)	K size (voxels)	P value NDI-ve
L Primary Motor Ctx	-2, -38, 62mm	17	0.015

Figure 4.9.2. **Greater Treg:CD4 ratio associated with lower NDI in the left precentral cortex** extending towards the post-central gyrus using PCGs ROI TFCE analysis (A-C). Location, size ("K") and significance of the cluster maximum is outlined in table D. NDI values within this cluster showed a moderate linear association on scatterplot (E; adjusted R^2=0.18). Colour bar represents p value range. *R=right; L=left; Post=posterior; PCG th=precentral gyrus thickness covariate.*

4.10 Relationships between NODDI ID=1.1 and Clinical Measures in the New Patients

No significant positive or negative associations between NDI, ODI or ISO and ALSFRS, Duration of Disease, Rate of Disease Progression, ECAS total score or the ECAS ALS-specific sub score were found at the level of the Whole Brain and PCGs ROI, particularly within any grey matter regions.

4.11 Group Differences: NODDI ID=1.1 in Historical Patients versus Controls

Whole brain and PCGs ROI. Clusters of significantly decreased NDI were seen throughout the white matter of the right CST and body of the CC in patients using TFCE at whole brain level (Fig. 4.11.2 D-F), although not unexpectedly at a much reduced significance compared to similar whole brain analysis using NDI ID=1.7 (see Fig. 4.4.2 A-C). Significantly decreased ODI was also seen in a very small cluster of voxels within the left primary motor cortex using TFCE at the PCGs ROI level in patients (Fig.4.11.2 A-C), although fell marginally outside the significance threshold once precentral cortical thickness was used as a co-variate (p=0.057).

Table 4.11.1

	Whole Brain			PCGs ROIs		
	NDI	ODI	ISO	NDI	ODI	ISO
Controls>ALS	p=0.045				p=0.039*	
ALS>Controls						

Table 4.11.1. **Summary of significant group differences in NODDI ID=1.1 between the Historical Patients and Controls** using TFCE at the level of the Whole Brain and PCGs ROI. *Decreased ODI no longer found after correcting for precentral cortical thickness.

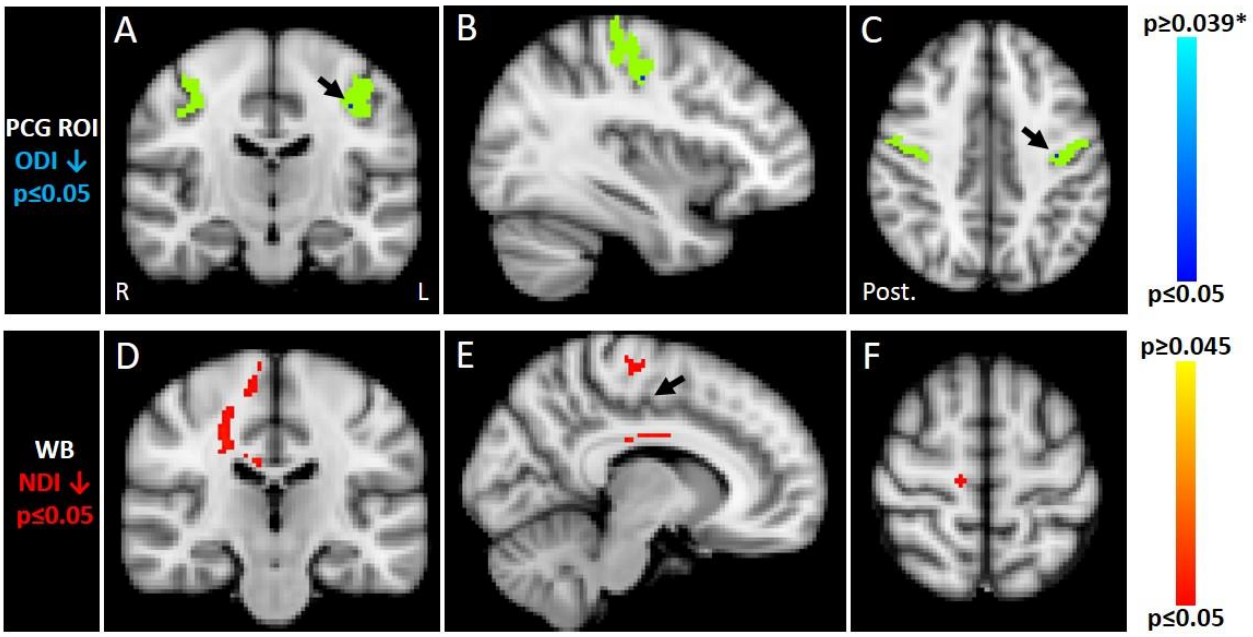

Cluster Peak PCGs ROi	MNI co-ordinates (x,y,z)	K size (voxels)	P value ODI ↓
CC Body	-14, -24, 30mm	2258	0.011

Cluster Peak WB	MNI co-ordinates (x,y,z)	K size (voxels)	P value NDI ↓
L Primary Motor Ctx	24, -22, 36mm	1	0.039

Figure 4.11.2. **ODI is reduced in New Patients compared to Controls within the left primary motor cortex** (arrows A-C) on PCGs ROI TFCE analysis, with the PCGs ROI mask shown in green. *Reduced ODI was no longer significant after correcting for cortical thickness. NDI was reduced within the right CST and subcortical PCG (D-F) on whole brain TFCE, as demonstrated from analyses at ID=1.7. Colour bar represents range of p values. Location, size ("K") and significance of the cluster maxima are outlined in the table. *R=right; L=left; Post=posterior; PCG th=precentral gyrus thickness as covariate.*

4.12 Relationships between NODDI ID=1.1 & Clinical Measures in Historical Patients

Whole brain and Motor ROIs. A significant negative association between a cluster of NDI within the right medial precentral gyrus cortex and ALSFRS was found using TFCE at the PCGs ROI level (Fig. 4.12.2 A-C). However, this did not survive correction for precentral cortex thickness (p=0.08). A significant negative association between a cluster of NDI within the left medial precentral gyrus cortex and the ECAS ALS Specific score was found also at the PCGs ROI level (Fig. 4.12.2 D-F), which did survive correction for precentral cortex thickness (p=0.007). NDI within this cluster demonstrated a strong linear relationship with the ECAS ALS Specific score on scatterplot (Fig. 4.12.2 H) with adjusted R^2=0.49. No other significant associations between NDI, ODI or ISO and ALSFRS, Duration of Disease, Rate of Disease Progression, ECAS total score or the ECAS ALS-specific sub score were found (Table 4.12.1).

Table 4.12.1

	Whole Brain						PCGs ROI					
	NDI		ODI		ISO		NDI		ODI		ISO	
	Pos	Neg	Pos	Neg	Pos	Neg	Pos	Neg	Pos	Neg	Pos	Neg
ALSFRS								p=0.008*				
Rate												
Duration												
ECAS												
ECAS ALS Spec								p=0.013†				

Table 4.12.1. **Summary of significant relationships between NODDI ID=1.1 and clinical factors** in Historical Patients using TFCE at Whole brain and PCGs ROI level. * Did not survive correction for precentral cortex thickness (p=0.08). † Did survive correction for precentral cortex thickness (p=0.007).

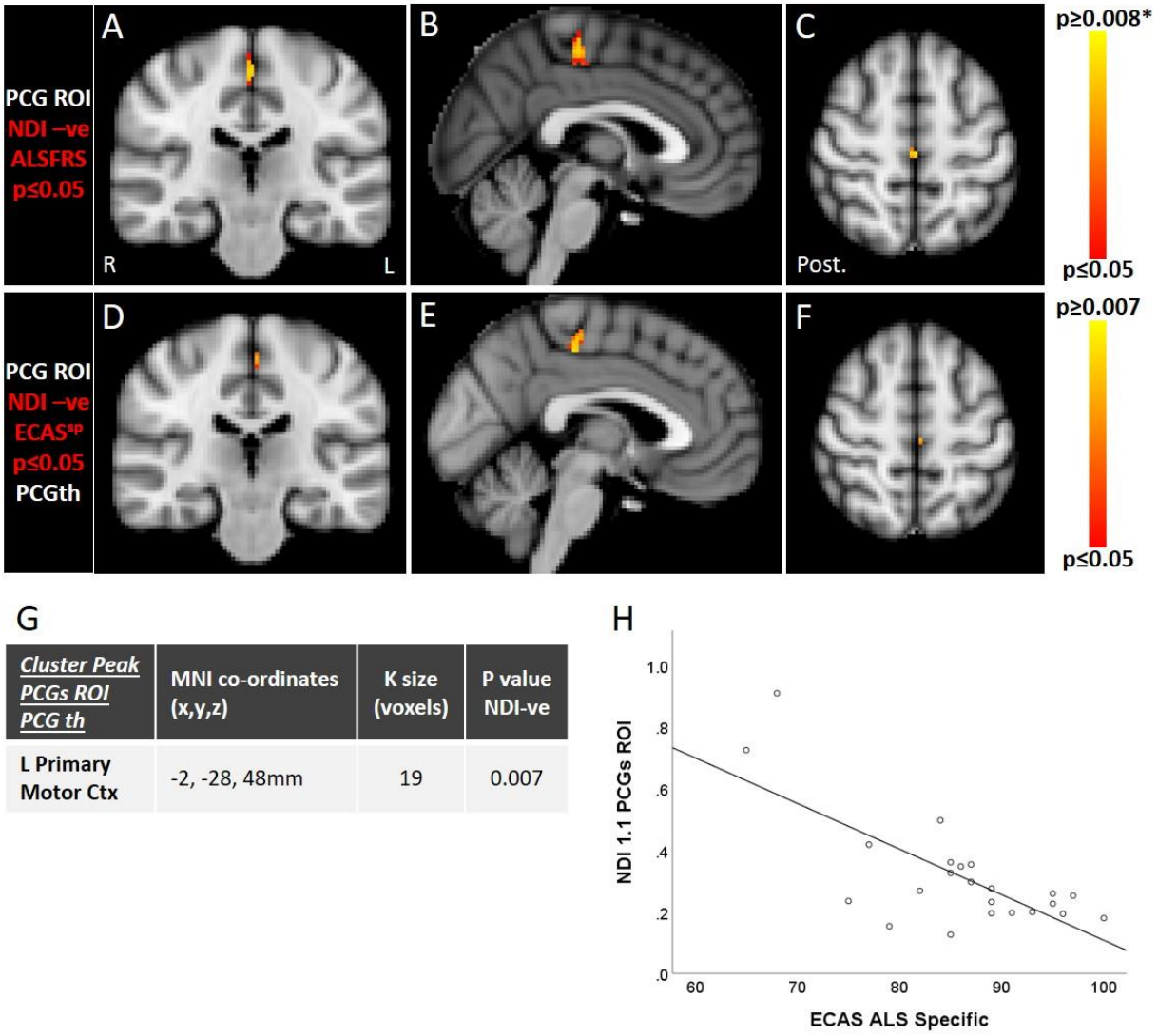

G

Cluster Peak PCGs ROI PCG th	MNI co-ordinates (x,y,z)	K size (voxels)	P value NDI-ve
L Primary Motor Ctx	-2, -28, 48mm	19	0.007

H

Figure 4.12.2. **Reduced ECAS ALS Specific score associated with increased NDI** within the left primary motor cortex of the PCGs (D-F) which survived cortical thickness correction. Location, size ("K") and significance of the cluster maximum shown in D-F is outlined in table G. NDI within this area demonstrated a strong linear relationship with the ECAS ALS Specific score on scatterplot (H; adjusted R^2=0.49). Colour bars represent range of p values. *R=right; L=left; Post=posterior.*

4.13 Relationships between NODDI ID=1.1 and Clinical Measures

Combined New + Historical Patients

Whole brain and Motor ROIs. A significant negative association between several clusters of NDI within the right and left medial precentral gyrus cortex and ALSFRS was found using TFCE at the PCGs ROI level (Fig. 4.13.2 A-C). NDI within these clusters demonstrated a strong linear relationship with ALSFRS on scatterplot (Fig. 4.13.2 E) with adjusted R^2=0.50. No other significant associations between NDI, ODI or ISO and ALSFRS, Duration of Disease, Rate of Disease Progression, ECAS total score or the ECAS ALS-specific sub score were found.

Table 4.13.1

	Whole Brain						PCG Motor ROI					
	NDI		ODI		ISO		NDI		ODI		ISO	
	Pos	Neg	Pos	Neg	Pos	Neg	Pos	Neg	Pos	Neg	Pos	Neg
ALSFRS								p=0.001*				
Rate												
Duration												
ECAS												
ECAS ALS Spec												

Table 4.13.1. **Summary of significant relationships between NODDI ID=1.1 and clinical factors** in Combined Patients using TFCE analysis at the Whole brain and PCGs ROI levels. *Survived correction for precentral cortex thickness (p=0.01).

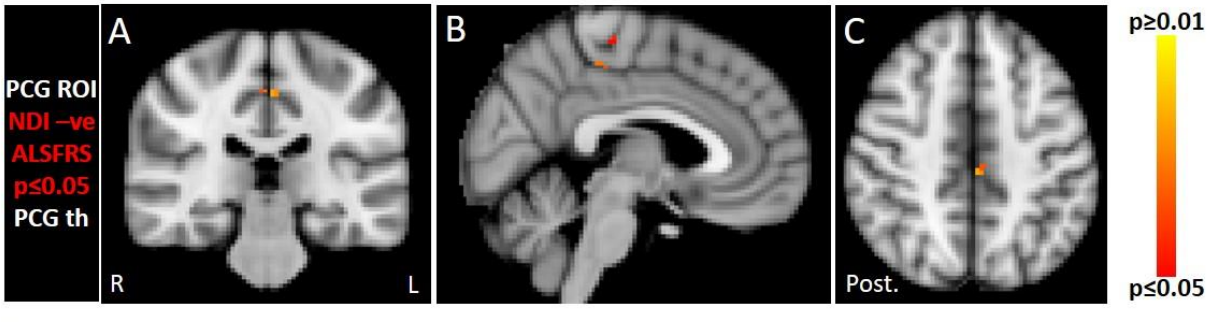

D

Cluster Peak PCGs ROI PCG th	MNI co-ordinates (x,y,z)	K size (voxels)	P value NDI-ve
R Primary Motor Ctx	2, -22, 48mm	13	0.01
L Primary Motor Ctx	-2, -26, 48mm	3	0.04

E

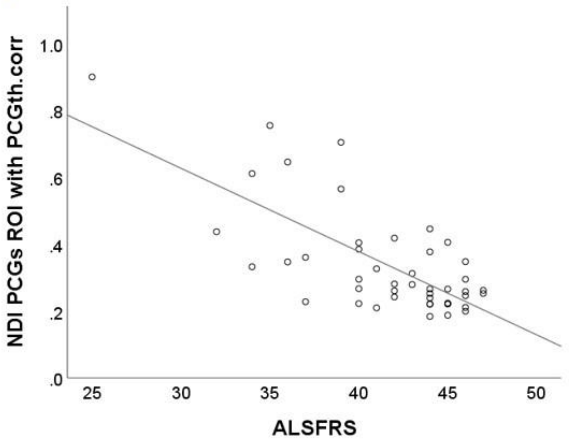

Figure 4.13.2. **Reduced functional score associated with increased NDI** within the primary motor cortex of the PCGs (A-C). Location, size ("K") and significance of the cluster maxima are outlined in table D. NDI within these areas demonstrated a strong linear relationship with ALSFRS on scatterplot (E; adjusted R^2=0.50). Colour bars represent range of p values. *R=right; L=left; Post=posterior.*

4.14 Summary of main NODDI ID=1.1 findings in Patients with ALS

A. ODI within the precentral gyrus cortex is *possibly* decreased in patients compared to controls on region-of-interest analysis, although may be confounded by cortical thickness.

B. NODDI 1.1 was sensitive, but less so, to the reduced NDI within the white matter CC and right CST compared to NODDI 1.7. See Table 4.14.1 for a summary of Patient versus Control group differences.

C. ALSFRS demonstrates the most consistent negative association with NDI within precentral gyrus cortex, demonstrated in the Historical and Combined Patient group analyses, and maintained after accounting for cortical thickness in the latter.

D. The ECAS ALS Specific score *may* have negative association with NDI within precentral gyrus cortex, although may be confounded by cortical thickness and was not found in the Combined Patient group analysis.

F. The ratio of blood Tregs:CD4 cells demonstrates a negative association with NDI within the (left) precentral gyrus cortex, and is maintained after accounting for cortical thickness.

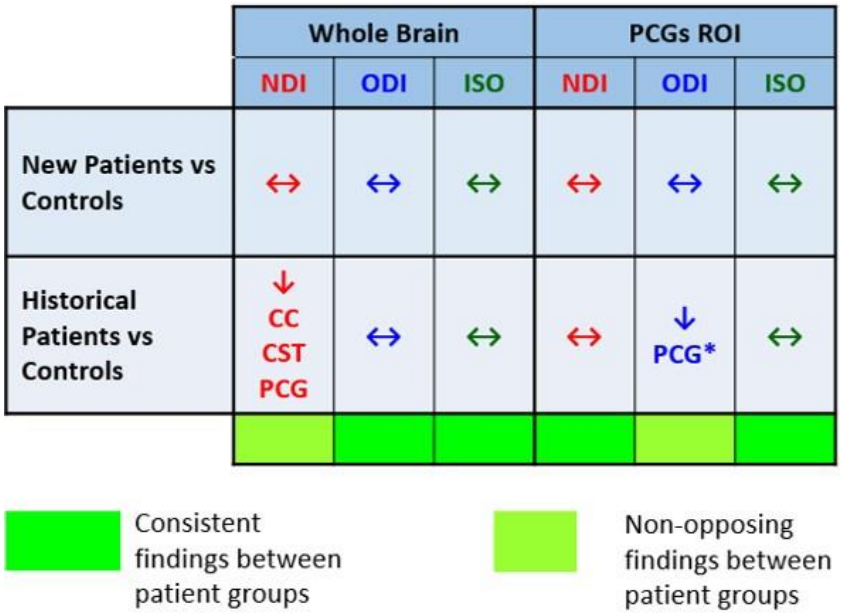

Table 4.14.1. **Summary of significant NODDI ID=1.1 changes between both Patient & Control groups.** Coloured boxes highlight similarities. *CC=corpus callosum; CSTs=corticospinal tracts; PCGs=precentral gyri; Cor=corona radiata.*

Chapter 5. Results: Quantitative Magnetisation MRI (qMTi) in ALS

Quantitative magnetisation imaging has not yet been explored in ALS and, as such, this results chapter presents entirely novel cross-sectional image analyses using this MRI modality. Differences between the New and Historical cohorts of participants, relationships with measures of clinical severity in patients and associations with 'wet' blood biomarkers [CD4 cells and Regulatory T Cells (Tregs)] in the New Patients will be presented. The findings will be then discussed and interpreted in Chapter 7.

As described in Chapter 2, non-parametric permutation testing with age included as a co-variate throughout using Threshold-Free Cluster Enhancement (TFCE) was undertaken to identify clusters of voxels whose parameters significantly differed between groups or in association with clinical and 'wet' biomarker blood measures:

- At Whole Brain level;
- Using skeletonised parameters through Tract Based Spatial Statistics (TBSS);
- Within the Motor ROIs;

Rate of disease progression was included as a covariate in analyses involving the 'wet' biomarker blood cell levels. P value outputs within each analysis are quoted with correction for multiple comparisons at cluster level and considered significant where $p \leq 0.05$.

Participants

Sections 5.1-5.3: 20 patients with El Escorial definite, probable or laboratory-supported ALS recruited within ANNALS-QuICT (mean age 57.7 years; n=14 male) and 21 healthy controls recruited within MultiNICS (mean age 62.5 years; n=8 male; n=17 limb onset). Demographics and patients' clinical characteristics are summarised in Table 5a with statistical analyses performed in IBM SPSS Statistics (SPSS; version 24). Shapiro-Wilk Testing revealed evidence of non-normality in age distribution in both groups (p=0.044 and p=0.026, respectively). A Mann-Whitney U (MWU) Test demonstrated no significant differences in group medians (p=0.13). A Pearson-Chi Square test, however, demonstrated a statistically different gender mix between groups (p=0.041).

Sections 5.4-5.5: 23 Historical patients with El Escorial definite, probable or laboratory-supported ALS (mean age 64.4 years; n=16 male) and 23 Historical healthy controls (mean age 61.5 years; n=14 male; n=20 limb onset). Shapiro-Wilk Testing revealed evidence of non-normality in patients' age distribution (p=0.002). MWU Test confirmed no significant differences in group medians (p=0.286). A Pearson-Chi Square test demonstrated no significantly different gender mix (p=0.536). See Table 5b.

Section 5.6: all 43 participants with ALS. Evidence of non-normality was found in one or other group and so non-parametric tests were employed throughout. The ANNALS-QuICT patient group were younger than the Historical patients by a mean 6.7 years (MWU p=0.013), had significantly shorter disease duration by a mean 7.9 months (MWU p=0.002) and less impaired function on the ALSFRS by a mean 3.3 points (MWU p=0.019). The gender mix, sites of onset, rates of disease progression, total ECAS and ALS-specific ECAS sub scores did not differ significantly between patient groups. See Table 5c.

	MultiNICS Healthy Controls [n=21]§	ANNALS-QuICT Patients with ALS [n=20]	Statistical Comparison
Age in years Mean (SD) Range Median	 62.5 (6.4) 47-71 65	 57.7 (10.4) 31-70 59.5	**Shapiro-Wilk Test** Controls: p=0.026 ALS: p=0.044 **MWU Test** p=0.13
Sex Male Female	 8 13	 14 6	Pearson Chi-Square p=0.041
Disease site of onset Limb Bulbar		 17 3	
Disease duration Mean (SD) Range Median		 11.4 (6.2) 4-23 9	
Total ALSFRS (max. 48) Mean (SD) Range Median		 43.3 (3.4) 34-47 44	
Rate of change of ALSFRS* Mean (SD) Range Median		 0.53 (0.45) 0.09-1.83 0.42	
Total ECAS (max.136) Mean (SD) Range Median		 110.8 (14.3) 77-132 116	
ALS-specific ECAS (max.100)† Mean (SD) Range Median		 82.0 (12.2) 57-98 85.5	
Blood Treg cell levels Mean absolute Tregs (SD) Range Median Mean absolute CD4 (SD) Range Median Mean % of total CD4 (SD) Range Median		 725.3 (410) 303-1679 592 11166 (5444) 4384 - 22783 10248 6.68 (2.56) 4.07-15.50 5.78	
MIROCALS inclusion to scan Mean days (SD) Range Median		 39.5 (20.6) 7-84 35.5	

Table 5a. New Participant demographics and clinical characteristics for qMTi analyses. *MWU=Mann Whitney U Test; * points lost per month duration; † sub-total of language, verbal fluency and executive scores.*

	Historical Controls [n=23]	Historical Patients with ALS [n=23]	Statistical Comparison
Age in years Mean (SD) Range Median	 61.5 (9.3) 43-76 64	 64.4 (8.0) 45-73 67	**Shapiro-Wilk Test** Controls: p=0.162 ALS: p=0.002 **MWU Test** p=0.286
Sex Male Female	 14 9	 16 7	Pearson Chi-Square p=0.536
Disease site of onset Limb Bulbar		 20 3	
Disease duration (months) Mean (SD) Range Median		 19 (8.9) 9-39 17	
Total ALSFRS (max. 48) Mean (SD) Range Median		 40 (5.2) 25-46 40	
Rate of change of ALSFRS* Mean (SD) Range Median		 0.44 (0.29) 0.09-1.33 0.37	
Total ECAS (max.136) Mean (SD) Range Median		 112.5 (13.7) 83-135 113	
ALS-specific ECAS (max.100)† Mean (SD) Range Median		 86.0 (8.8) 65-100 87	

Table 5b. Historical Participant demographics and clinical characteristics for qMTi analyses. *MWU = Mann Whitney U Test; * = points lost per month duration; † = sub-total of language, verbal fluency and executive scores.*

	Historical Patients with ALS [n=23]	ANNALS-QuICT Patients with ALS [n=20]	Statistical Comparisons
Age (years) Mean (SD) Range Median	 64.4 (8.0) 45-73 67	 57.7 (10.4) 31-70 59.5	**Shapiro-Wilk Test** Historical: p=0.002 ANNALS: p=0.044 **MWU Test p=0.013**
Sex Male Female	 16 7	 14 6	Pearson Chi-Square p=0.98
Disease site of onset Limb Bulbar	 3 20	 3 17	Pearson Chi-Square p=0.85
Disease duration Mean (SD) Range Median	 19.3 (8.9) 9-39 17	 11.4 (6.2) 4-23 9	**Shapiro-Wilk Test** Historical: p=0.025 ANNALS: p=0.049 **MWU Test p=0.002**
Total ALSFRS (max. 48) Mean (SD) Range Median	 40 (5.2) 25-46 40	 43.3 (3.4) 34-47 44	**Shapiro-Wilk Test** Historical: p=0.023 ANNALS: p=0.013 **MWU Test p=0.019**
Rate of change of ALSFRS* Mean (SD) Range Median	 0.44 (0.29) 0.1-1.33 0.37	 0.53 (0.45) 0.09-1.83 0.42	**Shapiro-Wilk Test** Historical: p=0.001 ANNALS: p=0.002 **MWU Test p=0.91**
Total ECAS (max.136) Mean (SD) Range Median	 112.5 (13.7) 83-135 113	 110.8 (14.3) 77-132 116	**Shapiro-Wilk Test** Historical: p=0.76 ANNALS: p=0.08 **MWU Test p=0.83**
ALS-specific ECAS (max.100)† Mean (SD) Range Median	 86.0 (8.8) 65-100 87	 82.0 (12.2) 57-98 85.5	**Shapiro-Wilk Test** Historical: p=0.267 ANNALS: p=0.03 **MWU Test p=0.34**

Table 5c. New and Historical Patient demographics and clinical characteristics for qMTi analyses. The groups demonstrated statistically significant differences in age, disease duration and functional impairment as measured by ALSFRS. *MWU = Mann Whitney U Test; * = points lost per month duration; † = sub-total of language, verbal fluency and executive scores.*

5.1 Group Differences: New Patients versus New Controls qMTi

No significant differences were found between f, kf or t2f between the New Patients and New Controls at the level of Whole Brain, Motor ROIs, TBSS whole skeleton or TBSS Motor ROIs.

5.2 qMTi relationships with Blood CD4 cells in the New Patients

Whole brain and Motor ROIs. No associations were found between f, kf and t2f and total blood $CD4^+$ count, blood $CD4^+$ $CD25^+$ $FoxP3^+$ Treg count or blood Treg:CD4 Ratio.

TBSS Motor ROIs. Skeletonised f within the Motor ROIs demonstrated a significant negative correlation (p=0.032) with the total blood CD4 count in a small cluster of voxels in the posterior aspect of the corpus callosum / deep cingulate gyrus white matter on the right side (Fig. 5.2.2 A-C). Scatterplot of skeletonised f values in this area demonstrated a negative linear association with total blood CD4 (Fig. 5.2.2 E) with adjusted R^2=0.15. Accounting for a clear outlier f value the linear relationship was maintained with an adjusted R^2=0.16 (Fig. 5.2.2 F). No other associations were found between f, kf and t2f and total blood $CD4^+$ count, blood $CD4^+$ $CD25^+$ $FoxP3^+$ Treg count or blood Treg:CD4 Ratio (Table 5.2.1).

When adding the rate of disease progression as an additional co-variate (to age), the significant negative association between skeletonised f within the Motor ROIs and the total blood CD4 count was maintained (p=0.039) but with no new significant associations

Table 5.2.1	TBSS Entire Skeleton						TBSS Motor ROIs					
	f		kf		t2f		f		kf		t2f	
	Pos	Neg	Pos	Neg	Pos	Neg	Pos	Neg	Pos	Neg	Pos	Neg
Blood CD4 total								p=0.032				
Blood Treg total												
Treg:CD4 Ratio												

Table 5.2.1. **TBSS and TBSS Motor ROIs qMTi parameters in New Patients vs blood CD4 cells and Tregs** with the significant association shown bold/underlined. The negative association between skeletonised f within the Motor ROIs and the total blood CD4 count was maintained (p=0.039) after adding rate of progression as a covariate.

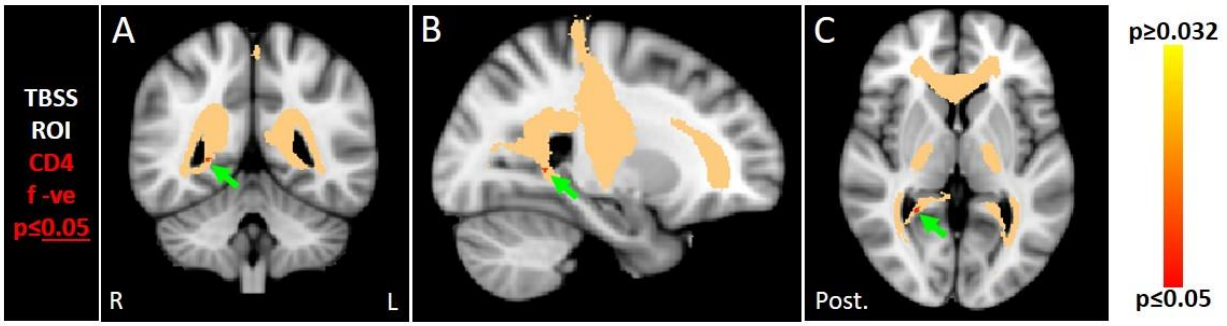

D

Cluster Peak TBSS ROI	MNI co-ordinates (x,y,z)	K size (voxels)	P value f -ve
R CC post.	26, -48, 4 mm	25	0.032

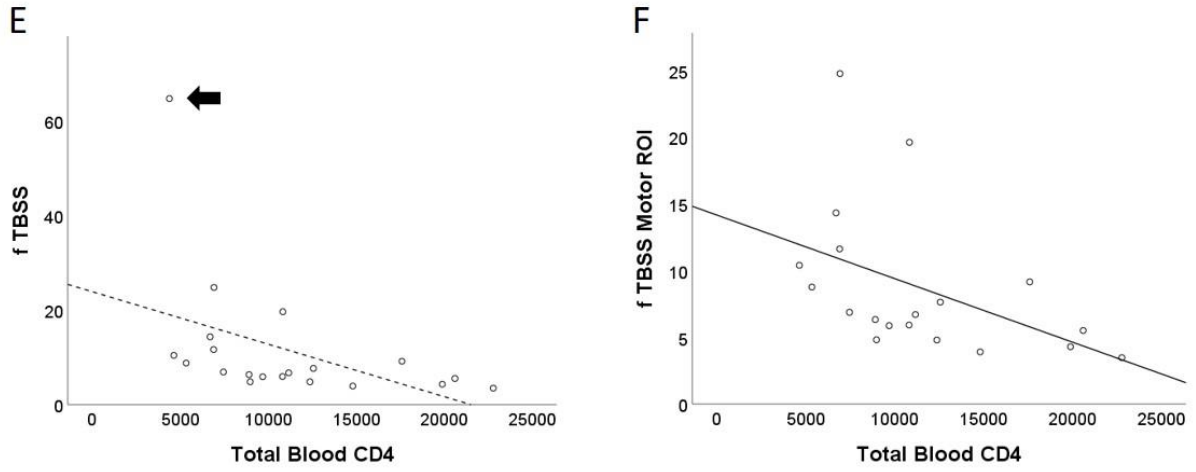

Figure 5.2.2. **Skeletonised f shows a negative association with total blood CD4 count** within the right posterior corpus callosum (A-C; green arrows). The Motor ROI mask shown in beige. Location, size ("K") and significance of the cluster maximum is outlined in table D. Scatterplot of skeletonised f values in this area demonstrated a negative linear association with total blood CD4 (E; dashed line with adjusted R^2=0.15) with a clear outlier shown (E; arrow). With this highest f value considered a spurious f result, the linear relationship is maintained with an adjusted R^2=0.16 (F). *R=right; L=left; Post=posterior.*

5.3 qMTi relationships with Clinical Measures in New Patients

No positive or negative associations were found between f, kf and t2f and the ALSFRS score, Rate of Disease Progression or Disease Duration at the level of Whole Brain, Motor ROIs, TBSS whole skeleton or TBSS Motor ROIs.

5.4 Group Differences: Historical Patients versus Historical Controls qMTi

Whole brain and Motor ROIs. Contiguous voxel clusters demonstrating significant reductions in unmasked kf ($p \leq 0.003$) were seen within the CSTs, CC body, left middle frontal gyrus and cingulate gyrus (Fig. 5.4.2 A-C), in addition to significant increases in t2f ($p=0.025$) within the left CST and CC body (Fig. 5.4.2 D-F) in patients compared to controls, confirmed by quantifying mean kf and t2f in these areas (Fig. 5.4.2 G and H, respectively). These findings were replicated at greater significance following analysis within the masked Motor ROIs (Fig. 5.4.3 A-C and Fig. 5.4.3 D-F, respectively), also confirmed by quantifying kf and t2f in these areas (Fig. 5.4.3 G and H, respectively).

TBSS and TBSS Motor ROIs. Skeletonised kf was significantly reduced ($p \leq 0.008$) extensively throughout the CSTs, PCGs, corpus callosum, the corona radiata and deep frontal white matter on both sides in patients compared to controls (Fig. 5.4.4 A-C). Significantly increased skeletonised t2f ($p=0.026$) was also seen within the CSTs, PCGs, the entire length of the corpus callosum, cingulate gyri, the corona radiata and deep frontal white matter bilaterally (Fig. 5.4.4 D-F). Quantifying mean kf and t2f in these areas also reaffirmed the group differences (Fig. 5.4.4 G and H, respectively).

Analysis using the Motor ROIs only TBSS skeleton showed significantly decreased skeletonised kf (p=0.001) within the CSTs, PCGs and CC (Fig. 5.4.5 A-C), and increased t2f (p=0.005) within the subcortical white matter of the PCGs, both CSTs and throughout the whole CC (Fig. 5.4.5 D-F), confirmed by quantifying mean kf and t2f in these areas (Fig. 5.4.5 G and H, respectively). No other comparative group increases in decreases or increases in f, kf or t2f were demonstrated (see Table 5.4.1).

Table 5.4.1	Whole Brain			Motor ROIs			TBSS Entire Skeleton			TBSS Motor ROIs		
	f	kf	t2f	f	kf	t2f	f	kf	t2f	f	kf	t2f
Controls>ALS		p=0.003			p=0.001			p=0.008			p=0.001	
ALS>Controls			p=0.025			p=0.013			p=0.026			p=0.005

Table 5.4.1. **Summary of significant group differences in qMTi between Historical Patients and Controls** using TFCE at Whole brain, Motor ROIs, TBSS and TBSS Motor ROIs levels. The main findings are of reduced kf and increased t2f within the CC and CSTs.

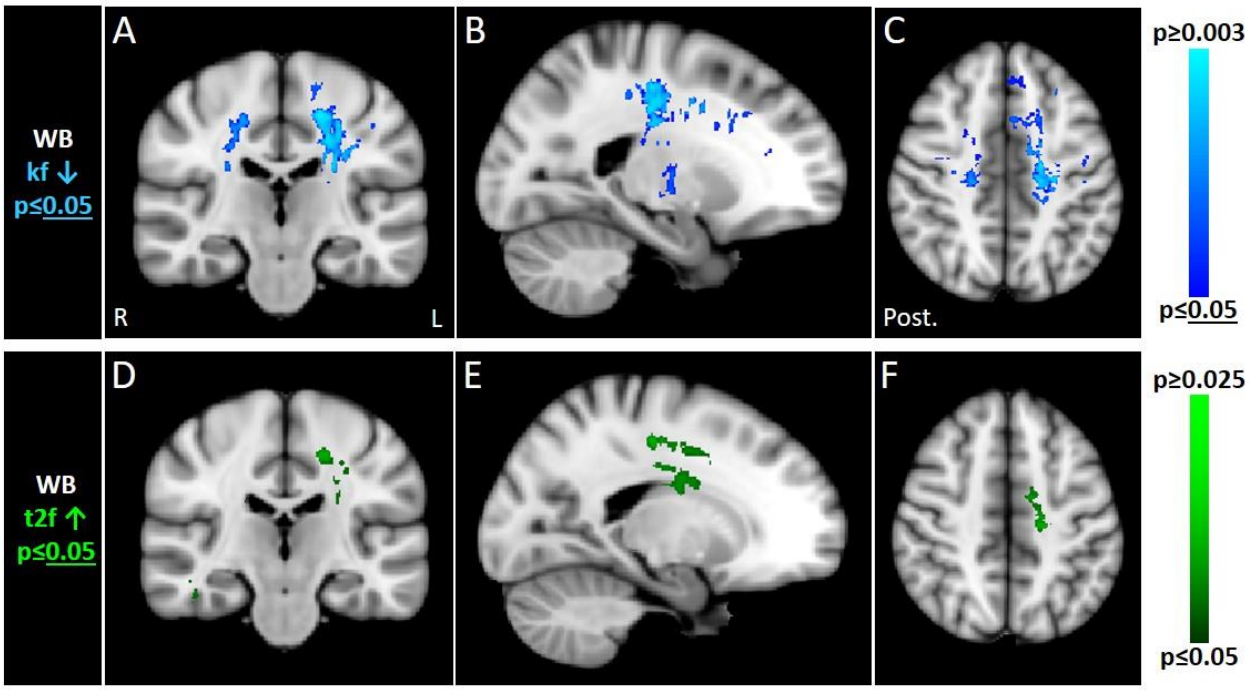

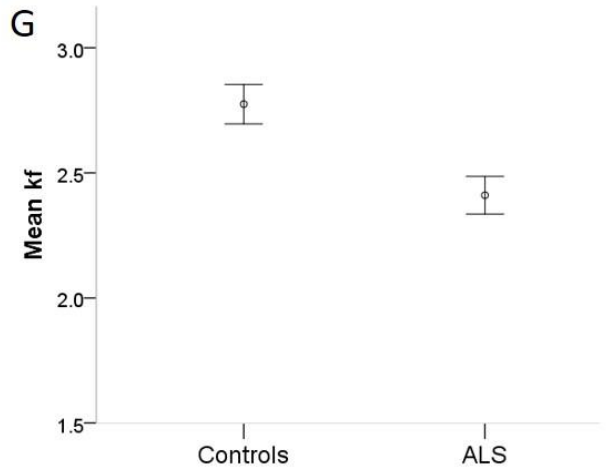

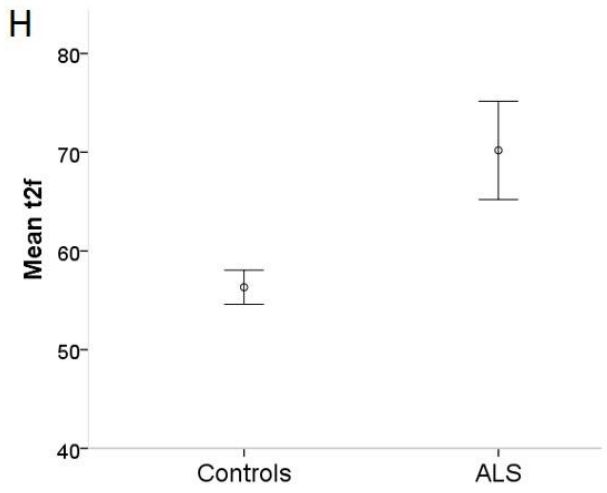

Cluster Peak Wholebrain	MNI co-ordinates (x,y,z)	K size (voxels)	P value kf ↓
L CST	-18, -17, 47mm	10125	0.003
R CST	26, -19, 25mm	1990	0.02
LCST	-20, -13, -2mm	366	0.029
CC Body	8, 24, -3mm	172	0.025
CC Body	21, 3, 40mm	121	0.04
CC Body	-7, 23, -3mm	89	0.042
Cingulate	15, -8, 45mm	67	0.043
R PCG	35, 4, 27mm	47	0.034
MFG	35, 26, 49mm	10	0.044

Cluster Peak Wholebrain	MNI co-ordinates (x,y,z)	K size (voxels)	P value t2f ↑
CC Body	7, 23, -4mm	1663	0.025
L CST	-17, -22, 47mm	1579	0.027
CC Body	-9, 25, -4mm	408	0.026
L CST	-23, -11, 27mm	218	0.036
L CST	-27, -28, 31mm	73	0.04

Figure 5.4.2. **Whole brain qMTi comparisons between Historical Participants.** Clusters of reduced kf are seen throughout the CSTs, cingulate gyrus, middle frontal gyrus and corona radiata (A-C), and increased t2f in the left CST and corona radiata (D-F) in Patients compared to Historical Controls, confirmed by quantifying mean kf and t2f in these areas (G and H, respectively). Location, size ("K") and significance of cluster maxima are outlined in the tables. *R=right; L=left; Post=posterior.*

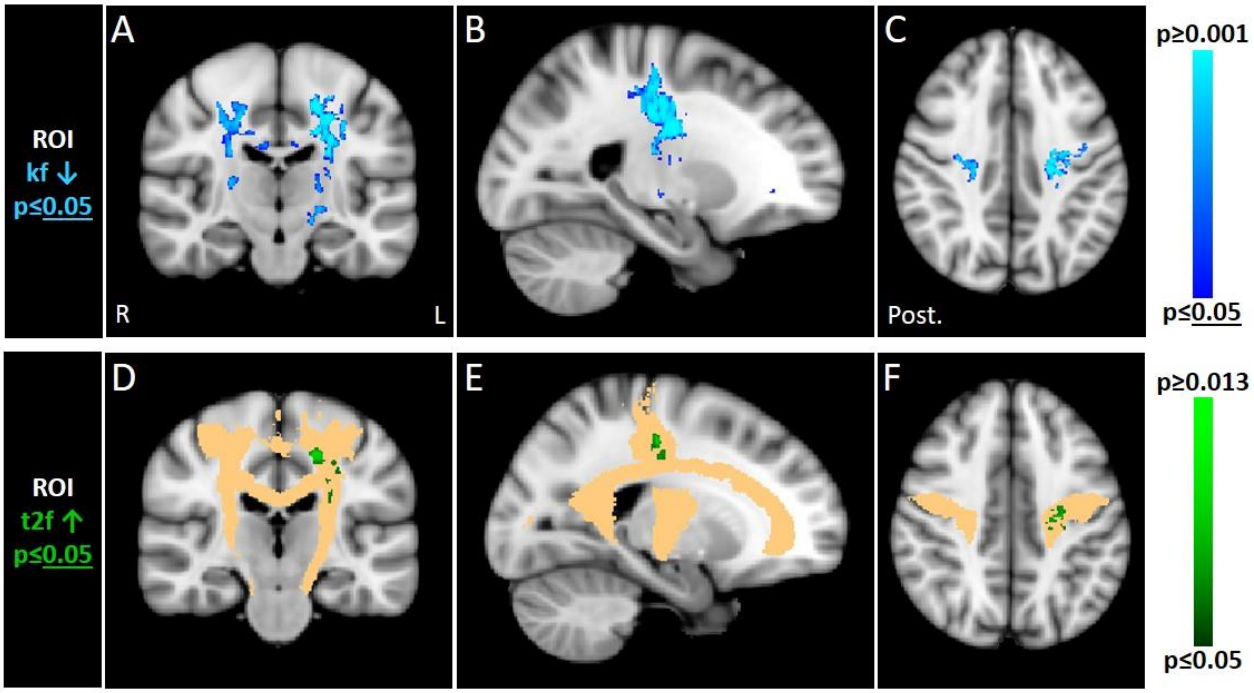

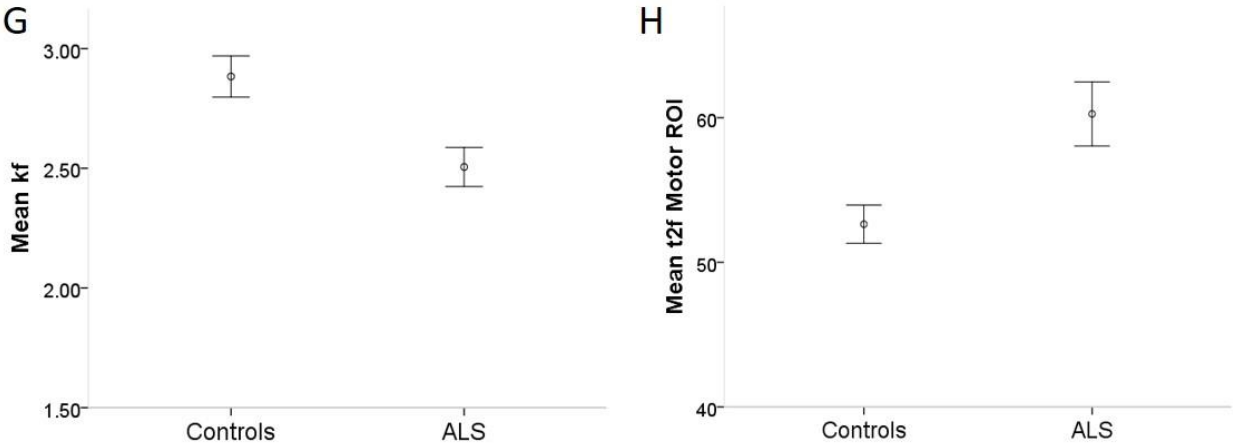

Cluster Peak ROI	MNI co-ordinates (x,y,z)	K size (voxels)	P value kf ↓
L CST	-18, -16, 46mm	6467	<0.001
R CST	26, -19, 25mm	2450	0.007
CC Body	8, 24, -3mm	1117	0.009
CC Body	8, -15, 27mm	206	0.021
CC Body	-5, -11, 26mm	108	0.033
R CST	16, -32, 51mm	45	0.04
CC Body	15, 30, -2mm	11	0.048

Cluster Peak ROI	MNI co-ordinates (x,y,z)	K size (voxels)	P value t2f ↑
L CST	-17, -22, 47mm	729	0.013
CC Body	6, 22, -3mm	610	0.013
CC Body	--8, 24, -4mm	262	0.014
L CST	-23, -11, 27mm	224	0.023
L CST	-27, -28, 31mm	80	0.028

Figure 5.4.3. **Motor ROI qMTi comparisons between Historical Participants.** Clusters of reduced kf are seen throughout the CSTs and extending into the subcortical white matter of the PCGs (A-C), in addition to increased t2f in the left CST (D-F; ROI mask shown in beige) in patients compared to Historical Controls confirmed by quantifying mean kf and t2f in these areas (G and H, respectively). Location, size ("K") and significance of cluster maxima are outlined in the tables. *R=right; L=left; Post=posterior.*

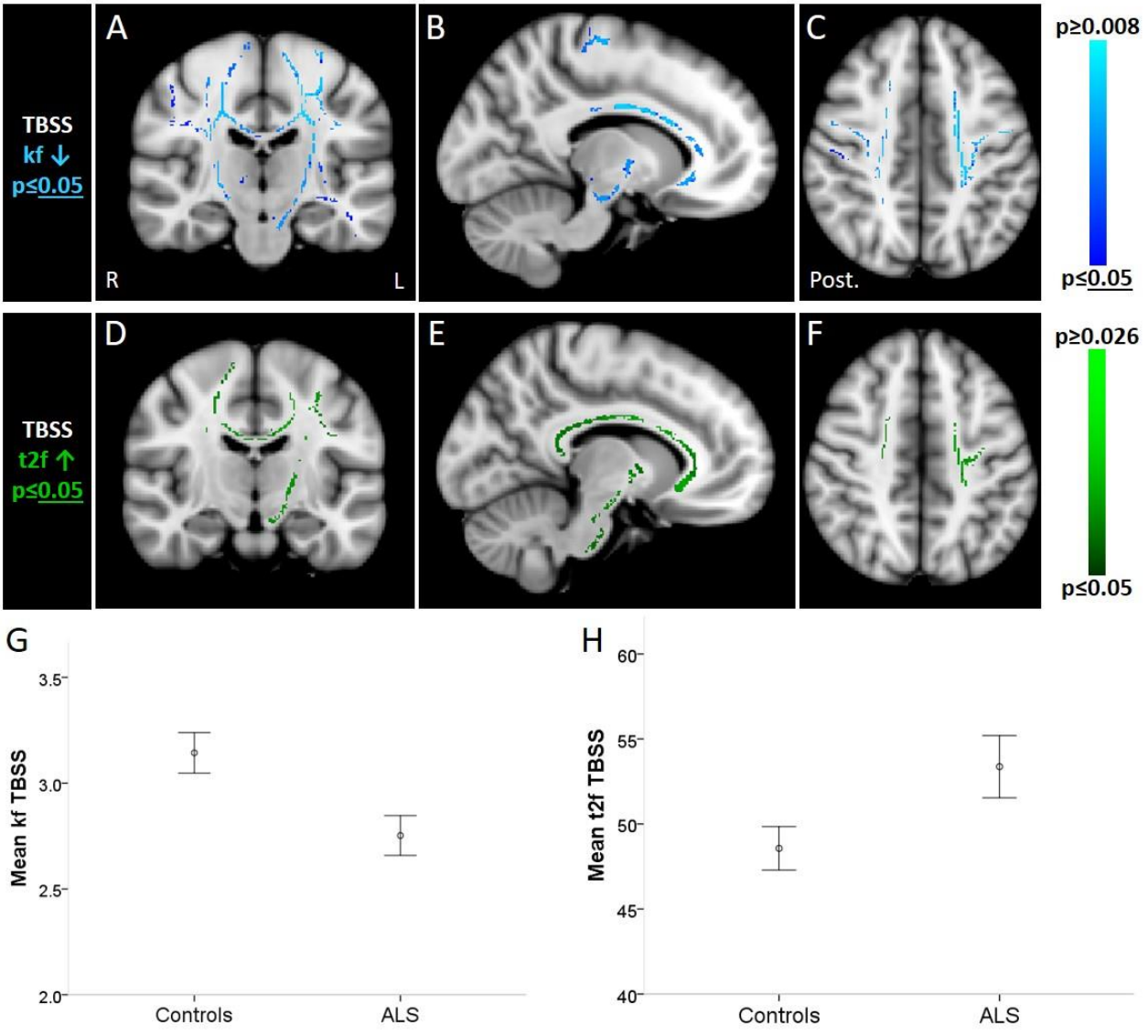

Cluster Peak TBSS	MNI co-ordinates (x,y,z)	K size (voxels)	P value kf ↓
L CST	-23, -21, 35mm	16705	0.008

Cluster Peak TBSS	MNI co-ordinates (x,y,z)	K size (voxels)	P value t2f ↑
CC Body	9, 21, -8mm	10694	0.026

Figure 5.4.4. **TBSS qMTi comparisons between Historical Participants.** Clusters of reduced kf (A-C) and increased t2f (D-F) are seen throughout the rostro-caudal CSTs, cingulate gyrus and corona radiata in patients compared to Historical Controls confirmed by quantifying mean kf and t2f in these areas (G and H, respectively). Location, size ("K") and significance of the cluster maxima are outlined in the tables. *R=right; L=left; Post=posterior.*

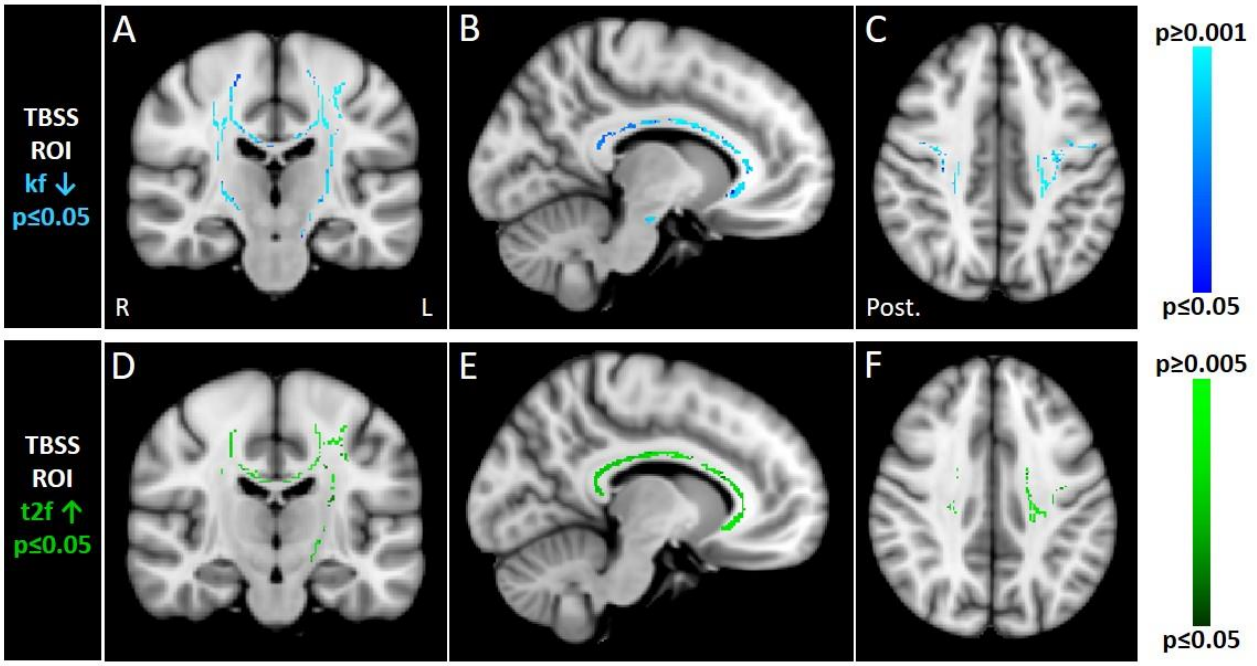

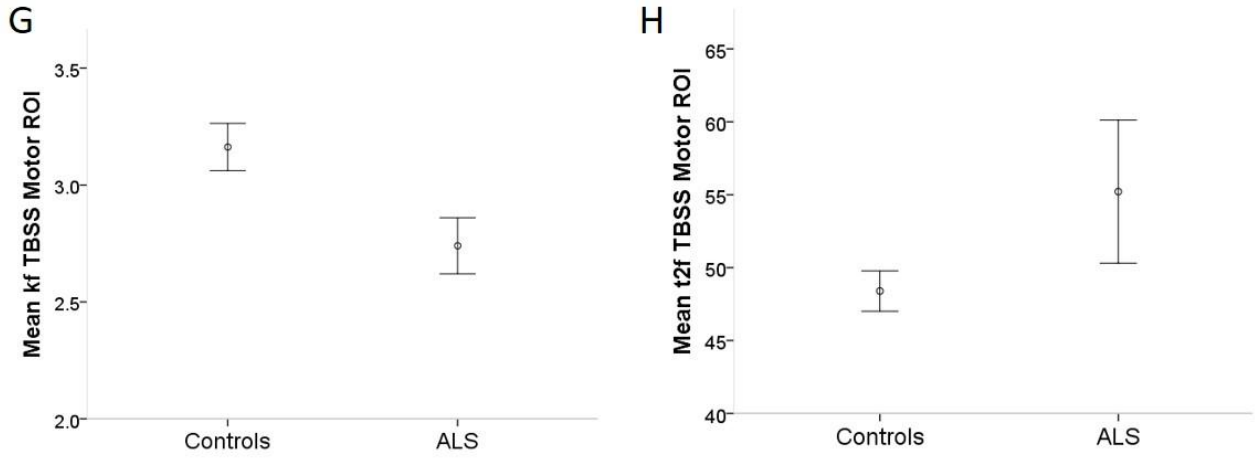

Cluster Peak TBSS ROI	MNI co-ordinates (x,y,z)	K size (voxels)	P value kf ↓
L CST	-23, -21, 35mm	9423	0.001

Cluster Peak TBSS ROI	MNI co-ordinates (x,y,z)	K size (voxels)	P value t2f ↑
CC Body	12, 26, -7mm	8306	0.005

Figure 5.4.5. **TBSS Motor ROIs analyses using qMTi in Historical Participants.** Clusters of reduced kf (A-C) are seen throughout the corticospinal tracts and corpus callosum (D-E), and increased t2f (D-F) throughout the corpus callosum and left CST, confirmed by quantifying mean kf and t2f in these areas (G and H, respectively). Location, size ("K") and significance of the cluster maxima are outlined in the tables. *R=right; L=left; Post=posterior.*

5.5 qMTi Relationships with Clinical Measures in the Historical Patients

Whole brain and Motor ROIs. Clusters of voxels within the left medial precentral cortex and bilateral cingulate cortices showed a significant positive correlation (p=0.029) between kf and the ALSFRS at the whole brain level (Fig. 5.5.3 A-C). kf values within these clusters demonstrated a strong linear association with ALSFRS on scatterplot (Fig. 5.5.3 E) and adjusted R^2=0.59.

TBSS and TBSS Motor ROIs. A small cluster of voxels within the distal right CST at the level of the anterior pons showed a significant negative correlation (p=0.046) between the total ECAS score and unmasked skeletonised f (Fig. 5.5.4 A-C). Scatterplot of skeletonised f values [in percentage units] in these clusters demonstrated two clear outliers (Fig. 5.5.4 E; arrows), removing which enabled the weak linear relationship to be appreciated (Fig. 5.5.4 F) and an adjusted R^2=0.16. Clusters of voxels within both distal CSTs at the level of the anterior pons and medulla also demonstrated a significant negative correlation (p=0.008) between the ECAS ALS Specific score and the unmasked skeletonised f parameter (Fig. 5.5.5 A-C). Scatterplot of skeletonised f values [in percentage units] in these clusters demonstrated the same two clear outlier values (Fig. 5.5.5 E) as seen in Fig. 5.5.4, but their removal did not enable a clear linear relationship to be appreicated (Fig. 5.5.5 F) suggesting that the association was predominantly driven by the outliers. Of note, these areas of the CSTs lie outside the distal-most coverage of the brain Motor ROIs mask use which terminates just above the pons.

Furthermore, a cluster of voxels within the central and anterior CC revealed a significant positive correlation (p=0.028) between the ECAS ALS Specific score and the unmasked skeletonised kf parameter (Fig. 5.5.6 A-C), which was also reproduced following analysis applying the Motor ROI mask (p=0.02). kf values within these clusters demonstrated a

strong positive linear association with ALSFRS on scatterplot (Fig. 5.5.6 E) and adjusted R^2=0.42.

No other positive or negative associations were found between f, kf and t2f and ALSFRS, Rate of Progression, Disease Duration, total ECAS score or ECAS ALS Specific score at the level of Whole Brain, Motor ROIs, TBSS whole skeleton or TBSS Motor ROIs (Tables 5.5.1 and 5.5.2).

Table 5.5.1

	Whole Brain						Motor ROIs					
	f		kf		t2f		f		kf		t2f	
	Pos	Neg	Pos	Neg	Pos	Neg	Pos	Neg	Pos	Neg	Pos	Neg
ALSFRS			**p=0.029**									
Rate												
Duration												
ECAS												
ECAS ALS Spec												

Table 5.5.1. Whole brain and Motor ROIs qMTi parameters in the Historical Patients vs clinical factors with the significant association shown bold/underlined.

Table 5.5.2

	TBSS Entire Skeleton						TBSS Motor ROIs					
	f		kf		t2f		f		kf		t2f	
	Pos	Neg	Pos	Neg	Pos	Neg	Pos	Neg	Pos	Neg	Pos	Neg
ALSFRS												
Rate												
Duration												
ECAS		**p=0.046**										
ECAS ALS Spec		**p=0.008**	**p=0.028**						**p=0.02**			

Table 5.5.2. TBSS and TBSS Motor ROIs qMTi parameters in the Historical Patients vs clinical factors with the significant associations shown bold/underlined.

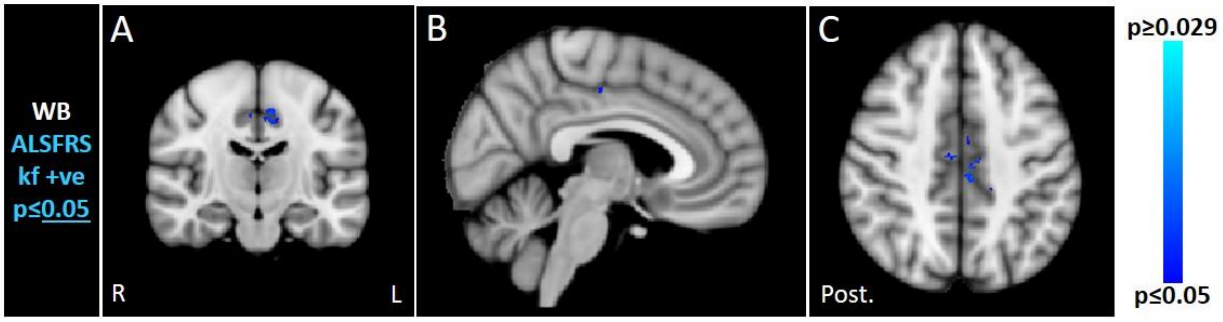

D

Cluster FA Wholebrain	MNI co-ordinates (x,y,z)	K size (voxels)	P value kf +ve
L Cing. Gy.	-4, -24, 46 mm	273	0.029
L Cing. Gy,	-5, -10, 47 mm	62	0.034
L PCG	-15, -34, 43 mm	47	0.034
Postcent. L	-14, -39, 51 mm	38	0.033
R Cing. Gy.	7, -16, 44 mm	31	0.04

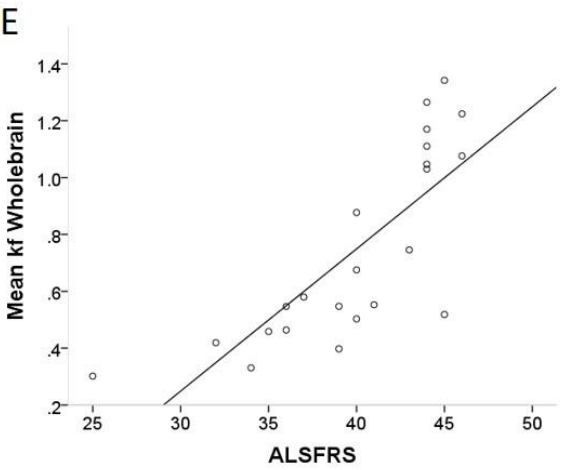

Figure 5.5.3. **Whole brain kf shows a significant positive correlation with ALSFRS** within bilateral cingulate cortices, the left precentral cortex and the left postcentral gyrus in Historical Patients on TFCE analysis (A-C). Location, size ("K") and significance of the cluster maxima are outlined in table D. kf values demonstrated a strong linear association with ALSFRS on scatterplot (E; adjusted R^2=0.59). *R=right; L=left; Post=posterior.*

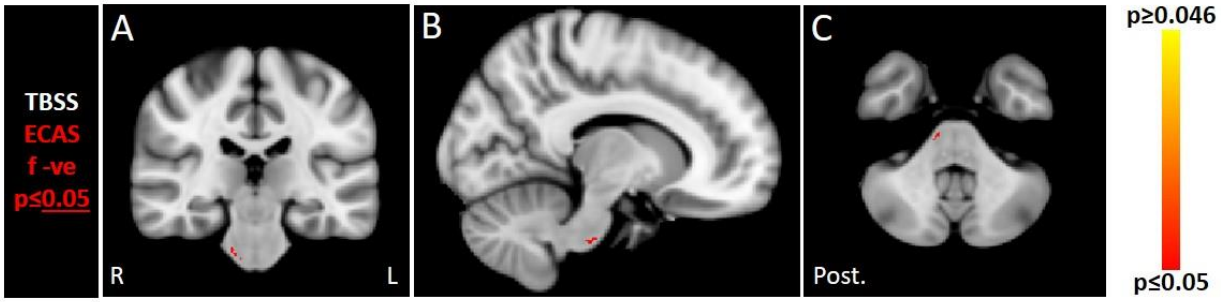

D

Cluster Peak TBSS	MNI co-ordinates (x,y,z)	K size (voxels)	P value f -ve
R Brainstem	10, -24, -42mm	36	0.046

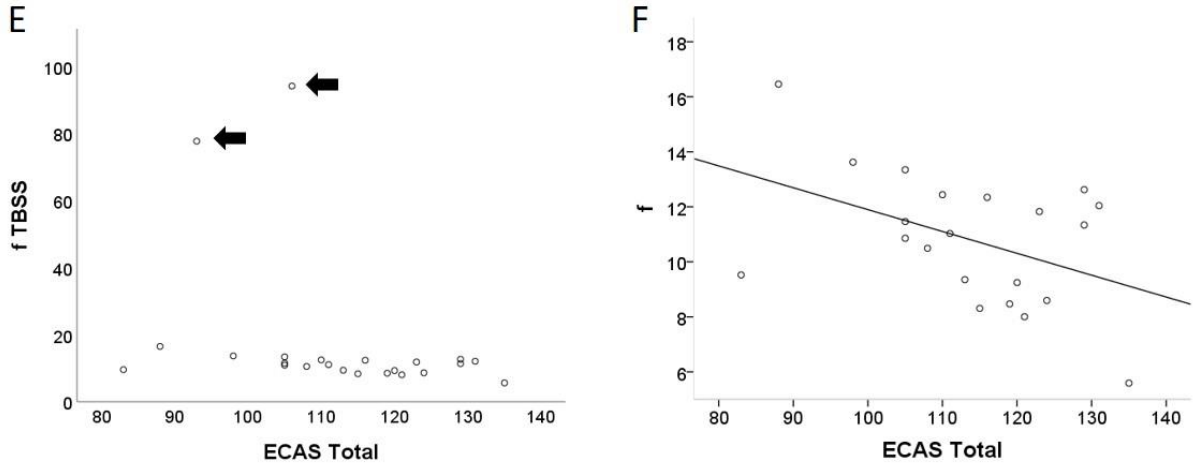

Figure 5.5.4. **Skeletonised f shows a significant negative correlation with total ECAS score** within the distal right CST at the level of the anterior pons in Historical Patients (A-C). Location, size ("K") and significance of the cluster maximum is outlined in table D. Scatterplot of skeletonised f values [in percentage units] in this area demonstrated two clear outliers (E; arrows). If these highest f values are considered spurious f results, the weak linear relationship emerges (F; line with an adjusted R^2=0.16). *R=right; L=left; Post=posterior.*

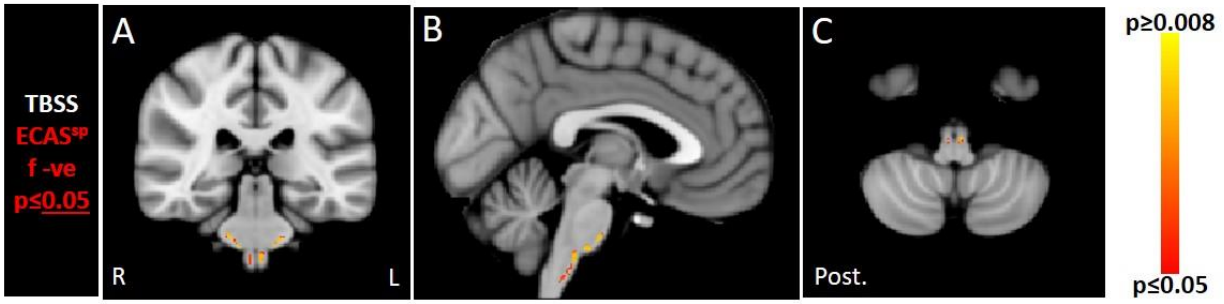

D

Cluster Peak TBSS	MNI co-ordinates (x,y,z)	K size (voxels)	P value f -ve
L Brainstem	-10, -27, -42mm	322	0.008
R Brainstem	11, -24, -40mm	225	0.007

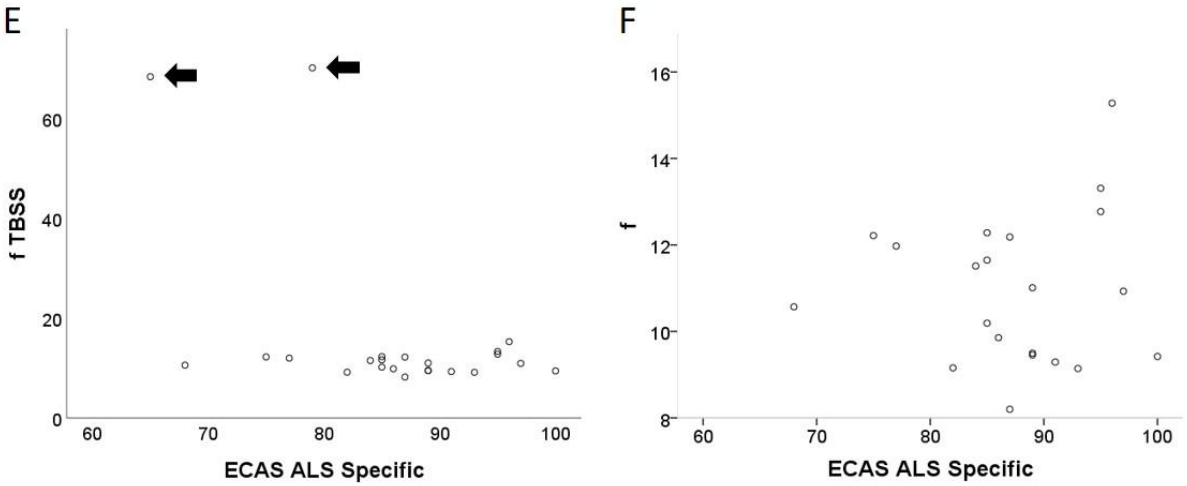

Figure 5.5.5. **Skeletonised f shows a significant negative correlation with the ECAS ALS Specific score** within both distal CSTs at the level of the anterior pons and medulla in Historical Patients (A-C). Location, size ("K") and significance of the cluster maxima are outlined in table D. Scatterplot of skeletonised f values [in percentage units] in these areas demonstrate the same two clear outlier values (E; arrows) as seen in Fig. 5.5.4. If these highest f values are also considered spurious f results, a linear relationship remains poorly discerned (F). *R=right; L=left; Post=posterior.*

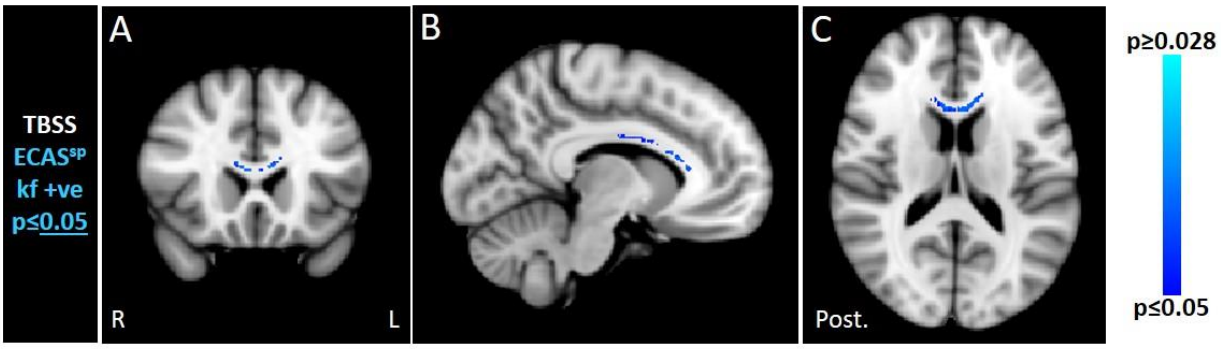

D

Cluster Peak TBSS	MNI co-ordinates (x,y,z)	K size (voxels)	P value kf -ve
CC Body	-7, 24, 12mm	558	0.028
CC Body	11, -15, 29mm	222	0.036
CC Body	-8, -1, 27mm	134	0.039

E

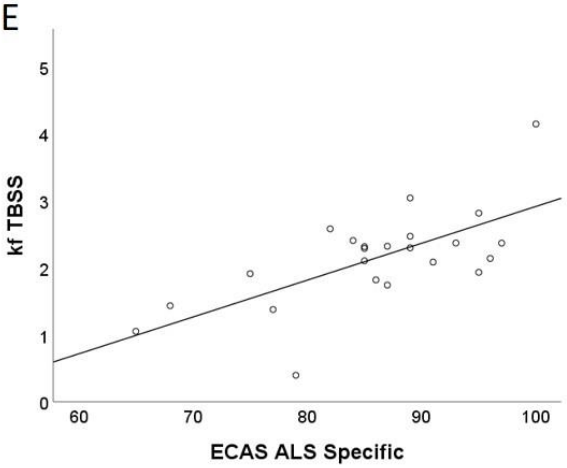

Figure 5.5.6. **Skeletonised kf shows a significant positive correlation with the ECAS ALS Specific score** within the central and anterior CC in Historical Patients (A-C). Location, size ("K") and significance of the cluster maxima are outlined in table D. kf values demonstrated a strong positive linear association with ALSFRS on scatterplot (E; adjusted R^2=0.42). *R=right; L=left; Post=posterior.*

5.6 Relationships with Clinical Measures and qMTi

Combined New + Historical Patients

No significant positive or negative associations were found between f, kf and t2f and clinical measures ALSFRS, Disease Duration, Rate of Disease Progression, ECAS and ECAS ALS Specific score at the level of the Whole Brain and Motor ROIs, or the TBSS whole skeleton and TBSS Motor ROIs.

5.7 Summary of main qMTi findings in Patients with ALS

A. In the Historical Patient group, kf is shown to be reduced and t2f increased within the CSTs and CC compared to controls on Whole brain, TBSS and Motor ROIs analyses. Group differences were not seen in the New Patients.

B. In the Historical Patient group, kf within extra-motor cortical (grey matter) areas of the left medial precentral cortex and bilateral cingulate cortices demonstrate a positive association with the ALSFRS score. Skeletonised kf within the CC demonstrates a positive association with the ECAS ALS Specific score. Neither was replicated in Combined patient group analyses.

C. In the Historical Patient group, skeletonised f within the distal CSTs demonstrates a positive association with the ECAS and ECAS ALS Specific scores, not replicated in Combined patient group analyses.

D. The total blood CD4 cell count demonstrates a negative association with skeletonised f within the posterior CC on TBSS analyses, which is also independent of the Rate of disease progression.

Chapter 6. Results Appendices: Post Hoc Analyses

6.1 CD4+ Cells and Rate of Disease Progression

The patients with ALS recruited within ANNALS-QuICT and whose scans have been analysed in this Doctoral Thesis constitute a small sub group of the patients enrolled into MIROCALS. As the overall Neuroimaging Study was powered to detect differences between patients and controls with respect to imaging parameters (principally NODDI), it is not within the remit of ANNALS-QuICT to present evidence for associations between non-imaging biomarkers (such as CD4+ cell populations) and clinical measures of disease severity. Indeed, this is the remit of the MIROCALS trial. However, given that the evidence for intrinsically higher levels of blood $CD4^+$ $CD25^+$ $FoxP3^+$ Treg cells being associated with a slower rate of disease progression has informed the hypothesis for this Neuroimaging Study, limited statistical analyses of correlations between the total blood CD4 count, total blood $CD4^+$ $CD25^+$ $FoxP3^+$ Treg count, or the Treg:CD4 Ratio and the Rate of Disease Progression, have been performed in SPSS on the 23 patients with ALS recruited within ANNALS-QuICT (whose clinical measures and blood CD4+ cell counts are summarised in Chapter 3 Table 3a).

Non parametric, one-tailed Spearman's Rank correlative analyses were performed owing to evidence on non-normality and a poor linear relationships visually evident on scatterplots. No significant results were found (see Table 6.1.1). However, there was a trend towards a positive correlation with total CD4 count, and a negative correlation with Treg:CD4 ratio. Total blood Treg count showed no trend. A boxplot of the rate of progression in the New Patients demonstrates a median rate of 0.37 ALSFRS points lost per month and a predominance of more slowly progressing patients.

	Spearman's Correlation with Rate	
Blood CD4 total	Rho = +0.204	p=0.18
Blood Treg total	Rho = +0.008	p=0.49
Treg:CD4 Ratio	Rho = -0.262	p=0.11

Table 6.1.1. Spearman's rho and significance between Rate of progression and the blood CD4 count, total blood $CD4^+$ $CD25^+$ $FoxP3^+$ Treg count and the Treg:CD4 Ratio. No significant associations were found.

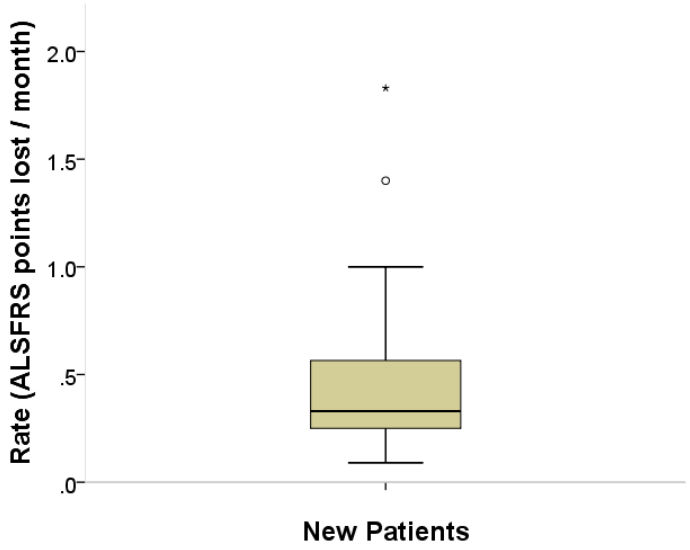

Figure 6.1.2. **Boxplot of the rate of disease progression in the New Patients** who underwent testing for total CD4 and Treg count levels. The median rate of 0.37 (and mean 0.44) would suggest the group predominantly contains 'slow' rather than 'fast' progressors.

6.2 Historical versus New MRI scans: Diffusion and qMT Imaging

All the MRI scans used for analysis in the New and Historical cohorts (patients and controls) were serially acquired using identical MRI protocols and on the same 1.5 Tesla Siemens Magnetom Avanto scanner at the Clinical Imaging Sciences Centre (CISC) over periods of 18 months. The control scans were captured in parallel with those of the accompanying patient group, although the Historical and current imaging studies were themselves separated by roughly 18 months also. Quality and performance checks have been conducted regularly with no overt alteration in scanner performance detected.

In light of the prominent kf and t2f differences seen between the Historical Patients and Controls, but the paucity of differences between the New Patients and New Controls, an additional analysis has been performed whereby the control groups have been compared with each other in order to screen simply for any gross discrepancies between the two data sets which may be a result of scanner performance drift. This is warranted due to absence of previous qMTi imaging studies in ALS to guide expected findings.

TFCE analysis on skeletonised kf and t2f, in addition to FA, NDI, ODI and ISO, parameters has been chosen given the consistency of differences found using TBSS in this study. Firstly, no statistical differences were found in age or gender between the Control groups (Tables 6.2.1 and 6.2.2) despite the smaller number of New participants included for qMTi analyses. Non-parametric permutation testing was then undertaken in *randomise_parallel* as described in Chapter 2 and the output p-value files corrected for multiple comparisons. No significant differences in FA, NDI, ISO, kf or t2f were found. In the New Controls, a small cluster of voxels demonstrated significantly higher ODI within the right anterior temporal lobe only (Fig. 6.2.1), and no differences were seen elsewhere or along the CSTs or CC.

	Historical Healthy Controls [n=23]	MultiNICS Controls [n=24]	Statistical Comparison
Age in years Mean (SD) Range Median	 61.5 (9.3) 43-76 64	 62.4 (6.5) 47-71 65	**Shapiro-Wilk Test** Historical: p=0.162 MultiNICS: p=0.074 **MWU Test** p=0.98
Sex Male Female	 14 9	 11 13	Pearson Chi-Square p=0.30

Table 6.2.1. Demographics for the Historical Controls and New Controls used in the Diffusion TBSS analyses. No statistically significant differences are found.

	Historical Healthy Controls [n=23]	MultiNICS Controls [n=21]	Statistical Comparison
Age (years) Mean (SD) Range Median	 61.5 (9.3) 43-76 64	 62.5 (6.4) 47-71 65	**Shapiro-Wilk Test** Historical: p=0.162 MultiNICS: p=0.03 **MWU Test** p=0.99
Sex Male Female	 14 9	 8 13	Pearson Chi-Square p=0.13

Table 6.2.2. Demographics for the Historical Controls and New Controls used in the gMTi TBSS analyses. No statistically significant differences are found.

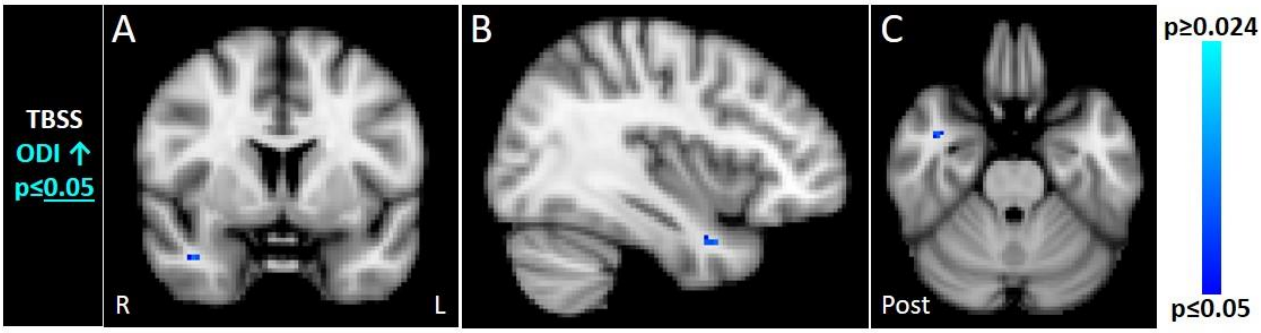

Figure 6.2.3. **Skeletonised ODI showed a small area of increase in the New Controls compared to the Historical Controls** within the right temporal lobe white matter. No other differences were seen with FA, NDI, ISO, kf or t2f. *R=right; L=left; Post=posterior.*

Furthermore, substantially reducing the viewing threshold of the original corrected 1-p output files from *randomise_parallel* comparing the entire skeleton for kf and t2f in the New Patients to the New Controls revealed that decreases in kf were seen to emerge within the CSTs bilaterally along with a cluster in the left middle frontal gyrus, and increases in t2f within the left CST and right middle frontal gyrus (Fig. 6.2.4). This may suggest that subtle changes within the CSTs primarily, as demonstrated in the Historical Patients, are present in the New Patients but may only reach significance with a much larger group size.

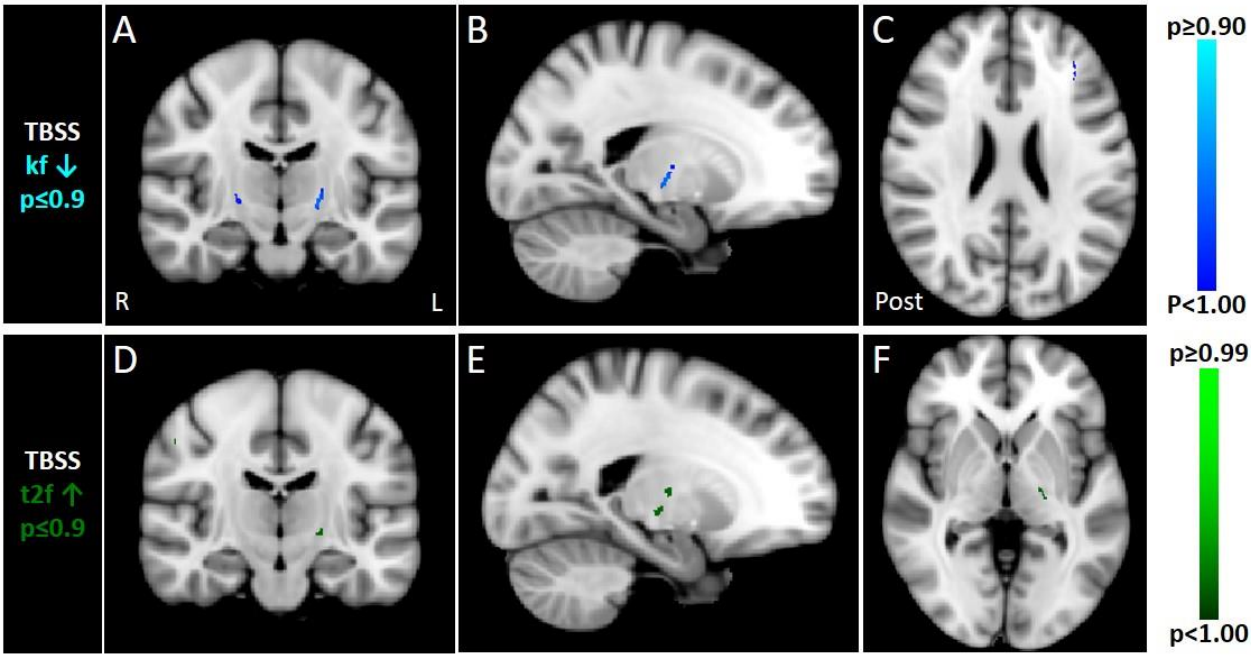

Figure 6.2.4. **Subthreshold TBSS qMTi comparisons between New Patients and Controls** show reductions in kf within both CSTs and left middle frontal gyrus (A-C) and increases in t2f within the left CST and right middle frontal gyrus (D-F). Colour columns represent range of p values. *R=right; L=left; Post=posterior.*

6.3 Effect Sizes for Patient and Control Group Differences

In order to report the substantive significance independent of sample size for group differences between the Patient and Control groups, the Cohen's *d* effect size has been calculated, as outlined in Chapter 2.12.4, for each of the imaging parameters. The Tables below display the effect size in place of the significant p value as previously shown in the respective Results Chapter for FA, NODDI and qMTi.

Table 6.3.1

	Effect Sizes in New Patients vs Controls – Mean FA			
	Whole Brain	Motor ROIs	TBSS Entire Skeleton	TBSS Motor ROIs
Controls>ALS		0.75	0.99	0.85
ALS>Controls				

Table 6.3.1. **Summary of effect sizes for significant group differences in FA between the New Patients and Controls** using TFCE at Whole brain, Motor ROIs, TBSS and TBSS Motor ROIs levels. See Chapter 3.1 for the significant p values.

Table 6.3.2

	Effect Sizes in Historical Patients vs Controls – Mean FA			
	Whole Brain	Motor ROIs	TBSS Entire Skeleton	TBSS Motor ROIs
Controls>ALS	1.63	1.41	1.20	1.16
ALS>Controls				

Table 6.3.2. **Summary of effect sizes for significant group differences in FA between the Historical Patients and Controls** using TFCE at Whole brain, Motor ROIs, TBSS and TBSS Motor ROIs levels. See Chapter 3.4 for the significant p values.

Table 6.3.3	Effect Sizes in New Patients vs Controls – Mean NODDI											
	Whole Brain			Motor ROIs			TBSS Entire Skeleton			TBSS Motor ROIs		
	NDI	ODI	ISO	NDI	ODI	ISO	NDI	ODI	ISO	NDI	ODI	ISO
Controls>ALS												
ALS>Controls					1.22			0.97			0.80	

Table 6.3.3. **Summary of effect sizes for significant group differences in NODDI parameters between the New Patients and Controls** using TFCE at Whole brain, Motor ROIs, TBSS and TBSS Motor ROIs levels. See Chapter 4.1 for the significant p values.

Table 6.3.4	Effect Sizes in Historical Patients vs Controls – Mean NODDI											
	Whole Brain			Motor ROIs			TBSS Entire Skeleton			TBSS Motor ROIs		
	NDI	ODI	ISO	NDI	ODI	ISO	NDI	ODI	ISO	NDI	ODI	ISO
Controls>ALS	1.53	1.83		1.41		1.33	1.18		1.53	1.30		1.57
ALS>Controls		1.46			1.07						1.15	1.15

Table 6.3.4. **Summary of effect sizes for significant group differences in NODDI parameters between the Historical Patients and Controls** using TFCE at Whole brain, Motor ROIs, TBSS and TBSS Motor ROIs levels. See Chapter 4.4 for the significant p values.

Table 6.3.5	Effect Sizes in Historical Patients vs Controls qMTi											
	Whole Brain			Motor ROIs			TBSS Entire Skeleton			TBSS Motor ROIs		
	f	kf	t2f	f	kf	t2f	f	kf	t2f	f	kf	t2f
Controls>ALS		1.63			1.52			1.44			1.46	
ALS>Controls			1.61			1.80			1.32			0.82

Table 6.3.5. **Summary of effect sizes for significant group differences in qMTi parameters between the Historical Patients and Controls** using TFCE at Whole brain, Motor ROIs, TBSS and TBSS Motor ROIs levels. See Chapter 5.4 for the significant p values. [No differences in the New Participant groups was seen.]

6.4 Relationships between FA / NODDI ID=1.7 and Disease Duration with ALSFRS as a co-variate

Widespread associations emerged on TBSS analyses between disease duration and ALSFRS, and both FA and NDI within similarly widespread regions of the CC and CSTs, across all patients, which may have been facilitated by the distributions of these clinical measures being significantly different between the New and Historical Patient groups. Furthermore, the ALSFRS and disease duration themselves demonstrate a significant negative correlation on Spearman's Rank test (p=0.01; Rho -0.34) which would be expected given their opposing associations with the imaging parameters.

To determine their relative contribution to the variability in FA in these areas, the association between skeletonised FA or NDI and ALSFRS were repeated in *randomise_parallel* using TFCE with disease duration as an additional co-variate (along with age) and, similarly, the associations between FA or NDI and disease duration were repeated with ALSFRS as an additional co-variate. The output p-value files were corrected for multiple comparisons, as described.

The positive associations between both FA and NDI and the ALSFRS no longer reached significance at either the full skeleton TBSS or TBSS Motor ROI levels. However, the negative associations between both FA (p=0.049) and NDI (p=0.035) and disease duration survived using TBSS Motor ROI, with a reduced volume of clusters still observed within the CC (Fig. 6.4.1).

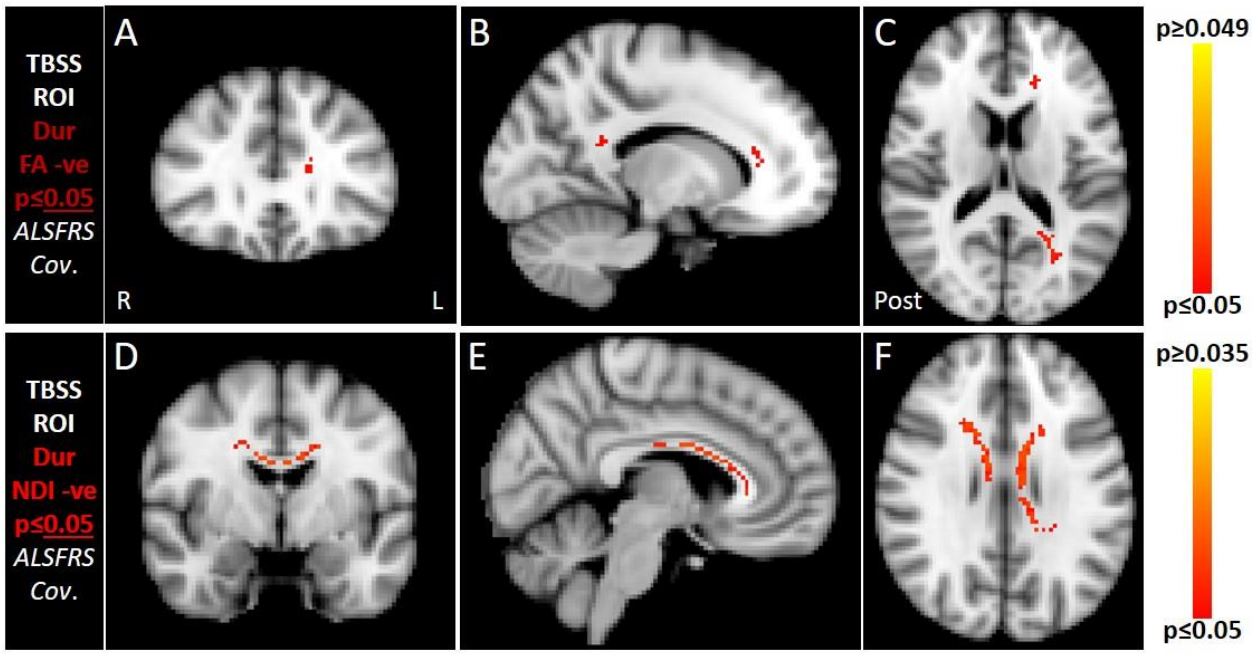

G

Cluster FA TBSS ROI	MNI co-ordinates (x,y,z)	K size (voxels)	P value
L CC body	-24, -60, 12 mm	55	0.049
CC Splenium	-16, 34, 12 mm	34	0.049

H

Cluster NDI TBSS ROI	MNI co-ordinates (x,y,z)	K size (voxels)	P value
CC body	-10, 4, 28 mm	662	0.035

Figure 6.4.1. **Longer disease duration remains associated with reduced skeletonised FA (A-C) or NDI (D-F)** within the corpus callosum after accounting for the ALSFRS score. The size ("K") of each cluster and the location and significance of maxima are listed in panels G (for FA) and H (for NDI). Colour columns represent range of p values. *R=right; L=left; Post=posterior.*

Chapter 7. Discussion

Encapsulated within a larger longitudinal neuroimaging study using multimodal MRI for the first time in newly-diagnosed patients with ALS enrolled into clinical drug trial, this Doctoral Thesis is able not only to present and discuss the use of novel brain imaging approaches in ALS but also unique insights into cross-sectional relationships between imaging parameters, markers of symptom severity and biological measures of immune system function [CD4 cells and Regulatory T Cells (Tregs)] as revealed in the preceding Results Chapters. In particular, quantitative magnetisation transfer imaging (qMTi) remained unexplored in ALS up until now, and has demonstrated promising sensitivity to tissue change alongside more established diffusion imaging techniques including Neurite Orientation Dispersion and Density Imaging (NODDI), with this being just the second cohort of patients symptomatic of the disease to undergo NODDI scans - the first being the Historical Participants although previously analysed at whole brain level only.[1] Accordingly, methods of image analysis presented here have included, but extended beyond, the whole brain level to include tract-based spatial statistics (TBSS) for a closer assessment of how parameters may be altered within the white matter tracts, in addition to a novel modification of the NODDI processing pipeline proposed to better characterise its indices for grey matter neurite architecture.

7.1 Diffusion Imaging in ALS: FA and NODDI 1.7

Patients versus Controls. The main findings in this study comparing diffusion MRI from patients to controls were that, firstly, fractional anisotropy (FA) was reduced within the corticospinal tracts (CSTs) and corpus callosum (CC) using diffusion tensor imaging (DTI) model and that, secondly, the reduced FA was associated with either a reduction in the neurite density index (NDI) or an increase in the orientation dispersion index (ODI), or a combination of the two, in these motor regions using NODDI. Thirdly, the NODDI

measure of free water diffusion (ISO) was interestingly decreased within the CST and increased within the CC. Importantly, the results demonstrated a reassuring consistency between whole brain and TBSS voxel-wise analyses, the latter of which has not previously been undertaken using NODDI in patients with ALS, and with a greater extent of change in parameters manifest using TBSS methods.

Diffusion MRI is well-established as the only MRI technique able to infer tissue microstructure by modelling the signal change from displacement of mobile (water) protons along a magnetic field gradient.[2] DTI, in particular, has been used extensively to pinpoint the sites of change in patients with a range of neurodegenerative conditions.[3] The reductions in FA here chime in well with the original hypothesis [Chapter 2.9.1(a)(i)] informed by a wealth of DTI studies in patients with ALS in whom the overarching theme has been reduced FA within the CSTs[4-18] and the interconnecting motor fibres traversing the body of the corpus callosum,[5,7-10,12,14,18-20] sometimes accompanied by an increase in one of the other (mean or radial) diffusivity indices, thus forming a colloquial 'horseshoe' appearance.[12] Furthermore, this had been replicated using either whole brain and masked region-of-interest (ROI) analysis[12,15,20-27] or entire and ROI-masked skeleton TBSS[5,14,16,18,28-31] methods which, if when undertaken even in the same group of patients, similar to this study, have reassuringly shown concordant results.[13,31] However, detecting significantly diminished FA in these tracts is not guaranteed,[12,29,32] as clearly demonstrated in a study amalgamating DTI data from multiple research centres, with one centre's patients failing to demonstrate any difference to controls, at the whole brain level at least.[12] This may have been influenced by their control group's average age being seven years higher than the patient group although the twenty-one patients included is not dissimilar to the Historical Patient cohort in this study who showed highly significant and extensive reductions in FA at whole brain level. On the other hand, reduced FA in

the New Patients was not seen at the whole brain level prior to restricting analysis to the masked Motor ROIs despite having the same number of patients and an age-matched New Controls group. Even then, the change in FA was patchy and reached a much lower significance compared to the Historical Patients. This may relate, instead, to differences in clinical factors between our patient groups, which shall be discussed below, but is a taste of the diversity of findings between studies using DTI in ALS.

As a way of controlling for between-subject inconsistencies in alignment introduced by linear and non-linear warping of parameter maps from the native into the standard space,[33] TBSS was performed in both of our patient groups. Analysis across the whole white matter skeleton more readily demonstrated reduced skeletonised FA throughout the rostral CSTs and CC body with a wider pattern of distribution in the New Patients, even though FA reduction in the CC was seen at far higher significance in the Historical Patients. Interestingly, in the Historical Patients, reduced FA was also seen more anteriorly within the genu of the CC and encroaching into the forceps minor, a nerve fibre bundle interconnecting the medial prefrontal cortices.[34] Changes here have been reported using DTI in ALS previously[35,36] and may be more extensively abnormal in patients with frontotemporal dementia (FTD).[36] Although none of our participants met diagnostic criteria for FTD, it is not unusual for regions of the frontal white matter to demonstrate reduced FA in patients with ALS with respect to controls on whole brain[13,23] or TBSS[31,37,38] analyses. This would also be in accordance with neuropathological loss of frontally-projecting motor fibres[39] and patterns of inclusion body deposition,[40] although no other such additional areas were identified here. Nevertheless, the findings of this study add to the weight of evidence that FA is predominantly sensitive to whatever disease processes are occurring within the CSTs and CC in patients with ALS.

What is perhaps more difficult is understanding the nature of altered tissue architecture to which the reduced FA may be ascribed. FA is reflective of the overall degree of directionality of water movement within tissue at the voxel level and is classically higher in regions rich in white matter tracts such as the CSTs where water movement is largely restricted along compact, parallel fibre bundles.[41] It would be tempting to interpret the FA in light of end-stage neuropathological data and ascribe lowering of FA to the known loss of axons and myelin within the CSTs and of the interhemispheric fibres traversing the CC.[39,40,42-45] However, equating specific alterations in anatomical configuration to a directional change in FA is ill-advised, not only given the accepted susceptibilities of the diffusion tensor model to normal variations in neurite morphology across the brain[2,46-48] but also the inherent difficulties of relating even *post mortem* imaging to post-fixed histopathological specimens.[49] Data relating the pattern and burden of TDP-43 inclusion bodies to a proportionate axonal loss (indirectly measured by staining for lipofuscin remnants) across certain tracts in the brain,[40] for instance, have formed the basis of interesting studies seeking to 'stage' patients *in vivo* using the reduced FA found on DTI as a surrogate for tract 'involvement', at least. Although the cumulative burden of selected tracts demonstrating a reduced FA correlated with the ALSFRS and disease duration (similar to this study's findings, as discussed below), the original study of inclusion body deposition itself found no relationship with these clinical factors and a up to quarter of patients in the imaging studies could not easily be categorised into these cumulative 'stages'.[50,51] Indeed, neurite configuration is not the only factor capable of determining diffusion anisotropy which may be differentially influenced by infiltration of lymphocytes or glial cells and also iron accumulation within microglia,[46,49,52] for instance. Moreover, the distribution of FA reduction observed in both our patient cohorts is throughout the CC and proximal/*rostral* CSTs with no significant change manifest in caudal portions of the CSTs, such as across the posterior limb of the internal capsule which has often

demonstrated a difference compared to controls in other DTI studies.[5,12,15,20,22,24,26,30,53-55] Depletion of pyramidal somata or their proximal CST axons has not been universally observed neuropathologically[42,56,57] with degeneration not infrequently more discernible in the *distal* CSTs even at extended epochs.[42,44,58] This has lent support to the idea that axons are sequentially 'pruned back' over time prior to parent cell death suggested from the observations of anterior horn cells in animal models of ALS,[59-62] albeit that the subpopulation of Cells of Betz appear to be particularly susceptible and have often largely disappeared by the time the patient has died. However, no clear gradient of neuropathological change along the CST has been found when specifically examined[42] and, at the very least, there is no consensus either from the pattern of changes in FA with regards to a rostro-caudal direction of tract 'abnormality' using DTI.[4,11,13,15,16,23,63,64] Therefore, relating the two is not straightforward and the FA, on its own, may not be providing the full picture.

NODDI has, therefore, been performed in this study with the principal objectives of trying to disentangle the possible contributions of neurite density, orientation dispersion or isometric water diffusion to a unidirectional deflection in FA, and also ascertain whether it is sensitive to changes which the FA is not, particularly within the CC and CSTs. As hypothesised [Chapter 2.9.1(a)(ii)], and based upon the whole brain findings previously reported in this cohort of participants,[1] a widespread reduction in the NDI was again seen along the length of both intracranial CSTs and across the body and anterior CC in the Historical Patients on whole brain and ROI analyses. In contrast to the rostral 'horseshoe' distribution of FA reduction, clusters of reduced NDI encompassed a greater voxel number and extended caudally into the medullary portions of the CSTs. In contrast to the hypothesis [1(a)(ii); see below], and not previously reported using NODDI, *raised* ODI was seen within the body and anterior CC on whole brain analysis clearly overlapping the

reductions in NDI and FA, although over a far less extensive area. Similar appearances of reduced skeletonised NDI and increased ODI in the Historical Patients were observed using TBSS. Conversely, in the New Patients, it was changes in ODI, not NDI, which dominated the NODDI abnormalities. ODI *increases* were demonstrated within the body of the CC on ROI analysis, followed by much more extensive increases throughout the rostral, and also caudal, CSTs using TBSS and TBSS ROI analyses, respectively, essentially mirroring the NDI changes in the Historical Patients. Furthermore, the extent of ODI change within these areas was in excess of that seen in FA on corresponding analyses in the same patients, as reflected by the voxel sizes of the main clusters. Rather surprisingly, however, no significant decreases in NDI were seen at all in the New Patient group.

These findings, now in two independent patient groups, may have several implications. Importantly, they illustrate how a shared, unidirectional change in FA within the same brain regions can arise from potentially disparate alterations in tissue microstructure inferred by diffusion MRI parameters. In the Historical Patients, the reduced FA within the white matter motor tracts would appear to be driven in part by increased ODI but overwhelmingly by reduced NDI which, in turn, suggests that loss of corticospinal and interhemispheric axon fibres in the CSTs and CC, respectively, is the dominant underlying pathological mechanism rather than a disturbance in fibre alignment, orientation or geometric complexity of the extra-axonal space. Reduced NDI over FA could also reflect a profound loss of myelin in place of axons themselves,[65,66] but this would be out of keeping with the neuropathological data from patients with ALS and animal models of the disease which suggests proportional loss of axons and their myelin.[39,42,44,67] That is not to say, however, that the axon-myelin relationship is necessarily *normal* in surviving pyramidal or motor neurons. Studies in rodents with SOD1 mutations using very high

field strength *ex vivo* DTI[68-71] and, more recently, NODDI[67] of the spinal cord in the symptomatic and pre-symptomatic[67-69] phases of disease have similarly shown either reduced FA and increased radial diffusivity, or reduced NDI and increased ODI, particularly in the ventrolateral cord white matter which contains exiting motor neuron axons and vertically interconnecting pathways necessary for locomotion.[72] Histologically, loss of neuronal markers and reduced expression of myelin proteins is accompanied by expansion in the extra-axonal space even in pre-symptomatic cases[67] which may imply an early breakdown of neuron-oligodendrocyte relationships and corroborate the several plausible explanations for the changes in diffusivity reported in this study (that being less hindered diffusion of water in directions other than the original tract orientation). Indeed, in the New Patients, the drop in FA seems almost entirely to be driven by an increased dispersion in fibre orientation. Accordingly, this could stem from either a warping of the fibre tracts, such as through infiltration of astrocytes, microglia or other inflammatory cells without substantial depletion in fibre quantity, or through increased branching of surviving axons (which may then partially restore NDI) after the most susceptible fibres have degenerated. Furthermore, given the different profile of NODDI changes shown by the New and Historical Patients, particularly with respect to NDI, it may be that changes in diffusion parameters are dependent on the severity of impairment or duration of disease, particularly given the two patient groups do differ in these regards. Of course, each scenario may be relevant to some extent and are discussed further below, in light of relationships with clinical factors and blood CD4+ lymphocytes.

Nevertheless, there were newly-reported changes in ISO detected primarily using TBSS in the Historical Patients which warrant consideration, especially as the majority were not found to correspond to any significant reduction in skeletonised FA. The decreased ISO shown within the right CST, corona radiata and longitudinal fasciculus was accompanied

by a reduction in NDI in these areas (but no change in ODI). This may imply a preferential degeneration of axons possessing the very largest diameters (within which ISO can, conversely, be elevated), although why the reduced ISO was exclusively on the right side (whereas the NDI loss was on both sides) is unclear. Conversely, there was increased skeletonised ISO seen within the body and anterior aspect of the CC accompanied by co-localised NDI reduction and ODI elevation. As there are no extended cerebrospinal fluid compartments here or dilated perivascular spaces, the ISO may be suggestive of either expansion of the extra-neurite space due to loss of axons (supported by the lower NDI), increased space between axon-oligodendrocyte membranes or cytoplasmic changes (perhaps from an influx of cells) resulting in increased free water diffusion but also a greater dispersion of diffusion orientation between cell membranes (to explain the increased ODI). Association fibres crossing the anterior CC, particularly, are felt to be less densely packed and of smaller diameter on average[34] and so their loss, as opposed to loss of larger diameter fibres in the CSTs or CC body, might not be expected to tip the balance towards a reduced ISO within this region.

The small area of reduced ODI in the right lateral putamen seen in the Historical Patients at the whole brain level might represent a focal loss of axonal or dendritic tree complexity, as reported neuropathologically in ALS,[73] although no basal ganglia ODI changes were observed in the New Patients nor was the reduced ODI accompanied by a change in FA which has been recognised previously but may be difficult to detect without a directed deep grey matter ROI approach.[74]

The unexpected differences in some findings between the whole brain analyses in the Historical Patients performed by Broad and colleagues[1] and those at whole brain level in the present study should be acknowledged at this point, given that our hypotheses for

ODI and ISO in Chapter 2.9.1(a)(ii) were informed by the original study. Reassuringly, essentially identical changes in NDI were found and FA changes were largely replicated in these patients. However, reduced FA had extended more caudally within both CSTs, ODI was actually *decreased* within a small area of the right anterior internal capsule (not *increased* within the CC as in this report), and ISO only increased in an anterior region of the caudate and adjacent to the right lateral ventricle - no such ISO increase was seen in this study at whole brain, or Motor ROI, level for that matter. Notwithstanding the overall consistency in FA and NDI changes, the congruent ODI increases seen in both independent Patient groups in this study (and clearly confirmed using TBSS) may indicate that the explanation lies in the different methods of image processing and analysis used by Broad and colleagues. In the present study, no smoothing of the parameters maps was undertaken prior to statistical analyses (see below in section 7.4), *dtifit* was used instead of *Camino* (UCL; open-access software) to generate the FA maps, and non-parametric permutation testing was conducted using TFCE and FSL software rather than parametric statistics using SPM12. Whether or not these differences would have been observed using ROI or TBSS is, of course, uncertain as this is the first study to undertake these approaches using NODDI parameters in ALS.

Relationships to Clinical Factors. The most consistent findings in this study relating patients' diffusion MRI parameters across all the patients with ALS to clinical factors (including ALSFRS-R, Rate of Progression, Disease Duration, total ECAS score and ECAS ALS Specific score) were that FA and NDI both showed a positive association with ALSFRS-R and a negative association with Disease Duration principally within substantial regions of the CSTs and CC. Furthermore, these particular relationships were only demonstrated using TBSS as opposed to analyses at whole brain level.

FA and measures of clinical severity have shown variable and, sometimes, opposing relationships across the plethora of studies using brain DTI in ALS. A positive correlation with ALSFRS-R is perhaps most often observed and localised to the CSTs with additional regions in the CC, corona radiata, frontal lobes or cingulum also found.[12,13,23,26,55,75-77] However, almost as many studies have failed to find an association between FA and the ALSFRS-R despite reporting reduction in FA along the CSTs compared to controls.[14-16,20,22,27,30,38] This may, in part, be explained by impairment on the ALSFRS-R score being more dependent on a relative loss of anterior horn cells rather than pyramidal cells within the brain,[78] and may underlie why a number of these studies instead showed negative associations between intracranial FA and measures tailored to UMN impairment[14,15,21,22,38] which are usually based around a composite score of brisk reflexes on bedside examination.[21,22,79] Interestingly, the author is aware of only one study which showed a negative association with ALSFRS-R although this did not survive the significance threshold after correction for multiple comparisons.[80] Therefore, the finding in the present study, of greater reduction in (skeletonised) FA within the CC and rostral CSTs being associated with worsening function, is consistent with previous work and with the hypothesis in Chapter 2.9.2. Likewise a positive relationship with NDI in the CC and CSTs was also identified which only became evident once the patient groups were combined, as neither showed the association with NDI on their own. This is perhaps surprising for the Historical Patients who so clearly demonstrated the reduced NDI (and FA) in these same areas compared to controls, but would suggest overall that declining function is partly mediated by axonal loss. Interestingly though, the positive association between ALSFRS-R and FA was demonstrated in the Historical Patient group alone (unlike with NDI). Given that neither ODI nor ISO subsequently showed associations with the ALSFRS-R in these or across all patients, particularly in light of the increases in ODI

shown in patients with ALS compared to controls, it implies that factors other than those to which NDI, ODI or ISO are sensitive might underlie the relationship with FA.

Disease duration has shown a much more polarised relationship to intracranial FA with a handful of studies showing either positive[14,22,27] or negative[23,26] associations, but many being unable to identify a link at all. In this study, a clear negative association was observed both with FA and, if not more markedly, with NDI suggesting that as time from symptom onset increases (and ALSFRS-R score is decreasing, as expected from the natural history of the disease) a greater degree of axon loss is detectable within the CC and CSTs. This seems logical and is in accordance with the original hypothesis. Nevertheless, it is important to observe that the ALSFRS-R and disease duration were the very clinical factors (in addition to age) which significantly differed between the New and Historical Patients: the New Patients were scanned earlier in their disease course and with higher levels of preserved function. Furthermore, there was no difference in the rates of disease progression between the groups with the mean and median loss of ALSFRS-R points per month all ≤0.5, and rate itself showing no significant associations with clinical factors across all diffusion parameters. When TBSS and TBSS Motor ROI analyses for FA and NDI against the ALSFRS were repeated adding disease duration (to age) as a co-variate, and against disease duration with ALSFRS as a covariate, the associations with ALSFRS-R fell below the significance threshold. Those for duration were preserved but emerged only using TBSS Motor ROI. Accepting that these analyses do not directly compare the effects of the two clinical factors, the implication is that the patterns of variability in FA and NDI linked to the ALSFRS-R and to disease duration are very similar, but that there remains some significant variability linked to disease duration which is different.

Circumstances where a *positive* association with disease duration could conceivably emerge are when there are a higher proportion of patients within the group progressing rapidly, such that a short duration, indicative of highly-active disease, might be conversely associated with *more* abnormality within the intracranial motor system (accepting they are still patients with an ALS phenotype with spinal motor neuron degeneration and not PLS which usually progresses more slowly[81,82]). If disease duration is then driving the association with imaging changes, this could then render any association with ALSFRS-R more difficult to detect. Interestingly, each of the studies showing a *positive* association between FA and disease duration were also ones in which a link with ALSFRS could not be demonstrated,[14,22,27] although without knowing the distribution of durations or rates of progression in these studies it is purely speculative. Yet it does highlight the interplay between heterogeneous clinical factors and the variable tempo of disease progression. As with the ALSFRS, the negative association between duration and NDI only became evident once the patient groups were combined, despite the Historical Patients demonstrating a clear negative association between the FA and disease duration. The possibility thus remains that some additional aspect of FA change in the Historical Patients is not so sensitively reflected by NODDI parameters in proportion to markers of severity, as considered above. Having said that, unlike with ALSFRS-R, the extent of the changes seen in NDI on the combined group analyses in relation to disease duration were then more marked compared to FA, and remained so after ALSFRS-R was added as a co-variate.

Clusters of voxels across other regions of the brain were found to bear significant associations with diffusion parameters on combined group analysis. Positive associations were demonstrated between disease duration and a small area of skeletonised FA within right temporal fusiform subcortical white matter, and between the

ECAS ALS Specific score and a small region of the right intraparietal sulcus. These regions did not display significantly altered FA compared to controls or any clear link to rate of progression. Higher FA in the intraparietal sulcus associating with a better performance on a combined score of executive, verbal fluency and language abilities may imply either better preservation of FA in these patients or a mechanism of compensation that increases the FA, such as local fibre plasticity. The intraparietal sulcus borders the superior and inferior parietal lobes and is part of a network connecting occipito-temporal areas to the premotor cortex for observed manipulative action such as the planning of object grasping.[83,84] It is also adjacent to areas of the inferior parietal lobe which shows functional abnormalities during confrontational naming task of word-retrieval in patients with ALS,[85] and thus would plausibly be relevant to the ECAS ALS Specific score. The first study to investigate DTI measures against ECAS scores was recently published and similarly reported a positive relationship between FA and, specifically, the verbal fluency component of the ECAS ALS Specific score but in more frontal areas such as the longitudinal and uncinate fasciculi.[18] In the current study exploring novel ECAS cognitive score relationships to NODDI, individual cognitive domains were not separately explored and so it may be useful to segregate all the ECAS sub-scores to fully characterise which domain may be driving these changes.

The fusiform gyrus, on the other hand, is concerned with facial recognition, forming a network with limbic and prefrontal areas.[86] Although recognition of familiar faces itself is not typically impaired in ALS, there is increasing evidence for altered ability to recognise affect and emotion in others (so-called social cognition[87,88] which is, incidentally, tested as part of the ECAS) and could conceivably explain a structural link to this brain area in ALS with respect to duration of symptoms. As NODDI did not detect associations with

these clinical factors it is not clear what the FA may represent on a structural level and clarification should be sought in future studies.

Within the Historical Patients only, positive associations between skeletonised FA and NDI and the ECAS ALS Specific score were seen within the CC and the CST which, together, would credibly relate the extent of motor tract neurite density loss to worsening cognitive function. A tiny patch of ISO within the CC also demonstrated a negative relationship to the total ECAS score. Given the higher proportion of smaller diameter association fibres found there normally and the increased ISO located here in these same Patients compared to controls, it may imply greater extra-neurite free water movement, within infiltrating cells and/or between fibres for instance, is driving the association with worsening cognition. However, these findings were not replicated in the combined group analyses which were dominated by the associations with ALSFRS-R and disease duration. ECAS scores did not significantly differ between patient groups and less consistent associations are likely symbolic of the disease heterogeneity which is evident from across different diffusion studies as a whole.

Relationships to blood CD4+ cells (New Patients only). This is the first study to relate diffusion MRI to CD4+ lymphocytes and the subpopulation of T regulatory cells (Tregs) in an attempt to further characterise the role of the immune system in patients with ALS. Certainly the most robust findings across FA and NODDI parameters were of an association between higher levels of circulating blood CD4+ cells and either lower skeletonised FA or higher ODI (on either whole brain, ROI or TBSS analyses) within the body and anterior corpus callosum, and maintained despite accounting the rate of disease progression as a co-variate. Indeed, a positive association between whole brain FA and the Treg:CD4 ratio was additionally seen to emerge within the parietal cortex.

Involvement of immunologically active cells and inflammatory signalling cascades are now widely recognised not only as integral components of neurodegenerative disease processes but also of normal nervous system development and optimal maintenance in health.[89-91] Although astrocytes, endothelial cells and even neurons themselves respond to stimulation of innate immune receptors, microglia are considered the most highly vigilant and morphologically dynamic resident immune cell type of the brain. They continuously survey the local environment for any evidence of damage, debris or pathogen attack and coordinate an appropriately limited 'beneficial' inflammatory response tailored towards neural protection and repair in their so-called 'M1' state.[90,91] Far from being segregated behind an impenetrable blood-brain-barrier, microglia communicate with and recruit circulating immune cells, particularly T cells and macrophages, via the cerebrospinal fluid and meninges to modulate brain function and plasticity, and are sensitive to peripheral inflammatory signalling.[91-95] In chronic neurodegenerative states, the spectrum of microglial phenotypes throughout the brain is felt to become tipped disproportionately towards a detrimental and inflammatory 'M2' state determined by a complex interplay of sustained signals from dying neurons and

humoral factors, perhaps exacerbated by their intrinsic dysfunction with age.[91,94] Whether or not this is a primary event or secondary to deposition of abnormal TDP-43 inclusion bodies, in ALS for instance, is unclear although several of the known genetic mutations associated with ALS impact microglial and astrocytic operations too.[96,97]

In patients with ALS, end-stage neuropathological examination reveals activated microglia within the lateral funiculi and anterior horn compartments of the spinal cord in addition to the precentral and frontal gyri.[98-100] The degree of activation in frontal regions correlates with executive cognitive impairment[101] and in the spinal cord with rates of disease progression.[102] Ligand PET studies in ALS[79] and FTD[103] using first generation binders to the TSPO protein on activated microglia have shown increased binding in motor and frontal areas *in vivo*. Furthermore, widespread astrogliosis is seen in these areas along with T cells predominantly positive for $CD8^+$ and smaller numbers of $CD4^+$ cells,[42,45,99-101,104-108] with animal models of the disease demonstrating that the $CD4^+$ cell type may predominate at earlier disease stages when their levels are actually increased compared to controls.[109] Interestingly, restoration of $CD4^+$ cells, particularly the $CD4^+$ $CD25^+$ $FoxP3^+$ Tregs, in T cell deficient mSOD1 rodents extends the stable phase of disease and maintains microglia in their 'M2' phenotype, providing evidence not only that peripheral immune cells influence the CNS inflammatory milieu but that this can be a positive phenomenon. Patients with ALS themselves also demonstrate an elevated Tregs:$CD4^+$ ratio compared to controls which itself,[110] or the absolute Treg number,[111] also correlates negatively with rates of disease progression.

Although not an outcome measure for which the present neuroimaging study was powered to address, non-significant trends towards a *positive* correlation with the baseline total $CD4^+$ cell count and a negative correlation with the baseline Treg:$CD4^+$

ratio were found with respect to the rate of disease progression for the subgroup of MIROCALS trial patients included here. Certainly the latter of the two correlations would be in keeping with the literature discussed[110,111] whereas the increased total $CD4^+$ cell count being associated with a faster rate of progression may seem counter-intuitive. In the rodent mSOD1 model of ALS at least, blood levels of all $CD4^+$ cells do increase in the established phase of disease and CD8+ towards the end stage,[109] mirroring the neuropathology reports. However, there are diverse subsets of $CD4^+$ cells, such as T effector cells, which accompany Tregs in this single measure and hence the Treg:$CD4^+$ ratio may be more relevant in terms of the overall effect on the inflammatory environment within the brain. Indeed, absolute Treg counts may appear less influential for this reason, coupled with the uncertainty regarding how functionally active or effective the Tregs are in the disease state. In any case, the trends observed are useful in contextualising the imaging findings.

A negative association between FA and total blood $CD4^+$ was found within the anterior body of the corpus callosum, bearing a striking resemblance to the positive associations found with ODI in this area in the New Patients. Indeed, the associations with ODI were reproduced using whole brain, ROI and TBSS methods whereas the FA associations were observed using TBSS only. Overall, this would highly suggest that a change in orientation dispersion, rather than neurite density, is responsible for the variation in FA in relation to total blood $CD4^+$ cell count. Interestingly, the New Patients also demonstrated reduced FA and, particularly, increased ODI in the same aspect of the corpus callosum when compared to Controls, which could support the inference that a higher total blood $CD4^+$ count relates to an increased degree of disease-associated change in the imaging parameters (that is, changes compared to controls), thus aligning with the trend shown between total blood $CD4^+$ and increasing rate of disease progression. However, it would

be premature to conclude that the FA and ODI changes in the CC relating to the total blood $CD4^+$ levels, or change with disease itself, are definitely representative of detrimental processes for several reasons. Firstly, as discussed earlier, the underlying nature of microstructural changes inferred by an increased ODI (or reduced FA) in the CSTs and CC between patients and controls may be indicative of greater dispersion in the orientation of neurites themselves due to tract bending or branching, but may alternatively denote increased extra-neurite diffusion within cells including glia or, potentially, infiltrating lymphocytes. Furthermore, these tissue changes wouldn't necessarily be mutually exclusive and could even represent a positive attempt to contain the damage. Filling in the steps between variations in blood $CD4^+$ cell counts and altered water diffusion in the brain is, of course, speculative without simultaneous pathological data but does provide evidence for relevant immunological crosstalk with the central nervous system.

Secondly, it is noteworthy that the rate of progression itself did not demonstrate a clear association with any imaging parameters (including ODI). When rate of disease progression was included as a co-variate in the analyses, the associations between total blood $CD4^+$ levels and the ODI were less easily detected (except with TBSS) suggesting that a rate-dependent influence may indeed be relevant, whereas associations with FA became more easily detectable, perhaps conversely indicating residual effects independent of rate. Rate of progression, therefore, does appear to relate to peripheral immune activity. In due course, additional biochemical information regarding the range of cell types comprising the total CD4 count, the functionality of the Tregs and their change over time will become available from MIROCALS at the end of the trial, which may help interrogate this relationship further, particularly as a clear relationship between corpus callosum imaging parameters and Tregs themselves was not demonstrated.

However, with rate added as a co-variate, a positive association emerged between the Treg:$CD4^+$ ratio and a cluster of FA within the subcortical white matter of the left superior parietal lobule. The superior parietal lobe is in close proximity to the intraparietal sulcus which interestingly, as discussed previously, contains some of the larger-sized pyramidal cells of the parietal lobe, connects to frontal and temporal lobes via the medial and longitudinal fasciculi and appears to have a role in sensorimotor decision tasks,[112-114] all having plausible relevance to the symptoms in ALS.

7.2 Diffusion Imaging in ALS: NODDI ID=1.1

This is the first study in patients with ALS which has explored NODDI parameter maps calculated using two different assumptions for the intrinsic diffusivity (ID). The established value of ID=1.7 x 10^{-9} $m^2.s^{-1}$ is believed to be optimised for white matter analyses, whereas grey matter structures may be better represented using a lower ID value of ID=1.1 x 10^{-9} $m^2.s^{-1}$ given the higher complexity of neurite (axonal and dendritic) architecture.[115,116] The principal findings not previously demonstrated using NODDI ID=1.7 are that precentral cortex NDI shows negative associations with the ALSFRS-R and the ECAS ALS Specific score on ROI analyses, and is also seen to demonstrate a negative association with the Treg:$CD4^+$ ratio which is independent of variation due to cortical thickness. A reduction in precentral cortex ODI in patients with ALS compared to controls was also found which may be dependent on cortical thickness.

NODDI is based upon a model of water diffusion comprising three main compartments, between which it is assumed there is negligible water exchange. Aside from unrestricted free water movement in cerebrospinal fluid, intraneurite diffusion is modelled as 'sticks' and extraneurite diffusion linked to an axially symmetric tensor.[117] Diffusion along the plane of the 'sticks' is termed the intrinsic diffusivity (ID) and has been assumed mathematically from diffusion tensor data in white matter tracts from structurally 'normal' brains.[118] However, the optimal assumption is more accurately dependent not only on whether white or grey matter is being mapped but also on age, potential differences between intra- and extra-cellular water movement parallel to the 'sticks', and even changes mediated by pathological conditions.[117] The ID value of 1.1 x 10^{-9} $m^2.s^{-1}$ used to recalculate the NDI, ODI and ISO parameter maps was in broad agreement across a range of recent studies,[115-117] in order to interrogate the deep grey matter on whole brain and the precentral motor cortex on ROI analyses. Recalibrating the ID to 1.1 has been

shown previously to enhance the signal-to-noise ratio of the grey matter ODI maps in particular[115] although, interestingly, the majority of new findings in this study relate to changes in the NDI within the precentral cortices. No group differences were seen in the white or grey matter between the New Patients and Controls, which is not unexpected given the ODI changes using ID=1.7 were seen on ROI analysis only and limited to within the corpus callosum, as earlier discussed. The widespread reduction in white matter NDI throughout the CSTs and CC in the Historical Patients compared to Controls seen using ID=1.7 was replicated but, as might be expected, at much lower significance and over a reduced distribution with the ID=1.1. However, the small cluster of reduced ODI in the right putamen was not reproduced which, if the alteration to ID is correct across the grey matter, may suggest that this small change in basal ganglia microstructure using ID=1.7 was a product of suboptimal signal modelling. A small cluster of reduced ODI was detected within the left precentral cortex in the Historical Patients compared to controls which is in line with the proposed hypothesis. Neuropathological data in ALS has usually shown loss of the largest pyramidal somata along with retraction and stumping of surviving pyramidal cell dendritic architecture, which might be expected to reduce the dispersion of diffusion orientation. ODI has demonstrated a positive association with the dispersion of neurites in grey matter of rodent cortex[119] and the human spinal cord,[120] although it is not possible at lower field strengths (here 1.5 Tesla, but even at 3 Tesla) to ascribe these changes to a particular cortical layer.[121] Furthermore, although NODDI does inherently account for partial volume effects from white matter or CSF, correction for cortical thickness in the context of any significant cortical findings has been recommended given the potential for residual variation, particularly where the cortex may be comparatively thinner.[116,121,122] Of course there would be an effect from age already accounted for, but the precentral cortex reliably demonstrates reduced thickness as a consequence of ALS itself.[123-127] Significantly decreased ODI was no longer seen

following this correction. As both the patients and controls would be expected to be adjusted proportionally, this may indeed indicate that the cortical ODI was confounded by partial voluming or the normal variation in cortical measurement between individuals.[121] Alternatively, a significant reduction in cortical ODI may only be detectable much later in the disease, given that the hypothesis is based upon end-stage pathological appearances and may additionally explain why no relationship between cortical ODI and measures of disease severity were subsequently identified in the patient groups. However, it is possible that using an average thickness across the whole precentral gyrus is too crude given that left and right hemispheres show asymmetric thickness in health and there may be focal volumetric loss depending on the phenotypic presentation of ALS.[128] Co-registration of a high-resolution T1 anatomical image and the diffusion data in native space prior to statistical analysis might help to hone any significant differences in NODDI grey matter parameters using ID=1.1,[121] and could even enable skeletonised cortical parameters, for NODDI and FA, to be calculated using a modified forms of TBSS, called grey matter based spatial statistics (GBSS).[122,129-131]

Accepting the limitations of the current method, however, precentral cortex NDI consistently showed a negative association with ALSFRS-R both in the Historical Patients alone and in the combined patient analysis which survived correction for cortical thickness in the latter. The negative association with the ECAS ALS Specific score was seen in the Historical Patient group only but did also survive cortical thickness correction despite not being replicated across the combined patient group (reminiscent of the association with ID=1.7 skeletonised white matter NDI within the CC and left CST). The strength of association was statistically very weak though, and was likely engulfed by heterogeneity within a larger cohort of patients, especially as the cognitive scores themselves and the proportions of other potential confounders such as bulbar- versus limb-onset cases were

not significantly different between groups. Nevertheless, both these negative relationships with cortical NDI are, intriguingly, the *reverse* of those shown with white matter NDI, whereby higher NDI values relate to more impaired function or cognition. Furthermore, no clear large scale changes in in FA or in NDI using NODDI ID=1.7 or ID=1.1 were seen within the precentral cortex grey matter between in patients compared to controls. This could imply that patients with a higher precentral cortex NDI to begin with do worse or that there is some limited compensatory sprouting of neurites despite the loss in function, although the neuropathological evidence has not been suggestive of this rendering it tricky to interpret the mechanism of this association.

Moreover, in the New Patients, the blood Treg:$CD4^+$ ratio demonstrated a negative association with NDI in the left precentral cortex also, suggesting the lower the NDI the higher the proportion of Tregs. Not only is this similarly counterintuitive at first glance, but it is otherwise in alignment with at least the negative association found with ALSFRS on combined patient group analyses. The borderline positive association between white matter ODI and the total $CD4^+$count, as seen at much greater significance using ID=1.7, was replicated and so provides reassurance that the new cortical associations are reflecting an equally valid relationship with tissue microstructure. It may be important, therefore, to step back from the notion of reducing NDI (or FA) always equating to a worsened outcome in ALS, given that these concepts emanate from diffusion modalities principally optimised for, and sensitive to, changes in white matter tract morphology. Changes in cortical grey matter structures using diffusion imaging in ALS remain largely unexplored. Cortical NDI calculated with ID=1.1 is still considered to be reflective of the density of neurites[121] and so it may, indeed, be the case that a raised precentral cortical NDI with lower Treg:$CD4^+$ ratio is somehow unfavourable. On the other hand, there is no definite evidence yet in this limited (New) patient cohort from MIROCALS that the

Treg:$CD4^+$ ratio mediates a beneficial effect on survival or relates directly to particular levels of Tregs and other cellular infiltrates within the brain parenchyma. If it did, one might have expected the extra-neurite diffusion to change, and hence the ODI to associate. It could even be the case that the density of cortical neurites is disproportionately reduced by an advantageous microglial or lymphocytic infiltration. These possibilities of course need further exploration and it may not be unreasonable to consider the possibility that the cortical NDI parameter reflected by NODDI ID=1.1 is actually sensitive to alternative cellular phenomena in ALS, such as the rather stellate astrocytic processes seen to encase degenerating pyramidal somata.[132] The only other significant association with the Treg:$CD4^+$ ratio found across this study was the positive association with FA within the superior parietal lobule but this region was not found to relate to disease severity measures or replicated using NODDI. Given the extensive changes in white matter tracts demonstrated using ID=1.7 TBSS, grey matter changes may be further elucidated using techniques such as GBSS with ID=1.1 parameters, as mentioned.

7.3 Quantitative Magnetisation Imaging in ALS

This is the first study to undertake quantitative magnetisation transfer imaging in patients with ALS and to explore relationships between its parameters in the brain and patients' clinical factors or levels of circulating immune cells. The main findings are of reduced kf and increased T2f within the CSTs on whole brain and ROI analyses and also, using TBSS, across the CC in the Historical Patients compared to Controls. Whole brain kf within the cingulate cortices and left pre- and post-central gyri showed a positive association with ALSFRS-R; skeletonised kf in the CC showed a positive association with the ECAS ALS Specific score; whereas skeletonised f within the lower CSTs showed negative associations with both total and ALS Specific ECAS scores. Skeletonised f within the right posterior corpus callosum was also negatively associated with total blood $CD4^+$ levels in the New Patients who otherwise showed no differences with respect to controls or clinical factors.

Unlike diffusion MRI techniques which attempt to infer architectural configuration through the movement of water molecules, magnetisation transfer (MT) imaging aims to interrogate macromolecular integrity and composition indirectly by assessing how protons bound to these lipids and proteins affect magnetisation of free water protons. The technique is already used clinically to better delineate body tissues of differing lipid/protein content but, within the central nervous system, would primarily be sensitive to changes in myelin which is the dominant macromolecule. Qualitative T1 MT contrast (MTC) imaging has previously revealed hyperintense appearances in the brain throughout the CST[133,134] and CC[133] compared to controls in a highly variable proportion of patients with ALS. Furthermore, when present, reduced MTC has been related to the degree of diminished FA in the CSTs.[133] The semi-quantitative MT ratio (MTR; essentially denoting the proportion of altered contrast produced by the MT pulse) has shown a reduction within

the white matter of the CSTs,[135] in addition to the precentral cortex and frontal gyri grey matter[136,137] in patients with ALS compared to controls. However, it is unclear what macromolecular changes the MTC and MTR represent as they are both relative measures dependent on a range of imaging variables.[138] Indeed, CST MTR has also been reported to be increased in ALS, similarly accompanied by reduced CST FA,[139] rendering it difficult to ascribe the biophysical meaning to these MT changes between different patient cohorts, particularly in the face of largely consistent decreases in FA (which may itself denote several biophysical phenomena as already discussed).

Decreased kf and increased T2f within the CSTs and CC so clearly seen here in the Historical Patients supports the sensitivity of quantitative MT imaging to the disease process in ALS and interestingly echoes the changes observed using qMTi in the brain lesions of multiple sclerosis. Acute inflammatory brain plaques have demonstrated reduced f and kf, and increased T2f followed by normalisation of these parameters over several months, consistent with demyelination, disturbed macromolecular composition or metabolism, and oedema and then a slow resolution with remyelination.[140] Although the tempo and pathophysiology of MS lesions is not directly applicable to ALS, the absence of a significant change in f in this present study would suggest that there is no significant loss of macromolecular density within the CSTs and CC. However, the Historical Patients did demonstrate extensive reduction in FA and NDI within these areas, along with a less marked increase in ODI. If reduced NDI is presumed to imply loss of axon fibres, loss of their myelin sheaths would also be expected. It is possible, therefore, that the density of intact myelin around surviving axons and/or remnants of degenerating myelin, as seen neuropathologically using the Marchi staining method,[39,42] maintain the f value despite significant loss of fibres suggested by NODDI. On the other hand, semisolid non-myelin macromolecules may also be upholding this parameter such as from lipid rich glia or

immune cells which are known to infiltrate the damaged CSTs and CC in ALS.[46,49] Indeed, there is debate over exactly which macromolecular breakdown products in actually reduce the osmium tetroxide in Marchi fluid.[141] Furthermore, as discussed above, early breakdown of neuron-oligodendrocyte relationships are seen in animal models of ALS and are accompanied by reduced FA and NDI or increased ODI even in the presymptomatic stages.[67-71] With abnormal expression of myelin proteins and expansion of the extra-axonal space also reported in such rodents,[67] these non-mutually exclusive mechanisms could plausibly explain a decreased kf, FA and NDI with increased T2f and even ODI without a significant drop in f. Furthermore, the extensive rise in non-bound water protons indicated by the increase in T2f throughout the corpus callosum on TBSS particularly may complement the more focussed patch of raised skeletonised ISO in its anterior aspect.

In sharp contrast to the Historical Patients, the New Patient cohort failed to demonstrate any significant differences in any qMTi parameters compared to controls. Although the principle changes in diffusion imaging within the New Patient group, of increased ODI rather than reduced NDI accompanying a somewhat less extensive reduction in FA, differed in proportions from the Historical Patients one still might have anticipated either kf or T2f changes on at least the TBSS analyses, especially in light of the consistent findings relating raised ODI in the CC to an increased peripheral $CD4^+$ cell count. Re-inspection of the statistical output files for skeletonised kf and T2f in the New participant group comparisons with the significance threshold substantially reduced did begin to reveal expected changes in the CSTs across the internal capsules on both sides. Skeletonised qMTi and, indeed, diffusion parameters for both the New and Historical Control groups were additionally compared with each other to screen for evidence of any substantial scanner performance drift over the time between participant recruitment

periods. Apart from a tiny cluster of increased ODI within the anterior right temporal lobe white matter in the New Controls compared to the Historical Controls, which itself was not a location for any significant group changes across any of the analyses, no other differences were identified. It is, therefore, very possible that qMTi and even NDI changes in the New Patients compared to controls are subtle, and may be detected more readily either with a larger group size or after interval scanning which can be explored once the neuroimaging study itself finishes in due course. The latter is tantalisingly suggested for NDI given its upheld relationships with disease duration and deteriorating ALSFRS scores across the patient groups combined.

The New Patients, however, did demonstrate an association between increasing total blood $CD4^+$ cell count and reducing f values within the posterior CC on TBSS ROI analysis, which was also independent to the rate of disease progression. Changes in FA within the CC and forceps major, into which posterior CC fibres may project, have been found to relate to interhemispheric functional connectivity in ALS[35] and the posterior CC is also said to contain larger myelinated fibres[34] which could plausibly underlie variations in f. Interestingly, reduced MTR has been reported in the forceps major and CC in patients with ALS in the absence of changes in DTI parameters.[142] However, changes compared to controls in diffusion imaging and qMTi were seen more towards the CC body and relationships between qMTi and clinical factors were not found in these patients, rendering the relationship to immune activity denoted by the blood $CD4^+$ cell count unclear. It is possible that the $CD4^+$ cell count influences the amount of myelin and/or other macromolecules in the posterior CC without reducing fibre density or increasing dispersion of diffusion orientation, but in the absence of $CD4^+$ cell counts in the controls it is not possible to be more specific.

The Historical Patients demonstrated some interesting clinical associations with qMTi parameters both in the white and grey matter. Worsening functional impairment on the ALSFRS was associated with decreasing kf within bilateral cingulate cortices and both the PCG and post-central cortices on the left but, unlike with the widespread areas seen with NODDI, not with kf in the CSTs or CC. Indeed, even on whole brain analysis, reductions in kf were not seen in cortical areas compared to controls in this study. The cingulum has previously demonstrated hypometabolism on SPECT[143] and reduced FA[26] in relation to the ALSFRS, with MTR also showing reductions in the cingulate and frontal gyri compared to controls.[136] Pyramidal neurons within the postcentral somatosensory cortices in addition to the PCGs contribute directly to the CSTs and pyramidal cells from cingulate cortices project to the red nucleus and spinal cord thus mediating motor function,[144-146] and so their collective involvement may suggest that the macromolecular changes in and around pyramidal cell somata are driving this association. Indeed, NODDI with ID=1.1 also suggested that worsening ALSFRS was associated with greater NDI within the PCGs at least, and together could indicate that morphological and metabolic cortical anomalies are reflected in the functional score.

On the other hand, kf did demonstrate a positive association with the ECAS ALS Specific score within the anterior CC where reductions had been seen compared to controls, strongly suggesting, as with the diffusion imaging indices, that disease-related change in kf is proportionate to worsening function, in this case cognitive. Furthermore, the anterior CC accommodates frontal interhemispheric fibres whose roles will credibly impact on executive capabilities assessed by the ECAS ALS Specific score. Moreover this and the total ECAS score intriguingly demonstrated negative associations with f along distal segments of the CSTs in the brain stem rather than, as might be expected, from cortical regions. Without having ascertained increases or decreases in f across the brain or brain

stem in ALS, it is tricky to interpret this finding. If f truly represents myelin content, it would reasonably be deduced that in the context of disease, a lower myelination in the CSTs should equate to worsened function, not better. Thus it may leave the biophysical basis for f here open to being macromolecules other than myelin which could include protein emanating from the extra-neurite compartment such as from glia or other immune cells, whereby more 'f' is associated with poorer (cognitive) function. However, it is noteworthy that scatterplots of the f values against ECAS scores revealed clear outlier values for f in two patients. Upon their removal, the association with the ECAS ALS Specific score was essentially lost and suggests these associations may be driven by spurious results. Further analyses in the New Patients whose full blood (and in due course CSF) immune and chemical profiles will be available may shed further light on these associations between and qMTi clinical factors, given that none sadly reached significance across the combined patient group.

7.4 Limitations of the current study

The results presented and discussed in this thesis relating particularly to all qMTi and NODDI ID=1.1 findings but also to all MR imaging modalities and relationships to blood CD4 cell populations in ALS are novel. Despite being part of a longer term study of the MIROCALS cohort, the size of the patient and control groups included for analysis here were exactly as anticipated from the study's original power calculations based on DTI data to show cross-sectional differences in NODDI ID=1.7 parameters, the primary imaging modality, between patients and controls. This would not have necessarily been the case for grey matter changes assessed with NODDI ID=1.1 and larger group sizes may be required to show group differences in these parameters in addition to pre-processing methods tailored for cortical analyses such as GBSS. Furthermore, owing to technical issues with several qMTi scans in the New Patients, fewer patients were included in this group meaning that associations between patients and the clinical factors or 'wet' biomarkers may alter once group numbers are at least equal to the Historical Patients, who showed clear differences to controls with 23 participants. Their disease severity and duration are also different to the patients being recruited soon after diagnosis into ANNALS-QuICT, and yet no significant associations with these particular clinical measures were found across the Combined Patient group. Thus, it may be that kf and T2f do not change in a linear fashion across the disease.

All of our imaging data was acquired at 1.5T as opposed to 3.0T which can affect the signal-to-noise ratio, although has been shown not to significantly alter the sensitivity for changes associated with ALS using DTI at least.[147] For NODDI the reduced field strength may be compensated by the longer T2 relaxation time and a larger voxel size as elsewhere[1] in comparison to other NODDI studies using 3.0T and smaller voxel size.[66,148,149] The FA was also calculated from the full multi-shell dataset from NODDI

with b-values in excess of most other studies with dedicated DTI protocol. However, the findings for FA in this study in relation to differences from controls and associations with common clinical factors were in keeping with the literature and were performed primarily to contextualise newer findings with NODDI and qMTI. Indeed, the qMTi acquisition protocol was exactly as used for previous studies at 1.5T.[150,151]

The maps for each imaging parameter were also not subjected to spatial smoothing prior to non-parametric analyses using TFCE. Although skeletonising parameters in the white matter using the TBSS method bypasses an obligation to pre-smooth data,[28,32,33] smoothing may have improved the signal-to-noise ratio and lessened effects of mis-registration during normalisation techniques for the non-TBSS-based analyses at whole brain or ROI level. Nevertheless, the decision was taken not to perform smoothing because the method of TFCE aims to minimise the requirement for smoothing through its advantages over cluster-based analysis methods of optimising detection of both diffuse low amplitude and focal high amplitude clusters without needing to specify a priori cluster thresholds, and because the amount of smoothing remains defined arbitrarily according to signal extent.[152] Furthermore, anticipated sizes of significant clusters across the brain using unexplored imaging techniques in ALS, such as qMTi, were unknown in advance and smoothing has recognised disadvantages to the sensitivity for such clusters. Nevertheless, a degree of smoothing is considered reasonable when applying TFCE, particularly for data with a low signal-to-noise ratio, and may have served to strengthen or even negate some of the smaller cluster sizes identified in this study at whole brain or ROI level.

Age was used as a co-variate throughout although other potential co-variates such as handedness and gender were not included in the statistical analyses, although they have

been found elsewhere not to significantly influence MRI diffusion parameters in ALS.[78,121] The New Patients with ALS recruited into ANNALS-QuICT were also scanned an average of 39 days after their Inclusion visit for enrolment into MIROCALS which had to be completed (including the baseline blood tests and lumbar puncture) prior to the ancillary neuroimaging study being considered. The delay was partly driven by the Inclusion visit and subsequent visits constituting a significant time commitment around which an extra appointment for brain imaging needed to be scheduled, the fact that the research NODDI/qMTi scans are only available at the CISC at the University of Sussex for all eligible UK participants and due to geographically distant participants needing to be contacted remotely in the first instance. It was decided in the neuroimaging study protocol not to perform repeat ECAS or ALSFRS-R assessments or recalculate duration of disease and rate of progression on the day of scanning, especially given that the baseline blood and CSF samples could not be repeated. However, days to scan could be added as a co-variate when looking for associations with clinical measures and blood $CD4^+$ cells.

Correction for multiple comparisons within each group of related tests was not additionally performed over-and-above the intrinsic family-wise error correction for the individual significant cluster results generated using TFCE. Although this may have increased type I statistical errors and false positive results, an indiscriminate correction without enabling interpretation of the potential biological/anatomical plausibility of cluster location in reference to regions known to be damaged in ALS may have overlooked fresh clues relating to disease mechanisms using these newer neuroimaging techniques. Indeed, the heterogeneity of clinical symptoms and signs in patients with ALS is widely appreciated to influence the neuroimaging findings across multiple studies[12] and smaller sample sizes are also recognised to increase the likelihood of either false positives and false negatives in voxel-based analyses independently of confounding methodological

influences.[153] On a related theme, analyses of patient versus control group differences, and associations between patients and their clinical factors, were undertaken separately rather than amalgamating New and Historical patient cohorts from the outset. The Historical Patients with ALS were not part of the MIROCALS trial and thus had no accompanying fluid biomarker data relating to blood CD4 cell populations. In addition, unlike the New Patients, the Historical Patients were not enrolled from a population eligible for a demanding clinical trial (MIROCALS) and their Inclusion Criteria for imaging differed slightly: age 18 to 70 years-of-age; FVC>60% predicted; and unrestricted length of disease. Furthermore, group comparisons using the Historical Patients and Controls had already been performed and published at whole brain level using NODDI and would serve as a point of reference for an entirely new cohort of patients (being only the second cohort of symptomatic patients studied with NODDI). Therefore, in order to discuss and interpret entirely novel associations between imaging parameters and blood immune cells in the cohort of New Patients aligned to MIROCALS, and explore why differences between patient cohorts may arise, group comparisons between the Patient groups and their respective Control groups were presented separately prior to amalgamating patients for extended relationships between imaging parameters and shared markers of clinical severity. Several associations between clinical scores and NODDI or qMTi seen within the Historical Patients, particularly, were not replicated once combined with the New Patients, and it is acknowledged that small sample sizes, correction for multiple comparisons between tests and clinical heterogeneity may contribute to some extent.

The present study's group sizes were not powered to look at phenotypic subgroups, such as sALS versus fALS or site of onset. Given that 87% of the patients in both the New and Historical cohorts were limb-onset a post-hoc analysis was not performed. Once the full breakdown of baseline ALSFRS sub-scores are available from MIROCALS it may be

possible to look at the severity of bulbar impairment, for instance, on each of the imaging parameters to see which may be driving the associations with FA and NDI in the white and grey matter reported here. Furthermore, the influence of riluzole on diffusion and qMTi is unknown and all patient participants were already taking this medicine at the time of scanning. MIROCALS, on the other hand, is investigating the change in clinical measures and 'wet' biomarkers during the riluzole-only (run-in) period and a future neuroimaging study (here being an ancillary study to MIROCALS only) could seek to ascertain this information.

7.5 Further work

The data presented here relates to cross-sectional diffusion and qMTi MRI alone in patients with ALS. The imaging protocol also included high resolution T1 sequences to enable volumetric analyses across the brain, beyond the isolated measurement of precentral cortical thickness used as a co-variate, and also resting state functional MRI (rsfMRI) using the multi-echo acquisition technique which has not been explored in patients with ALS. It is anticipated that multi-echo rsfMRI may screen out a higher percentage of non-BOLD-like signal artefacts and improve the consistency of sensorimotor, default mode, fronto-parietal and executive network resting network connectivity differences between patients and controls assessed by independent component analysis. In addition, combined functional and structural connectivity of selected "seed" regions using rsfMRI and FA, respectively, can explore the somewhat conflicting results yielded with single-echo rsfMRI data. Increased functional connectivity of the sensorimotor or other cortical regions has been associated with average CST FA values being either better preserved (and thus closer to control values)[154] or, conversely, reduced.[5,155] Accordingly, potential associations between multi-echo resting network connectivity and NODDI, qMTi and blood $CD4^+$ cells have not hitherto been investigated and may build better understanding into mechanisms of disease.

Simultaneous acquisition of several MRI modalities also permit additional parameters relating to tissue characteristics to be calculated. For instance, as diffusion MRI is insensitive to myelin, the combination of the intraneurite and isotropic fractions from NODDI and the f value from qMTi can be used to estimate the myelinated fibre "g-ratio" across the brain. G-ratio equals the axon diameter divided by the diameter of its ensheathing myelin and is estimated to be around 0.7 in the central nervous system.[156] The g-ratio for optimal nerve conduction is considered to lie around 0.6,[157,158] and it tends

to demonstrate a *positive* association with large axonal diameters – that is, the larger the axon fibre diameter the bigger the g-ratio.[159] Within the CSTs, at the medullary pyramid level at least, microscopic g-ratio has between shown to be 0.6-0.7,[159] with similar estimates suggested by MRI.[157] Following adolescence, white matter g-ratio tends to steadily increase with age inferring myelin reduction and knock on effects with respect to the velocity of neuronal conduction.[160] Premature increases in the g-ratio are accordingly seen within MS plaques.[161,162] Although ALS is not primarily a demyelinating disease, new insights into the secondary effects of the neurodegenerative process may be revealed with this technique and correlate with clinical measures.

It would be very interesting to determine the sensitivity and specificity of NODDI and qMTi for ALS given the differences between the patients and controls, generally seen most clearly using TBSS. A meta-analyses has probed whether CST FA values alone may be diagnostic of ALS and found that the overall sensitivity was up to 0.68 and specificity 0.73,[147,163] using FA averaged either throughout the whole intracranial CST or focussed within the internal capsule.[147] Moreover, the average difference in mean FA between patients and healthy controls (not even disease mimics which would eventually be more clinically relevant) is only marginally in excess of one standard deviation and not improved by using 3.0T MRI in preference to 1.5T.[147]

ANNALS-QuICT continues to recruit participants for baseline and identical follow-up imaging. Therefore, not only can the cross-sectional image analyses be repeated in due course with a larger patient group size (which may be of particular relevance to the NODDI ID=1.1 and qMTi analyses given that studies to guide power calculations had not been performed in ALS at the time of designing the study) and inclusive of g-ratio, volumetric and network analyses, but also longitudinal changes in these MRI approaches

can be assessed. Longitudinal scans using DTI in ALS have[23,55,63,64,164] or have not[4,165] demonstrated FA change within the CSTs over intervals of between 6-9 months, whereas very little data exists regarding resting state networks using single-echo rsfMRI,[166] and there is currently no longitudinal imaging study using qMTi or NODDI. Furthermore, once MIROCALS has followed-up its last participants, a greater wealth of serial clinical and 'wet' biomarker measures will become available for investigating potential associations with the neuroimaging which may even be able to predict the degree of change seen on repeat imaging. These measures will include further breakdown on the ALSFRS functional scores and, excitingly, CSF and blood immune cell profiles in addition to levels of neuronal cytoskeletal neurofilament proteins, levels of which begin rising early in the symptomatic phase of disease,[167] appear to remain stable in both CSF and blood thereafter[168] and have been reported to increase in line with the extent of change within the CSTs as assessed by DTI.[169] Importantly, the heavy chain form in CSF negatively correlates with clinical severity on the ALSFRS-R and, with largely stable CSF levels over time,[170] would be a potential candidate for monitoring therapeutic effect. Whether or not the group of follow-up scans performed in ANNALS-QuICT, divided according to treatment with active ld-IL-2 or placebo, will be powered sufficiently to detect a change with respect to MRI parameters is uncertain, however, but may provide sufficient data to justify use of neuroimaging techniques in future clinical trials.

In this regard, thinking beyond the confines of the present imaging study, it would be ideal to undertake combined brain and cord imaging to substantially advance the understanding of how changes within the distal corticospinal tracts in addition to the spinal motor neuron compartment relate to each other and to clinical phenotype. Several studies in patients using DTI of the cervical cord have shown reduced FA,[165,171-173] frequently in the context of reduced cord cross-sectional area,[165,172] and a significant

association with the symptom severity scale ALSFRS[171,172] or finger tapping speed,[173] although in other studies the association is less clear.[165] Reduced MTR has also been reported within the cervical spinal cord[174-176] accompanied by diminished CSA and average FA,[175] and a longitudinal decline between sequential scans.[174] With the encouraging findings with spinal cord NODDI in rodents, albeit at ultra-high field strengths, there is a scientific justification for developing use of NODDI and qMTi techniques in patients with ALS.

7.6 Conclusion

ALS is a highly heterogeneous clinical syndrome comprising features of progressive motor weakness and cognitive impairment for which objective, sensitive and specific biological markers of disease activity for diagnosis, prognosis and response to treatment *in vivo* are greatly desired, ultimately to improve clinical care and assist the search for more effective treatments for patients. Non-invasive quantitative MR neuroimaging is generally well-tolerated and a promising biomarker candidate for ALS able to reveal abnormalities in the corticospinal tracts and corpus callosum, in addition to wider brain regions. Its ever-evolving techniques are being harnessed not only to demonstrate *that* a change exists and where it might be in the brain, but also *why* and *how* the tissue is different which enables a better understanding of disease mechanisms and informs hypotheses for potential therapies. Linking changes seen indirectly on brain imaging to precise conformational or metabolic alterations in living tissue, however, is far from straightforward and, more often than not, precipitates more questions than answers. Nevertheless, this is exactly what is required in order to interrogate existing assumptions which may not be entirely accurate. Thus, NODDI parameters used in this neuroimaging study have offered a deeper interpretation of the changes in FA relating to neurite microstructure primarily in the white matter seen so widely across a wealth of DTI studies and have been complimented by the use of qMTi which has added novel information concerning the macromolecular milieu, including myelin. NODDI adapted for the grey matter has also been undertaken for the first time in ALS and the findings strongly suggest that white and grey matter diffusion properties show disparate changes in ALS. Furthermore, changes detected by each of these imaging modalities have been explored with respect to peripherally circulating $CD4^+$ cells and T regulatory cells which are recently considered to be important mediators of disease outcomes in ALS. Novel relationships with FA, NODDI and qMTi have been revealed which may also relate partially to disease-

associated change on diffusion imaging, particularly within the corpus callosum, thus broadening the possible factors contributing to a unidirectional change in FA. Resting state functional MRI acquired using a newer multi-echo technique and other parameters new to the ALS neuroimaging field, such as the g-ratio, await exploration in these patients, as do as yet unexplored longitudinal changes and associations with a greater range of blood and CSF biological compounds.

References

1. Broad, R.J., *et al.* Neurite orientation and dispersion density imaging (NODDI) detects cortical and corticospinal tract degeneration in ALS. *J Neurol Neurosurg Psychiatry* (2018).
2. Jones, D.K., Knosche, T.R. & Turner, R. White matter integrity, fiber count, and other fallacies: the do's and don'ts of diffusion MRI. *Neuroimage* **73**, 239-254 (2013).
3. Goveas, J., *et al.* Diffusion-MRI in neurodegenerative disorders. *Magn Reson Imaging* **33**, 853-876 (2015).
4. Blain, C.R., *et al.* A longitudinal study of diffusion tensor MRI in ALS. *Amyotroph Lateral Scler* **8**, 348-355 (2007).
5. Douaud, G., Filippini, N., Knight, S., Talbot, K. & Turner, M.R. Integration of structural and functional magnetic resonance imaging in amyotrophic lateral sclerosis. *Brain* **134**, 3470-3479 (2011).
6. Huynh, W., *et al.* Assessment of the upper motor neuron in amyotrophic lateral sclerosis. *Clin Neurophysiol* **127**, 2643-2660 (2016).
7. Menke, R.A.L., Agosta, F., Grosskreutz, J., Filippi, M. & Turner, M.R. Neuroimaging Endpoints in Amyotrophic Lateral Sclerosis. *Neurotherapeutics*, 1-13 (2016).
8. Simon, N.G., *et al.* Quantifying disease progression in amyotrophic lateral sclerosis. *Ann Neurol* **76**, 643-657 (2014).
9. Turner, M.R. & Verstraete, E. What does imaging reveal about the pathology of amyotrophic lateral sclerosis? *Curr Neurol Neurosci Rep* **15**, 45 (2015).
10. Verstraete, E. & Foerster, B.R. Neuroimaging as a New Diagnostic Modality in Amyotrophic Lateral Sclerosis. *Neurotherapeutics* **12**, 403-416 (2015).
11. Grolez, G., *et al.* The value of magnetic resonance imaging as a biomarker for amyotrophic lateral sclerosis: a systematic review. *BMC Neurol* **16**, 155 (2016).
12. Muller, H.P., *et al.* A large-scale multicentre cerebral diffusion tensor imaging study in amyotrophic lateral sclerosis. *J Neurol Neurosurg Psychiatry* **87**, 570-579 (2016).
13. Sage, C.A., Peeters, R.R., Gorner, A., Robberecht, W. & Sunaert, S. Quantitative diffusion tensor imaging in amyotrophic lateral sclerosis. *Neuroimage* **34**, 486-499 (2007).
14. Iwata, N.K., *et al.* White matter alterations differ in primary lateral sclerosis and amyotrophic lateral sclerosis. *Brain* **134**, 2642-2655 (2011).
15. Iwata, N.K., *et al.* Evaluation of corticospinal tracts in ALS with diffusion tensor MRI and brainstem stimulation. *Neurology* **70**, 528-532 (2008).
16. Stagg, C.J., *et al.* Whole-brain magnetic resonance spectroscopic imaging measures are related to disability in ALS. *Neurology* **80**, 610-615 (2013).
17. Sarica, A., *et al.* The corticospinal tract profile in amyotrophic lateral sclerosis. *Hum Brain Mapp* **38**, 727-739 (2017).
18. Trojsi, F., *et al.* Microstructural correlates of Edinburgh Cognitive and Behavioural ALS Screen (ECAS) changes in amyotrophic lateral sclerosis. *Psychiatry Res Neuroimaging* **288**, 67-75 (2019).
19. Kollewe, K., Korner, S., Dengler, R., Petri, S. & Mohammadi, B. Magnetic resonance imaging in amyotrophic lateral sclerosis. *Neurol Res Int* **2012**, 608501 (2012).
20. Agosta, F., *et al.* Voxel-based morphometry study of brain volumetry and diffusivity in amyotrophic lateral sclerosis patients with mild disability. *Hum Brain Mapp* **28**, 1430-1438 (2007).

21. Ellis, C.M.*, et al.* Diffusion tensor MRI assesses corticospinal tract damage in ALS. *Neurology* **53**, 1051-1058 (1999).
22. Filippini, N.*, et al.* Corpus callosum involvement is a consistent feature of amyotrophic lateral sclerosis. *Neurology* **75**, 1645-1652 (2010).
23. Keil, C.*, et al.* Longitudinal diffusion tensor imaging in amyotrophic lateral sclerosis. *BMC Neurosci* **13**, 141 (2012).
24. Prell, T.*, et al.* Diffusion tensor imaging patterns differ in bulbar and limb onset amyotrophic lateral sclerosis. *Clin Neurol Neurosurg* **115**, 1281-1287 (2013).
25. Sach, M.*, et al.* Diffusion tensor MRI of early upper motor neuron involvement in amyotrophic lateral sclerosis. *Brain* **127**, 340-350 (2004).
26. Thivard, L.*, et al.* Diffusion tensor imaging and voxel based morphometry study in amyotrophic lateral sclerosis: relationships with motor disability. *J Neurol Neurosurg Psychiatry* **78**, 889-892 (2007).
27. Wong, J.C.*, et al.* Spatial profiling of the corticospinal tract in amyotrophic lateral sclerosis using diffusion tensor imaging. *J Neuroimaging* **17**, 234-240 (2007).
28. Alruwaili, A.R.*, et al.* A combined tract-based spatial statistics and voxel-based morphometry study of the first MRI scan after diagnosis of amyotrophic lateral sclerosis with subgroup analysis. *J Neuroradiol* **45**, 41-48 (2018).
29. Cardenas-Blanco, A.*, et al.* Central white matter degeneration in bulbar- and limb-onset amyotrophic lateral sclerosis. *J Neurol* **261**, 1961-1967 (2014).
30. Menke, R.A.*, et al.* Fractional anisotropy in the posterior limb of the internal capsule and prognosis in amyotrophic lateral sclerosis. *Arch Neurol* **69**, 1493-1499 (2012).
31. Sage, C.A.*, et al.* Quantitative diffusion tensor imaging in amyotrophic lateral sclerosis: revisited. *Hum Brain Mapp* **30**, 3657-3675 (2009).
32. Cardenas-Blanco, A.*, et al.* Structural and diffusion imaging versus clinical assessment to monitor amyotrophic lateral sclerosis. *Neuroimage Clin* **11**, 408-414 (2016).
33. Smith, S.M.*, et al.* Tract-based spatial statistics: voxelwise analysis of multi-subject diffusion data. *Neuroimage* **31**, 1487-1505 (2006).
34. Aboitiz, F., Scheibel, A.B., Fisher, R.S. & Zaidel, E. Fiber composition of the human corpus callosum. *Brain Res* **598**, 143-153 (1992).
35. Kopitzki, K.*, et al.* Interhemispheric connectivity in amyotrophic lateral sclerosis: A near-infrared spectroscopy and diffusion tensor imaging study. *Neuroimage Clin* **12**, 666-672 (2016).
36. Lillo, P.*, et al.* Grey and white matter changes across the amyotrophic lateral sclerosis-frontotemporal dementia continuum. *PLoS One* **7**, e43993 (2012).
37. Ciccarelli, O.*, et al.* Investigation of white matter pathology in ALS and PLS using tract-based spatial statistics. *Hum Brain Mapp* **30**, 615-624 (2009).
38. Menke, R.A.*, et al.* Widespread grey matter pathology dominates the longitudinal cerebral MRI and clinical landscape of amyotrophic lateral sclerosis. *Brain* **137**, 2546-2555 (2014).
39. Smith, M.C. Nerve Fibre Degeneration in the Brain in Amyotrophic Lateral Sclerosis. *J Neurol Neurosurg Psychiatry* **23**, 269-282 (1960).
40. Brettschneider, J.*, et al.* Stages of pTDP-43 pathology in amyotrophic lateral sclerosis. *Ann Neurol* **74**, 20-38 (2013).
41. Basaia, S., Filippi, M., Spinelli, E.G. & Agosta, F. White Matter Microstructure Breakdown in the Motor Neuron Disease Spectrum: Recent Advances Using Diffusion Magnetic Resonance Imaging. *Front Neurol* **10**, 193 (2019).
42. Brownell, B., Oppenheimer, D.R. & Hughes, J.T. The central nervous system in motor neurone disease. *J Neurol Neurosurg Psychiatry* **33**, 338-357 (1970).
43. Davison, C. Amyotrophic lateral sclerosis. Origin and extent of the upper motor neuron lesion. *Arch Neurol & Psychiat* **46**, 1039-1056 (1941).

44. Chou, S.M. Pathology of Motor System Disorder. in *Motor Neuron Disease: Biology and Management* (eds. Leigh, P.N. & Swash, M.) 53-92 (Springer-Verlag, London, 1995).
45. Martin, J.E. & Swash, M. The Pathology of Motor Neuron Disease. in *Motor Neuron Disease: Biology and Management* (eds. Leigh, P.N. & Swash, M.) 93-118 (Springer-Verlag, London, 1995).
46. Bede, P. The histological correlates of imaging metrics: postmortem validation of in vivo findings. *Amyotroph Lateral Scler Frontotemporal Degener*, 1-4 (2019).
47. Budde, M.D. & Annese, J. Quantification of anisotropy and fiber orientation in human brain histological sections. *Front Integr Neurosci* **7**, 3 (2013).
48. Lampinen, B.*, et al.* Searching for the neurite density with diffusion MRI: Challenges for biophysical modeling. *Hum Brain Mapp* **40**, 2529-2545 (2019).
49. Pallebage-Gamarallage, M.*, et al.* Dissecting the pathobiology of altered MRI signal in amyotrophic lateral sclerosis: A post mortem whole brain sampling strategy for the integration of ultra-high-field MRI and quantitative neuropathology. *BMC Neurosci* **19**, 11 (2018).
50. Kassubek, J.*, et al.* Diffusion tensor imaging analysis of sequential spreading of disease in amyotrophic lateral sclerosis confirms patterns of TDP-43 pathology. *Brain* **137**, 1733-1740 (2014).
51. Lule, D.*, et al.* Cognitive phenotypes of sequential staging in amyotrophic lateral sclerosis. *Cortex* **101**, 163-171 (2018).
52. Cardenas, A.M.*, et al.* Pathology of callosal damage in ALS: An ex-vivo, 7 T diffusion tensor MRI study. *Neuroimage Clin* **15**, 200-208 (2017).
53. Turner, M.R.*, et al.* Neuroimaging in amyotrophic lateral sclerosis. *Biomark Med* **6**, 319-337 (2012).
54. Li, J.*, et al.* A meta-analysis of diffusion tensor imaging studies in amyotrophic lateral sclerosis. *Neurobiol Aging* **33**, 1833-1838 (2012).
55. Zhang, Y.*, et al.* Progression of white matter degeneration in amyotrophic lateral sclerosis: A diffusion tensor imaging study. *Amyotroph Lateral Scler* **12**, 421-429 (2011).
56. Gredal, O., Pakkenberg, H., Karlsborg, M. & Pakkenberg, B. Unchanged total number of neurons in motor cortex and neocortex in amyotrophic lateral sclerosis: a stereological study. *J Neurosci Methods* **95**, 171-176 (2000).
57. Toft, M.H., Gredal, O. & Pakkenberg, B. The size distribution of neurons in the motor cortex in amyotrophic lateral sclerosis. *J Anat* **207**, 399-407 (2005).
58. Mizutani, T.*, et al.* Development of ophthalmoplegia in amyotrophic lateral sclerosis during long-term use of respirators. *J Neurol Sci* **99**, 311-319 (1990).
59. Conforti, L., Adalbert, R. & Coleman, M.P. Neuronal death: where does the end begin? *Trends Neurosci* **30**, 159-166 (2007).
60. Fischer, L.R.*, et al.* Amyotrophic lateral sclerosis is a distal axonopathy: evidence in mice and man. *Exp Neurol* **185**, 232-240 (2004).
61. Pun, S., Santos, A.F., Saxena, S., Xu, L. & Caroni, P. Selective vulnerability and pruning of phasic motoneuron axons in motoneuron disease alleviated by CNTF. *Nat Neurosci* **9**, 408-419 (2006).
62. Saxena, S. & Caroni, P. Mechanisms of axon degeneration: from development to disease. *Prog Neurobiol* **83**, 174-191 (2007).
63. van der Graaff, M.M.*, et al.* Upper and extra-motoneuron involvement in early motoneuron disease: a diffusion tensor imaging study. *Brain* **134**, 1211-1228 (2011).
64. Nickerson, J.P.*, et al.* Linear longitudinal decline in fractional anisotropy in patients with amyotrophic lateral sclerosis: preliminary results. *Klin Neuroradiol* **19**, 129-134 (2009).

65. Jespersen, S.N.*, et al.* Neurite density from magnetic resonance diffusion measurements at ultrahigh field: comparison with light microscopy and electron microscopy. *Neuroimage* **49**, 205-216 (2010).
66. Zhang, H., Schneider, T., Wheeler-Kingshott, C.A. & Alexander, D.C. NODDI: practical in vivo neurite orientation dispersion and density imaging of the human brain. *Neuroimage* **61**, 1000-1016 (2012).
67. Gatto, R.G.*, et al.* Neurite orientation dispersion and density imaging can detect presymptomatic axonal degeneration in the spinal cord of ALS mice. *Funct Neurol* **33**, 155-163 (2018).
68. Gatto, R.G., Li, W., Gao, J. & Magin, R.L. In vivo diffusion MRI detects early spinal cord axonal pathology in a mouse model of amyotrophic lateral sclerosis. *NMR Biomed* **31**, e3954 (2018).
69. Gatto, R.G., Li, W. & Magin, R.L. Diffusion tensor imaging identifies presymptomatic axonal degeneration in the spinal cord of ALS mice. *Brain Res* **1679**, 45-52 (2018).
70. Kim, J.H., Wu, T.H., Budde, M.D., Lee, J.M. & Song, S.K. Noninvasive detection of brainstem and spinal cord axonal degeneration in an amyotrophic lateral sclerosis mouse model. *NMR Biomed* **24**, 163-169 (2011).
71. Underwood, C.K., Kurniawan, N.D., Butler, T.J., Cowin, G.J. & Wallace, R.H. Non-invasive diffusion tensor imaging detects white matter degeneration in the spinal cord of a mouse model of amyotrophic lateral sclerosis. *Neuroimage* **55**, 455-461 (2011).
72. Arvanian, V.L.*, et al.* Chronic spinal hemisection in rats induces a progressive decline in transmission in uninjured fibers to motoneurons. *Exp Neurol* **216**, 471-480 (2009).
73. Piao, Y.S.*, et al.* Neuropathology with clinical correlations of sporadic amyotrophic lateral sclerosis: 102 autopsy cases examined between 1962 and 2000. *Brain Pathol* **13**, 10-22 (2003).
74. Sharma, K.R., Sheriff, S., Maudsley, A. & Govind, V. Diffusion tensor imaging of basal ganglia and thalamus in amyotrophic lateral sclerosis. *J Neuroimaging* **23**, 368-374 (2013).
75. Bao, Y.*, et al.* Radial diffusivity as an imaging biomarker for early diagnosis of non-demented amyotrophic lateral sclerosis. *Eur Radiol* **28**, 4940-4948 (2018).
76. de Albuquerque, M.*, et al.* Longitudinal evaluation of cerebral and spinal cord damage in Amyotrophic Lateral Sclerosis. *Neuroimage Clin* **14**, 269-276 (2017).
77. Wang, S.*, et al.* Amyotrophic lateral sclerosis: diffusion-tensor and chemical shift MR imaging at 3.0 T. *Radiology* **239**, 831-838 (2006).
78. Toosy, A.T.*, et al.* Diffusion tensor imaging detects corticospinal tract involvement at multiple levels in amyotrophic lateral sclerosis. *J Neurol Neurosurg Psychiatry* **74**, 1250-1257 (2003).
79. Turner, M.R.*, et al.* Evidence of widespread cerebral microglial activation in amyotrophic lateral sclerosis: an [11C](R)-PK11195 positron emission tomography study. *Neurobiol Dis* **15**, 601-609 (2004).
80. Rajagopalan, V., Yue, G.H. & Pioro, E.P. Brain white matter diffusion tensor metrics from clinical 1.5T MRI distinguish between ALS phenotypes. *J Neurol* **260**, 2532-2540 (2013).
81. Gordon, P.H., Cheng, B., Katz, I.B., Mitsumoto, H. & Rowland, L.P. Clinical features that distinguish PLS, upper motor neuron-dominant ALS, and typical ALS. *Neurology* **72**, 1948-1952 (2009).
82. Gordon, P.H.*, et al.* The natural history of primary lateral sclerosis. *Neurology* **66**, 647-653 (2006).

83. Orban, G.A., Ferri, S. & Platonov, A. The role of putative human anterior intraparietal sulcus area in observed manipulative action discrimination. *Brain Behav* **9**, e01226 (2019).
84. Grefkes, C. & Fink, G.R. The functional organization of the intraparietal sulcus in humans and monkeys. *J Anat* **207**, 3-17 (2005).
85. Abrahams, S.*, et al.* Word retrieval in amyotrophic lateral sclerosis: a functional magnetic resonance imaging study. *Brain* **127**, 1507-1517 (2004).
86. Rapcsak, S.Z. Face Recognition. *Curr Neurol Neurosci Rep* **19**, 41 (2019).
87. Bora, E. Meta-analysis of social cognition in amyotrophic lateral sclerosis. *Cortex* **88**, 1-7 (2017).
88. Goldstein, L.H. & Abrahams, S. Changes in cognition and behaviour in amyotrophic lateral sclerosis: nature of impairment and implications for assessment. *Lancet Neurol* **12**, 368-380 (2013).
89. DiSabato, D.J., Quan, N. & Godbout, J.P. Neuroinflammation: the devil is in the details. *J Neurochem* **139 Suppl 2**, 136-153 (2016).
90. Heneka, M.T., Kummer, M.P. & Latz, E. Innate immune activation in neurodegenerative disease. *Nat Rev Immunol* **14**, 463-477 (2014).
91. Sochocka, M., Diniz, B.S. & Leszek, J. Inflammatory Response in the CNS: Friend or Foe? *Mol Neurobiol* **54**, 8071-8089 (2017).
92. Dantzer, R., O'Connor, J.C., Freund, G.G., Johnson, R.W. & Kelley, K.W. From inflammation to sickness and depression: when the immune system subjugates the brain. *Nat Rev Neurosci* **9**, 46-56 (2008).
93. Yirmiya, R. & Goshen, I. Immune modulation of learning, memory, neural plasticity and neurogenesis. *Brain Behav Immun* **25**, 181-213 (2011).
94. Bright, F.*, et al.* Neuroinflammation in frontotemporal dementia. *Nat Rev Neurol* (2019).
95. London, A., Cohen, M. & Schwartz, M. Microglia and monocyte-derived macrophages: functionally distinct populations that act in concert in CNS plasticity and repair. *Front Cell Neurosci* **7**, 34 (2013).
96. Haukedal, H. & Freude, K. Implications of Microglia in Amyotrophic Lateral Sclerosis and Frontotemporal Dementia. *J Mol Biol* **431**, 1818-1829 (2019).
97. Umoh, M.E.*, et al.* A proteomic network approach across the ALS-FTD disease spectrum resolves clinical phenotypes and genetic vulnerability in human brain. *EMBO Mol Med* **10**, 48-62 (2018).
98. Engelhardt, J.I., Tajti, J. & Appel, S.H. Lymphocytic infiltrates in the spinal cord in amyotrophic lateral sclerosis. *Arch Neurol* **50**, 30-36 (1993).
99. Kawamata, T., Akiyama, H., Yamada, T. & McGeer, P.L. Immunologic reactions in amyotrophic lateral sclerosis brain and spinal cord tissue. *Am J Pathol* **140**, 691-707 (1992).
100. Sta, M.*, et al.* Innate and adaptive immunity in amyotrophic lateral sclerosis: evidence of complement activation. *Neurobiol Dis* **42**, 211-220 (2011).
101. Brettschneider, J.*, et al.* Microglial activation and TDP-43 pathology correlate with executive dysfunction in amyotrophic lateral sclerosis. *Acta Neuropathol* **123**, 395-407 (2012).
102. Henkel, J.S.*, et al.* Presence of dendritic cells, MCP-1, and activated microglia/macrophages in amyotrophic lateral sclerosis spinal cord tissue. *Ann Neurol* **55**, 221-235 (2004).
103. Cagnin, A., Rossor, M., Sampson, E.L., Mackinnon, T. & Banati, R.B. In vivo detection of microglial activation in frontotemporal dementia. *Ann Neurol* **56**, 894-897 (2004).

104. Stephens, B.*, et al.* Widespread loss of neuronal populations in the spinal ventral horn in sporadic motor neuron disease. A morphometric study. *J Neurol Sci* **244**, 41-58 (2006).
105. Schiffer, D., Attanasio, A., Chio, A., Migheli, A. & Pezzulo, T. Ubiquitinated dystrophic neurites suggest corticospinal derangement in patients with amyotrophic lateral sclerosis. *Neurosci Lett* **180**, 21-24 (1994).
106. Schiffer, D., Cordera, S., Cavalla, P. & Migheli, A. Reactive astrogliosis of the spinal cord in amyotrophic lateral sclerosis. *J Neurol Sci* **139 Suppl**, 27-33 (1996).
107. Nihei, K., McKee, A.C. & Kowall, N.W. Patterns of neuronal degeneration in the motor cortex of amyotrophic lateral sclerosis patients. *Acta Neuropathol* **86**, 55-64 (1993).
108. Philips, T. & Robberecht, W. Neuroinflammation in amyotrophic lateral sclerosis: role of glial activation in motor neuron disease. *Lancet Neurol* **10**, 253-263 (2011).
109. Beers, D.R.*, et al.* Endogenous regulatory T lymphocytes ameliorate amyotrophic lateral sclerosis in mice and correlate with disease progression in patients with amyotrophic lateral sclerosis. *Brain* **134**, 1293-1314 (2011).
110. Menon, P.*, et al.* Regulatory T cells in amyotrophic lateral sclerosis: A role for disease modulation. *J Clin Neurosci* **21**, 2050 (2014).
111. Henkel, J.S.*, et al.* Regulatory T-lymphocytes mediate amyotrophic lateral sclerosis progression and survival. *EMBO Mol Med* **5**, 64-79 (2013).
112. Caspers, S. & Zilles, K. Microarchitecture and connectivity of the parietal lobe. *Handb Clin Neurol* **151**, 53-72 (2018).
113. Corbetta, M.*, et al.* A common network of functional areas for attention and eye movements. *Neuron* **21**, 761-773 (1998).
114. Yeo, B.T.*, et al.* The organization of the human cerebral cortex estimated by intrinsic functional connectivity. *J Neurophysiol* **106**, 1125-1165 (2011).
115. Bouyagoub, S., Clarke, C.L., Wood, T.C., Zhang, H. & Cercignani, M. Evaluating NODDI's a priori □?xed parameters by combining NODDI and mcDESPOT. in *International Society for Magnetic Resonance in Medicine (ISMRM)* (Honolulu, HI, USA, 2017).
116. Fukutomi, H.*, et al.* Neurite imaging reveals microstructural variations in human cerebral cortical gray matter. *Neuroimage* (2018).
117. Guerreiro, J.M.*, et al.* Optimizing the fitting initial condition for the parallel intrinsic diffusivity in NODDI: An extensive empirical evaluation. *BioRxiv* (2019).
118. Alexander, D.C.*, et al.* Orientationally invariant indices of axon diameter and density from diffusion MRI. *Neuroimage* **52**, 1374-1389 (2010).
119. Jespersen, S.N., Leigland, L.A., Cornea, A. & Kroenke, C.D. Determination of axonal and dendritic orientation distributions within the developing cerebral cortex by diffusion tensor imaging. *IEEE Trans Med Imaging* **31**, 16-32 (2012).
120. Grussu, F.*, et al.* Neurite dispersion: a new marker of multiple sclerosis spinal cord pathology? *Ann Clin Transl Neurol* **4**, 663-679 (2017).
121. Schmitz, J.*, et al.* Hemispheric asymmetries in cortical gray matter microstructure identified by neurite orientation dispersion and density imaging. *Neuroimage* **189**, 667-675 (2019).
122. Parker, T.D.*, et al.* Cortical microstructure in young onset Alzheimer's disease using neurite orientation dispersion and density imaging. *Hum Brain Mapp* **39**, 3005-3017 (2018).
123. Agosta, F.*, et al.* The cortical signature of amyotrophic lateral sclerosis. *PLoS One* **7**, e42816 (2012).
124. Schuster, C.*, et al.* Focal thinning of the motor cortex mirrors clinical features of amyotrophic lateral sclerosis and their phenotypes: a neuroimaging study. *J Neurol* **260**, 2856-2864 (2013).

125. Schuster, C.*, et al.* Longitudinal course of cortical thickness decline in amyotrophic lateral sclerosis. *J Neurol* **261**, 1871-1880 (2014).
126. Verstraete, E.*, et al.* Structural MRI reveals cortical thinning in amyotrophic lateral sclerosis. *J Neurol Neurosurg Psychiatry* **83**, 383-388 (2012).
127. Walhout, R.*, et al.* Cortical thickness in ALS: towards a marker for upper motor neuron involvement. *J Neurol Neurosurg Psychiatry* **86**, 288-294 (2015).
128. Bede, P.*, et al.* Grey matter correlates of clinical variables in amyotrophic lateral sclerosis (ALS): a neuroimaging study of ALS motor phenotype heterogeneity and cortical focality. *J Neurol Neurosurg Psychiatry* **84**, 766-773 (2013).
129. Ball, G.*, et al.* Development of cortical microstructure in the preterm human brain. *Proc Natl Acad Sci U S A* **110**, 9541-9546 (2013).
130. Nazeri, A.*, et al.* Functional consequences of neurite orientation dispersion and density in humans across the adult lifespan. *J Neurosci* **35**, 1753-1762 (2015).
131. Parvathaneni, P.*, et al.* Gray Matter Surface based Spatial Statistics (GS-BSS) in Diffusion Microstructure. *Med Image Comput Comput Assist Interv* **10433**, 638-646 (2017).
132. Hammer, R.P., Jr., Tomiyasu, U. & Scheibel, A.B. Degeneration of the human Betz cell due to amyotrophic lateral sclerosis. *Exp Neurol* **63**, 336-346 (1979).
133. Carrara, G.*, et al.* A distinct MR imaging phenotype in amyotrophic lateral sclerosis: correlation between T1 magnetization transfer contrast hyperintensity along the corticospinal tract and diffusion tensor imaging analysis. *AJNR Am J Neuroradiol* **33**, 733-739 (2012).
134. da Rocha, A.J.*, et al.* Detection of corticospinal tract compromise in amyotrophic lateral sclerosis with brain MR imaging: relevance of the T1-weighted spin-echo magnetization transfer contrast sequence. *AJNR Am J Neuroradiol* **25**, 1509-1515 (2004).
135. Tanabe, J.L.*, et al.* Reduced MTR in the corticospinal tract and normal T2 in amyotrophic lateral sclerosis. *Magn Reson Imaging* **16**, 1163-1169 (1998).
136. Cosottini, M.*, et al.* Mapping cortical degeneration in ALS with magnetization transfer ratio and voxel-based morphometry. *PLoS One* **8**, e68279 (2013).
137. Cosottini, M.*, et al.* Magnetization transfer imaging demonstrates a distributed pattern of microstructural changes of the cerebral cortex in amyotrophic lateral sclerosis. *AJNR Am J Neuroradiol* **32**, 704-708 (2011).
138. Cercignani, M., Dowell, N.G. & Tofts, P. Quantitative MRI of the brain : principles of physical measurement. in *Series in medical physics and biomedical engineering* pages cm. (2018).
139. Verstraete, E.*, et al.* Multimodal tract-based analysis in ALS patients at 7T: a specific white matter profile? *Amyotroph Lateral Scler Frontotemporal Degener* **15**, 84-92 (2014).
140. Levesque, I.R.*, et al.* Quantitative magnetization transfer and myelin water imaging of the evolution of acute multiple sclerosis lesions. *Magn Reson Med* **63**, 633-640 (2010).
141. Strich, S.J. Notes on the Marchi method for staining degenerating myelin in the peripheral and central nervous system. *J Neurol Neurosurg Psychiatry* **31**, 110-114 (1968).
142. Borsodi, F.*, et al.* Multimodal assessment of white matter tracts in amyotrophic lateral sclerosis. *PLoS One* **12**, e0178371 (2017).
143. Habert, M.O.*, et al.* Brain perfusion imaging in amyotrophic lateral sclerosis: extent of cortical changes according to the severity and topography of motor impairment. *Amyotroph Lateral Scler* **8**, 9-15 (2007).
144. Agosta, F.*, et al.* Structural brain correlates of cognitive and behavioral impairment in MND. *Hum Brain Mapp* **37**, 1614-1626 (2016).

145. Devinsky, O., Morrell, M.J. & Vogt, B.A. Contributions of anterior cingulate cortex to behaviour. *Brain* **118 (Pt 1)**, 279-306 (1995).
146. Lemon, R.N. Descending pathways in motor control. *Annu Rev Neurosci* **31**, 195-218 (2008).
147. Foerster, B.R.*, et al.* Diagnostic accuracy using diffusion tensor imaging in the diagnosis of ALS: a meta-analysis. *Acad Radiol* **19**, 1075-1086 (2012).
148. Billiet, T.*, et al.* Age-related microstructural differences quantified using myelin water imaging and advanced diffusion MRI. *Neurobiol Aging* **36**, 2107-2121 (2015).
149. Wen, J.*, et al.* Neurite density is reduced in the presymptomatic phase of C9orf72 disease. *J Neurol Neurosurg Psychiatry* (2018).
150. Dowell, N.G.*, et al.* Acute Changes in Striatal Microstructure Predict the Development of Interferon-Alpha Induced Fatigue. *Biol Psychiatry* **79**, 320-328 (2016).
151. Harrison, N.A.*, et al.* Quantitative Magnetization Transfer Imaging as a Biomarker for Effects of Systemic Inflammation on the Brain. *Biol Psychiatry* **78**, 49-57 (2015).
152. Smith, S.M. & Nichols, T.E. Threshold-free cluster enhancement: addressing problems of smoothing, threshold dependence and localisation in cluster inference. *Neuroimage* **44**, 83-98 (2009).
153. Lorca-Puls, D.L.*, et al.* The impact of sample size on the reproducibility of voxel-based lesion-deficit mappings. *Neuropsychologia* **115**, 101-111 (2018).
154. Agosta, F.*, et al.* Sensorimotor functional connectivity changes in amyotrophic lateral sclerosis. *Cereb Cortex* **21**, 2291-2298 (2011).
155. Schmidt, R.*, et al.* Correlation between structural and functional connectivity impairment in amyotrophic lateral sclerosis. *Hum Brain Mapp* **35**, 4386-4395 (2014).
156. Chomiak, T. & Hu, B. What is the optimal value of the g-ratio for myelinated fibers in the rat CNS? A theoretical approach. *PLoS One* **4**, e7754 (2009).
157. Mohammadi, S.*, et al.* Whole-Brain In-vivo Measurements of the Axonal G-Ratio in a Group of 37 Healthy Volunteers. *Front Neurosci* **9**, 441 (2015).
158. Rushton, W.A. A theory of the effects of fibre size in medullated nerve. *J Physiol* **115**, 101-122 (1951).
159. Graf von Keyserlingk, D. & Schramm, U. Diameter of axons and thickness of myelin sheaths of the pyramidal tract fibres in the adult human medullary pyramid. *Anat Anz* **157**, 97-111 (1984).
160. Cercignani, M.*, et al.* Characterizing axonal myelination within the healthy population: a tract-by-tract mapping of effects of age and gender on the fiber g-ratio. *Neurobiol Aging* **49**, 109-118 (2017).
161. Hagiwara, A.*, et al.* Analysis of White Matter Damage in Patients with Multiple Sclerosis via a Novel In Vivo MR Method for Measuring Myelin, Axons, and G-Ratio. *AJNR Am J Neuroradiol* **38**, 1934-1940 (2017).
162. Stikov, N.*, et al.* In vivo histology of the myelin g-ratio with magnetic resonance imaging. *Neuroimage* **118**, 397-405 (2015).
163. Foerster, B.R.*, et al.* Diagnostic accuracy of diffusion tensor imaging in amyotrophic lateral sclerosis: a systematic review and individual patient data meta-analysis. *Acad Radiol* **20**, 1099-1106 (2013).
164. Abhinav, K.*, et al.* Use of diffusion spectrum imaging in preliminary longitudinal evaluation of amyotrophic lateral sclerosis: development of an imaging biomarker. *Front Hum Neurosci* **8**, 270 (2014).
165. Agosta, F.*, et al.* A longitudinal diffusion tensor MRI study of the cervical cord and brain in amyotrophic lateral sclerosis patients. *J Neurol Neurosurg Psychiatry* **80**, 53-55 (2009).

166. Menke, R.A.L., Proudfoot, M., Talbot, K. & Turner, M.R. The two-year progression of structural and functional cerebral MRI in amyotrophic lateral sclerosis. *Neuroimage Clin* **17**, 953-961 (2018).
167. Weydt, P.*, et al.* Neurofilament levels as biomarkers in asymptomatic and symptomatic familial amyotrophic lateral sclerosis. *Ann Neurol* **79**, 152-158 (2016).
168. Lu, C.H.*, et al.* Neurofilament light chain: A prognostic biomarker in amyotrophic lateral sclerosis. *Neurology* **84**, 2247-2257 (2015).
169. Menke, R.A.*, et al.* CSF neurofilament light chain reflects corticospinal tract degeneration in ALS. *Ann Clin Transl Neurol* **2**, 748-755 (2015).
170. Xu, Z., Henderson, R.D., David, M. & McCombe, P.A. Neurofilaments as Biomarkers for Amyotrophic Lateral Sclerosis: A Systematic Review and Meta-Analysis. *PLoS One* **11**, e0164625 (2016).
171. Cohen-Adad, J.*, et al.* Involvement of spinal sensory pathway in ALS and specificity of cord atrophy to lower motor neuron degeneration. *Amyotroph Lateral Scler Frontotemporal Degener* **14**, 30-38 (2013).
172. Valsasina, P.*, et al.* Diffusion anisotropy of the cervical cord is strictly associated with disability in amyotrophic lateral sclerosis. *J Neurol Neurosurg Psychiatry* **78**, 480-484 (2007).
173. Nair, G.*, et al.* Diffusion tensor imaging reveals regional differences in the cervical spinal cord in amyotrophic lateral sclerosis. *Neuroimage* **53**, 576-583 (2010).
174. El Mendili, M.M.*, et al.* Multi-parametric spinal cord MRI as potential progression marker in amyotrophic lateral sclerosis. *PLoS One* **9**, e95516 (2014).
175. Querin, G.*, et al.* Multimodal spinal cord MRI offers accurate diagnostic classification in ALS. *J Neurol Neurosurg Psychiatry* (2018).
176. Querin, G.*, et al.* Spinal cord multi-parametric magnetic resonance imaging for survival prediction in amyotrophic lateral sclerosis. *Eur J Neurol* **24**, 1040-1046 (2017).

Appendix

Candidate's Published Work in Relation to the Thesis

Review:

Barritt AW, Gabel M, Cercignani M and Leigh PN.

Novel Magnetic Resonance Imaging Techniques and Analysis Methods in Amyotrophic Lateral Sclerosis.

Front Neurol. 9:1065 DOI: 10.3389/fneur.2018.01065.

frontiers in Neurology

MINI REVIEW
published: 04 December 2018
doi: 10.3389/fneur.2018.01065

Emerging Magnetic Resonance Imaging Techniques and Analysis Methods in Amyotrophic Lateral Sclerosis

Andrew W. Barritt[1,2*], *Matt C. Gabel*[3], *Mara Cercignani*[1] *and P. Nigel Leigh*[2,3]

[1] Clinical Imaging Sciences Centre, Brighton and Sussex Medical School, Falmer, United Kingdom, [2] Hurstwood Park Neurological Centre, Haywards Heath, West Sussex, United Kingdom, [3] Department of Neuroscience, Trafford Centre for Biomedical Research, Brighton and Sussex Medical School, Falmer, United Kingdom

Objective markers of disease sensitive to the clinical activity, symptomatic progression, and underlying substrates of neurodegeneration are highly coveted in amyotrophic lateral sclerosis in order to more eloquently stratify the highly heterogeneous phenotype and facilitate the discovery of effective disease modifying treatments for patients. Magnetic resonance imaging (MRI) is a promising, non-invasive biomarker candidate whose acquisition techniques and analysis methods are undergoing constant evolution in the pursuit of parameters which more closely represent biologically-applicable tissue changes. Neurite Orientation Dispersion and Density Imaging (NODDI; a form of diffusion imaging), and quantitative Magnetization Transfer Imaging (qMTi) are two such emerging modalities which have each broadened the understanding of other neurological disorders and have the potential to provide new insights into structural alterations initiated by the disease process in ALS. Furthermore, novel neuroimaging data analysis approaches such as Event-Based Modeling (EBM) may be able to circumvent the requirement for longitudinal scanning as a means to comprehend the dynamic stages of neurodegeneration *in vivo*. Combining these and other innovative imaging protocols with more sophisticated techniques to analyse ever-increasing datasets holds the exciting prospect of transforming understanding of the biological processes and temporal evolution of the ALS syndrome, and can only benefit from multicentre collaboration across the entire ALS research community.

Keywords: motor neuron disease, MRI—magnetic resonance imaging, event-based model, quantitative magnetization transfer imaging, neurite orientation dispersion and density imaging (NODDI)

OPEN ACCESS

Edited by:
Peter Bede,
Trinity College Dublin, Ireland

Reviewed by:
Efstratios Karavasilis,
National and Kapodistrian University of Athens Medical School, Greece
Cristina Moglia,
Dipartimento di Neuroscienze Rita Levi Montalcini, Università degli Studi di Torino, Italy

***Correspondence:**
Andrew W. Barritt
a.barritt@bsms.ac.uk

Specialty section:
This article was submitted to Neurodegeneration, a section of the journal Frontiers in Neurology

Received: *29 October 2018*
Accepted: *22 November 2018*
Published: *04 December 2018*

Citation:
Barritt AW, Gabel MC, Cercignani M and Leigh PN (2018) Emerging Magnetic Resonance Imaging Techniques and Analysis Methods in Amyotrophic Lateral Sclerosis. Front. Neurol. 9:1065. doi: 10.3389/fneur.2018.01065

Neuroimaging modalities sensitive to the dynamics and patterns of tissue degeneration in amyotrophic lateral sclerosis (ALS) are required as objective biological markers of disease activity *in vivo*. Standard clinical assessment is usually adequate for diagnosis, however there is a pressing need for non-invasive neuroimaging biomarkers that may differentiate between the various phenotypes within the ALS syndrome, provide more accurate prognostic information, and monitor responses to therapeutic interventions. There is also a need for neuroimaging techniques which have the potential to interrogate the specific mechanisms of neurodegeneration, given that conventional MRI primarily aims to exclude alternative diagnoses (1). As such, it will be important to integrate new modalities of structural and functional imaging (including MRI and PET) with molecular

biomarkers of neuronal damage, and indicators of neuroinflammation if the therapeutic impasse for more effective disease treatments is to be broken. Diffusion MRI, particularly diffusion tensor imaging (DTI), has been extensively researched in patients with ALS to infer structural alterations within the brain and spinal cord by virtue of the movement of water molecules induced by magnetic field gradients. Fractional anisotropy (FA) is consistently reduced, often alongside increased mean or radial diffusivity (MD or RD, respectively), within the corticospinal tracts (CSTs) (2–15) and body of the corpus callosum through which pass the fibers connecting hemispheric motor areas (3, 5–8, 10, 12, 16, 17). Indeed, DTI changes are perhaps most reliably encountered within the posterior limb of the internal capsule (18, 19) which forms a common conduit for several descending motor pathways including the CST, cortico-rubro-spinal, and cortico-reticulo-spinal connections (20). Additional areas within the frontal, temporal (11, 21, 22), and parietal areas (11, 23) have shown reduced FA, all of which is consistent with the multisystem motor and extra-motor regions involved clinically and neuropathologically (24–26). Nevertheless, establishing the precise substrate or substrates underlying these changes observed on MRI is not straightforward and may be complimented by novel magnetic resonance imaging techniques and emerging big data analysis methods.

NEURITE ORIENTATION DISPERSION AND DENSITY IMAGING (NODDI)

Diffusion MRI is sensitive to the motion of water molecules at microscopic level. Nevertheless the signal it measures is averaged across volumes of 1–2 mm^3 (the so-called "voxel"). For this reason, any interpretation of the signal and its origin requires some degree of "modeling." More than one model has been proposed and each typically incorporates slightly differing mathematical assumptions to interpret and model the signal, thus providing only indirect inferences on anatomical configurations. For instance, DTI assumes that water movement will obey Gaussian properties and is widely accepted to lose consistency when neuronal fibers bend or fan out within a voxel, or where otherwise aligned fiber tracts are crossing each other (5) which is common to areas such as the centrum semiovale and even regions of the foliated corpus callosum (27, 28). Moreover, a reduction in FA signifies changes in both neurite density and orientation dispersion without distinguishing their individual contributions (28, 29). Therefore, variations on the diffusion tensor model have been created in an attempt to address these limitations. One such model is neurite orientation dispersion and density imaging (NODDI).

NODDI requires acquisition over a longer time than DTI and compartmentalizes non-Gaussian water diffusion into three geometric spaces encompassing isotropic (or free), hindered anisotropic and restricted anisotropic components. These are known as V_{ISO}, V_{IC}, and V_{EC} and each broadly correspond to free water/CSF, intra-neurite water (of axons and dendrites), and extra-neurite water (but potentially including glial cells and neuronal somata), respectively (29–31). The NODDI parameters ISO, NDI (neurite density index), and ODI (orientation dispersion index; a marker of the geometric complexity of neurites) can then be derived, the latter two of which are considered to provide a more structurally useful breakdown of single FA values (29) (see **Figure 1**). NODDI is able to better delineate white from gray matter, in which normal white matter displays higher NDI and lower ODI with the reverse in gray matter (33), and differentiate between different gray matter structures although might be more susceptible to changes in field strength in these areas (31). Compared to DTI, NODDI indices, particularly ODI, have been shown to correlate with histological measures of orientation dispersion in the spinal cord and might also display more inter-subject variability with implications for the sample sizes required for group analyses (33, 34). However, this may not necessarily be an inaccuracy in modeling rather a more accurate depiction of tissue composition (31). In addition, regions which might be expected to demonstrate considerable axon density and higher NDI values might counterintuitively show higher ISO due to the larger diameter axons enabling more freedom of water movement (31, 34).

NODDI has been used to demonstrate tissue alterations associated with normal aging (35–37) and in a range of conditions including focal cortical dysplasia (38), stroke (39), Wilson's disease (40), multiple sclerosis (33), neurofibromatosis type 1 (38, 41), and neurodegenerative diseases. Reduction in NDI and ODI of the contralateral substantia nigra pars compacta has been shown to correlate negatively with clinical severity of Parkinson's disease (42) whereas in pre-manifest Huntington's disease reductions in NDI and ODI are seen in a range of white matter tracts with reduced NDI in the corpus callosum correlating positively with markers of severity (43). In patients with young onset Alzheimer's disease reduction in NDI and ODI is seen corrected for reduced thickness within several relevant cortical areas, with lower NDI values in patients scoring less well on cognitive tests (44), while in a rodent model NODDI indices correlate more consistently than DTI parameters with the burden of tau pathology harbored by the cortex, corpus callosum, and hippocampus (45).

Use of NODDI imaging in ALS has only recently been undertaken. Whole brain analysis in patients with manifest disease has demonstrated a significant NDI reduction throughout the intracranial CSTs up to the subcortical matter of the precentral gyri and across the corpus callosum, with increased ODI in the anterior limb of right internal capsule and increased ISO adjacent to the right lateral ventricle relative to healthy controls (46). NDI within the right corona radiata and precentral subcortical white matter was decreased to a greater extent in those patients with both limb and bulbar involvement compared to limb alone, and longer disease durations correlated with reduced ODI in the precentral gyri, dorsolateral prefrontal cortices, and precuneus. Furthermore, at the statistical threshold used, FA was reduced as expected within the CSTs but less extensively than NDI, and changes were not observed within the corpus callosum, implying NODDI may be more sensitive than DTI. Indeed, combined NODDI and DTI has also been performed in pre-manifest C9orf72 mutation carriers alongside first degree relatives not possessing the pathological repeat

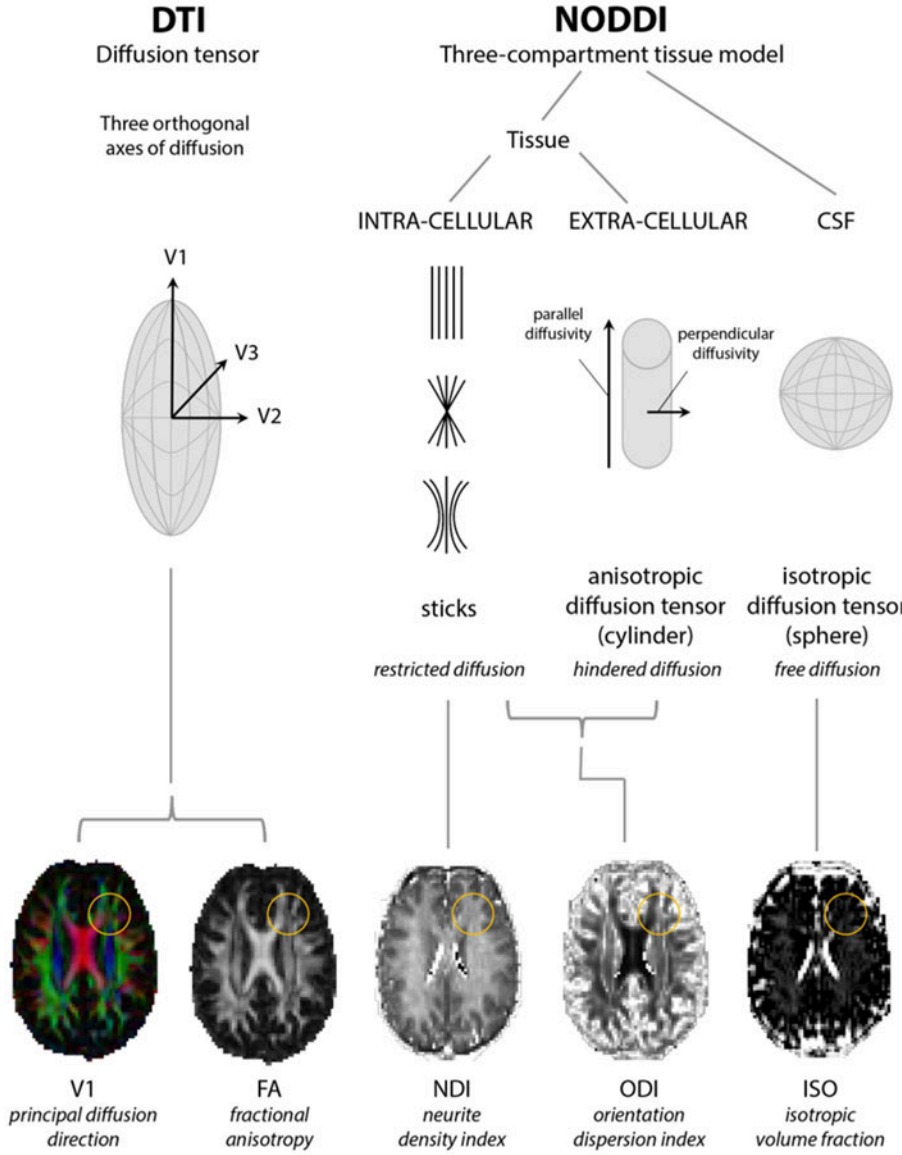

FIGURE 1 | Models of diffusion for neurite orientation dispersion and density imaging (NODDI) and diffusion tensor imaging (DTI). The diffusion tensor model of DTI is based upon three orthogonal axes of diffusion (V1, V2, and V3) yielding radial, axial, and mean diffusivity from which fractional anisotropy (FA) can be estimated. NODDI considers diffusion within three compartments: restricted diffusion in the intracellular compartment, hindered diffusion in the extracellular compartment, and free diffusion in cerebrospinal fluid (CSF), from which parameter maps representing neurite density (NDI), orientation dispersion (ODI), and isotropic fraction (ISO) indices can be estimated. Yellow circles highlight a region where changes in FA can be accompanied by changes in both NDI and ODI. Adapted from Rae et al. (32).

expansion (47). The effect size relating to detectable reductions of NDI within 7 of 11 white matter tracts, including the CSTs, is greater than that for DTI metrics (in this case increased axial diffusivity, RD, and MD rather than decreased FA) albeit statistically significant in just two. Therefore, the results appear to corroborate the implication that lowered FA (or increased diffusivity) in the CSTs and corpus callosum results from the loss of axon fibers rather than increased complexity or dispersion within tracts. Longitudinal NODDI scans have not yet been investigated although results from an ancillary imaging study to the Modifying Immune Response and Outcomes in ALS (MIROCALS) trial of low dose Interleukin-2 treatment are awaited.

In any case, neuroimaging techniques are constantly evolving with a raft of acronyms and employing different protocols aiming to reflect the true histological framework of gray and white matter. Although NODDI is considered non-inferior to other MRI modalities of high-angular resolution in this regard (48), it may be that acquisition protocols or MRI data modeling methods undertaken in NODDI, such as spherical (rather than linear) tensor encoding (49) along with tract-based (50), gray matter based (37), and gray matter surface based (51) spatial statistics

are further refined in due course to overcome its own recognized limitations.

QUANTITATIVE MAGNETIZATION TRANSFER IMAGING (QMTI)

Magnetization transfer imaging, unlike the NODDI model of diffusion MRI, essentially utilizes a "two pool" model in which hydrogen protons are either free or bound to macromolecules (lipids and proteins) within the semisolid tissue. The latter protons do not directly contribute to the MRI signal and are "silent" in diffusion sequences (increased radial diffusivity with DTI is not specific for demyelination) (52), but can be indirectly probed thanks to their interaction with the free protons following off-frequency radiofrequency pulses. The exchange in magnetization between the two compartments allows the state of the semisolid pool (saturated) to affect that of the free protons, resulting in partial saturation and in a decrease of its overall magnetization (53). The magnetization transfer (MT) effect can thereby produce a qualitative magnetization transfer tissue contrast (MTC) image and is already clinically utilized as part of MR angiography and gadolinium-enhanced T1-weighted sequences, for instance. Indeed, MTC T1 images in patients with ALS have shown hyperintensity along the CST (54, 55) and CC (54) in a proportion of cases (and more conspicuously than FLAIR) (55) compared to control subjects which was significantly related to the degree of reduced FA in the same regions and presumed to reflect damage to the white matter tracts, although with no clear association with clinical rating scales or disease duration (54). Acquiring a proton-density image with and without a MT pulse renders it possible to semi-quantify the MT effect and produce a voxel-wise magnetization transfer ratio (MTR) to reflect changes in macromolecular integrity. Accordingly, reduced MTR within the brain has been reported within the CSTs (56), the precentral and other frontal and extramotor gyri (57, 58), in patients with ALS compared to healthy controls, and independently of gray matter atrophy as measured by voxel-base morphometry (57). Significantly reduced average MTR within the spinal cord has also been reported with respect to controls (59–61), accompanied by diminished cord cross-sectional area and average FA (60), and with a longitudinal decline between sequential scans (59). More recent segmentation of the cord into gray and white matter areas, and using a particular adjusted MT protocol called inhomogeneous MT, has demonstrated localized reductions in MTR to the CSTs and dorsal columns in addition to the anterior horns at several non-contiguous cervical levels (62). However, the MTC and MTR are dependent on a range of imaging variables and their biophysical basis is undefined (53).

The development of mathematical models able to describe the MT-weighted signal as a function of the saturating pulses has enabled more biologically applicable parameters to be derived from quantitative magnetization transfer imaging (qMTi), including the macromolecular pool fraction [f; modeled to essentially represent myelin content], forward exchange rate of magnetization transfer [k_f], and transverse relaxation time of the free pool [$T_2{}^F$]. Although qMTi is yet to be explored in patients with ALS, studies in multiple sclerosis (MS) have demonstrated reductions in f and k_f, and increased $T_2{}^F$ in acute inflammatory lesions with a subsequent return to baseline over several months (63). Compared to healthy controls, normal appearing white matter (NAWM) has reduced f, kf, and MTR (64), and reduced MTR in chronic MS plaques and has been shown to correlate with greater disability (65). Incidentally, reduced MTR in the context of MS is generally considered to be a marker of demyelination, although a small study subdivided NAWM according to distance from a T2 hyper-intense plaque and degree of MTR reduction and found that, whereas at the edge of plaques reduced MTR correlates with reduced myelin content reduced MTR in NAWM may be result from to swollen microglia and, perhaps, axons (66), thus highlighting the uncertainty of its interpretation. MTR in normal appearing gray matter is also reduced in patients with relapsing-remitting MS (67–69) and may also correlate with disability, although variable results are reported (68). Acute increases in kf (but without change in f or T2f) on qMTi have also been induced within the insula in the context of a systemic inflammatory stimulus comprising intramuscular injection of typhoid vaccination and are associated with increased levels of reported fatigue, in addition to a co-localized increase in glucose metabolism measured by FGD-PET (70). Although the mechanisms underlying changes in magnetization transfer parameters are likely to be very different between diseases, it is plausible that qMTi would be sensitive to structural alterations in ALS given the likely role for the immune system in its pathogenesis (71, 72).

MULTIMODAL MRI

Furthermore, it may be that performing simultaneous qMTi with several other MR neuroimaging sequences, such as diffusion and (resting state) functional MRI, will be most helpful in building a better understanding how both tissue structure and function are affected by the disease process and, ultimately, the difference between certain phenotypes to guide more personalized treatments. Indeed, this is exemplified by the estimations of the myelinated fiber "g-ratio," the axon diameter divided by the diameter of its ensheathing myelin, which is estimated to ideally be around 0.7 in the central nervous system (73). As diffusion MRI is insensitive to myelin, the combination of intraneurite and isotropic fractions from NODDI and the *f* value from qMTi is required to calculate the g-ratio across the brain. Following adolescence, white matter g-ratio tends to steadily increase with age inferring myelin reduction and knock on effects with respect to the velocity of neuronal conduction (74) and premature increases in the g-ratio are accordingly seen within MS plaques (75, 76). Although ALS is not primarily a demyelinating disease, new insights into the secondary effects of the neurodegenerative process may be revealed with these techniques and correlate with clinical measures.

EVENT-BASED MODELING

Aside from interpreting the deviations of imaging parameters in terms of current tissue configuration, collecting longitudinal

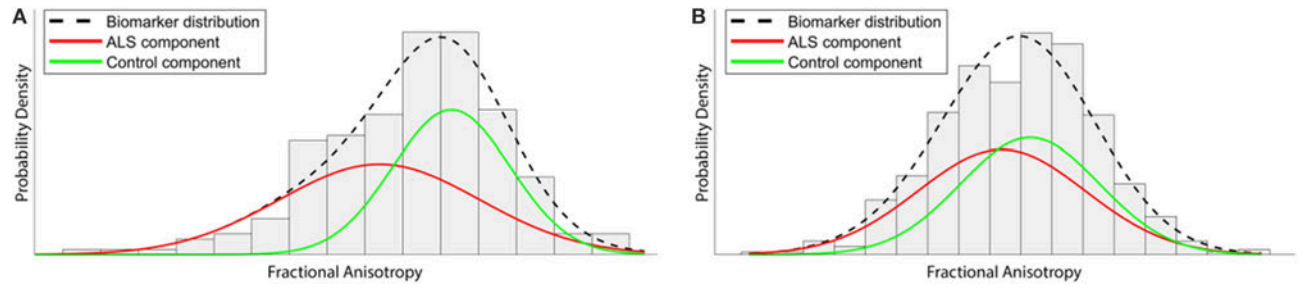

FIGURE 2 | Illustration of how the event-based model (EBM) aims to extract temporal information from a cross-sectional data set. Gaussian distributions of fractional anisotropy (FA) biomarker readings within a tract affected early in the course of the disease, such as the corticospinal tract, would be expected to demonstrate substantial separation between ALS and Control imaging data **(A)**. However, FA from another area affected at later stages demonstrates much less separation between distributions **(B)**. By exploiting and characterizing these differences across all biomarkers, the EBM attempts to order the change from "normal" to "diseased" across the entire disease course.

data is, at least conceptually, the most straightforward approach to understanding the temporal evolution of neurodegenerative pathology. However, patient tolerability for repeated MRI acquisition remains challenging in ALS, particularly, due to the rapid accumulation of symptoms and perhaps accounts for the relatively few studies conducted to date (5). Furthermore, it can be argued that participants who are included would be those harboring more slowly-progressing disease, and therefore may not be representative of the majority of patients with ALS.

Given these limitations, alternative methods such as "big data" analysis techniques and new modeling approaches have the potential to greatly increase our understanding of the mechanisms of disease progression. One such approach is the Event-Based Model (EBM) (77–79), a generative probabilistic model originally developed for use in Alzheimer's disease (AD) for which it has been validated in addition to Huntington's disease (80) and recently in ALS using oculomotor data (81). The EBM is designed to extract temporal information from cross-sectional data sets and, unlike traditional models of disease progression, does not rely on *a priori* staging of patients but instead extracts the event ordering directly from the data, thereby minimizing subjective bias.

The EBM defines a disease as a series of "events," where each event is the change of a biomarker reading from a "healthy" to a "diseased" state. Crucially, biomarker cut-off points are not determined beforehand, but are derived from the data during the modeling process. This not only reduces subjective bias, but also allows for much finer temporal characterization of disease progression than is possible under existing clinically-based staging systems. Healthy control data are used as a fixed reference, and each biomarker is modeled as a mixture of two Gaussian distributions (**Figure 2**). In order to perform temporal modeling, the EBM assumes that the disease progression is monotonic for individual biomarkers (i.e., the severity of disease burden can only increase). Thus, for biomarkers affected early on in the course of the disease, there will be larger differences between patient and control readings, while biomarkers that are affected late on will have smaller differences between patients and controls. Markov Chain Monte Carlo (MCMC) techniques can then be used to determine the most likely event order across the entire cohort (77).

As with any modeling approach, the EBM has strengths and weaknesses. The ability to extract fine-grained temporal information from cross-sectional data is exceptionally novel and valuable. Use of MCMC techniques also enables the model to quantify the positional variance of individual biomarkers across the cohort, thereby allowing a comparison of their relative importance and variability. In its current form, the EBM reveals aspects of disease progression that are common across the entire cohort (an "average" disease progression). The heterogeneity of ALS means that EBM analyses of stratified subgroups, based on genetic/prognostic factors, are an important future area for investigation.

The accuracy of the EBM output, as with any modeling process, will depend on the quality of the input biomarker data. As a consequence, ALS event-based modeling can require large quantities of data, particularly as individual mean cerebral CST FA values are known to have modest diagnostic power for ALS [found to have a pooled sensitivity and specificity of 0.68 and 0.73, respectively, in a meta-analysis (82)]. Current applications of the EBM to ALS data in progress include analysis of mean FA of white matter (WM) fiber bundles, modeling of patterns of cortical thinning, volumetric changes of brain structures, and oculomotor data. Future areas for development include the application of the EBM to multi-modal ALS biomarker data. Excitingly, the application of the EBM to higher order models of diffusion such as NODDI has the potential to give greater insight into ALS degeneration by simultaneously modeling the changes within ISO, NDI, and ODI parameters.

CONCLUSION

Ultimately, all modeling is an attempt to separate meaningful information from randomness. MRI techniques differentially model the signal to derive parameters that plausibly relate to tissue microstructure properties; these parameters can then be

modeled further using the EBM to reveal patterns that exist within the data, but which still require human assessment and interpretation (as well as clinical and histological validation). Although the innovative imaging and data analysis techniques presented here constitute a selection of available methods or protocols, their use singly and in combination has the potential to transform our understanding of the biological processes and temporal evolution of ALS, which is likely to benefit further from multicenter collaboration across the entire ALS research community.

AUTHOR CONTRIBUTIONS

AWB and MCG performed a review of the literature and drafted the paper. MC and PNL provided specialized expertise and critical appraisal of the article for submission.

FUNDING

MCG was funded by the MND Association (MNDA Gabel/Oct16/966-799).

REFERENCES

1. Turner MR, Talbot K. Mimics and chameleons in motor neurone disease. *Pract Neurol.* (2013) 13:153–64. doi: 10.1136/practneurol-2013-000557
2. Blain CR, Williams VC, Johnston C, Stanton BR, Ganesalingam J, Jarosz JM, et al. A longitudinal study of diffusion tensor MRI in ALS. *Amyotroph Lateral Scler.* (2007) 8:348–55. doi: 10.1080/17482960701548139
3. Douaud G, Filippini N, Knight S, Talbot K, Turner MR. Integration of structural and functional magnetic resonance imaging in amyotrophic lateral sclerosis. *Brain* (2011) 134:3470–9. doi: 10.1093/brain/awr279
4. Huynh W, Simon NG, Grosskreutz J, Turner MR, Vucic S, Kiernan MC. Assessment of the upper motor neuron in amyotrophic lateral sclerosis. *Clin Neurophysiol.* (2016) 127:2643–60. doi: 10.1016/j.clinph.2016.04.025
5. Menke RA, Agosta F, Grosskreutz J, Filippi M, Turner MR. Neuroimaging endpoints in amyotrophic lateral sclerosis. *Neurotherapeutics* (2016) 14:11–23. doi: 10.1007/s13311-016-0484-9
6. Simon NG, Turner MR, Vucic S, Al-Chalabi A, Shefner J, Lomen-Hoerth C, et al. Quantifying disease progression in amyotrophic lateral sclerosis. *Ann Neurol.* (2014) 76:643–57. doi: 10.1002/ana.24273
7. Turner MR, Verstraete E. What does imaging reveal about the pathology of amyotrophic lateral sclerosis? *Curr Neurol Neurosci Rep.* (2015). 15:45. doi: 10.1007/s11910-015-0569-6
8. Verstraete E, Foerster BR. Neuroimaging as a new diagnostic modality in amyotrophic lateral sclerosis. *Neurotherapeutics* (2015) 12:403–16. doi: 10.1007/s13311-015-0347-9
9. Grolez G, Moreau C, Danel-Brunaud V, Delmaire C, Lopes R, Pradat PF, et al. The value of magnetic resonance imaging as a biomarker for amyotrophic lateral sclerosis: a systematic review. *BMC Neurol.* (2016) 16:155. doi: 10.1186/s12883-016-0672-6
10. Müller HP, Turner MR, Grosskreutz J, Abrahams S, Bede P, Govind V, et al. A large-scale multicentre cerebral diffusion tensor imaging study in amyotrophic lateral sclerosis. *J Neurol Neurosurg Psychiatry* (2016) 87:570–9. doi: 10.1136/jnnp-2015-311952
11. Sage CA, Peeters RR, Görner A, Robberecht W, Sunaert S. Quantitative diffusion tensor imaging in amyotrophic lateral sclerosis. *Neuroimage* (2007) 34:486–99. doi: 10.1016/j.neuroimage.2006.09.025
12. Iwata NK, Kwan JY, Danielian LE, Butman JA, Tovar-Moll F, Bayat E, et al. White matter alterations differ in primary lateral sclerosis and amyotrophic lateral sclerosis. *Brain* (2011) 134:2642–55. doi: 10.1093/brain/awr178
13. Iwata NK, Aoki S, Okabe S, Arai N, Terao Y, Kwak S, et al. Evaluation of corticospinal tracts in ALS with diffusion tensor MRI and brainstem stimulation. *Neurology* (2008) 70:528–32. doi: 10.1212/01.wnl.0000299186.72374.19
14. Stagg CJ, Knight S, Talbot K, Jenkinson M, Maudsley AA, Turner MR. Whole-brain magnetic resonance spectroscopic imaging measures are related to disability in ALS. *Neurology* (2013) 80:610–5. doi: 10.1212/WNL.0b013e318281ccec
15. Sarica A, Cerasa A, Valentino P, Yeatman J, Trotta M, Barone S, et al. The corticospinal tract profile in amyotrophic lateral sclerosis. *Hum Brain Mapp.* (2017) 38:727–39. doi: 10.1002/hbm.23412
16. Kollewe K, Körner S, Dengler R, Petri S, Mohammadi B. Magnetic resonance imaging in amyotrophic lateral sclerosis. *Neurol Res Int.* (2012) 2012:608501. doi: 10.1155/2012/608501
17. Agosta F, Pagani E, Rocca MA, Caputo D, Perini M, Salvi F, et al. Voxel-based morphometry study of brain volumetry and diffusivity in amyotrophic lateral sclerosis patients with mild disability. *Hum Brain Mapp.* (2007) 28:1430–8. doi: 10.1002/hbm.20364
18. Turner MR, Agosta F, Bede P, Govind V, Lulé D, Verstraete E. Neuroimaging in amyotrophic lateral sclerosis. *Biomark Med.* (2012) 6:319–37. doi: 10.2217/bmm.12.26
19. Li J, Pan P, Song W, Huang R, Chen K, Shang H. A meta-analysis of diffusion tensor imaging studies in amyotrophic lateral sclerosis. *Neurobiol Aging* (2012) 33:1833–8. doi: 10.1016/j.neurobiolaging.2011.04.007
20. Lindenberg R, Renga V, Zhu LL, Betzler F, Alsop D, Schlaug G. Structural integrity of corticospinal motor fibers predicts motor impairment in chronic stroke. *Neurology* (2010) 74:280–7. doi: 10.1212/WNL.0b013e3181ccc6d9
21. Sage CA, Van Hecke W, Peeters R, Sijbers J, Robberecht W, Parizel P, et al. Quantitative diffusion tensor imaging in amyotrophic lateral sclerosis: revisited. *Hum Brain Mapp.* (2009) 30:3657–75. doi: 10.1002/hbm.20794
22. Agosta F, Ferraro PM, Riva N, Spinelli EG, Chiò A, Canu E, et al. Structural brain correlates of cognitive and behavioral impairment in MND. *Hum Brain Mapp.* (2016) 37:1614–26. doi: 10.1002/hbm.23124
23. Senda J, Kato S, Kaga T, Ito M, Atsuta N, Nakamura T, et al. Progressive and widespread brain damage in ALS: MRI voxel-based morphometry and diffusion tensor imaging study. *Amyotroph Lateral Scler.* (2011) 12:59–69. doi: 10.3109/17482968.2010.517850
24. Brownell B, Oppenheimer DR, Hughes JT. The central nervous system in motor neurone disease. *J Neurol Neurosurg Psychiatry* (1970) 33:338–57.
25. Martin JE, Swash M. The pathology of motor neuron disease. In: Leigh PN, Swash M, editors. *Motor Neuron Disease: Biology and Management.* London: Springer-Verlag (1995). p. 93–118. doi: 10.1007/978-1-4471-1871-8_5
26. Smith, M.C. Nerve fibre degeneration in the brain in amyotrophic lateral sclerosis. *J Neurol Neurosurg Psychiatry* (1960) 23:269–82. doi: 10.1136/jnnp.23.4.269
27. Budde MD, Annese J. Quantification of anisotropy and fiber orientation in human brain histological sections. *Front Integr Neurosci.* (2013) 7:3. doi: 10.3389/fnint.2013.00003
28. Jones DK, Knösche TR, Turner R. White matter integrity, fiber count, and other fallacies: the do's and don'ts of diffusion MRI. *Neuroimage* (2013) 73:239–54. doi: 10.1016/j.neuroimage.2012.06.081
29. Zhang H, Schneider T, Wheeler-Kingshott CA, Alexander DC. NODDI: practical *in vivo* neurite orientation dispersion and density imaging of the human brain. *Neuroimage* (2012) 61:1000–16. doi: 10.1016/j.neuroimage.2012.03.072
30. Caverzasi E, Papinutto N, Castellano A, Zhu AH, Scifo P, Riva M, et al. Neurite orientation dispersion and density imaging color maps to characterize brain diffusion in neurologic disorders. *J Neuroimaging* (2016) 26:494–8. doi: 10.1111/jon.12359
31. Chung AW, Seunarine KK, Clark CA. NODDI reproducibility and variability w th magnetic field strength: a comparison between 1.5 T and 3 T. *Hum Brain Mapp.* (2016) 37:4550–65. doi: 10.1002/hbm.23328
32. Rae CL, Davies G, Garfinkel SN, Gabel MC, Dowell NG, Cercignani M, et al. Deficits in neurite density underlie white matter structure abnormalities in first-episode psychosis. *Biol Psychiatry* (2017) 82:716–25. doi: 10.1016/j.biopsych.2017.02.008

33. Grussu F, Schneider T, Tur C, Yates RL, Tachrount M, Ianuş A, et al. Neurite dispersion: a new marker of multiple sclerosis spinal cord pathology? *Ann Clin Transl Neurol.* (2017) 4:663–79. doi: 10.1002/acn3.445
34. Grussu F, Schneider T, Zhang H, Alexander DC, Wheeler-Kingshott CA. Neurite orientation dispersion and density imaging of the healthy cervical spinal cord *in vivo*. *Neuroimage* (2015) 111:590–601. doi: 10.1016/j.neuroimage.2015.01.045
35. Billiet T, Vandenbulcke M, Mädler B, Peeters R, Dhollander T, Zhang H, et al. Age-related microstructural differences quantified using myelin water imaging and advanced diffusion MRI. *Neurobiol Aging* (2015) 36:2107–21. doi: 10.1016/j.neurobiolaging.2015.02.029
36. Merluzzi AP, Dean DC, Adluru N, Suryawanshi GS, Okonkwo OC, Oh JM, et al. Age-dependent differences in brain tissue microstructure assessed with neurite orientation dispersion and density imaging. *Neurobiol Aging* (2016) 43:79–88. doi: 10.1016/j.neurobiolaging.2016.03.026
37. Nazeri A, Chakravarty MM, Rotenberg DJ, Rajji TK, Rathi Y, Michailovich OV, et al. Functional consequences of neurite orientation dispersion and density in humans across the adult lifespan. *J Neurosci.* (2015) 35:1753–62. doi: 10.1523/JNEUROSCI.3979-14.2015
38. Winston GP, Micallef C, Symms MR, Alexander DC, Duncan JS, Zhang H. Advanced diffusion imaging sequences could aid assessing patients with focal cortical dysplasia and epilepsy. *Epilepsy Res.* (2014) 108:336–9. doi: 10.1016/j.eplepsyres.2013.11.004
39. Adluru G, Gur Y, Anderson JS, Richards LG, Adluru N, DiBella EV. Assessment of white matter microstructure in stroke patients using NODDI. *Conf Proc IEEE Eng Med Biol Soc.* (2014) 2014:742–5. doi: 10.1109/EMBC.2014.6943697
40. Song YK, Li XB, Huang XL, Zhao J, Zhou XX, Wang YL, et al. A study of neurite orientation dispersion and density imaging in wilson's disease. *J Magn Reson Imaging* (2018) 48:423–30. doi: 10.1002/jmri.25930
41. Billiet T, Mädler B, D'Arco F, Peeters R, Deprez S, Plasschaert E, et al. Characterizing the microstructural basis of "unidentified bright objects" in neurofibromatosis type 1: A combined *in vivo* multicomponent T2 relaxation and multi-shell diffusion MRI analysis. *Neuroimage Clin.* (2014) 4:649–58. doi: 10.1016/j.nicl.2014.04.005
42. Kamagata K, Hatano T, Okuzumi A, Motoi Y, Abe O, Shimoji K, et al. Neurite orientation dispersion and density imaging in the substantia nigra in idiopathic Parkinson disease. *Eur Radiol.* (2016) 26:2567–77. doi: 10.1007/s00330-015-4066-8
43. Zhang J, Gregory S, Scahill RI, Durr A, Thomas DL, Lehericy S, et al. *In vivo* characterization of white matter pathology in pre-manifest Huntington's disease. *Ann Neurol.* (2018) 84:497–504. doi: 10.1002/ana.25309
44. Parker TD, Slattery CF, Zhang J, Nicholas JM, Paterson RW, Foulkes AJM, et al. Cortical microstructure in young onset Alzheimer's disease using neurite orientation dispersion and density imaging. *Hum Brain Mapp.* (2018) 39:3005–17. doi: 10.1002/hbm.24056
45. Colgan N, Siow B, O'Callaghan JM, Harrison IF, Wells JA, Holmes HE, et al. Application of neurite orientation dispersion and density imaging (NODDI) to a tau pathology model of Alzheimer's disease. *Neuroimage* (2016) 125:739–44. doi: 10.1016/j.neuroimage.2015.10.043
46. Broad RJ, Gabel MC, Dowell NG, Schwartzman DJ, Seth AK, Zhang H, et al. Neurite orientation and dispersion density imaging (NODDI) detects cortical and corticospinal tract degeneration in ALS. *J Neurol Neurosurg Psychiatry* (2018). doi: 10.1136/jnnp-2018-318830. [Epub ahead of print].
47. Wen J, Zhang H, Alexander DC, Durrleman S, Routier A, Rinaldi D, et al. Neurite density is reduced in the presymptomatic phase of C9orf72 disease. *J Neurol Neurosurg Psychiatry* (2018). doi: 10.1136/jnnp-2018-318994. [Epub ahead of print].
48. Schilling KG, Janve V, Gao Y, Stepniewska I, Landman BA, Anderson AW. Histological validation of diffusion MRI fiber orientation distributions and dispersion. *Neuroimage* (2018) 165:200–21. doi: 10.1016/j.neuroimage.2017.10.046
49. Lampinen B, Szczepankiewicz F, Mårtensson J, van Westen D, Sundgren PC, Nilsson M. Neurite density imaging versus imaging of microscopic anisotropy in diffusion MRI: a model comparison using spherical tensor encoding. *Neuroimage* (2017) 147:517–31. doi: 10.1016/j.neuroimage.2016.11.053
50. Smith SM, Jenkinson M, Johansen-Berg H, Rueckert D, Nichols TE, Mackay CE, et al. Tract-based spatial statistics: voxelwise analysis of multi-subject diffusion data. *Neuroimage* (2006) 31:1487–505. doi: 10.1016/j.neuroimage.2006.02.024
51. Parvathaneni P, Rogers BP, Huo Y, Schilling KG, Hainline AE, Anderson AW, et al. Gray matter surface based spatial statistics (GS-BSS) in diffusion microstructure. *Med Image Comput Comput Assist Interv.* (2017) 10433:638–46. doi: 10.1007/978-3-319-66182-7_73
52. Cohen-Adad J. Microstructural imaging in the spinal cord and validation strategies. *Neuroimage* (2018) 182:169–83. doi: 10.1016/j.neuroimage.2018.04.009
53. Cercignani M, Dowell NG, Tofts P. *Quantitative MRI of the Brain : Principles of Physical Measurement*. Series in Medical Physics and Biomedical Engineering. CRC Press; Taylor & Francs Group (2018).
54. Carrara G, Carapelli C, Venturi F, Ferraris MM, Lequio L, Chiò A, et al. A distinct MR imaging phenotype in amyotrophic lateral sclerosis: correlation between T1 magnetization transfer contrast hyperintensity along the corticospinal tract and diffusion tensor imaging analysis. *AJNR Am J Neuroradiol.* (2012) 33:733–9. doi: 10.3174/ajnr.A2855
55. da Rocha AJ, Oliveira AS, Fonseca RB, Maia AC, Buainain RP, Lederman HM. Detection of corticospinal tract compromise in amyotrophic lateral sclerosis with brain MR imaging: relevance of the T1-weighted spin-echo magnetization transfer contrast sequence. *AJNR Am J Neuroradiol.* (2004) 25:1509–15.
56. Tanabe JL, Vermathen M, Miller R, Gelinas D, Weiner MW, Rooney WD. Reduced MTR in the corticospinal tract and normal T2 in amyotrophic lateral sclerosis. *Magn Reson Imaging* (1998) 16:1163–9. doi: 10.1016/S0730-725X(98)00129-5
57. Cosottini M, Cecchi P, Piazza S, Pesaresi I, Fabbri S, Diciotti S, et al. Mapping cortical degeneration in ALS with magnetization transfer ratio and voxel-based morphometry. *PLoS ONE* (2013) 8:e68279. doi: 10.1371/journal.pone.0068279
58. Cosottini M, Pesaresi I, Piazza S, Diciotti S, Belmonte G, Battaglini M, et al. Magnetization transfer imaging demonstrates a distributed pattern of microstructural changes of the cerebral cortex in amyotrophic lateral sclerosis. *AJNR Am J Neuroradiol.* (2011) 32:704–8. doi: 10.3174/ajnr.A2356
59. El Mendili MM, Cohen-Adad J, Pelegrini-Issac M, Rossignol S, Morizot-Koutlidis R, Marchand-Pauvert V, et al. Multi-parametric spinal cord MRI as potential progression marker in amyotrophic lateral sclerosis. *PLoS ONE* (2014) 9:e95516. doi: 10.1371/journal.pone.0095516
60. Querin G, El Mendili MM, Bede P, Delphine S, Lenglet T, Marchand-Pauvert V, et al. Multimodal spinal cord MRI offers accurate diagnostic classification in ALS. *J Neurol Neurosurg Psychiatry* (2018) 89:1220–1. doi: 10.1136/jnnp-2017-317214
61. Querin G, El Mendili MM, Lenglet T, Delphine S, Marchand-Pauvert V, Benali H, et al. Spinal cord multi-parametric magnetic resonance imaging for survival prediction in amyotrophic lateral sclerosis. *Eur J Neurol.* (2017) 24:1040–6. doi: 10.1111/ene.13329
62. Rasoanandrianina H, Grapperon AM, Taso M, Girard OM, Duhamel G, Guye M, et al. Region-specific impairment of the cervical spinal cord (SC) in amyotrophic lateral sclerosis: a preliminary study using SC templates and quantitative MRI (diffusion tensor imaging/inhomogeneous magnetization transfer). *NMR Biomed.* (2017) 30:e3801. doi: 10.1002/nbm.3801
63. Levesque IR, Giacomini PS, Narayanan S, Ribeiro LT, Sled JG, Arnold DL, et al. Quantitative magnetization transfer and myelin water imaging of the evolution of acute multiple sclerosis lesions. *Magn Reson Med.* (2010) 63:633–40. doi: 10.1002/mrm.22244
64. Liu Z, Pardini M, Yaldizli Ö, Sethi V, Muhlert N, Wheeler-Kingshott CA, et al. Magnetization transfer ratio measures in normal-appearing white matter show periventricular gradient abnormalities in multiple sclerosis. *Brain* (2015) 138:1239–46. doi: 10.1093/brain/awv065
65. Amann M, Papadopoulou A, Andelova M, Magon S, Mueller-Lenke N, Naegelin Y, et al. Magnetization transfer ratio in lesions rather than normal-appearing brain relates to disability in patients with multiple sclerosis. *J Neurol.* (2015) 262:1909–17. doi: 10.1007/s00415-015-7793-5
66. Moll NM, Rietsch AM, Thomas S, Ransohoff AJ, Lee JC, Fox R, et al. Multiple sclerosis normal-appearing white matter: pathology-imaging correlations. *Ann Neurol.* (2011) 70:764–73. doi: 10.1002/ana.22521
67. Davies GR, Altmann DR, Hadjiprocopis A, Rashid W, Chard DT, Griffin CM, et al. Increasing normal-appearing grey and white matter magnetisation

transfer ratio abnormality in early relapsing-remitting multiple sclerosis. *J Neurol.* (2005) 252:1037–44. doi: 10.1007/s00415-005-0808-x
68. Gracien RM, Jurcoane A, Wagner M, Reitz SC, Mayer C, Volz S, et al. Multimodal quantitative MRI assessment of cortical damage in relapsing-remitting multiple sclerosis. *J Magn Reson Imaging* (2016) 44:1600–7. doi: 10.1002/jmri.25297
69. Samson RS, Cardoso MJ, Muhlert N, Sethi V, Wheeler-Kingshott CA, Ron M, et al. Investigation of outer cortical magnetisation transfer ratio abnormalities in multiple sclerosis clinical subgroups. *Mult Scler.* (2014) 20:1322–30. doi: 10.1177/1352458514522537
70. Harrison NA, Cooper E, Dowell NG, Keramida G, Voon V, Critchley HD, et al. Quantitative magnetization transfer imaging as a biomarker for effects of systemic inflammation on the brain. *Biol Psychiatry* (2015) 78:49–57. doi: 10.1016/j.biopsych.2014.09.023
71. Schwartz M, Baruch K. Breaking peripheral immune tolerance to CNS antigens in neurodegenerative diseases: boosting autoimmunity to fight-off chronic neuroinflammation. *J Autoimmun.* (2014) 54:8–14. doi: 10.1016/j.jaut.2014.08.002
72. Zhao W, Beers DR, Appel SH. Immune-mediated mechanisms in the pathoprogression of amyotrophic lateral sclerosis. *J Neuroimmune Pharmacol.* (2013) 8:888–99. doi: 10.1007/s11481-013-9489-x
73. Chomiak T, Hu B. What is the optimal value of the g-ratio for myelinated fibers in the rat CNS? a theoretical approach. *PLoS ONE* (2009) 4:e7754. doi: 10.1371/journal.pone.0007754
74. Cercignani M, Giulietti G, Dowell NG, Gabel M, Broad R, Leigh PN, et al. Characterizing axonal myelination within the healthy population: a tract-by-tract mapping of effects of age and gender on the fiber g-ratio. *Neurobiol Aging* (2017) 49:109–18. doi: 10.1016/j.neurobiolaging.2016.09.016
75. Hagiwara A, Hori M, Yokoyama K, Nakazawa M, Ueda R, Horita M, et al. Analysis of white matter damage in patients with multiple sclerosis via a novel *in vivo* MR method for measuring myelin, axons, and G-Ratio. *AJNR Am J Neuroradiol.* (2017) 38:1934–40. doi: 10.3174/ajnr.A5312
76. Stikov N, Campbell JS, Stroh T, Lavelée M, Frey S, Novek J, et al. *In vivo* histology of the myelin g-ratio with magnetic resonance imaging. *Neuroimage* (2015) 118:397–405. doi: 10.1016/j.neuroimage.2015.05.023
77. Fonteijn HM, Clarkson MJ, Modat M, Barnes J, Lehmann M, Ourselin S, et al. An event-based disease progression model and its application to familial Alzheimer's disease. *Inf Process Med Imaging* (2011) 22:748–59. doi: 10.1007/978-3-642-22092-0_61
78. Oxtoby NP, Young AL, Cash DM, Benzinger TLS, Fagan AM, Morris JC, et al. Data-driven models of dominantly-inherited Alzheimer's disease progression. *Brain* (2018) 141:1529–44. doi: 10.1093/brain/awy050
79. Young AL, Oxtoby NP, Daga P, Cash DM, Fox NC, Ourselin S, et al. A data-driven model of biomarker changes in sporadic Alzheimer's disease. *Brain* (2014) 137:2564–77. doi: 10.1093/brain/awu176
80. Fonteijn HM, Modat M, Clarkson MJ, Barnes J, Lehmann M, Hobbs NZ, et al. An event-based model for disease progression and its application in familial Alzheimer's disease and Huntington's disease. *Neuroimage* (2012) 60:1880–9. doi: 10.1016/j.neuroimage.2012.01.062
81. Gabel MC, Schmidt DG, Leigh NP, Pinkhardt EH, Ludolph AC, Kassubek J, et al. *Event-Based Modelling Resembles the Sequential Development of Eye Movement Dysfunctions in Amyotrophic Lateral Sclerosis*. Berlin: Neurowoche (2018). Available online at: https://www.dgnkongress.org/
82. Foerster BR, Dwamena BA, Petrou M, Carlos RC, Callaghan BC, Pomper MG. Diagnostic accuracy using diffusion tensor imaging in the diagnosis of ALS: a meta-analysis. *Acad Radiol.* (2012) 19:1075–86. doi: 10.1016/j.acra.2012.04.012

Conflict of Interest Statement: The authors declare that the research was conducted in the absence of any commercial or financial relationships that could be construed as a potential conflict of interest.